January 2021

Hole Cleaning And Cuttings Transportation Modelling And Optimization

Foued Badrouchi

HOLE CLEANING AND CUTTINGS TRANSPORTATION MODELLING AND OPTIMIZATION

by

Foued Badrouchi

Petroleum Engineering Bachelor of Science, University of Boumerdes, Algiers, Algeria, 2015

Petroleum Engineering Masters of Science, University of Boumerdes, Algiers, Algeria, 2017

A Dissertation

Submitted to the Graduate Faculty

of the

University of North Dakota

In fulfillment of the requirements

for the degree of

Doctor of Philosophy

Grand Forks, North Dakota

May
2021

Name: Foued Badrouchi

Degree: Doctor of Philosophy

This document, submitted in partial fulfillment of the requirements for the degree from the University of North Dakota, has been read by the Faculty Advisory Committee under whom the work has been done and is hereby approved.

DocuSigned by:
Vamegh Rasouli
0EB956E8C9C9456...
Vamegh Rasouli

DocuSigned by:
Hui Pu
C63B8AB854E4448...
Hui Pu

DocuSigned by:
Minou Rabiei
DB5B8BA42D59466...
Minou Rabiei

DocuSigned by:
Kegang Ling
AE10F7CCAFC7487...
Kegang Ling

DocuSigned by:
Iraj Hossein Pouli Mamaghani
76231706E0AA4C6...
Iraj Hossein Pouli Mamaghani

This document is being submitted by the appointed advisory committee as having met all the requirements of the School of Graduate Studies at the University of North Dakota and is hereby approved.

DocuSigned by:
Chris Nelson
2E0AF0886795463...
Chris Nelson
Dean of the School of Graduate Studies

4/26/2021
Date

PERMISSION

Title Hole Cleaning and Cuttings Transportation Modelling and Optimization

Department Petroleum Engineering

Degree Doctor of Philosophy

In presenting this thesis in partial fulfillment of the requirements for a graduate degree from the University of North Dakota, I agree that the library of this University shall make it freely available for inspection. I further agree that permission for extensive copying for scholarly purposes may be granted by the professor who supervised my thesis work or, in his absence, by the chairperson of the department or the dean of the Graduate School. It is understood that any copying or publication or other use of this thesis or part thereof for financial gain shall not be allowed without my written permission. It is also understood that due recognition shall be given to me and to the University of North Dakota in any scholarly use which may be made of any material in my thesis.

Foued Badrouchi
February 19th, 2021

DEDICATION

This research is lovingly dedicated to my parents Salah Badrouchi and Sihem Kahloul Badrouchi, my brothers Abdenasser and Nidhal, my beloved sister Dr. Samaara and my soulmate Nourelhouda Benouadah who have been my source of inspiration. They have given me the drive and discipline to tackle any task with enthusiasm and determination. Without their love and support, this project would not have been made possible.

Foued Badrouchi

ACKNOWLEDGMENTS

First and foremost, I am extremely grateful to my advisor, Prof. Vamegh Rasouli for his invaluable advice, continuous support, and patience during my PhD study. His immense knowledge and plentiful experience have encouraged me in all the time of my academic research and daily life. I wish to express my sincere appreciation to the members of my advisory committee for their guidance and support during the course of my Ph.D program at the University of North Dakota.

I want to thank Harry Feilen for his help in building the Slurry Loop Unit.

Finally, I want to thank my former advisor at Schlumberger Mohammed Kelkouli for his continuous support.

The financial support of the North Dakota Industrial Commission (NDIC) is highly appreciated.

ABSTRACT

Efficient hole cleaning in drilling operation is essential to ensure optimum rate of penetration. This complex problem involves simultaneous analysis of multiple parameters, including cuttings characteristics, fluid rheology and the geometry of the annulus space. For instance, accurate calculations of the equivalent circulation density (ECD) requires the effect of the mud density increase due to the cuttings' concentration to be considered, which itself is a function of the settling velocity and the rate of penetration (ROP). Analytical models, lab experiments and numerical simulations have been used to determine the optimum flow rate for efficient hole cleaning. Most of these models are based on the drag coefficient-Reynolds number relationship, where both parameters are velocity dependent, making the calculation workflow to be implicit, tedious and time consuming. While several attempts have been made to present explicit correlations, precise equations covering a wide range of Reynolds numbers are not available.

Terminal settling velocity was used in this research to determine the minimum required transportation velocity of drilling cuttings in the annulus space to ensure an optimal cleaning. The ROP also affects the hole cleaning as it defines the volume of the cuttings produced. We first used analytical models to investigate the effect of the cuttings size, density, and fluid properties as a function of wellbore deviation and circulation rate on hole cleaning efficiency. The results were compared with lab experiments using a slurry loop. The analytical models predict the critical velocities for lifting and rolling the cuttings particles based on the equilibrium cuttings bed height model and forces acting on a cuttings bed. For vertical sections of the wellbore, the critical transportation velocity showed to be proportional to the terminal settling velocity of the drill cuttings. Hence, we developed two new methods to predict the hindered terminal settling velocity due to the presence of wellbore and pipe walls and particle shape.

We then used the Artificial Neural Network (ANN) algorithm and generated two models to predict the terminal velocity of drill cuttings and proppants considering the particles shape and the wall effect. The results of both analytical models and ANN were applied to estimate ECD. In addition, the drilling Mechanical Specific Energy (MSE) was calculated to determine the effect of different drilling parameters on hole cleaning and ECD. A new model was proposed for predicting the ECD in vertical and deviated wellbores that considers fluid and formation properties as well as wellbore and drill string geometry and drilling operational parameters. The developed model was used to study the effect of different drilling parameters on ECD and help engineers to optimize their operational parameters.

The final step of this study was to investigate the effect of stabilizers geometry on hole cleaning. A total of more than 30 different designs of straight, straight with offset and helical blades geometries were built numerically and the results were compared. The reliability of the numerical simulation was confirmed against experimental and field data from the literature. The effect of size and shape of the stabilizer blades on the motion of the particles was investigated. Numerical simulation results showed that the straight blade geometry causes less disturbance to the cuttings transportation as compared to the straight with offset and helical blades, respectively.

CONTENT

LIST OF FIGURES

LIST OF TABLES

Nomenclature

ΔP_T	Total Pressure Loss
A_b	Drill bit area (in^2)
A_p	surface area of the particle (m^2)
C_D	Drag Coefficient (N/A)
C_L	Lift Coefficient (N/A)
$C_{c\%}$	Cuttings concentration (N/A)
D_{hyd}	Hydraulic Diameter (in)
D_b	Drill bit diameter (in)
D_{cs}	Casing Shoe Setting Depth (ft)
E_m	Bit mechanical efficiency
$F_{\Delta P}$	Pressure Differential Force
F_B	Buoyance Force
F_D	Drag Force
F_L	Lift Force
F_P	Plastic Force
F_g	Gravity Force
L_{Cs}	Previous Casing Length (ft)
L_{DC}	Drill Colar Length (ft)
P_b	Back Pressure (psi)
P_p	Pore Pressure (psi)
Q_c	Cuttings feed rate (cft/hr)
Re_∞	Infinite medium Reynold's number
Re_p	Particle Reynold's number (N/A)
U_{Lift}	Critical Lifting Velocity (m/s)
U_{Roll}	Critical Rolling Velocity (m/s)
U_f	Fluid velocity (m/s)
U_p	Particle velocity (m/s)
V_{eq}	Equivalent volume (m^3)
V_{fCs}	Annular Fluid Velocity Between Drillpipe and Previous Casing (m/s)
V_{fDC}	Annular Fluid Velocity Between Drill Collar and Open Hole (m/s)

V_{fOH}	Annular Fluid Velocity Between Drillpipe and Open Hole (m/s)
V_{sl}	settling velocity (m/s)
V_{sl}	Particle's settling velocity (m/s)
d_p	Particle's Diameter (mm)
t_{csurf}	Cuttings travel time to surface (min)
v_∞	Infinite medium terminal settling velocity (unit: m/s)
v_{sl}	Terminal settling velocity (unit: m/s)
η_{PV}	Plastic viscosity (eq. cP)
μ_f	fluid viscosity (cP)
ρ_f	Fluid density (ppg)
ρ_f	Fluid Density (ppg)
ρ_p	Particles density (gcc)
ρ_s	Solids density (gcc)
ρ_s	Solid Density (gcc)
τ_w	Shear Stress at Wall (lb/100ft^2)
τ_y , τ_{YP}	Yield point (lb/100ft^2)
$\emptyset$	Angle of Internal Friction (deg)
WF	Wall effect factor (N/A)
α	Shape factor (N/A)
φ	Repose angle (deg)
CCS	Confining Compressive Strength (psi)
ECD	Equivalent circulation density (ppg)
ID_{Cs}	Casing Inner Diameter (in)
ID_{DP}	Drill Pipe Inner Diameter (in)
L	Section Length (ft)
MSE	Mechanical Specific Energy (psi)
OD_{DP}	Drillpipe Outer Diameter (in)
P	Padé approximation
P	Fluid Pressure (psi)
$P[m/n]$	Order of accuracy in Padé
Q	Flow rate (gpm)
$R(x)$	Residual function

ROP	Rate of penetration (ft/hr)
RPM	Rotary speed (rpm)
Re	Reynold's number (N/A)
T	Torque in bit (ft.lbf)
TVD	True Vertical Depth (ft)
U	velocity (m/s)
UCS	Uniaxial Compressive Strength (psi)
WOB	Weight om bit (lbf)
$a, b, c\ and\ d$	Constants
f	Friction factor
g	Acceleration due to gravity (m/s^2)
i	Number of nodes in ANN model
j	Number of layers in ANN model
k	Fluid consistency index
m	Particle's mass (kg)
n	Fluid behavior index
t	Time (s)
x	vertical position (m)
Ψ	Resistance coefficient (unit: s^2/m^2)
Ψ'	Spherical particle-fluid non-dimensional parameter (N/A)
Ψ''	Non-spherical particle-fluid non-dimensional parameter (N/A)
α	Well inclination (deg)
η	Coefficient of viscosity (cP)
μ	dynamic viscosity (kg/(m/s))
ρ	Density (kg/m^3)
φ	Sphericity (N/A)
φ	Porosity (N/A)
ω	ANN connection weight

CHAPTER 1

Borehole Cleaning Challenges

1.1 Introduction

Removal of cuttings from the wellbore during drilling is vital for a safe and successful operation. Apart from changing a worn bit, making a connection, coring, formation measurement and testing and well completion, drilling operation can be stopped for a variety of reasons. The pause of the drilling operation is followed by a suspension of the drilling fluid flow causing the cuttings left in the wellbore to deposit in the bottom of the wellbore (Chen et al., 2002; Mason and Chen, 2006; Moreira et al., 2017). Large amounts of settled cuttings left over in the wellbore lead to serious operational problems such as, high torque, low rate of penetration (ROP), stuck pipe, bit balling and bad cementing (Ahmed and Takach, 2008; Busahmin et al., 2017; Gaynor et al., 2001; Mason and Chen, 2006; Mohammadsalehi and Malekzadeh, 2011; Rasi, 1994).

The existence of the drilling hardware, such as centralizers and stabilizers, on cuttings transportation is another important topic for efficient hole cleaning. Drilling hardware can cause a restriction area to flow leading to an increase of the fluid velocity enhancing some pf the particles velocity. However, the blades and bows of these subs blocks some of the particles reducing their velocity. Therefore, appropriate design of these subs, helps enhance enhancement of the hole cleaning (Xiaofeng et al., 2013). Few researches are available in the literature considering the effect of stabilizers on hole cleaning (Anayo et al., 2012; Chen and Xiong, 2010; Shu, 2005; Shu

and Liu, 2006, 2005; Xiaofeng et al., 2013). Some researches on helical centralizers showed that for deviated to horizontal holes, helices in the helical centralizers help to enhance cuttings transport efficiency to some extent by generating eddies (Anayo et al., 2012; Chen and Xiong, 2010; Shu, 2005; Shu and Liu, 2006, 2005). However, these studies do not present a comparison between different blade geometries. Xiaofeng et al. (2013) compared two models of straight and helical blades stabilizers and showed that the straight blade ones are better in terms of hole cleaning without presenting a sensitivity analysis or a wide comparison between different types. Other researchers investigated the use of hole cleaning devices, similar geometries to stabilizer, to cleanout deviated wellbores (Nwagu et al., 2014; Yan et al., 2019).

Over the past 35 years or so, considerable efforts have been made on studying the cuttings transportation in vertical, deviated and horizontal wellbores. Investigators followed three approaches of experimental work, analytical models and numerical simulations.

The first approach relied on observations and empirical approach. Data obtained from experiments are correlated by dimensional analysis or semi-theoretical models. The second approach is a theoretical based analytical approach. Starting with forces equilibrium and physics principles, equations are developed and models are tested with experimental data. The third approach can be subdivided in two categories. The first one is using algorithms on analytically developed equations. Some of the equations developed based on the second approach cannot be solved by hand and needs computational tools. The second is using computational fluid dynamics (CFD) based software, mainly ANSYS.

Another alternative, considering the existing large experimental data available in the area of the settling velocity, is the Artificial Intelligence (AI) and Machine Learning (ML) techniques. Since its inception, technology has driven the development and transformation of the oil and gas

industry. AI and ML allow computers to assess large volumes of data and make decisions to solve problems in a manner that is similar to how the human brain does it (Badrouchi et al., 2019; Mitchell, 2006). Recently, some researchers focused on using AI techniques such as Artificial Neural Networks (ANN), support vector machine (SVM) and other generic programming algorithms to predict the settling velocity (Agwu et al., 2020; Barati et al., 2014; Goldstein and Coco, 2014; Kamyab et al., 2016; Li et al., 2014; Rooki et al., 2012; Sadat-Helbar et al., 2009). Experiments studies provide a visual and effective approach to investigate the effects of fluid, cuttings geometry and shape and drilling parameters on cuttings transportation. A number of set ups have been developed for this purpose. The Tulsa University Drilling Research Projects (TUDRP) (Tomren, 1979) is a field scale flow loop used to study cuttings transportation. Other flow loops labs include the Southwest Research (Sifferman and Becker, 1992), M.I. Drilling Fluids (Seeberger et al., 1989), Middle East Technical University (METU) (Sorgun, 2010). Recently a new field scale slurry loop unit (SLU) was set up at the University of North Dakota (see Figure 1.1).

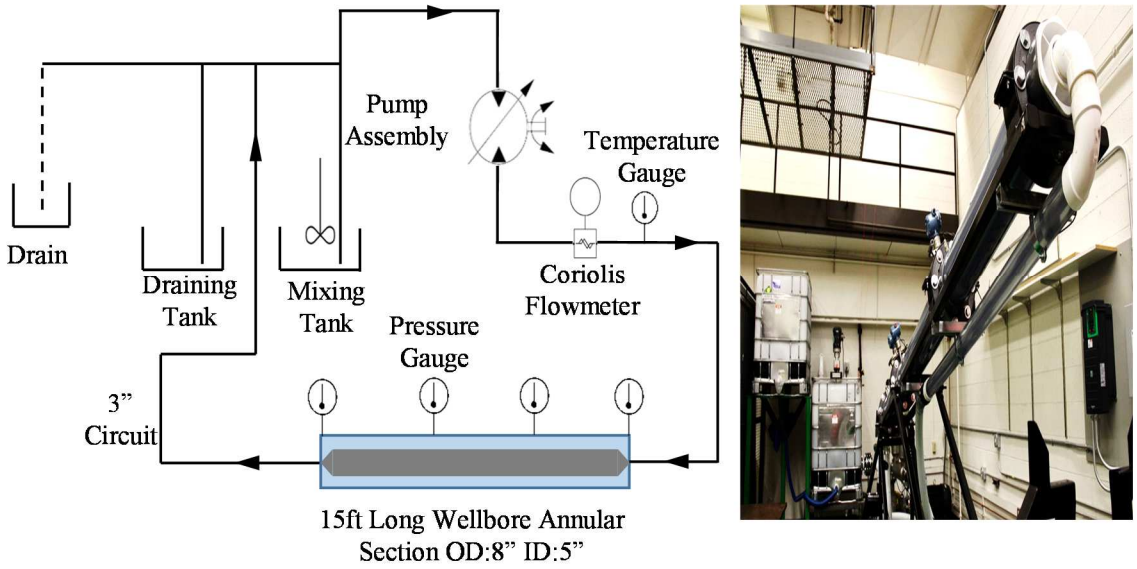

Figure 1.1 – Slurry Loop Unit at the University of North Dakota.

In this research study, we performed experimental, numerical simulations and artificial intelligence technique to study and model the effect of various parameters on efficient hole cleaning as well as the impact of stabilizers geometry.

In the following sections, the objectives of this study and the methodology used will be outlined. Also, the significance of the work will be presented and the structure of the thesis content will be reviewed.

1.2 Objectives

As explained above, predicting the settling velocity of drill cuttings is of significant importance in drilling operations to ensure that the cuttings are transported to the surface and the hole is clean. Also, providing an understanding of the effect of stabilizers geometry on hole cleaning is a novelty in the field of drilling and helps engineers to select appropriate designs to ensure the stability of the drillstring and wellbore and an efficient hole cleaning. Therefore, the two main goals of this study are to propose improved models for predicting the settling velocity of spherical and irregularly shaped drill cuttings and simulate the effect of stabilizers geometry on hole cleaning efficiency. The detailed objectives of this work can be summarized as followings:

1. Comprehensive review of existing literature on hole cleaning and settling velocity prediction. This includes analytical models, lab experimental studies and numerical simulations.
2. Determine critical velocities required to transport cuttings in deviated wellbores.
3. Outline the applications and limitations of analytical models in estimating the settling velocity of drill cuttings. This will be extended to validate numerical simulation using MfiX with experimental data in predicting the settling velocity.
4. Propose new empirical correlations for predicting the settling velocity of drill cuttings and graphical nomograms that account for the shape irregularity and the wellbore size effect.

5. Propose an artificial neural network models for predicting the settling velocity. These models will be used to generate new graphical nomograms that account for the particles shape irregularity.
6. Conduct numerical simulations to study the effect of straight, straight with offset and helical blade stabilizers to study their effects on hole cleaning efficiency. The simulation results are then compared to field data for validation.

1.3 Methodology

The methodology that will be used to achieve the above objectives comprises of data inventory, analytical solutions and numerical simulations. These are briefly explained below.

1. In order to propose correlations and graphical nomograms we will collect sets of lab data from our experiments using the Slurry Loop Unit (SLU) and from the literature.
2. Numerical simulations will be run using MFiX software to estimate the particles settling velocity. The impact of particle and fluid properties as well as wellbore geometry on cuttings transportation will be studied. Lab data will be used to validate the numerical simulation results.
3. The results of correlation and graphical models and numerical simulations will be compared to draw some practical conclusions in terms of determining the hindered setting velocity of drill cuttings.
4. Numerical simulation will be used also to study the effect of stabilizers geometry on hole cleaning. The results of the simulations will be compared to field data obtained from the literature.

1.4 Significance

The results of this research study will present multifold novelties including the followings:

1. New analytical models to predict the critical velocities to initiate the cleaning of different cuttings in deviated wellbores.
2. High accuracy correlations and easy to use graphical nomograms to predict the particles settling velocity.
3. An Artificial Neural Network to generate models and graphical nomograms for predicting the settling velocity of irregularly shaped drill cuttings with high accuracy compared to previous models present in the literature.
4. The use of the MFiX software, and Eulerian-Lagrangian simulations, with their special features implemented in this study are one of the first attempts to study the impact of different stabilizers geometries on hole cleaning efficiency.

1.5 Thesis Structure

This thesis consists of eight chapters.

Chapter 1 provides the background to the project and a brief explanation of the basics of the cuttings transportation, emphasizing on the approaches used in studying the hole cleaning. It also contains the objectives of this study, the methodology used and the significance of this research.

In **Chapter 2** a brief review of the literature regarding the hole cleaning will be presented. Also, a summary of past studies related to the lab work, numerical simulations and analytical models to study the effect the drilling, particle and fluid properties on hole cleaning will be presented.

Chapter 3 presents the proposed analytical models used to predict critical velocities for lifting and rolling the cuttings particles based on the equilibrium cuttings bed height model and forces acting on a cuttings bed. The results will be compared to experimental data obtained using the Slurry Loop Unit. The range of applications and limitations of these models will be discussed.

Chapter 4 comprises of different analytical models that study the terminal settling velocity of drill cuttings. These models integrate the unsteady state region of the particles motion. Numerical simulations are conducted and results are compared to experimental data obtained from the Slurry Loop. The range of applications and limitations of these models will be discussed.

Chapter 5 presents the proposed correlations and graphical nomograms developed to predict terminal settling velocity of drill cuttings. The models account for the particles shape and wall retarding effect. The proposed models were compared to experimental and simulation results.

Chapter 6 presents different ANN models to predict the terminal settling velocity of spherical and irregularly shaped cuttings. The models were used to develop wide range of graphical nomograms. The proposed models were compared to experimental results.

Chapter 7 presents a new model to predict the cuttings concentration and equivalent circulation density in vertical and deviated wells. The workflow followed implements the critical and settling velocity models developed in chapters 3, 5 and 6 and the drilling mechanical specific energy. The developed model aids to optimize both drilling performance and hole cleaning.

Chapter 8 presents the simulation results of the impact of stabilizers geometry on hole cleaning efficiency. More than 30 different designs of straight, straight with offset and helical blade stabilizers were simulated. The results were compared to field observations.

In **Chapter 9** a summary of the findings from this study will be presented along with some recommendations and future studies that can be carried out.

1.6 Summary

This Chapter introduced the hole cleaning and the research gaps in cuttings transportation. It was highlighted that the knowledge of critical drilling fluid flow rate is crucial to ensure an efficient

hole cleaning. Also, it was explained that the settling velocity of cuttings and the stabilizers geometry are important in studying cuttings transportation. Also, in this Chapter, a summary of the main objectives of this research, the methodology which will be implemented, distinguished aspects of this study and the structure of this thesis were presented.

In the next Chapter, a review of the literature will be presented to give a background to the different methods and models that are used for studying the transportation of cuttings and hole cleaning in vertical, deviated and horizontal wells.

CHAPTER 2

Review of Literature

2.1 Introduction

Of the many functions that ae performed by the drilling fluid, the most important is to transport cuttings from the bit up the annulus to the surface. If the cuttings cannot be removed from the wellbore, drilling cannot proceed for long.

Hole cleaning in vertical wells has been studied for many years, with the earliest analysis of the problem being that of Pigott (1941). For vertical wells, hole cleaning efficiency is usually assessed by determining the settling velocity, which is dependent on cuttings particles properties and shapes, the drilling fluid density and rheological properties, flow rate, and the annular space configuration (Clark and Bickham, 1994). Since the 1980s, more studies focused on inclined wellbores (Ford et al., 1990; Larsen et al., 1997; Larsen, 1990; Luo et al., 1992; Pilehvari et al., 1996; Rasi, 1994). This focus came from the considerable difficulties encountered when drilling directional wells, as cuttings may accumulate either in a stationary, moving or churning bed at lower hole sections (Clark and Bickham, 1994).

Extensive work can be found in the literature studying the cuttings transportation. This work ranges from experimental, analytical, numerical simulations and application of artificial intelligence.

2.2 Borehole Cleaning Overview

2.2.1 Experimental and Analytical Studies

Among the early experimental studies on hole cleaning in vertical and deviated wellbores include the work of Sifferman et al. (1974) and Tomren (1979) at the University of Tulsa (TUDRP). Sifferman et al. (1974) used the Transport Ratio (R_t) defined by the ratio the particle and annular velocities to study the hole cleaning efficiency. He concluded that only particle settling velocity (should be overcome by the annular fluid velocity) and fluid rheological properties have major effect on cuttings transportation, while, the pipe rotation, cuttings percentage, annulus size, and eccentricity have a minor effect. Tomren (1979) reported that the pipe rotation effect on hole cleaning is minor for deviated wellbores and the height of the cuttings bed formed increases with inclination up to a certain angle under a constant flow rate. A year later, Iyoho (1980) expanded the work of Tomren (1979) and developed a General Transport Ratio (R_{tg}) to evaluate cuttings transportation performance in directional wells which was initially was proposed by Sifferman et al. (1974) for vertical annuli and did not consider the effect of cuttings beds presence. His new ratio was proposed based on a combination of experimental data, of material balance, and particle settling velocity theory.

Few years later, Tomren et al. (1986) presented a study on the effect of drilling fluid velocity, hole inclination, and fluid rheological properties on cuttings transportation and described the cuttings behavior as a function of wellbore inclination (θ). A summary of their observations is presented in Table 2.1. Tomren et al. (1986) recommended to apply turbulent flow regimes to remove cuttings beds from directional wells.

Okrajni and Azar (1986) focused on studying the effect of fluid rheological properties on hole cleaning when drilling operation is stopped and the bit is off bottom. They found that the yield

point (YP) and the plastic viscosity (PV) have a major effect on cuttings transportation at laminar flow regime, however, their effect is dramatically reduced when turbulent flow regime takes place. They also observed that laminar flow regime provides a better hole cleaning in vertical to low inclined wellbores (0° to 45°) compared to turbulent flow regime. The situation reverses for high inclination to horizontal wellbores (55° to 90°). A similar performance is observed for both turbulent and laminar flow regimes for the intermediate inclination angles (45° to 55°).

Similarly, Brown et al. (1989) conducted experiments using the flow loop facility at the BP Research Centre to determine the minimum transport velocity (MTV) required to initiate the transportation of cuttings and the effectiveness of water and HEC polymer-based water solutions in hole cleaning. They observed that water is more effective than HEC polymer-based fluid for cuttings transportation.

Becker (1982, 1987) and Becker et al. (1991) continued the studies and experimental works of Tomren (1979) and Iyoho (1980) with a focus on the effect of the drilling fluid properties on hole cleaning. Their observation was in agreement with that of Okrajni and Azar (1986) in that the drilling fluid density increase enhances the cleaning of the cuttings.

Later, Larsen (1990) proposed several correlations to predict the critical fluid flow velocity (CTVF) as the minimum fluid velocity required to maintain a continuously upward movement of cuttings, blow which the cuttings will settle and build up in the annuls.

Sifferman and Becker (1992), based on their extensive experimental work on the effect of various drilling parameters on hole cleaning, reported that the flow rate, mud weight, borehole inclination and drill pipe rotation have, in order, the major influence on hole cleaning. They also mentioned that cuttings size, fluid rheology and borehole eccentricity have a moderate effect. However, the cuttings feeding rate (or rate of penetration), mud type and drillpipe size have minor to insignificant

effect on hole cleaning. Similar to previous findings, they observed that the pipe rotation has more effect on hole cleaning for highly inclined to horizontal wellbores, small cuttings (diameter less than 0.2 mm) and low flow rate and ROP.

Ford et al. (1990) and Peden et al. (1990) used video camera recording technology in their experiments at the Heriot-Watt University to study the different cuttings movement patterns in deviated small annulus. Their observations were similar to those of Govier and Khalid (1972). A summary of their findings are listed in Table 2.2.

Gavignet and Sobey (1989), following the two-layer model for pipeline developed by Wilson (1970), proposed a two-layer model for annuli using simple momentum Balance. They concluded that at wellbore inclinations higher than 60°, the rate of penetration (cuttings concentration) and fluid rheology have a minor effect of the bed forming critical flow rate above which no beds are formed. It is important to mention that they considered that the flow regime in the region above the bed to be always turbulent. Brown et al. (1989) mentioned that in their model Gavignet and Sobey (1989) the dry friction force between the cuttings and the confining walls were not rigorously analyzed as proposed by Wilson (1970) and the effects of interfacial shear stress and fluid velocity in eccentric annuli were neglected. Both models of Wilson (1970) and Gavignet and Sobey (1989) consider the cuttings bed always sliding regardless of its height and fluid flow rate and ignore the particles moving on top of the bed and in suspension in the fluid area contrary to what is reported by Tomren (1979) and Iyoho (1980).

The two-layer model proposed by Gavignet and Sobey (1989) was improved using experimental and field data analysis by Martin et al. (1987) who developed a numerical model to improve cuttings movement in the inclined wellbores. Their observations, later confirmed by Ford et al. (1990) and Peden et al. (1990), showed that high viscosity drilling fluids provide a better carrying

capacity of drill cuttings, however, at high inclinations, less viscosity is required to perform a good cleaning in addition to higher fluid density that improves the carrying capacity in this situation.

Martins and Santana (1992) extended the two-layer model proposed by Doron et al. (1987) for slurry transport studies in pipes to improve the model of Gavignet and Sobey (1989). Their model introduced the transportation of solid particles by turbulent suspension. The proposed model allows to predict the particles flow pattern for high inclination to horizontal wellbores. However, their new model did not resolve all the limitations in the model of Gavignet and Sobey (1989).

Luo et al. (1992) ameliorated the model of (Luo (1988) to propose a physical model for predicting the minimum transportation velocity based on forces acting on a cuttings particle.

Clark and Bickham (1994) proposed a mechanistic model for cuttings transportation. The model used a combination of mechanical relationships based on forces acting on particle, including the settling, lifting, and rolling forces. They compared their model to experimental data and found that it under-predicted the annular cuttings concentrations at angles higher than 50°.

Consideing the shortcomings of the two layer models, three layer models of cuttings transportation were developed by other researchers (Cho et al., 2000; D. Nguyen, 1997; Nguyen and Rahman, 1998; Ozbayoglu et al., 2009; Wang et al., 2010). These models are comprised of suspended layer, stationary and mobile cuttings bed. These models considered the key factors including cuttings distribution of suspended layer, particle settling, and mass exchange between layers.

With advances in computers technology in recent years, simulation has become an integrated part of any experimental work with the ability to run several models to conduct sensitivity analysis of different parameters in a more cost effective and timely manner. Simulation modeling solves real-world problems safely and efficiently. It provides an important method of analysis which is easily verified, communicated, and understood. Across industries and different disciplines, simulation

modeling provides valuable solutions by giving clear insights into complex systems (Wang and He, 2020).

Alongside with experimental studies, analytical work, and simulations, correlations have been proposed to study the cuttings behaviour in the annulus (Bassal, 1995; Duan et al., 2008; Li et al., 2010; Loureiro et al., 2010; M E Ozbayoglu et al., 2010; Ozbayoglu et al., 2008; Wang et al., 1995) and predict the critical velocity (Clark and Bickham, 1994; Duan et al., 2009; Larsen et al., 1997; Luo et al., 1992; Mirhaj et al., 2007; Mohammadsalehi and Malekzadeh, 2011; M E Ozbayoglu et al., 2010; Peden et al., 1990).

A summary of such correlations is given in Table 2.3 and Table 2.4 a and b, respectively.

Table 2.1 – Experimental observations on hole cleaning (Tomren et al., 1986)

Inclination	Description	Observations
$0° < \theta < 10°$	Near vertical	Cuttings are transported in suspension similar to the vertical wellbores
$10° < \theta < 30°$	Low inclination	Attempts of bed of cuttings forming at low drilling fluid flow rates
$30° < \theta < 60°$	Critical inclination	Cuttings bed tends to slide downward if insufficient drilling fluid flow rate is provided
$60° < \theta < 90°$	High inclination	A stagnant cuttings bed forms instantaneously and above this bed particles move in two different zones: a moving layer and a suspension layer

Table 2.2 – Experimental observations on hole cleaning (Ford et al., 1990; Peden et al., 1990)

Description	Observations
Homogeneous Suspension	Particles are fully suspended and uniformly distributed throughout the annular space
Heterogeneous Suspension	Particles are in suspension; however, particles concentration increases with the depth
Suspension/Saltation	Densely populated particles near the bottom-side of the annular space move forward by jumping or saltating

Clusters	Clusters of particles are transported in suspension
Separated Moving Beds (Dunes)	Separated particles beds are formed on the bottom-side of the annular space and particles on the top layer of the bed are transported forward
Continuous Moving Bed	A layer of moving bed is formed on the low-side wall with particles travelling above it at a higher speed
Stationary Bed	A stationary bed of particles is formed on the low-side wall with particles sliding forward on the surface of the bed.

Table 2.3 – Experimental observations on hole cleaning (Tomren et al., 1986)

Author	Goal	Rate	ROP	Eccentricity	RPM	Inclination	Annulus size	Particle size
(Wang et al., 1995)	Bed Height	x	x	x	x	x		
(Bassal, 1995)		x	x		x	x	x	x
(Duan et al., 2008)		x				x	x	x
(Li et al., 2010)		x	x		x	x	x	x
(Ozbayoglu et al., 2008)	Cuttings bed area	x	x	x	x	x	x	
(M E Ozbayoglu et al., 2010)		x	x			x	x	
(Loureiro et al., 2010)	Cutting %	x	x	x	x		x	x

Table 2.4 a – Empirical correlations to predict the cuttings behavior in the annulus

Author	Rate	ROP	Eccentricity	RPM	Inclination	Annulus size	Particle size
(M E Ozbayoglu et al., 2010)	x	x	x	x	x		
(Luo et al., 1992)	x	x		x	x	x	x
(Mirhaj et al., 2007)	x				x	x	x
(Mohammadsalehi and Malekzadeh, 2011)	x	x		x	x	x	x

Table 2.5 b – Empirical and mechanistic correlations to predict the critical velocity

Author	Forces considered
(Peden et al., 1990)	Gravity, Drag, Lift and friction forces
(Clark and Bickham, 1994)	Buoyancy, plastic, gravity, lift, drag forces and pressure force
(Larsen et al., 1997)	Mass Balance: Mass generated by drillbit = mass transported by mud forces
(Duan et al., 2009)	Static, drag, lift and Van der Waals forces
(Badrouchi et al., 2020)	Buoyancy, plastic, gravity, lift and drag forces

2.2.2 Numerical Simulation studies

Analytical and mechanistic models presented in the leterature presented a good understanfing of suttings transportation process (Clark and Bickham, 1994; D. Nguyen, 1997). However, even the advanced trilayer model of (Nguyen and Rahman, 1998) was not proved by experimental results (Zakerian et al., 2018).

Ali (2002) investigated the effect of drilling parameters on the cuttings transportation in vertical and horizontal wells by Compututional Fluid Dynamics (CFD) and compared the simulation results with the results of experimental work of (Sifferman and Becker, 1992). He noted that flow regime and annular space configuration have an important effect on the cutting transportation process. Li et al. (2010) used CFD to study the effect of pipe rotation on hole cleaning and observed that rotary speeds (RPM) between 80 and 120 *rpm* affect at high degree the cuttings transportation. They also noted that below 80 *rpm* and high flow rates, the effect of the pipe rotation is minor and can be neglected. Their results are in agreement with the experimental investigation conducted by Wang et al. (1995). Sorgun (2010) used CFD to confirm the experimental results of Ozbayoglu et al., (2008). They reported that the increase of the pipe rotation decreases the minimum transport velocity (MTV) required to start transporting the cuttings, however, after certain limit (close to 120 *rpm*), pipe rotation effect on hole cleaning remains the same. Akhshik et al. (2015) used Compututional Fluid Dynamics- Discrete Element Method (CFD-DEM) numerical simulation

(fluid is considered as continuous phase and drilling cuttings as non-continuous phase) to examine drill pipe rotation effect on the cutting transport in vertical and horizontal wellbores. Zakerian et al. (2018) reported that the CFD-DEM model of (Akhshik et al., 2015b) and CFD model of Mehmet Evren Ozbayoglu et al. (2010) showed a better performance in modeling cutting transport than the analytical model of Yu et al. (2007). The CFD results obtained by Bilgesu et al. (2007) showing that pipe rotation enhances hole cleaning more for smaller sized particles, were confirmed experimentally by Duan et al. (2008).

Badrouchi and Rasouli, (2020) used Eulerian-Lagrangian simulation using MfiX to study the effect of different drill cuttings settling behavior in drilling fluids. They validated their simulation results against experimental results obatained using the Slurry Loop Unit (SLU). This simulation was able to predict the settling velocity of drill cuttings at high accuracy and counted for the effect of the annular space configuration.

A comparison summary on the experimental and numerical simulation investigation of the effect of pipe rotation on hole cleaning can be found in Table 2.6.

2.2.3 Artificial Intelligence studies

Recently, some researchers focused on using AI techniques such as Artificial Neural Networks (ANN), support vector machine (SVM) and other generic programming algorithms to predict the settling velocity (Agwu et al., 2020; Barati et al., 2014; Goldstein and Coco, 2014; Kamyab et al., 2016; Li et al., 2014; Rooki et al., 2012; Sadat-Helbar et al., 2009). A summary on the previous application of AI techniques in the prediction of the terminal settling velocity of cuttings can be found in Table 2.7. It is important to note that ANN and other AI techniques, do not take into consideration the physics of the process, however, they allow the machine to learn from field or experimental data (Alnuaim, 2019; Osborne, 1977).

Table 2.6 – Empirical correlations to predict the cuttings behavior in the annulus

	RPM limit	Study Factors	Key findings	Ref.
Experimental	120	Flow rate Eccentricity Fluid viscosity Annular size	As viscosity increases, the pipe rotation effect on the MTV increases. Pipe rotation enhanced cleaning in small annuli.	(Peden et al., 1990)
	60	Particle size Inclination Concentration	Pipe rotation effect increases for small cuttings and low ROP for highly deviated to horizontal wellbores.	(Sifferman and Becker, 1992)
	60	Flow rate	Pipe rotation effect on cuttings bed formation depends on the flow rate. At high flow rates, the pipe rotation has no significant effect on cuttings bed height.	(Wang et al., 1995)
	120	Particle size Inclination Fluid viscosity	For small particles and highly deviated wellbores, as viscosity increases, the pipe rotation enhances the hole cleaning.	(Bassal, 1995)
	175	Flow rate Inclination	For vertical wells, at low flow rates, high pipe rotation speeds help enhance hole cleaning.	(Sanchez et al., 1997a)
	120	Flow rate	Pipe rotation decreases MTV. After certain limit, pipe rotation effect on hole cleaning remains the same.	(Ozbayoglu et al., 2008)
	160	Flow rate Particle size	For small particles, the pipe rotation enhances the hole cleaning. The effect is reduced for bigger particles.	(Duan et al., 2008)
	120	Concentration Inclination	With the help of pipe rotation and increased concentration of polypropylene beads, there is a drastic increase in the cuttings transport ratio that is efficient for hole cleaning.	(Katende et al., 2020)

Simulation	120	Flow rate	Pipe rotation increase to a certain limit, decreases MTV. After that, MTV is not decreased.	(Sorgun, 2010)
	60	Flow rate Particle size	Pipe rotation enhances hole cleaning more for smaller sized particles.	(Bilgesu et al., 2007)
	200	-	Significant effect on hole cleaning is observed for RPM between 80-120.	(Li et al., 2010)
	200	Flow rate Eccentricity Fluid density	Drill pipe rotation increases the shear force exerted on solid particles and leads to the dispersion of settled cuttings in the annulus especially for higher eccentricities.	(Hajipour, 2020)

Table 2.7 – Previous AI application in terminal settling velocity prediction

Technique	Structure	Inputs			Outputs	Reference
		Fluid	Particle	Other		
ANN	6-12-1	ρ_f, k, n	ρ_P, d_P	g	v_{sl}	(Rooki et al., 2012)
ANN	7-12-1	ρ_f, k, n	ρ_P, d_P	$d_P/D, d_P/L_P$	WF	(Li et al., 2014)
ANN	2-5-1	φ	-	$Log(Re)$	f	(Kamyab et al., 2016)
ANN	4-4-1	d_n	v	$\rho_f/\rho_f, S_f$	v_{sl}	(Sadat-Helbar et al., 2009)
SVM	-	ρ_f, k, n	ρ_P, d_P	$d_P/D, d_P/L_P$	WF	(Li et al., 2014)
GP	-	d_n	v	ρ_f/ρ_f	v_{sl}	(Goldstein and Coco, 2014)
MGGP	-	-	-	Re	C_D	(Barati et al., 2014)

2.3 Cuttings Settling Velocity

All models and correlations proposed in the literature rely in one or another way on the prediction of the settling velocity. For vertical wells, the settling velocity directly determines the minimum flow rate required to ensure a good hole cleaning. Also, when drilling operation is ceased, cuttings are subjected to a free settling motion. Drilling can be stopped for different reasons such us making

a connection, changing a dull bit, stuck pipe, and well control or wireline operations. The suspension of the drilling fluid flow causes the cuttings transported in the annular space to settle in the bottom of the wellbore (Moreira et al., 2017). Cuttings settlement at large volume will present problems such us stuck pipe, high torque, bit balling, bad placement of casings and low rate of penetration (Ahmed and Takach, 2008; Busahmin et al., 2017; Kristiansen, 2004; Malekzadeh and Mohammadsalehi, 2011; Rasi, 1994; Tan et al., 2004).

Over the years, researchers found that predicting the settling velocity of the drill cuttings at which they settle down and accumulate in the bottom of the well is crucial and imperative to assess the hole cleaning process (Elgaddafi et al., 2016; Wang et al., 2010; Zhang et al., 2015).

Baldino et al. (2015a) mentioned that predicting the settling velocity of cuttings helps in understanding the cuttings concentration profile which in turn helps to improve the controll of the wellbore pressure for a better wllbore instability. Badrouchi and Rasouli, (2020) also noted that the prediction of the settling velocity enables the cuttings depth matching, i.e. estimating the depth of the formation where the cuttings are generated. However, an erronious prediction of the settling velocity of particles can lead to serious operational problems such as innacurate lag times and wrong interpretations of the mudlogger data, as well as imprecise estimation of cuttings concentrations, hence, incorrect wellbore pressure estimation (Agwu et al., 2018; Altindal et al., 2017).

Due to its importance in oil and gas drilling operations, the cuttings settling velocity was widely investigated and several models and correlations presented in the literature. From the simple correlation of Stokes (1850) to more complicated semi-analytical model of Zhu and Fan (1998) who presented the so called Basset–Boussinesq–Oseen equation (BBO) (Basset, 1888; Boussinesq, 1885; Oseen, 1911). The work ranges from experimental, mathematical modelling,

numerical simulations and artificial intelligence. A summary of such literature is presented in Table 2.8 and Table 2.9, respectively. Some literature on the use of AI in predicting the terminal settling velocity can be found in Table 2.7.

In recent years, artificial intelligence techniques such as artificial neural network, support vector machines and genetic programming have also become very popular in predicting settling velocity of cuttings. The large volume of experimental data generated over the years (e.g. see Table 2.9) is the main reason for the expansion of the Machine learning models to predict the settling velocity (Agwu et al., 2020; Barati et al., 2014; Goldstein and Coco, 2014; Kamyab et al., 2016; Li et al., 2014; Rooki et al., 2012; Sadat-Helbar et al., 2009).

Table 2.8 – Example of numerical studies on hole cleaning

Investigation	**Fluid Model**	**Particles shape**	**Algorithm (discretization method)**	**Key findings**	**Ref.**
Wall effect; Fluid properties	Power Law	Spherical	AXFINR Program (FEM)	The flow disturbance due to the particle motion as well as the wall effect is neglected when the flow index is reduces.	(Dazhi and Tanner, 1985)
Fluid properties; Drag Force	Modified Power Law	Spherical	SIMPLER Method (FDM)	Good numerical estimation of the drag coefficient comparing to experimental results.	(Butcher and Jr, 1990)
Elongational and shear fluid properties	Viscoelastic shear-thinning: (Phan-Thien Tanner fluid)	Spherical	POLYFLOW program	The need to consider the elongational properties of test fluids in addition to the shear properties. The	(Bush, 1994)

				elongational properties affect considerably the net response.	
creeping flow inside a pipe; Bingham numbers	Bingham plastic	Spherical	Papanastasiou modified Bingham constitutive Equation (FEM)	dramatic increase of the drag coefficient as the dimensionless yield stress increases.	(Blackery and Mitsoulis, 1997)
tube/sphere diameter ratio wall effect	Pseudoplastic shear-thinning (Power Law)	Spherical	FLOWCAD computer program (FEM) FIVOS computer program (FVM)	Tube/sphere diameter ratio has a significant influence on the drag. When the power-law index n approaches zero, the drag coefficient converges to a constant value of 1.18, which is independent of the tube/sphere diameter ratio.	(Missirlis et al., 2001)
Reynolds number Fluid properties	Incompressible power-law fluid	Spherical	Gauss-Seidel iterative algorithm (QUICK scheme- CDS)	Total drag always increases as the power-law index n increases. As Re increases, the contribution of the pressure drag increases, however, for n>1, this process is suppressed.	(Dhole and Chhabra, 2006)

Yield stress effect Reynolds number	Bingham plastic	Spherical	lattice-Boltzmann flow solver (LBM)	At low Reynolds number, two spheres settle with equal velocity. The settling velocity decreases with effective yield stress increase.	(Prashant and Derksen, 2011)
Fluid properties effect	shear thinning (thixotropic)	Spherical	VOF (FDM implicit-CDS)	As the relaxation time of the fluid increases, the drag force is decreased. Settling velocity is high at the sheared fluid regions.	(Gumulya et al., 2014)
Reynolds number Solid Volume Fraction	Newtonian (Water)	Spherical	IBM DEM	Average settling velocity of particles deviate from Richardson and Zaki relation for dilute suspension and higher range of Reynolds number. Moderate Reynolds number effect is neglected as the solid volume fraction increases.	(Zaidi et al., 2015a)
Fluid properties Particle properties	Viscoelastic shear-thinning	Spherical	ALA (Euler implicit and Semi-implicit Gear scheme)	Particles moves toward the closest wall when shear flow happens. Slippery particles have tendency toward alignment	(Trofa et al., 2015)

				along the flow channel center.	
Single particle settling behavior	Newtonian Bingham plastic	Spherical	PeliGRIFF Lagrangian loop (FV/SG scheme)	Fluid surrounding the particle can regain viscous properties and decreases the settling velocity until a critical Bingham number when the particle stops moving.	(Wachs and Frigaard, 2016)
Reynolds number Plastic effect	Herschel–Bulkley fluid	Spherical	SIMPLEC algorithm (QUICK scheme-FVM)	The drag in plastic fluid is higher than in fluid with no yield and with the same viscosity. As the Reynolds number increases the difference in the drag force decreases.	(Gavrilov et al., 2017)

Table 2.9 – Example of experimental studies on hole cleaning

Factors investigated	Fluid Used	Particles shape (diameter / density)	Key findings	Ref.
Wall effect	Water, olive oil, glycerol, glycerol and lead nitrate, glycerol and npropyl alcohol μ : 1-86cP ρ : 1-1.2 gcc	Spherical (0.7-5mm / 1.2-20gcc)	As Reynolds number increases, the wall retarding effect decreases.	(Fidleris and Whitmore, 1961a)
Particle shape effect	Liquid paraffin, sugar solution and water	Cylinders, cones and disks "brass and steel" (8-9 gcc)	When several cylinders are released in random orientation, they cluster to form pairs crossed at right angles. Flat cones with vertex angles higher than 45° tend to settle with their apex in the downward direction and vice versa.	(Jayaweera and Mason, 1965)
Critical Reynolds Number Particle properties	Water	Spherical "brass and aluminum (3-10mm / 2.6-8.43gcc)	The settling velocity of particles with Re higher than the critical value present a scatter as great as 20%, however, if Re is	(Nolan, 1970)

			less than this critical value, the particles displayed little scatter in their terminal velocities.	
Dispersion concentration Fluid properties	Salt solution Shear thinning polymer solutions	Spherical "polystyrene latex" (0.00155mm / 1.05gcc)	Particles' settling rate increases as the salt concentration in water increases. Zero shear rate for polymer solutions affects the settling velocity.	(Buscall et al., 1982)
Fluid properties Particle properties	Power law (polymer based muds) Viscoelastic (hydroxyethylcellulose based muds) Newtonian (Schell oil) n : 0.45-1 k : 0.0374-3.992	Spherical "sand, glass, marbles, steel", rectangular and disks "aluminum", disks "Plastic" and proppants (0.3-25mm / 2.3-7.8gcc)	For Newtonian fluids, the drag coefficient is a function of the Reynolds number, however, for non-Newtonian fluids it is function of the flow behavior index n.	(Peden and Luo, 1987)
Particle properties Fluid properties Wall and container geometry effects	Corn syrup solution Castor oil Carboxymethyl cellulose solution ρ : 0.965-1.154 gcc n : 0.62-1 k : 0.005-1	Cones "Perspex" (15-19.6mm / 1.204gcc)	At low Re, the wall effect is reduced for conic shaped particles in Newtonian fluids comparing to spherical ones. This phenomenon is	(Sharma and Chhabra, 1991)

			reversed at high Re.	
Particle properties Fluid properties Wall effect	Carboxymethyl cellulose solution Methocel cellulose solution ρ : 1 gcc n : 0.779-0.89	Needles "steel", cylinders "aluminum", discs "steel and copper", prisms "plastic", cubes "plastic" and thin square plates "brass" (1.2-8.4gcc)	At intermediate Re range between 2 and 40, disc shaped particles drag coefficient in non-Newtonian fluids is identical to Newtonian fluids. At increasing Re, the non-Newtonian flow properties becomes less important in effect.	(Chhabra et al., 1996)
Particle properties Fluid properties	Water Carboxymethyl cellulose solution n : 0.753-1 k : 0.001-0.265	Spherical "glass" (0.1-0.35mm / 2.26-2.727gcc)	Apparent viscosity can be used to determine the particle settling velocity.	(Kelessidis, 2003)
Particle properties Fluid properties Wall effect	Carboxymethyl cellulose solution Glucose solution ρ : 1-1.39 gcc n : 0.61-1 k : 0.0078-15.31	30 cubes "brass, steel, aluminum, teflon, nylon and acrylic" (6-25mm / 1.137-8.403gcc)	As Re increases, the wall effect on the settling velocity of the particles decreases.	(Agarwal and Chhabra, 2007)
Fibers concentration Fluid properties	Xanthan gum Solution (0.25%) Mineral oil	Spherical "glass" (1-15mm / 2.59-7.740gcc)	As the fibers concentration increases, the settling velocity	(Ahmed, 2012)

	PAC solution (0.5%) Fiber concentration by weight: 0 – 0.08%		of the cuttings decreases.	
Fluid properties	Water PAC solution Bayol 35 Paraffin oil	Spherical "glass, steel" (2-8mm / 2.6gcc)	The settling velocity of clustered cutting particles is higher than single particle one.	(Johnsen, 2014)
Fluid properties Particle properties Temperature Pipe inclination (60°, 75° and 90°) Pipe rotation	Synthetic based mud	High sphericity drill cuttings $\varphi = 0.65$	The modified Quemada model can accurately characterize a drilling fluid. The Concha and Barrientos correlation is also reasonably accurate in prediction of the slip velocity.	(Baldino et al., 2015b)
Particle properties	Water	Natural sand Industrial sand Synthetic sand	The settling velocity of sand increases as Stokes number increases.	(Jacobs et al., 2015)
Particle properties	Water	Spherical "Polycaprolactone" Cylindrical "short Polycaprolactone and long sections of fishing lines" (0.15-0.71mm / 1.131-1.168gcc)	The effect of the shape is attenuated as the size of the particles is increased. Cylindrical particles exhibits rotational and oscillatory	(Khatmullina and Isachenko, 2016)

			falling movement.	
Fiber length effect Fiber concentration effect	Glycerin and water solutions μ : 66-122cP	21 spheres "aluminum, titanium and steel" Monofilament synthetic fibers (1-10mm / 2.68-7.96gcc)	Fibers' length and concentration have minor effect on fluid viscosity. However, as their length increases, the particle settling velocity increases too.	(Xu et al., 2017)
Continuity theory for sphere settling process	Water Water and sand/perlite suspension "Newtonian" Water and fly ash suspension "Bingham" ρ : 1-1.39 gcc PV : 3-24cP	Spherical "steel" (28-40mm / 2.6-8.5gcc)	Steel balls can be considered as continuum in fine suspensions.	(Faitli, 2017)
Fluid properties Particle properties	Distilled Water and glycerin solution	133 calcareous sand particles of Highly irregular shapes were	As particles settling down in the fluid, the conditions of passage through which the flow passes between the particles, can predominate the drag force and thus terminal velocity of particles.	(Wang et al., 2018)

2.4 Effect of Downhole Devices

In field applications, to ensure the success of the drilling operation, different garniture components such as centralizer and stabilizer are added to the drilling string to ensure the right rate of penetration.

Hole cleaning is often assessed in relation to flow rate, fluid properties, cuttings properties, wellbore inclination and some drilling parameters such us rate of penetration and rotary speed (Badrouchi et al., 2020; Badrouchi and Rasouli, 2020a; Bilgesu et al., 2007; Gavignet and Sobey, 1989; Iyoho, 1980; Kenny et al., 1996; Martins et al., 1999; Menegbo et al., 2019; Mohammadsalehi and Malekzadeh, 2011; Nazari et al., 2010; Pilehvari et al., 1996; Saasen and Løklingholm, 2002; Saeid and Busahmin, 2016; Sanchez et al., 1997b; van Oort et al., 1996; Zeidler, 1972). The existence of wellbore hardware, such as stabilizer may present a large disturbance to the cuttings movement along the annulus space and ultimately result in poor hole cleaning. This concept has not been adequately studied in the past (Xiaofeng et al., 2013). These downhole components help to apply sufficient weight on the bit and avoid unintentional sidetracking, vibrations, and maintain the quality of the hole being drilled. Contrary to their benefits, these tools may also have considerable impact on the cutting's transportation and quality of the hole cleaning. Stabilizer selection was often based on mechanical stability under harsh downhole environment (Pastusek, 2018; Woods and Lubinski, 1955). Studying the effect of stabilizers geometry on hole cleaning helps field engineers to optimize the selection of these hardware to improve the drillstring stability, hole stability and ensure an efficient hole cleaning.

2.5 Summary

This Chapter presents a summary of different, analytical, experimental, numerical and artificial intelligence work to investigate the cuttings transportation behavior with the outputs of those researches presented. Also, the results of these studies demonstrate that the terminal settling velocity is a key parameter in hole cleaning optimization. Most of the experimental works available in the literature focused on using rigid spherical particles, due to the fact that they it easy for visualizing the flow and track the particle, as well as for easy numerical implementation. Artificial intelligence is an emerging modelling technique for the settling velocity phenomenon. This technique presents a unique way of modelling the settling velocity phenomena due to the complexities surrounding it.

This chapter also discusses a novel research area in the domain of hole cleaning which is the effect of stabilizers on cuttings transportation. Stabilizers come in different shapes and geometries and the selection of the appropriate design should consider both wellbore and drillstring stability as well as an efficient hole cleaning.

In the next Chapter, analytical models for cuttings movement pattern recognition in deviated wellbores will be presented.

CHAPTER 3

Modelling Cuttings Movement Pattern in Deviated Wellbores

3.1 Introduction

One of the main functions of the drilling fluid is the efficient removal of the cuttings from the bottom hole to the surface. Poor hole cleaning results in the deposition of drill cuttings at different wellbore locations possibly leading to several issues in drilling and completion such as stuck pipe, high torque and drag, and faulty cementing jobs.

Pigott (1941) pioneered the extensive study of hole cleaning in vertical and near-vertical wellbore geometries, which was followed by several other studies on the particle's settling velocity of the cuttings as a major factor influencing the hole cleaning. The settling velocity is dependent upon cuttings density, size, and shape, as well as fluid rheology and flow rate. Chien (1994) has introduced a correlation between the settling velocity and irregularly shaped cuttings by introducing a factor to account for the non-sphericity and apply it to a fictive spherical particle with an equivalent volume. His findings can expand the work from spherical to non-spherical particles.

In the early 1980s, experimental work was performed using different custom made flow loops (Brown et al., 1989; Iyoho, 1980; Larsen, 1990; Okrajni and Azar, 1986; Pilehvari et al., 1996;

Stenevik, 1991; Tomren et al., 1986). These researchers focused on the particle settling velocity; however, they studied multiple particles movements in inclined wellbores resulting in an extensive literature on experimental and modeling work from which we modified some analytical models to study the rolling and lifting of particles. Clark and Bickham (1994), Ford (1993), Larsen et al. (1997), Luo et al. (1992), and Rasi (1994) developed some of the analytical models in this research topic. The model developed by Larsen et al. (1997) was able to predict cuttings bed height at sub-critical flow conditions, the rate less than what is required to prevent cuttings deposition in the annular space. Their model was based on empirical correlations derived from experimental data collected from a 35-*ft* long 5-*in* diameter flow loop. Luo et al. (1992) and Ford, (1993) previously formulated the sub-critical flow region mathematically, validating their models against experimental data. Some models were validated against experiments carried out at inclinations that allow cutting beds to form, i.e., inclinations higher than 50° (Larsen et al., 1997; Luo et al., 1992; Rasi, 1994). Ford et al. (1990) developed a model available for different wellbore inclination. The results of their work showed that the flow regime and rheological properties of the fluid are the key parameters in hole cleaning.

Different observations have been reported regarding the effect of the drilling fluid rheology on hole cleaning, whether the fluid should be thick or thin to ensure better cleaning (Zamora and Hanson, 1991a, 1991b). Recently, Duan et al. (2010, 2007) conducted an experimental study to investigate smaller sized particle behavior and showed that water is more effective in terms of hole cleaning than low polymer concentration slurries.

Piroozian et al. (2012) investigated the effect of fluid viscosity on cuttings transportation. This showed that for a certain annular velocity that ensures turbulent flow in the annulus, the increase

of viscosity improved cuttings transportation. However, further increasing viscosity paired with transient to laminar flow regime significantly reduces the transport capacity of the cuttings.

Clark and Bickham (1994) developed a model for the lift and roll mechanisms of a particle that was used and modified in this work to fit our experimental observations.

The diversity of experimental work yields the same conclusion, namely, that at sufficiently high flow rates, cuttings can be removed regardless of the fluid properties, annulus size, or wellbore inclination. However, field experiences show that these high flow rates are not affordable for most of the cases of large holes and highly deviated wellbores due to different reasons, including high dynamic downhole or surface pressures and limited pump capacity. This can be remedied by applying high string rotation speeds in case of rotary or top-drive drilling (Clark and Bickham, 1994).

This Chapter reports the results of our study on the movement of cuttings in the annulus at different inclination angles and assesses critical velocity mechanistic models for predicting cuttings movement as a function of different cutting sizes and densities.

3.2 Analytical Models

3.2.1 Particle Slip Velocity

The earliest analytical studies of cuttings transportation considered the fall of particles in a stagnant fluid and these models also used for studying the particles movement in a moving fluid. Most researchers used the relationship developed by Stokes for creeping flow around a spherical particle (Clark and Bickham, 1994; Stokes, 1850).

The equation for particle-slip velocity is stated as:

$$V_{sl} = \frac{(\rho_s - \rho_f) g {d_p}^2}{18\mu_f} \tag{3.1}$$

where V_{sl} is the settling velocity, d_p is the diameter of the particle, ρ_s and ρ_f are the solid and fluid densities, respectively, μ_f is the fluid viscosity, and g is the gravity.

For a Newtonian fluid, with an assumption of turbulent flow and drag coefficient equal to 0.44, the Equation (3.1) can be written as:

$$V_{sl} = 2.46\left(\frac{(\rho_s - \rho_f)gd_p}{2\rho_f}\right)^{\frac{1}{2}} \tag{3.2}$$

The viscosity is not appearing in Equation (3.2) but its effect is included in the 0.44 value of the drag coefficient.

The drag force acting on a particle is described as:

$$V_{sl} = 2.46\left(\frac{(\rho_s - \rho_f)gd_p}{2\rho_f}\right)^{\frac{1}{2}} \tag{3.3}$$

where C_D is the drag coefficient. This coefficient is a function of the particle Reynolds number (N_{Re_p}):

$$N_{Re_p} = \frac{\rho_f V_{sl} d_p}{\mu_f} \tag{3.4}$$

$$C_D = \begin{cases} \dfrac{24}{N_{Re_p}} & Re < 0.1 \\ \left(\dfrac{24}{N_{Re_p}}\right)\left[1 + \dfrac{3}{16}N_{Re_p} + 9N_{Re_p}\dfrac{\ln(2N_{Re_p})}{160}\right] & 0.1<Re < 2 \\ \left(\dfrac{24}{N_{Re_p}}\right)\left[1 + 0.15{N_{Re_p}}^{0.687}\right] & 2<Re < 500 \\ 0.44 & 500<Re \end{cases} \tag{3.5}$$

3.2.2 Critical Velocities

Cuttings transportation is primarily affected by the flow rate in the annular space (Figure 3.2). The cuttings are completely removed from the wellbore without deposition at a certain flow velocity. At lower rates, these cuttings tend to settle on the bottom, forming cuttings beds. Their location, shape, and height depend on different parameters. The limit between deposition and the start of the removal process of the cuttings bed led to the notion of critical transport velocity (Clark and Bickham, 1994). This observation directed researchers to focus on the equilibrium state of cuttings beds. A bed will keep forming until the velocity in the open flow area reaches the critical velocity to remove cuttings. When reached, the bed height will remain unaffected.

During experimental laboratory tests on the Slurry Loop Unit (SLU) shown in Figure 1.1, rolling, lifting, and settling patterns of cuttings movement were observed and analyzed to study the cuttings bed development and removal process.

The cuttings were mixed with the fluid in a mixing tank and injected through a 15-ft long annulus made up of 5-*in* inner diameter drill pipe and 8-*in* outer diameter clear PVC tube. The wellbore deviation can be changed from horizontal to vertical configuration to simulate wellbores at different angles. All data are collected and plotted in real time using a built-in data acquisition system.

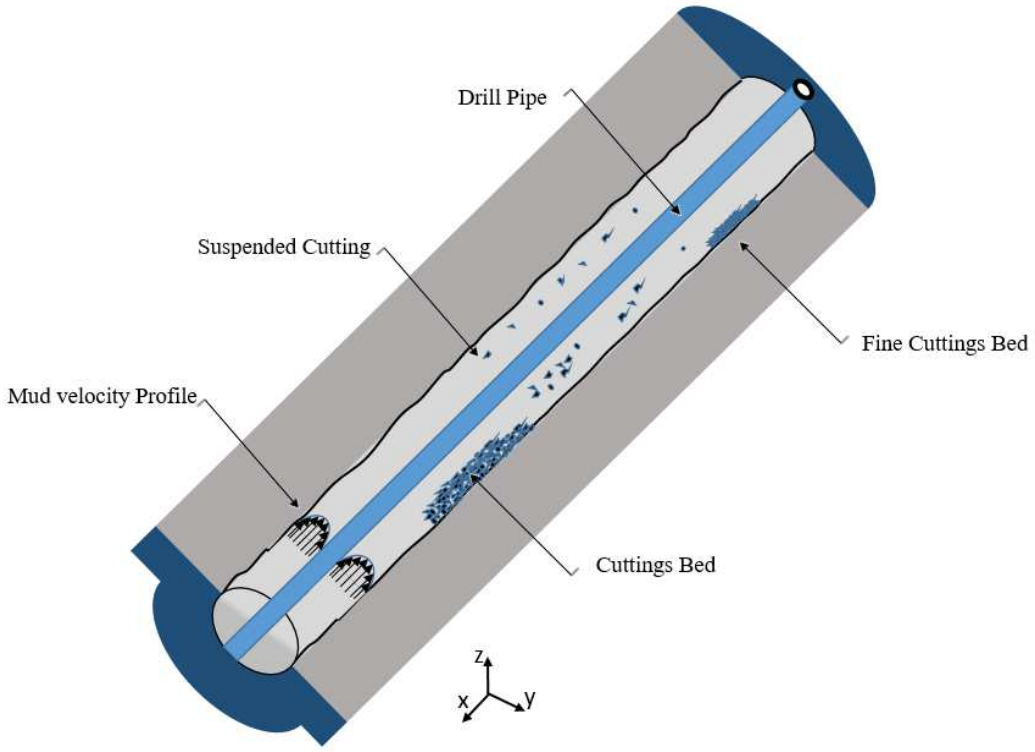

Figure 3.2 – Cuttings transportation in the annulus of a deviated wellbore.

As discussed above, to study the cuttings behavior, we need to study the bed equilibrium and find the critical velocity causing the rolling and lifting mechanisms. These two mechanisms are based on the forces required to move a single cutting in equilibrium from the surface of a bed. The equilibrium equation of forces will allow us to determine the critical state (velocities) that causes the rolling and lifting of the cutting from its equilibrium place.

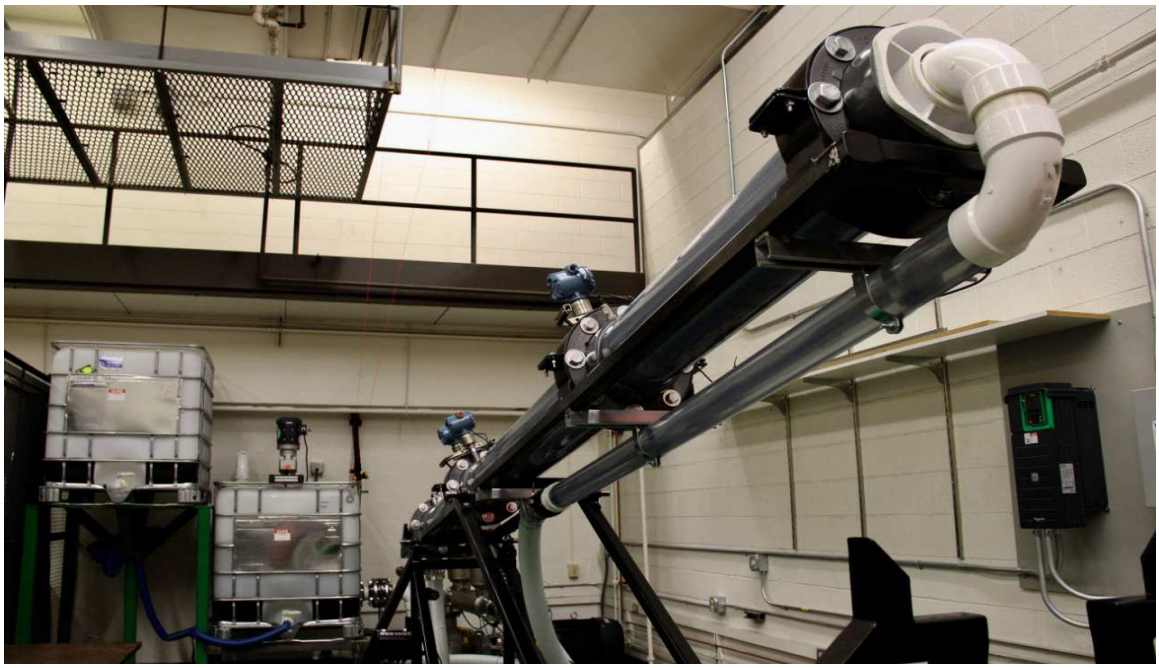

Figure 3.3 – Slurry Loop Unit at the University of North Dakota.

3.2.3 Single Cutting Modelling

3.2.3.1 Repose Angle

The repose angle, or critical angle of repose, is the steepest angle that a granular material can form relative to the horizontal plane (Mehta and Barker, 1994). Additionally, this angle is defined as the dip from horizontal, in which the material can be piled without slumping. Figure 3.4 shows Talus cones on the north shore of Isfjord in Svalbard, Norway, with a natural angle of repose for coarse sediment.

The repose angle depends on the sphericity and roundness of the particles, as shown in Figure 3.5 and Figure 3.6.

A good understanding of the repose angle can help the drill bit selection and design as well as choose the optimum drilling parameters to remove cuttings more effectively. Furthermore, a good understanding of the repose angle as a function of drilling parameters and lithology can help the

drilling industry in mud logging and depth matching, as well as understanding the cuttings mixing phenomena that was observed during experiments, which will be subjected to future studies.

Figure 3.4 – Talus cones showing the angle of repose for coarse sediment, on the north shore of Isfjord, Svalbard, Norway (Wilson, 2009).

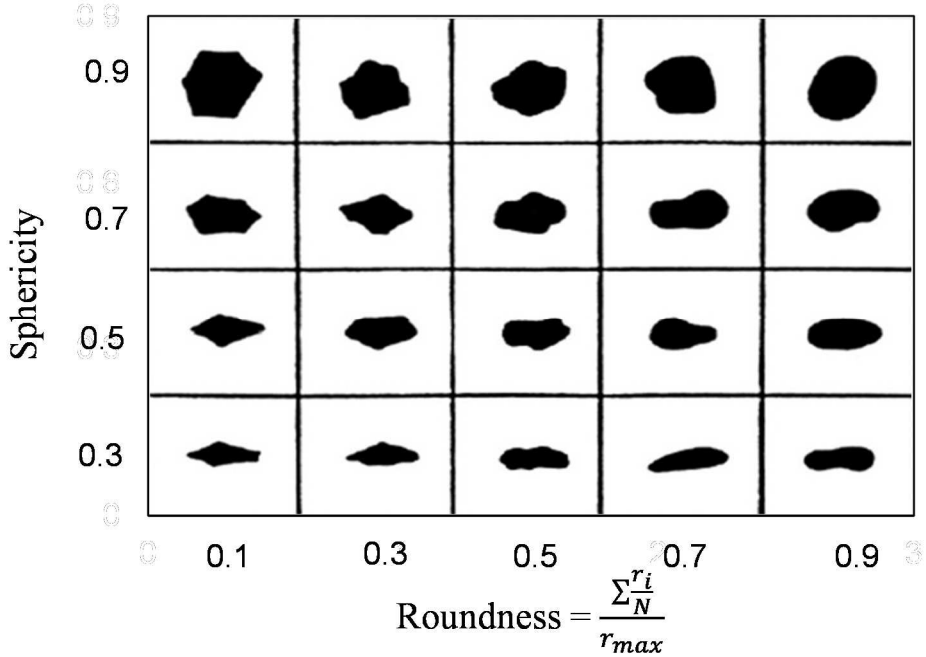

Figure 3.5 – Roundness-sphericity chart (Krumbein and Sloss, 1951).

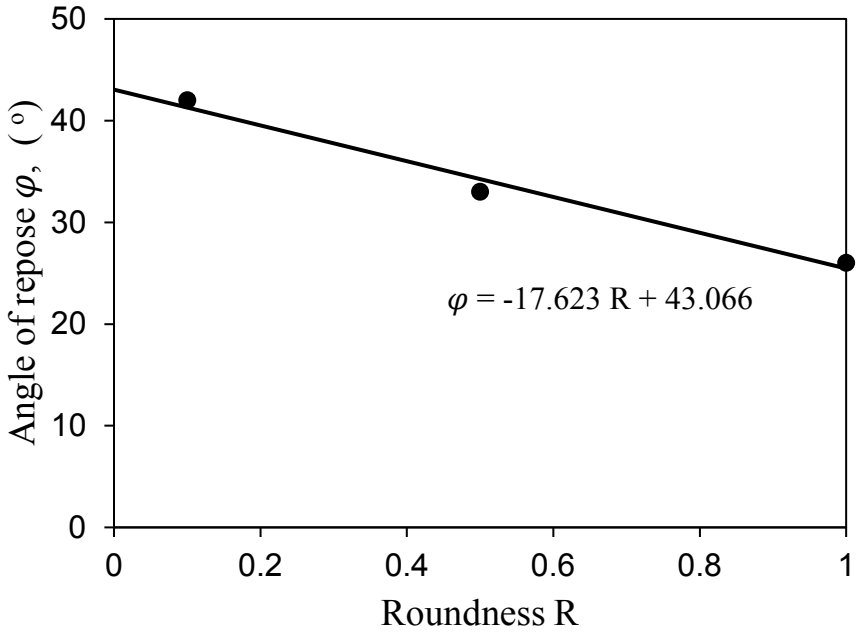

Figure 3.6 – Effect of roundness on the angle of repose (sand, gravel, and ceramic hydraulic fracturing proppants).

3.2.3.2 Model Description

At high inclination wellbore angles and a sub-critical flow regime, the cuttings tend to settle at the lower section of the wellbore annulus to form a stationary bed, while the cuttings at the surface are either rolled or lifted. This phenomenon was observed during our experimental work at inclination angles higher than the complementary angle of the repose angle. If the inclination angle from the vertical axis is α and the repose angle is φ, the stationary bed will clearly form at 90°- φ. The forces acting on a single cutting particle are shown in Figure 3.7. These forces are static and dynamic. Dynamic forces can be expressed as functions of the annular slurry velocity *U*. This means that we can solve the forces stated as a function of *U* to find at what limit this particle can move (either rolled or lifted). This leads to the determination of the critical velocity. Two situations are to be studied: rolling and lifting mechanisms.

This equilibrium study is an extension of work developed in different areas; sedimentation (Einstein and El-Samni, 1949; Samni, 1949), soil erosion (Chepil, 1958) and cuttings transport (Clark and Bickham, 1994; Wicks, 1971).

The single cutting particle is assumed to be a sphere with a diameter d_p and a density ρ_c. It is also assumed that at equilibrium state, the particle is retained in place due to a reactive force F_R applied at the contact point. The cuttings bed has a repose angle φ. The slurry is considered flowing at a constant rate and has a density ρ_f. The static forces are the gravity force F_g, the buoyance effect force F_B, and $F_{\Delta p}$, which is the plastic force due to the mud yield stress (in the case of a non-Newtonian fluid). The dynamic forces due to the flow are the lift force F_L, the drag force F_D, and the pressure due to the pressure gradient F_P.

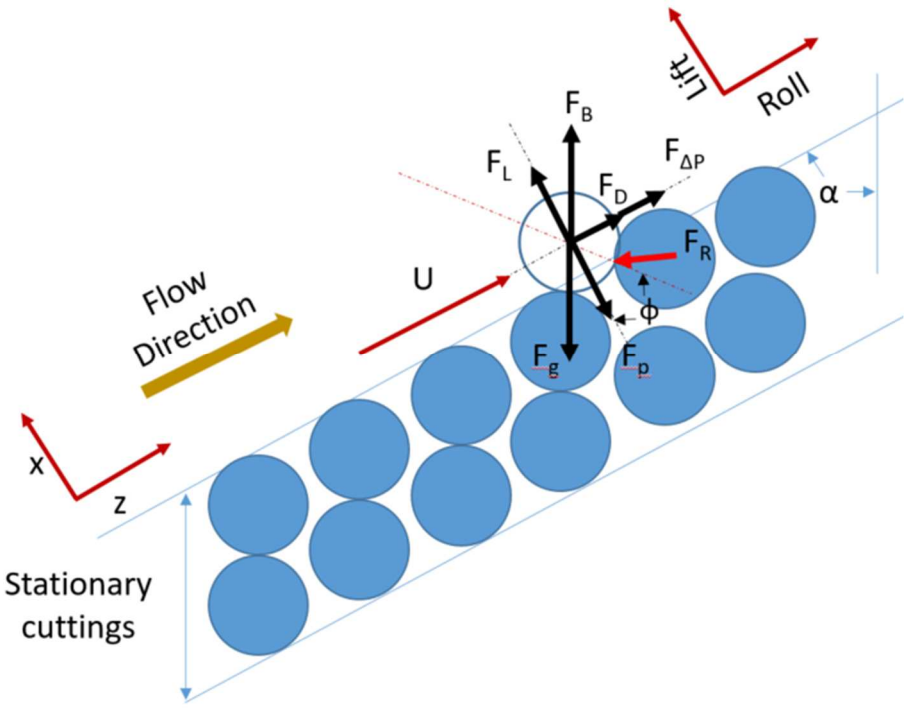

Figure 3.7 – Forces acting on a single cutting on a cutting bed.

3.2.3.3 Rolling Mechanism

Clark and Bickham (1994) studied the rolling mechanism, which is represented by the momentum conservation equation around the support pointo' $(-x, z)$:

$$|x|(F_D + F_{\Delta P}) + |z|(F_L - F_p) + \ell(F_B - F_g) = 0 \tag{3.6}$$

Here, ℓ is the momentum arm for the gravity and buoyancy forces, expressed as:

$$\ell = |z|\left(sin\alpha + \frac{cos\alpha}{tan\varphi}\right) \tag{3.7}$$

The repose angle can be expressed as a function of the coordinate of the support point:

$$tan\varphi = \frac{|z|}{|x|} \tag{3.8}$$

Dividing Equation (3.6) members by $|z|$ and then multiplying by $tan\varphi$ leads to:

$$tan\varphi\left(\frac{|x|}{|z|}(F_D + F_{\Delta P}) + \frac{|z|}{|z|}(F_L - F_p) + \frac{\ell}{|z|}(F_B - F_g)\right) = 0 \tag{3.9}$$

Rearranging Equation (3.9) gives:

$$(F_D + F_{\Delta P}) + tan\varphi(F_L - F_p) + (cos\alpha + sin\alpha.tan\varphi)(F_B - F_g) = 0 \tag{3.10}$$

After defining the forces acting on the particle, Equation (3.10) will help to define the rolling velocity of the particle.

3.2.3.4 Lifting Mechanism

For the case of lifting, F_R is assumed to equal the sum of the drag and pressure gradient forces. The lift is governed by the sum of the remaining forces in x direction, which can be mathematically written as follows (Clark and Bickham, 1994):

$$(F_L - F_p) + (F_B - F_g)sin\alpha = 0 \tag{3.11}$$

3.2.3.5 Critical Lift and Roll Velocities Solutions

In order to solve Equation (3.10) and (3.11) to estimate the critical rolling and lifting velocities, respectively, we need to define some ancillary equations describing the geometry, dynamics, and kinematics of the system based on the forces described in Figure 3.7. Flow mechanics textbooks have widely described these equations (Blevins, 1984). A summary of these equations can be found in Table 2.1.

Table 3.10 – Equilibrium forces ancillary equations

Force	Equation	
Drag Force	$F_D = \frac{1}{2} C_D \frac{\pi d_p^2}{4} \rho_f U^2$	(3.12)
Lift Force	$F_L = \frac{1}{2} C_L \frac{\pi d_p^2}{4} \rho_f U^2$	(3.13)
Buoyance Force	$F_B = \frac{\pi d_p^3}{6} \rho_f g U^2$	(3.14)
Gravity Force	$F_g = \frac{\pi d_p^3}{6} \rho_s g U^2$	(3.15)
Pressure Differential Force	$F_{\Delta P} = \frac{\pi d_p^3}{6}\left(\frac{4\tau_w}{D_{hyd}}\right)$ $D_{hyd} = \frac{4A}{wetted\ perimeters}$ $D_{hyd} = \frac{4\frac{\pi}{4}(d_0^2 - d_i^2)}{\pi(d_o + d_i)} = d_o - d_i$ where τ_w is the wall shear stress and the hydraulic diameter	(3.16)
Plastic Force	$F_p = \frac{\pi d_p^2}{2} \tau_y \left[\varphi + \left(\frac{\pi}{2} - \varphi\right) sin^2\varphi - cos\varphi sin\varphi\right]$ where τ_y is the yield stress of the fluid	(3.17)

By replacing Equations. (3.12) to (3.17), into Equations. (3.10) and (3.11), we obtain the following critical velocities:

- **Critical Roll Velocity, U_{Roll}:**

$$U_{Roll} = \left[\frac{4\left[\begin{array}{c} (\rho_s - \rho_f) g d_p (cos\alpha + sin\alpha . tan\varphi) - d_p \left(\frac{4\tau_w}{D_{hyd}}\right) + \\ 3\tau_y \left(\varphi + \left(\frac{\pi}{2} - \varphi\right) sin^2\varphi - cos\varphi sin\varphi\right) tan\varphi \end{array} \right]}{3\rho_f (C_D + C_L tan\varphi)} \right]^{1/2} \quad (3.18)$$

- **Critical Lift Velocity, U_{Lift}:**

$$U_{Lift} = \left[\frac{4\left[(\rho_s - \rho_f) g d_p sin\alpha + 3\tau_y \left(\varphi + \left(\frac{\pi}{2} - \varphi\right) sin^2\varphi - cos\varphi sin\varphi\right) tan\varphi \right]}{3\rho_f C_L} \right]^{1/2} \quad (3.19)$$

3.2.4 Asymptotic Solutions

In order to study the limits of the analytical solutions of critical velocities, we performed derivative calculations to determine the critical inclination angles.

3.2.4.1 Rolling Velocity

Rolling was observed at high wellbore angles. When the inclination angle approaches and remains under the complimentary angle, the rolling appears to disappear since the movement of the particles will become more arbitrary and lifting mechanisms accompanied by a boycott movement become dominant. Also, from experiment observations, when the inclination angle reaches a value equal to the repose angle or less, there is no bed forming.

Assuming $\tau_y = 0$ (non-plastic fluid) for simplification purposes, the derivative of the rolling velocity, $\frac{\partial U_{roll}}{\partial \alpha}$, will be:

$$\frac{\partial U_{roll}}{\partial \alpha} = \frac{\partial}{\partial \alpha}\left[\frac{4\left[(\rho_s - \rho_f) g d_p (cos\alpha + sin\alpha . tan\varphi) - d_p \left(\frac{4\tau_w}{D_{hyd}}\right)\right]}{3\rho_f (C_D + C_L tan\varphi)}\right]^{1/2} \tag{3.20}$$

A behavior change can be observed by equalizing the derivative to zero, $\frac{\partial U_{roll}}{\partial \alpha} = 0$, and solving it to obtain φ. By doing so, we find:

$$4\left[(\rho_s - \rho_f) g d_p (-sin\alpha + cos\alpha . tan\varphi)\right] = 0 \tag{3.21}$$

This leads to $tan\varphi = tan\alpha$, or $\varphi = \alpha$, which means that the inclination from the horizontal plane is equal to the repose angle. Many researchers reported this conclusion during their experimental work, where at the range of 50°, the particles are lifted, and no rolling is observed (Clark and Bickham, 1994). However, this angle was not identified as the repose angle, which is close to 50° in the case of sand particles.

3.2.4.2 Lifting Velocity

Following the same process for rolling velocity, we can determine the lifting velocity:

$$\frac{\partial U_{lift}}{\partial \alpha} = \frac{4\left[(\rho_s - \rho_f) g d_p cos\alpha\right]}{3\rho_f C_L} \tag{3.22}$$

This leads to $cos\alpha = 0$, which means $\alpha = 90°$, or in horizontal wellbores, particles are not likely to be lifted. This is confirmed through some experimental works; however, the particles are lifted at a very high rate (Cho et al., 2000; Clark and Bickham, 1994).

3.2.4.3 Discussion

The above results show that the analytical models for cuttings transportation are in good agreement with the experimental observations at some wellbore deviations. For rolling, the critical inclination was found to be equal to the repose angle, which is the limit of the bed formation in a wellbore

and cuttings are being lifted at higher angles. The inclination angle close to the complementary angle of repose angle was not found critical. For lifting velocity, the critical point was estimated to be at the inclination angle equal to 90° (horizontal wellbore), which is close to the experimental observations, where at high wellbore angles (near horizontal) to horizontal, the rolling is the dominant mechanism.

3.3 Experimental Studies

3.3.1 Experimental Procedure

In this study we used three different types of cuttings. Each type has a specific density, sphericity, and size. The use of cuttings with a wide range of properties will help to validate the applicability of the analytical solutions presented earlier.

For each case, first, we determined the size distribution of the cuttings samples based on the sieve analysis and identified the average particles' diameter. Then we measured the repose angle followed by measuring the density of the cuttings.

The experiments started with low cuttings concentration to prevent thick bed formation, which makes velocity measurements more complex due to the change of the area open to the flow.

3.3.2 Case 1: Lapis Lustre Clean Dry Sand

A clean Lapis Lustre Sand with a density of 2.6 *gcc* and a grain size distribution described in Table 3.11, was used as cuttings for the first experiment. The repose angle of this sand is 37°, as shown in Figure 3.8.

Table 3.11 – Equilibrium forces ancillary equations

Sieve nbr	Diameter (mm)	Mass (gr)	Percentage %
14	0.055	1.397	367
20	0.0331	0.84074	993
25	0.0278	0.70612	76
30	0.0234	0.59436	43
40	0.0165	0.4191	20
rest	<0.0165	<0.4191	1

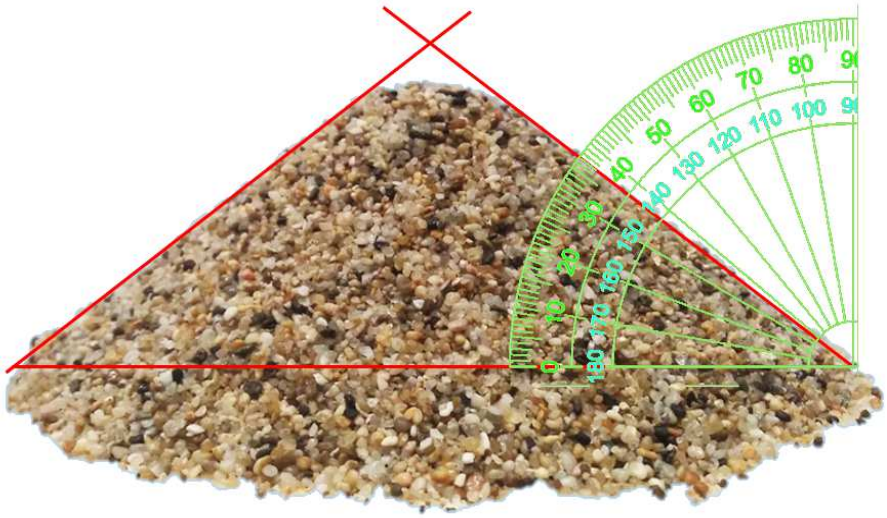

Figure 3.8 – Lapis Lustre Clean Dry Sand repose angle measurement.

3.3.3 Case 2: Ceramic Proppants

Ceramic Proppants with a density of 2.95 *gcc* and a grain size distribution described in Table 3.12 were used as cuttings for the second experiment. The repose angle of this sand is 26°, as shown in Figure 3.9.

Table 3.12 – Hydraulic Fracturing Ceramic Proppants grain size distribution

Sieve nbr	Diameter (mm)	Mass (gr)	Percentage %
14	1.4	390	55.71
16	1.18	286	40.86
rest	< 1.18	24	3.43

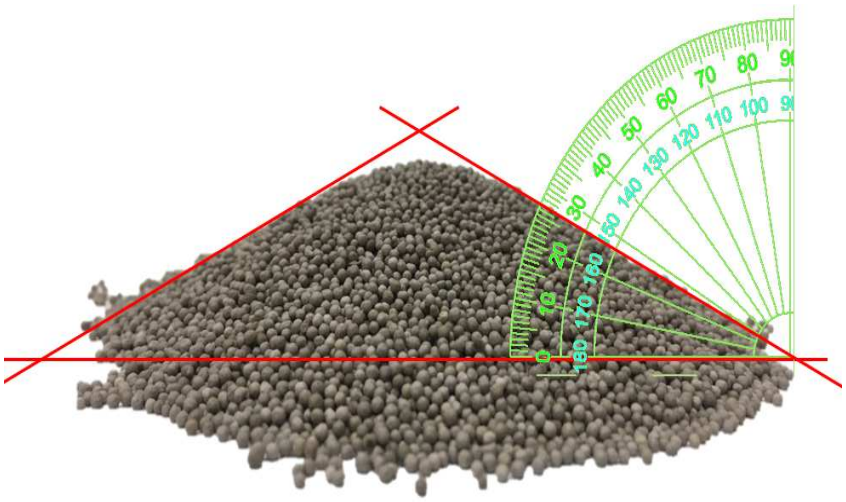

Figure 3.9 – Ceramic Proppants repose angle measurement.

3.3.4 Case 3: Rock Fragments

Rock fragments with a density of 3.11 *gcc* and a grain size distribution described in Table 3.13 were used as cuttings for the third experiment. The repose angle of this sand is 40°, as shown in Figure 3.10.

Table 3.13 – Rock fragments grain size distribution

Sieve nbr	Diameter (mm)	mass	percentage %
5-8	2.8	-	99
rest	< 3	-	1

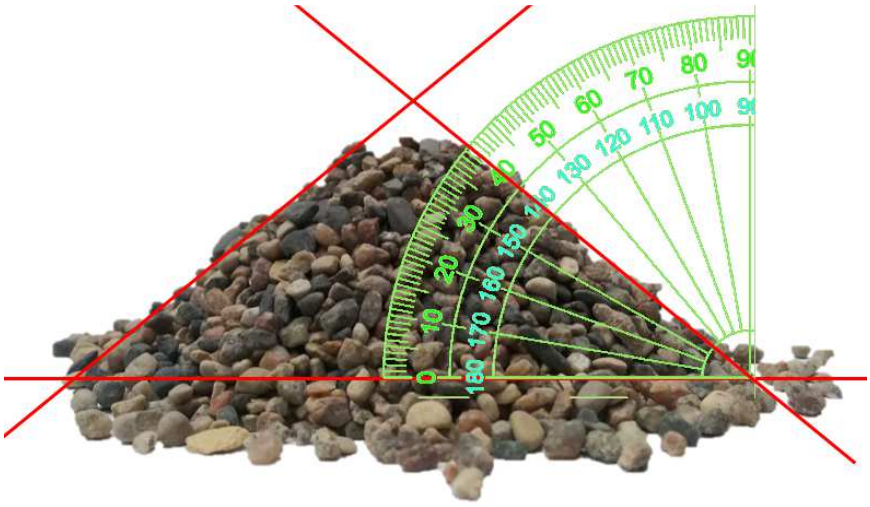

Figure 3.10 – Rock fragments repose angle measurement.

3.4 Results and Discussion

The experimental results of the initial velocity needed for the clean sand particles to start rolling and being lifted (Figure 3.8) were compared to analytical solutions for the lift and roll velocities (see Figure 3.11 to Figure 3.13).

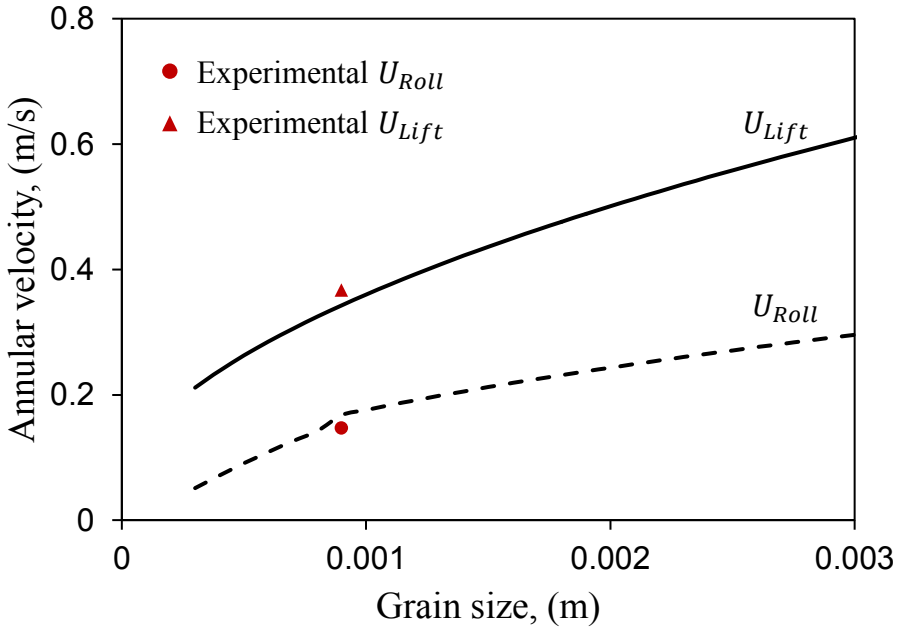

Figure 3.11 – Experimental vs. Analytical Rolling and Lifting at 90° inclination (Sand).

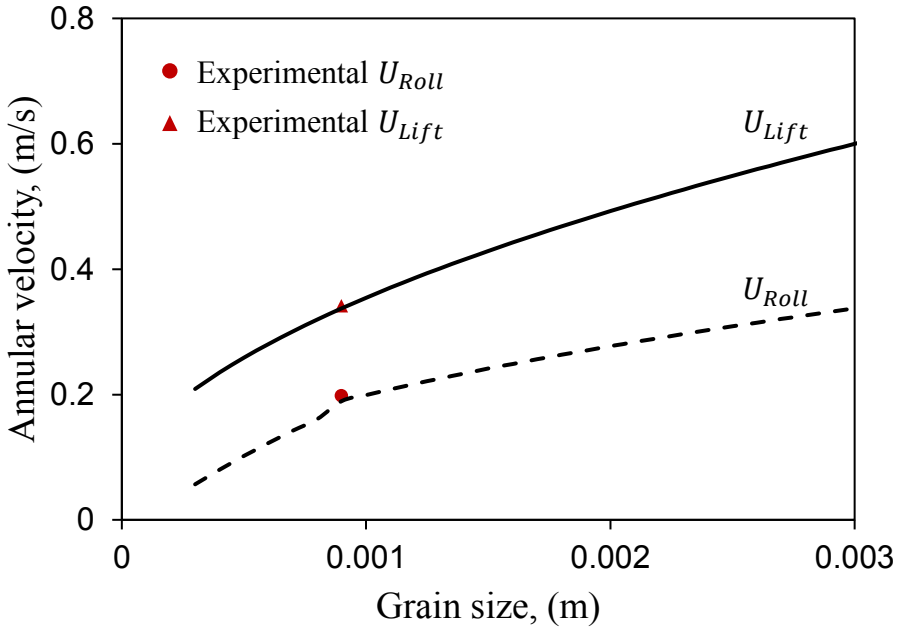

Figure 3.12 – Experimental vs. Analytical Rolling and Lifting at 75° inclination (Sand).

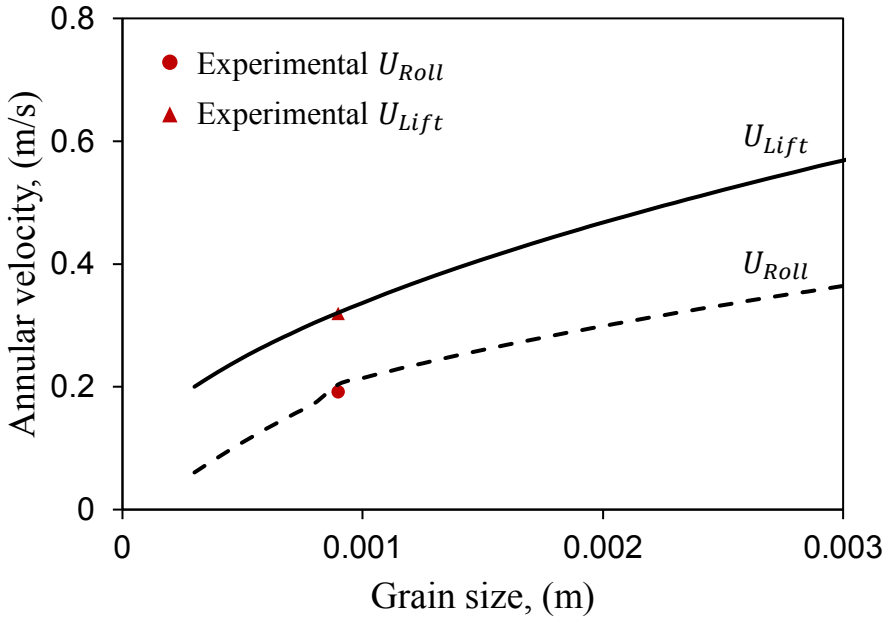

Figure 3.13 – Experimental vs. Analytical Rolling and Lifting at 60° inclination (Sand).

For the proppant particles (Figure 3.9), the results are also plotted for comparison with the analytical solution (see Figure 3.14 to Figure 3.16).

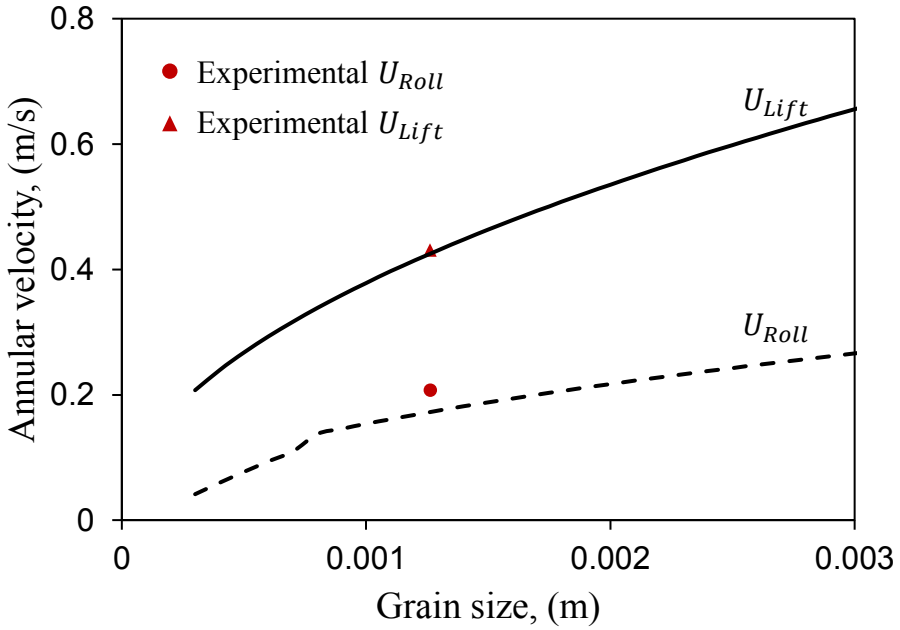

Figure 3.14 – Experimental vs. Analytical Rolling and Lifting at 90º inclination (Proppants).

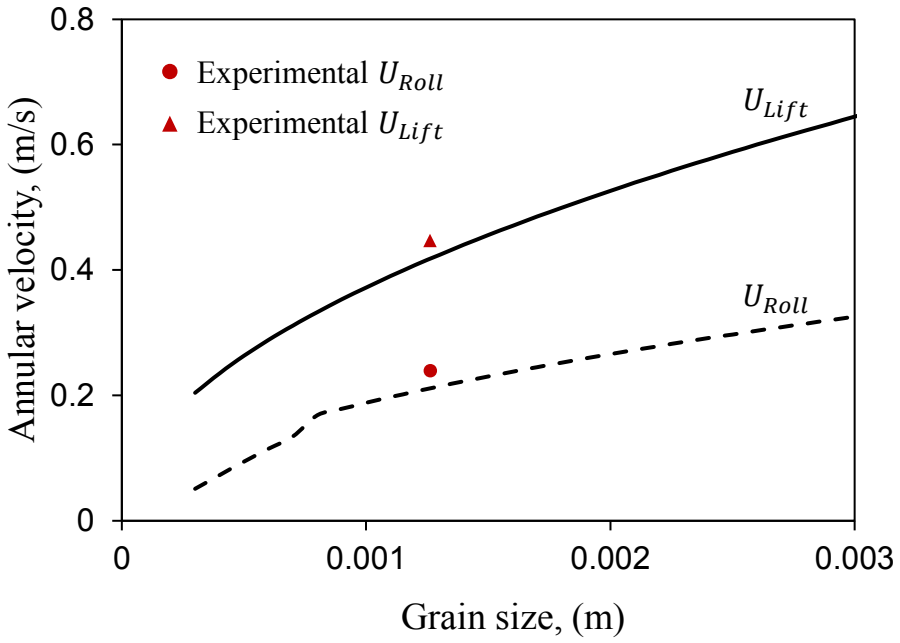

Figure 3.15 – Experimental vs. Analytical Rolling and Lifting at 75° inclination (Proppants).

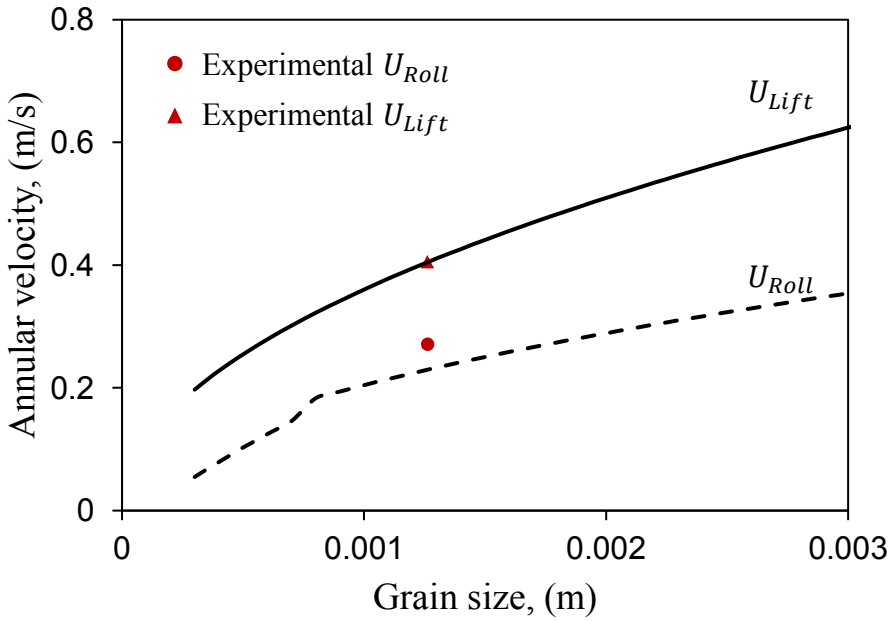

Figure 3.16 – Experimental vs. Analytical Rolling and Lifting at 65° inclination (Proppants).

The third cuttings used composed of rock fragments (Figure 3.10) showed the highest repose angle of 40°, and these results were compared with analytical predictions (Figure 3.17 to Figure 3.19).

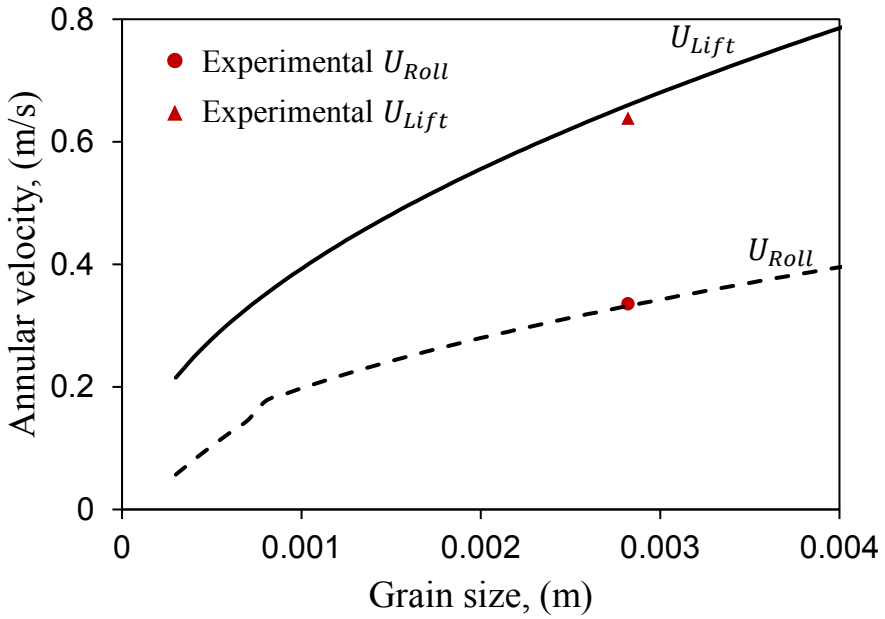

Figure 3.17 – Experimental vs. Analytical Rolling and Lifting at 90° inclination (Rock fragments).

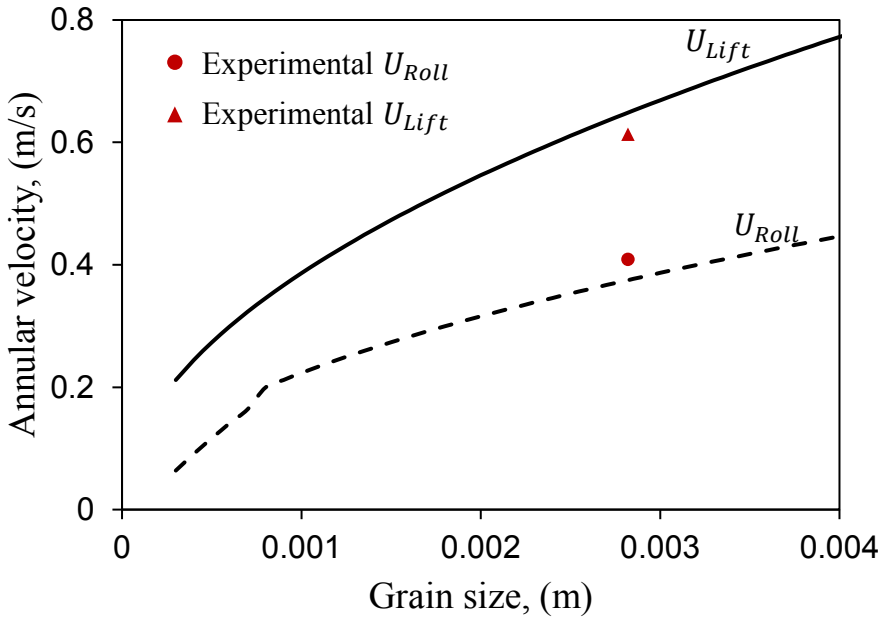

Figure 3.18 – Experimental vs. Analytical Rolling and Lifting at 75° inclination (Rock fragments).

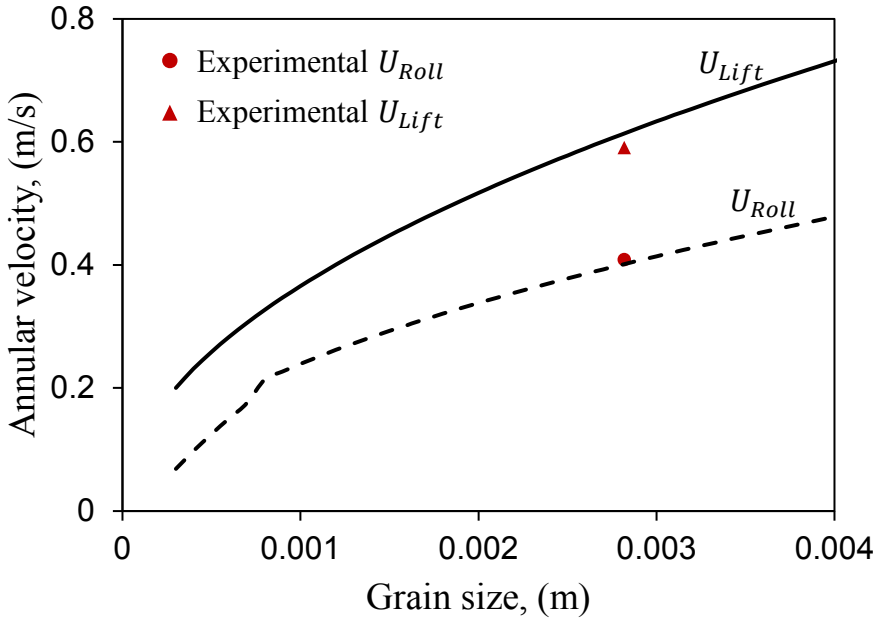

Figure 3.19 – Experimental vs. Analytical Rolling and Lifting at 60° inclination (Rock fragments).

The experimental results showed that the prediction of the rolling and lifting velocities are in good agreement with the experimental observations. The comparison of the analytical versus experimental results, as presented in Figure 3.20, Figure 3.21 and Figure 3.22, respectively, shows that the velocity data in all cases are clustered around the 45° line, which means a close agreement between the two methods. The points lay within the 25% margins, which is an accepted margin for analytical models.

For different cuttings' sizes, densities, repose angles, and wellbore inclinations, the analytical solution showed accurate predictions of the critical velocities.

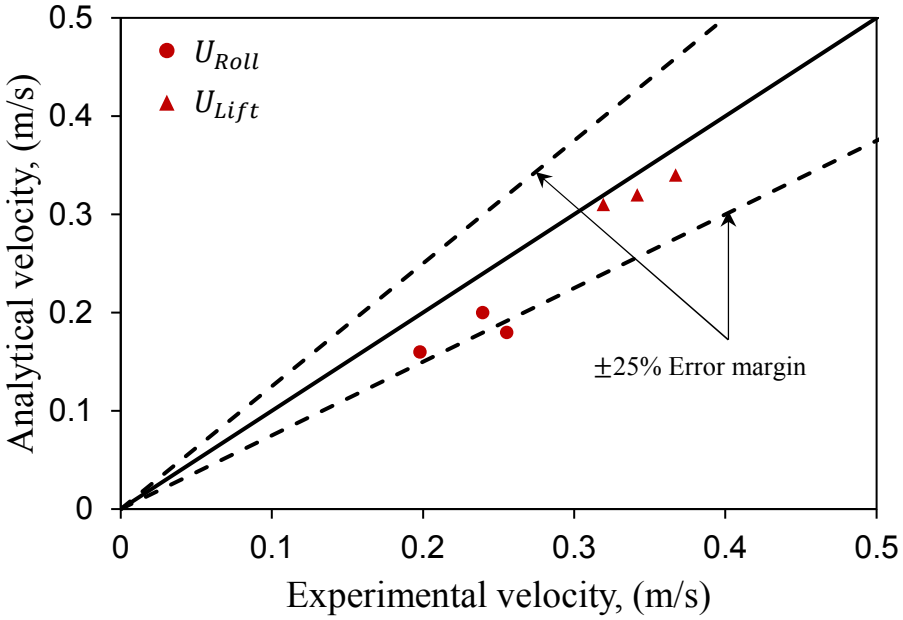

Figure 3.20 – Experimental vs. Analytical Rolling and Lifting (Sand).

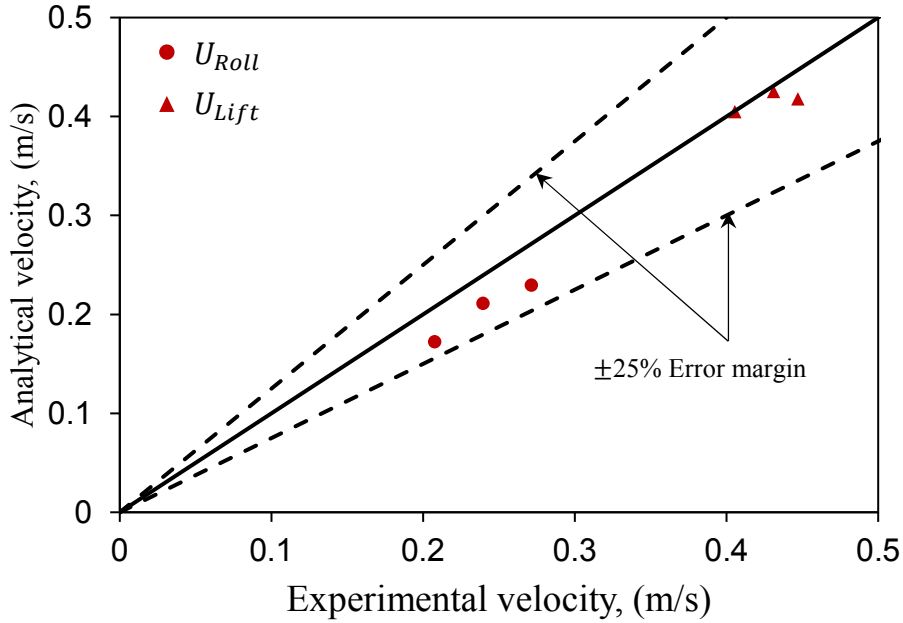

Figure 3.21 – Experimental vs. Analytical Rolling and Lifting (Proppants).

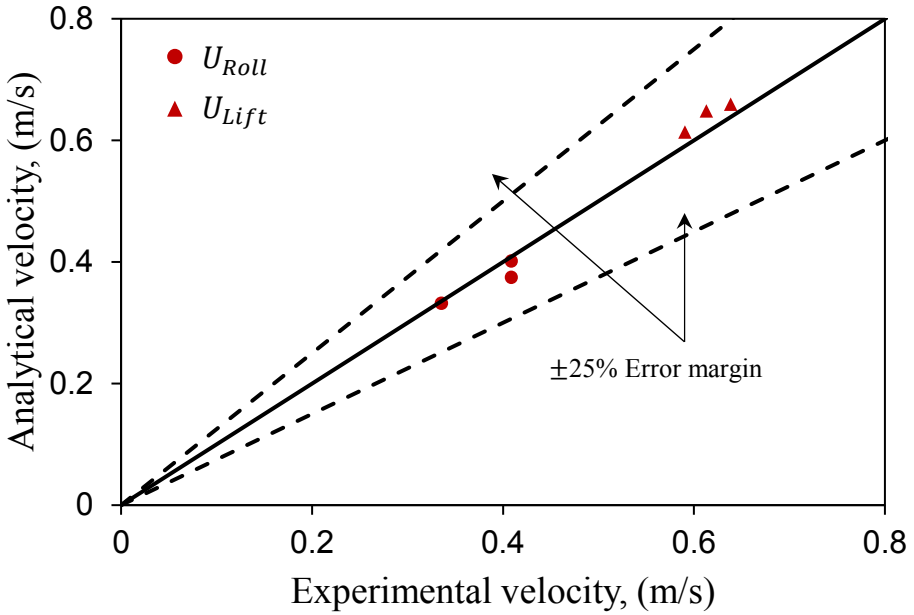

Figure 3.22 – Experimental vs. Analytical Rolling and Lifting results (Rock fragments).

3.5 Summary

In this Chapter three different cuttings types were used to estimate the critical rolling and lifting velocities at different wellbore inclinations. The results showed that:

1- The analytical models for lifting and rolling provided good estimates of velocities compared to experimental measurements.

2- The repose angle was shown to be an important parameter in hole cleaning efficiency. This assumption was confirmed analytically and experimentally.

3- The lift velocity is the limiting velocity needed to start cleaning a bed deposited at the wellbore. This value is not the optimum velocity for cleaning; however, it is the limit where the cuttings start to be transported out of the well.

4- The cuttings transportation becomes more difficult when increasing the angle until reaching a critical angle more than the complementary of the repose angle (from the horizontal plane); after this angle, the cleaning becomes easier.

CHAPTER 4

Simulation of Settling Velocity and Motion of Particles in Drilling Operation

4.1 Introduction

The study of cuttings transportation is an important topic in borehole cleaning, in particular in deviated and horizontal sections of the wellbore. In the simplest case, this problem can be studied as the settlement of a single particle in a fluid. When a particle is dropped into a stationary fluid, it will fall vertically and accelerates due to the gravitational force until this force is equilibrated with frictional and resistance forces (i.e. buoyancy and drag forces) (Nouri et al., 2014). When this equilibrium is reached, the particle acceleration drops to zero and the velocity becomes constant, this constant value is a function of the fluid and particles' properties as well as the geometry of the fluid container.

The motion of bubbles, drops and particles has been widely investigated by researchers in different fields such as chemical engineering, sediment transport, particle deposition in transport pipelines and drilling engineering. Clift et al. (1978) reported the settling mechanism of bubbles, drops and solid particles in Newtonian Fluids, whereas, Chhabra (2007) studied the settling mechanisms in non-Newtonian fluids. The behavior of falling objects and particle was also studied by many researchers (Chhabra, 2007; Guo, 2011). Some of these studies presented different drag coefficient

models depending on the particle types, i.e. spherical and non-spherical (Haider and Levenspiel, 1989).

Several industries rely on the determination of the terminal settling velocity to optimize their processes (e.g. slurry mixing, food processing, fluidized bed reactors and many others) (Clift et al., 1978). However, for the drilling industry and more specifically cuttings transportation and hole cleaning area, the motion of the particles has always been considered at steady state and correlations have been used for velocity calculations (Sifferman et al., 1974).

The wide research work on particle settlement was the continuity of the pioneering work of Stokes as the first analysis of particle motion (Agwu et al., 2018). In late 1850, a paper entitled: "*On the Effect of the Internal Friction of Fluids on the Motion of Pendulums*" was presented to the *Cambridge Philosophical Society* by Stokes (1850). Most researchers use the relation developed by Stokes for creeping flow around a spherical particle to study particle motion (Clark and Bickham, 1994).

In oil and gas drilling applications, the particle motion relates to the settlement and deposition of the cuttings drilled by the bit inside the drilling mud within the annulus space. During the drilling operation, mud circulation may be suspended for different reasons, such as workover and casing installment. During this time, the fluid becomes stagnant, resulting in loss of carrying capacity of the drilling fluid and settlement of the cuttings. Many studies have been done in the area of settling velocity related to cuttings transportation and hole cleaning. These studies focused on both experimental investigations (Agarwal and Chhabra, 2007; Baldino et al., 2015b; Buscall et al., 1982; Chhabra et al., 1996; Elgaddafi et al., 2012; Faitli, 2017; Fidleris and Whitmore, 1961a; Jacobs et al., 2015; Jayaweera and Mason, 1965; Johnsen, 2014; Kelessidis, 2003; Khatmullina and Isachenko, 2016; Nolan, 1970; Peden and Luo, 1987; Sharma and Chhabra, 1991; Wang et

al., 2018; Xu et al., 2017) and numerical simulations (Blackery and Mitsoulis, 1997; Bush, 1994; Butcher and Jr, 1990; Dazhi and Tanner, 1985; Dhole and Chhabra, 2006; Gavrilov et al., 2017; Ghosh and Stockie, 2015; Gumulya et al., 2014; Missirlis et al., 2001; Prashant and Derksen, 2011; Trofa et al., 2015; Wachs and Frigaard, 2016; Zaidi et al., 2015a). A summary of the previous work assumptions, tools and key findings is presented in Appendix A. The settling velocity was also investigated for studying proppants transport and settling in hydraulic fracturing fluids (Huang et al., 2019; Luo et al., 2014; Tong et al., 2019; Wei et al., 2020a; Zhu et al., 2019).

Experimental and numerical work focused on understanding the impact of three main factors affecting the hole cleaning including drilling cuttings, drilling fluid and wellbore geometry. As the rock is drilled, cuttings are mixed in a multitude of sizes, shapes and densities (Time and Rabenjafimanantsoa, 2014). Chien (1994) reported in his work the effect of the size and diameter of the cuttings and concluded that the rate of increase of the settling velocity with the particle size differs from one to another particle based on their size range. Baldino et al. (2015) showed the spiral, vibrating and rotational motion of irregularly shaped particles. Comparing the spherical and irregularly shaped particles (with equivalent volume and density), Luo (1988) and Reynolds and Jones (1989) found that the velocity decreases with shape irregularity. In terms of drilling fluid, as the fluid density increases, the settling velocity decreases (Hopkin, 1967), and similarly, as the fluid viscosity increases, the settling velocity is reduced (Chien, 1994). Hopkin (1967) demonstrated that the yield of the fluid is the main viscosity component that affects the settling velocity. Wellbore configuration (vertical or deviates) has a great effect on the particles settling motion as in deviated wellbores, the settling rate increases (Acrivos et al., 1983). This phenomenon was first presented by Boycott, and it was named later as the *Boycott Effect* after him (Cerny et al., 1988). Boycott (1920) reported that "when blood is put to stand in narrow tubes, the corpuscles

sediment a good deal faster if the tube is inclined than when it is vertical". The wall effect is the effect of the confining on the particle motion when the particles are adjacent to the wellbore wall (Faitli, 2017). The wall effect decreases the settling velocity by exerting a friction force on the adjacent particles (Clift et al., 1978; Malhotra and Sharma, 2014; Richardson et al., 1986; Song et al., 2019) Another wellbore related factor is the rotation speed (Hopkin, 1967; Time and Rabenjafimanantsoa, 2014). As the rotational speed increases, the particles are re-orientated causing them to settle slowly (Hopkin, 1967; Williams and Bruce, 1951).

Attempts have been made to develop analytical solutions for the particle falling motion based on the Basset–Boussinesq–Oseen equation (BBO). Some derived a semi-exact solution of the velocity by applying the Variational Iteration Method (VIM) (Domiri Ganji, 2012). In one study, the VIM was used to find the acceleration of the falling particle in different fluids (Yaghoobi and Torabi, 2012). Later, they applied the Padé approximation seeking a better convergence and accuracy of the solution (Torabi and Yaghoobi, 2011).

The main challenge when solving differential equations and partial differential equations (PDE) is the discretization and linearization. In 1986, Zhou (1986) introduced the concept of the differential transformation method (DTM). DTM can be applied to differential equations for both linear and non-linear as well as for partial differential equations (Hassan, 2008). It was shown to be an effective tool for solving extreme partial differential equations like the Fornberg-Whitham equation (Merdan et al., 2012). DTM provides the advantage of solving differential equations without requiring a linearization process (Aydemir and Mukhtarov, 2015). However, the main issue with DTM is its convergence. To overcome this issue, Rashidi et al. (2010) introduced the Padé approximation to the DTM solution and is called DTM-Padé approximation.

More recently, Nouri et al. (2014) developed analytical solutions of the Basset–Boussinesq–Oseen equation (BBO) for the unsteady state motion of spherical particles in Newtonian fluids using the differential transformation method (DTM), Galerkin method (GM) and collocation method (CM). In this work, the unsteady motion of a single particle as described by the BBO equation was solved analytically through DTM transformation and Padé approximation numerically using MATLAB. This solution is referred to as Numerical solution. Then the DTM and DTM-Padé approximation were applied to find corresponding analytical solutions. Also, numerical simulation results for single, multiple and heterogeneous particles settling using MfiX software were compared to the analytical and the numerical solutions. The MfiX solutions will be referred to as simulation. The simulation is used to define the extent of the Basset–Boussinesq–Oseen equation (BBO) as proposed by Torabi and Yaghoobi (2011). The effect of the container geometry is also considered in the simulations. The analytical and numerical results of single particle settling were projected to multiple particles settling to understand the settling process of homogeneous and heterogeneous suspensions of particles.

4.2 Methodology

4.2.1 Mathematical Formulation

Basset–Boussinesq–Oseen Equation

The settling velocity of a spherical particle in a stagnant fluid was first described by Stokes (2009).

The Stokes' equation for particle-slip velocity is stated as:

$$V_{sl} = \frac{(\rho_s - \rho_f) g {d_p}^2}{18\mu_f} \tag{4.23}$$

where V_{sl} is the settling velocity, ρ_s and ρ_f are the solid and fluid densities, respectively, μ_f is the fluid viscosity and g is the gravity.

For a Newtonian fluid, Equation (3.1) can be written as:

$$V_{sl} = 2.46\left(\frac{(\rho_s - \rho_f)gd_p}{2\rho_f}\right)^{\frac{1}{2}} \tag{4.24}$$

Based on the Stokes' relation, several researchers, including Boussinesq (1885), Basset (1888) and Oseen (1911), independently investigated the forces acting on a spherical particle in incompressible fluid flow. Their work established the main platform for studying the unsteady motion of spherical particles in fluids. Soo (1990) and Zhu and Fan (1998) continued the work of Boussinesq, Basset and Oseen and presented the so-called Basset–Boussinesq–Oseen equation (BBO). Parmar et al. (2011), extended the BBO equation for the application in compressible fluids. The main assumptions embedded in the BBO equation are the small particle size range and low Reynolds number. Nouri et al. (2014) and Torabi and Yaghoobi (2011) did not report in their work the extent and the validity of BBO equation for large size particles. Also, in their work, they didn't consider the Basset history force by neglecting the fluid density comparing to the particle density. This assumption may be questionable as they used aluminum particles of 2702 kg/m^3 (2.702 gr/cc or gcc) which is a high density comparing to water density of 1000 kg/m^3 (1 gcc).

The BBO equation, based on Newton's second law states that the momentum change rate is equal to the forces acting on the particle.

Table 4.14 presents the definition of the different components of the BBO equation. The BBO is presented as:

$$\frac{1}{6}\pi {d_p}^3 \rho_p \frac{dU_p}{dt} = \underbrace{3\pi d_p \mu \left(U_f - U_p\right)}_{term\ 1} - \underbrace{\frac{1}{6}\pi {d_p}^3 \nabla P}_{term\ 2} + \underbrace{\frac{1}{12}\pi {d_p}^3 \rho_f \frac{d\left(U_f - U_p\right)}{dt}}_{term\ 3}$$
$$+ \underbrace{\frac{3}{2}\pi {d_p}^2 \sqrt{\pi \rho_f \mu} \int_{t_0}^{t} \frac{1}{\sqrt{t-\tau}} \frac{d\left(U_f - U_p\right)}{d\tau} d\tau}_{term\ 4} + \underbrace{\sum_k F_k}_{term\ 5} \quad (4.25)$$

Table 4.14 – Definition of the terms in the BBO equation

Term	Formulation	Definition
Term 1	$3\pi d_p \mu \left(U_f - U_p\right)$	Stokes' drag force
Term 2	$-\frac{1}{6}\pi {d_p}^3 \nabla P$	Froude–Kriloff force: introduced by the unsteady pressure field generated by undisturbed
Term 3	$\frac{1}{12}\pi {d_p}^3 \rho_f \frac{d\left(U_f - U_p\right)}{dt}$	Added mass force
Term 4	$\frac{3}{2}\pi {d_p}^2 \sqrt{\pi \rho_f \mu} \int_{t_0}^{t} \frac{1}{\sqrt{t-\tau}} \frac{d\left(U_f - U_p\right)}{d\tau} d\tau$	Basset force
Term 5	$\sum_k F_k$	Gravity and other forces acting on the particle

Particle Velocity and Trajectory Calculations

Assuming a small rigid particle, falling in an infinite incompressible Newtonian fluid with a velocity $v(t)$, and that the density of the particle is very high compared to the fluid density, the Basset history force (see

Table 4.14) will be simplified as (Torabi and Yaghoobi (Torabi and Yaghoobi, 2011)):

$$m\frac{dv}{dt} = mg\left(1 - \frac{\rho_f}{\rho_p}\right) - \frac{1}{8}\pi {d_p}^2 \rho_f C_D v^2 - \frac{1}{12}\pi {d_p}^3 \rho_f \frac{dv}{dt} - 3\pi \mu d_p v \quad (4.26)$$

where d_p , m and ρ_p are respectively, the diameter, mass and density of the solid particle, μ and ρ_f are the fluid density and viscosity. C_D is the Drag coefficient and is related to Reynold's number Re. The forces considered in Equation (4.25) are gravity, drag, buoyancy and added or virtual mass effect forces. The non-linear nature of the drag coefficient term (see Table 1) introduces difficulty in solving Equation (4.26). Several researchers proposed different models as the solution of the drag coefficient term based on the particle velocity. However, the iterative calculations needed in these models add another complexity to the solution. Ferreira et al. (1998) performed an analytical study and proposed a correlation for the drag coefficient applicable for a wide range of particle velocities corresponding to the Reynolds numbers of $0 \leq Re \leq 10^5$. Jalaal et al. (2011) used this correlation successfully in their study in which they compared different correlations proposed by previous researchers to calculate the resistive particle forces. The correlation proposed by Ferreira et al. (1998) is expressed as:

$$C_D = \frac{24}{Re_p}\left(1 + \frac{Re_p}{48}\right) \tag{4.27}$$

where

$$Re_p = \frac{\rho v d_p}{\mu} \tag{4.28}$$

For non-spherical particles, d_p is replaced by d_{eq} which is the equivalent volume diameter. Sphericity parameter was first defined by Wadell (1935) as the ratio of the surface area of an equivalent volume spherical particle (V_{eq}) to the surface area of the particle itself (A_p) and is calculated as:

$$\Psi = \frac{\pi^{\frac{1}{3}}(6V_{eq})^{\frac{1}{3}}}{A_p} \tag{4.29}$$

For particles with $0.2 < \Psi < 1$ and $0.001 \leq Re \leq 10^4$ Chien (1994) proposed:

$$C_D = \frac{30}{Re_p} + 67.289e^{-5.03\Psi} \tag{4.30}$$

with

$$Re_p = \frac{\rho v d_{eq}}{\mu} \tag{4.31}$$

In this paper spherical particles are considered, while in terms of the analysis, the same workflow is applied.

The mass of a spherical particle is calculated as:

$$m = \frac{1}{6}\pi {d_p}^3 \rho_p \tag{4.32}$$

Substituting Equation (4.27) into Equation (4.28) and replacing the terms in Equation (4.26) yields the general form for the velocity as:

$$a\frac{dv}{dt} + bv + cv^2 - d = 0 \tag{4.33}$$

Here

$$a = \frac{1}{12}\pi {d_p}^3 (2\rho_p - \rho_f) \tag{4.34}$$

$$b = 3\pi d_p \mu \tag{4.35}$$

$$c = \frac{1}{16}\pi {d_p}^2 \rho_f \tag{4.36}$$

$$d = \frac{1}{6}\pi {d_p}^3 g(\rho_p - \rho_f) \tag{4.37}$$

Substituting Equation (4.33) into Equation (4.31), and using the velocity equation as:

$$v(t) = \frac{dx(t)}{dt} \tag{4.38}$$

results in trajectory equation in form of:

$$a\frac{d^2x(t)}{dt^2} + b\frac{dx(t)}{dt} + c\left(\frac{dx(t)}{dt}\right)^2 - d = 0 \tag{4.39}$$

This equation can be used to determine the position of the particle as a function of time during its settlement in a fluid.

4.2.2 Analytical and Semi-Analytical Solutions

In this section, we will be developing an analytical solution of the Basset–Boussinesq–Oseen equation (BBO) for both particle velocity and trajectory (vertical position) during its settlement in a fluid in stationary mode. DTM and DTM-Padé will be used for this purpose. Due to the complexity of the DTM and the Padé approximation at high orders, semi-analytical solutions of the BBO were developed using an algorithm in MATLAB.

Both Equations (4.33) and (4.39) are non-linear equations with known initial conditions of $v(0) = 0$ and $x(0) = 0$. This makes them resolvable analytically. For a better convergence, semi-analytical solutions are also possible using MATLAB, which is a powerful numerical computation software.

In this study we considered a variety of spherical shapes as cuttings. Table 2.1 shows different minerals that can be encountered during drilling. Fluids used in this work, under normal conditions of pressure and temperature, are water (Fluid 1) and other fluids with different viscosities and densities were used for sensitivity purposes.

Table 4.16 and

Table 4.17 show the calculated coefficients of Equation (4.33) and Equation (4.39) for different fluids and minerals presented in Table 2.1.

Table 4.15 – Rock properties

Lithology	Density, g/cc
Sandstone	2.65
Limestone	2.70
Dolomite	2.876
Anhydrite	3.00
Salt	2.032

Table 4.16 – Coefficients of Equations (4.31) and (4.34) for different cuttings densities and sizes falling in Fluid 1

Lithology	Diameter, mm	a	b	c	D
Salt	0.003	3.5795E-05	2.8274E-05	0.001767146	0.000143124
	0.006	0.00028636	5.6549E-05	0.007068583	0.001144988
	0.01	0.00132575	9.4248E-05	0.019634954	0.005300872
Sandstone	0.003	4.4532E-05	2.8274E-05	0.001767146	0.000228831
	0.006	0.00035626	5.6549E-05	0.007068583	0.00183065
	0.01	0.00164934	9.4248E-05	0.019634954	0.008475232

Limestone	0.003	0.000045380	0.000028274	0.001767146	0.000237152
	0.006	0.000363042	0.000056549	0.007068583	0.001897219
	0.01	0.001680752	0.000094248	0.019634954	0.008783422
Dolomite	0.003	4.7727E-05	2.8274E-05	0.001767146	0.000260174
	0.006	0.00038182	5.6549E-05	0.007068583	0.002081394
	0.01	0.00176767	9.4248E-05	0.019634954	0.009636081
Anhydrite	0.003	4.9155E-05	2.8274E-05	0.001767146	0.000274181
	0.006	0.00039324	5.6549E-05	0.007068583	0.002193452
	0.01	0.00182055	9.4248E-05	0.019634954	0.010154868

Table 4.17 – Coefficients of Equations (4.31) and (4.34) for sandstone cuttings with different sizes falling in Fluid 2

Lithology	Diameter, mm	a	b	c	d
Sandstone	0.003	0.000046653	0.000282743	0.002297290	0.000187226
	0.006	0.000373221	0.000565487	0.009189159	0.001497805
	0.01	0.001727876	0.000942478	0.025525440	0.006934280

Differential Transformation Method (DTM)

The DTM was described by Torabi and Yaghoobi (2011). The DTM transformation allows us to transform the velocity Equation (4.33) into a polynomial equation in the form of:

$$v(t) = \sum_{i=0}^{\infty} c_i t^i. \tag{4.40}$$

After applying the DTM transformation on the velocity Equation (4.33) it is expressed as:

$$a(k+1)V(k+1) + bV(k) + c\sum_{i=0}^{k} V(i)V(k-i) - d\delta(k) = 0 \tag{4.41}$$

where $V(k)$ represents the transformed velocity function and $v(t)$is the original velocity function.

Padé Approximant

Padé (1892) presented an approximation function of given order to improve convergence of non-linear equation solutions (Nouri et al., 2014). Padé approximation has two integers m and n representing the order of the fractional functions, generally denoted as $R(x)$ or $P[m/n]$.

For a function $f(x)$, its Padé approximation is given by Torabi and Yaghoobi (2011):

$$P[m/n] = R(x) = \frac{\sum_{i=0}^{m} a_i x^j}{1 + \sum_{j=1}^{n} a_k x^k} \tag{4.42}$$

Equation (4.42) agrees with the original function $f(x)$ to the highest order $(m+n)$, this agreement allows us to define a_i and a_j constants of the approximant by solving the agreement equation system:

$$\begin{cases} R(0) = f(0) \\ R'(0) = f'(0) \\ \quad . \\ \quad . \\ \quad . \\ R^{m+n}(0) = f^{m+n}(0) \end{cases} \tag{4.43}$$

Application Example

After applying the DTM to Equation (4.33), Equation (4.41) is rearranged to obtain

$$V(k+1) = \frac{d\delta(k) - c\sum_{i=0}^{k} v(i)v(k-i) - bV(k)}{a(k+1)} \tag{4.44}$$

where

$$d\delta(k) = \begin{cases} 1 \; if \; k = 0 \\ 0 \; if \; k \neq 0 \end{cases} \tag{4.45}$$

and the terms $V(0)$, $V(1)$, … and $V(n)$ obtained from Equation (4.44) are replaced in Equation (4.40) knowing that

$$c_i = V(i) \tag{4.46}$$

Equation (4.44) can be solved easily by hand up to $k = 5$, however, better convergence demands higher degrees of iterations $k \geq 10$, which requires a computing tool to obtain the polynomial representing the velocity equation.

For $k = 7$ the DTM terms obtained from Equation (4.44) are

$$\begin{cases} V(0) = 0 \\ V(2) = -\frac{1}{2}\frac{bd}{a^2} \\ V(3) = \frac{1}{6}\frac{d\left(b^2 - 2cd\right)}{a^3} \\ V(4) = -\frac{1}{24}\frac{bd\left(b^2 - 8cd\right)}{a^4} \\ V(5) = -\frac{1}{120}\frac{d\left(22cdb^2 - 16c^2d^2 - b^4\right)}{a^5} \\ V(6) = \frac{1}{720}\frac{db\left(52cdb^2 - 136c^2d^2 - b^4\right)}{a^6} \\ V(7) = -\frac{1}{5040}\frac{d\left(114cdb^4 - 720d^2b^2 + 272c^3d^3 - b^6\right)}{a^7} \end{cases} \tag{4.47}$$

At order 7 the velocity solution can be written as

$$v(t) = V(0) + V(1) \times t + V(2) \times t^2 + V(3) \times t^3 + V(4) \times t^4 + V(5) \times t^5 + V(6) \times t^6 + V(7) \times t^7 \tag{4.48}$$

Now applying Padé for different m and n values. For *m*=*n*=2:

$$P[2/2] = \frac{12adt}{12a^2 + 6abt + (b^2 + 4cd)t^2} \tag{4.49}$$

Similarly at Padé orders m and n higher than 2, for ease of computation a MATLAB code was developed. Equation (4.50) shows, as an example, the DTM-Padé approximation corresponding to $m = n = 4$.

$$P[4/4]$$

$$= \frac{\begin{array}{c} 5dt[168a^3(b^2 + 4cd)^3 + 420a^2bt(b^6 - 240b^4cd + \\ 3072b^2c^2d^2 - 3968c^3d^3) + 4at^2(b^2 + 4cd)^4 + \\ 7bt^3(b^6 - 240b^4cd + 3072b^2c^2d^2 - 3968c^3d^3)(b^2 + 4cd)] \end{array}}{\begin{array}{c} 840a^4(b^2 + 4cd)^3 + 2520a^3bt(b^6 - 198b^4cd + 2568b^2c^2d^2 - 3296c^3d^3) + \\ 60a^2t^2(19b^8 - 4176b^6cd + 53904b^4c^2d^2 - 69056b^2c^3d^3 + 384c^4d^4) + \\ 20abt^3(b^2 + 4cd)(11b^6 - 2514b^4cd + 32280b^2c^2d^2 - 41632c^3d^3) + \\ 2t^4(b^2 + 4cd)(9b^8 - 2096b^6cd + 26904b^4c^2d^2 - 34656b^2c^3d^3 + 64c^4d^4) \end{array}} \tag{4.50}$$

In this work, to obtain the calculate the values of velocity and trajectory in the vertical direction as a function of time we extracted a semi-analytical solution in MATLAB. The results are presented as the following two equations:

$$v(t) = -\frac{b - 2.tan(A)\left(-\frac{b^2}{4} - cd\right)^{\frac{1}{2}}}{2c} \tag{4.51}$$

$$x(t) = B \quad - \frac{a.log(A)(b^2 + 4cd)^{\frac{1}{2}}}{4c\left(\frac{b^2}{4} + cd\right)^{\frac{1}{2}}} - \frac{b}{2c}t \tag{4.52}$$

Where

$$A = tan\left(\left(a\frac{\tan\left(\frac{b}{(-b^2-4cd)^{\frac{1}{2}}}\right)}{\left(-\frac{b^2}{4}-cd\right)^{\frac{1}{2}}} - \frac{t}{a}\right)\left(-\frac{b^2}{4}-cd\right)^{\frac{1}{2}}\right)^2 + 1 \tag{4.53}$$

$$B = \frac{a.\log\left(1-\frac{b^2}{b^2+4cd}\right)(b^2+4cd)^{\frac{1}{2}}}{4c\left(\frac{b^2}{4}+cd\right)^{\frac{1}{2}}} \tag{4.54}$$

4.2.3 Basset–Boussinesq–Oseen Numerical Solution

The BBO equations of velocity and trajectory (Equation (4.33) and Equation (4.39)) are non-linear second order ordinary differential equation (ODE). Equation (4.39) is a general function describing the velocity and acceleration of an object (Oliveira, 2015). In order to find a numerical solution to any similar particular problem, specific initial conditions (ICs) are needed. When these ICs are applied to this equation, an explicit value of x can be derived.

Since different numerical methods to solve ODE can be implemented using standard programming techniques, they are generally part of the mathematical tools library of programming languages such us MATLAB, FORTRAN and C++ (Oliveira, 2015).

For a settling particle in a stagnant fluid, the BBO has two initial conditions; $v(0) = 0$ and $x(0) = 0$. For the velocity equation, Equation (4.33) can be solved using only one boundary condition which is $v(0) = 0$ or $\frac{dx}{dt}(0) = 0$. However, for the trajectory, Equation (4.39) needs both initial conditions. For the numerical solution, MATLAB was used.

The BBO equation considers the particle falling in an infinite medium.

4.3 Eulerian-Lagrangian Simulation

Eulerian and Lagrangian modeling are the two main multiphase solid-particle flow modeling methods (Razavi et al., 2019). In Eulerian modeling, the solid phase is considered as a continuous phase. Empirical equations are required to model the solids dispersed phase behavior. However, the Lagrangian approach considers each particle separately and models its movement by deriving the equations of motions based on the particles' mass and velocity. Both models consider the fluid as a continuous phase and local averaging is used in the governing equations (Crowe et al., 2011). For our simulation, we used a Particle-In-Cell (PIC) multiphase model in MFIX software, which is a Lagrangian-Eulerian simulation. The model considers the fluid phase as a continuum while assigning parcels to represent groups of real particles. This approach helps to reduce computational time and cost ("MFiX - Multiphase Flow Science Group at NETL," n.d.).

MFIX employ a parcel-based approach. This approach is also called as computational/notional/nominal particles based approach in literature. In the parcel approach a finite number of parcels are tracked rather than using individual particles (Strack and Cundall, 1978). Values between Eulerian cell centers, face cell centers, and parcel position are managed through interpolation operators. To accomplish this in MFiX-PIC, bi-linear operators are combined in each axial direction (Clarke and Musser, 2020).

In MFIX, the fluid–phase governing equations for mass and momentum conservation are similar to those in traditional fluid–phase CFD but with additional coupling terms due to drag from the solids–phase. The solids-phase is modeled using discrete particles. MFIX has recently been extended to include heat and mass transfer (Clarke and Musser, 2020).

Also, MFIX defines physical boundary by the intersection of the Eulerian grid with a STL (stereolithographic CAD file). Newtonian interaction with boundaries is discretely calculated (Clarke and Musser, 2020).

4.4 Experimental Set Up

In order to validate the results of analytical models, we conducted some experiments. Figure 1.1, shows the view of a slurry loop that was used for our lab experiments. Spherical ceramic proppants were mixed with the fluid in a mixing tank and injected through a 15 *ft* long annulus made up of 5 *in* inner diameter drill pipe and 8 *in* outer diameter clear PVC tube. The wellbore deviation was changed from horizontal to vertical to simulate the effect of wellbore angle.

The flow rate was changed until the particles remained in the same vertical position inside the annulus. At this point the settling velocity is nearly equal to the annular fluid velocity. The settling velocity was also estimated from the video of particle settlement taken during their settlement after the flow rate was brought down to zero.

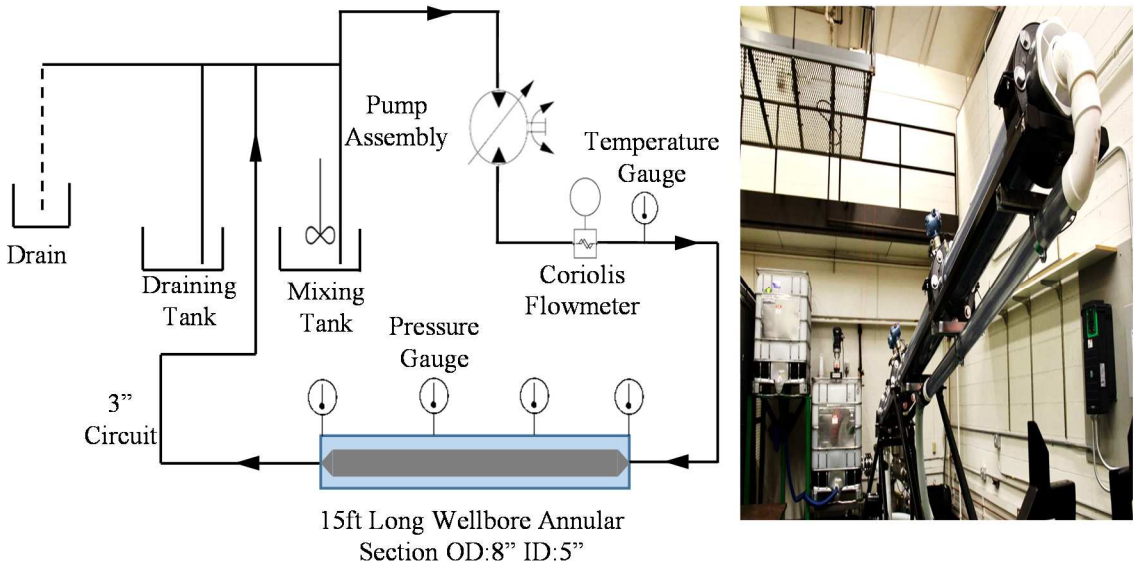

Figure 4.23 – Slurry Loop Unit at the University of North Dakota.

4.5 Single Particle Analysis

In this work, numerical solution refers to the solution of the BBO equation using MATLAB. However, Simulation refers to the solution delivered using MFIX Eulerian-Lagrangian Simulation software.

In this section, the velocity of a single particle falling in fluids is calculated using different methods and the results are compared. This provided a basis to continue with the analysis of multiple particles sedimentation in the next sections.

The time-dependent unsteady settling velocity of a single sandstone particle was calculated using DTM and DTM-Padé methods with different orders. For DTM orders of $k < 7$ and Padé orders of up to [2,2], the analytical solutions were used, as explained in the previous section. However, for higher orders, a semi-analytical solution using a MATLAB algorithm was used to solve the BBO. Also, a fully numerical solution of the BBO was developed using a MATLAB algorithm. Here, for the purpose of demonstration, a 3 mm sandstone spherical particle is considered. Figure 4.24 (a) presents the results over 0.35 s time span. From this Figure, it is seen that within this time period, even higher orders of the DTM ($k > 20$) do not yield convergence. However, for Padé approximation with orders exceeding [6,6] the solution appears to become stabilized. This result is consistent with earlier findings by others (Nouri et al., 2014).

A similar analysis to Figure 4.24 (a) over 2.00 second time span is presented in Figure 4.24 (b). The results show the divergence of the results even at higher DTM- Padé orders. This may suggest that the analytical and semi-analytical solutions can predict the steady state settling velocity for a short time span after the unsteady state regime, however, the results deviate shortly. Though, for any time interval, only the numerical solution of the BBO is consistent and converges to a constant settling velocity value. Therefore, in the remaining of this work, only the MATLAB numerical

solution of the BBO, due to its simplicity and stability, will be used for calculation purposes and its results will be compared to the MFIX numerical simulations.

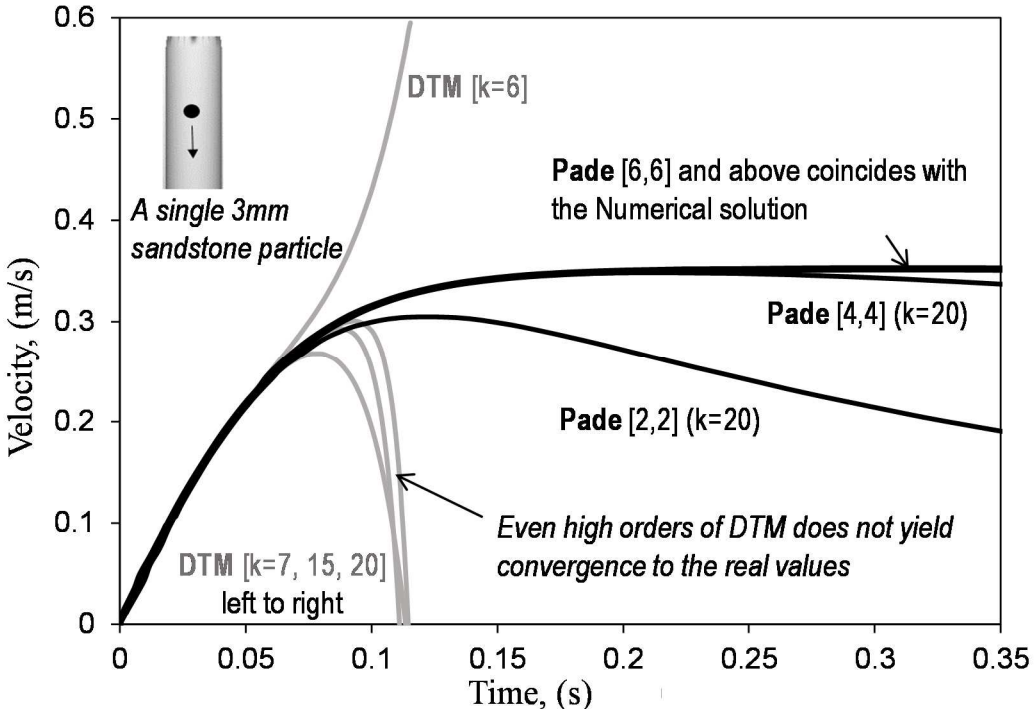

(a)

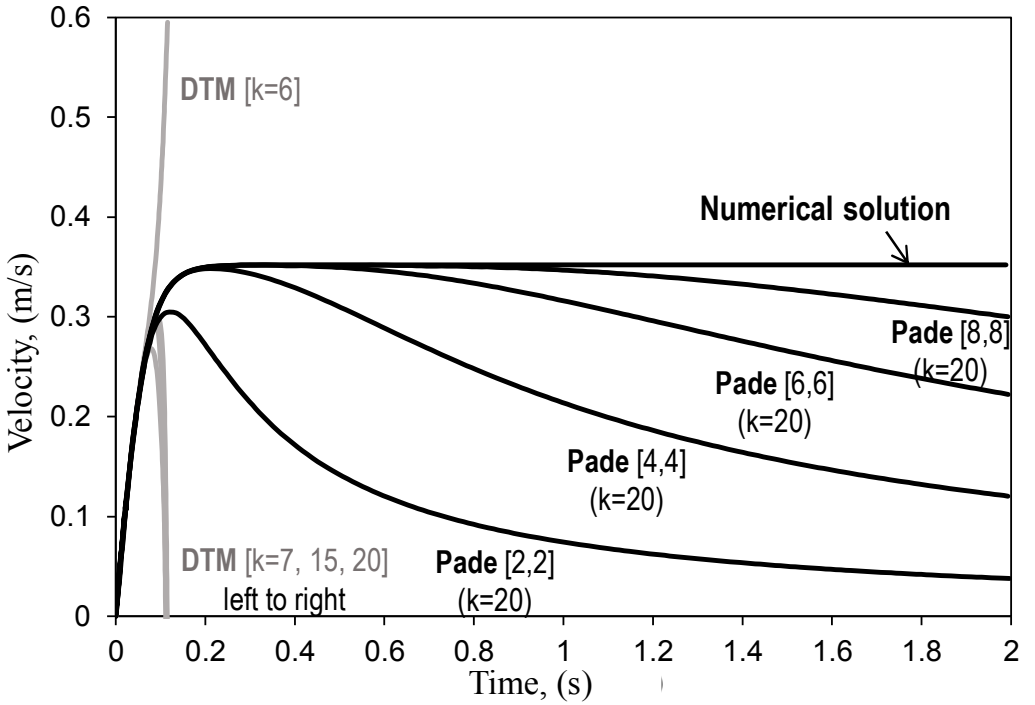

(b)

Figure 4.24 – Comparison of settling velocity for a single 3 *mm* sandstone particle (a) over 0.35 s time span (b) over 2.00 time span; using numerical model and analytical and semi-analytical models of DTM with three different orders and DTM-Padé with four different $[m, n]$ at $k = 20$.

The motion of the same sandstone particle was simulated inside Fluid 1 in a cylinder of 8.00cm radius and compared to the numerical solution, Stokes' correlation (Equation (4.24)) and experimental results from the Slurry Loop Unit (SLU). The cylinder radius was considered to be equivalent to the diameter of the annulus space of the SLU (8 *in* outer diameter and 5 *in* inner diameter). The SLU experiment using sandstone particles with an average diameter of approximately 3 *mm* showed that the particles are suspended on a vertical position (i.e. when annular velocity = settling velocity) at a rate of 105 *GPM* which is equivalent to an annular velocity or settling velocity of 0.3352 *m/s*. The results are presented in Figure 4.25. This figure demonstrates that the simulation prediction is in good agreement with the experimental measurement of the settling velocity. However, due to limitations discussed in the previous Sections, the agreement with the experimental results decreases when compared to numerical and correlation predictions.

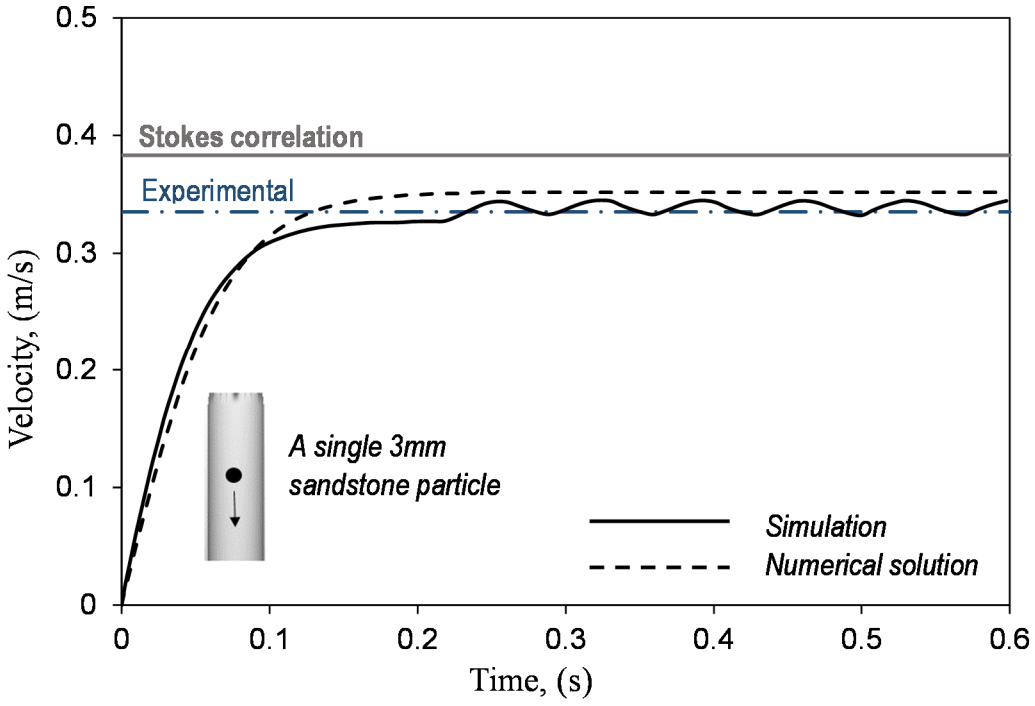

Figure 4.25 – Comparison of settling velocity for a single 3 *mm* sandstone particle using the numerical model, correlation, experimental measurement and simulation.

Since the BBO equation assumes the settlement of the particle in an infinite fluid, the wall effect when the particle is moving inside an annulus space was investigated using simulation which were run in three different pipes with a radius of 0.3 *m*, 0.096 *m* and 0.020 *m*, respectively. As presented in Figure 4.26, the results show that the radius of the pipe has an effect on the steady state settling velocity, however, for a small particle-to-pipe radius ratio of less than 0.0525 the settling velocity tends to remain constant. In order to apply the wall effect to the BBO equation for higher particle-to-pipe radius ratio, a correction factor can be used (see Appendix A).

Another limitation of the BBO is its assumption related to the small particle size range. The size of the particles in this work is not necessarily small enough to fall within the range of applications of the BBO. Therefore, to study this effect, three simulations were run on three single sandstone particles with sizes of 3 *mm*, 6 *mm* and 10 *mm* and the results were compared to the BBO numerical solution. The results presented in Figure 4.27 show that with increasing the particle size the deviation of the BBO numerical solution from the simulation result increases, and this holds true even for the smallest particle size of 3 *mm* used in these simulations. This may be due to the density of the particles since the BBO equation assumes that the particle density is very high compared to the fluid density. The experimental measurements in Figure 4.27 show that the simulation is able to predict the settling velocity with very high accuracy. However, for these sandstone particles, the fluid-to-particle density ratio is 0.38 which is relatively not negligible and might be the reason for the BBO solution deviation from the experimental and simulation results. To investigate this further, the simulation was repeated for a salt particle (Table 2.1) of 10 mm diameter. The results (see Figure 4.28) indicate the high impact of the particle size and the fluid-to-particle density ratio on the results of the numerical solution of the BBO equation. Further simulations with higher density particles showed that for particle size less than 6 *mm* and the fluid-to-particle density ratio

of less than 0.125 the settling velocity and particle trajectory predictions using the BBO equation may yield reasonable results. The results are shown, as an example, for a particle size of 3 *mm* and density of 8 *gcc* in Figure 4.29 (a) and (b) with respect to the particle velocity and position.

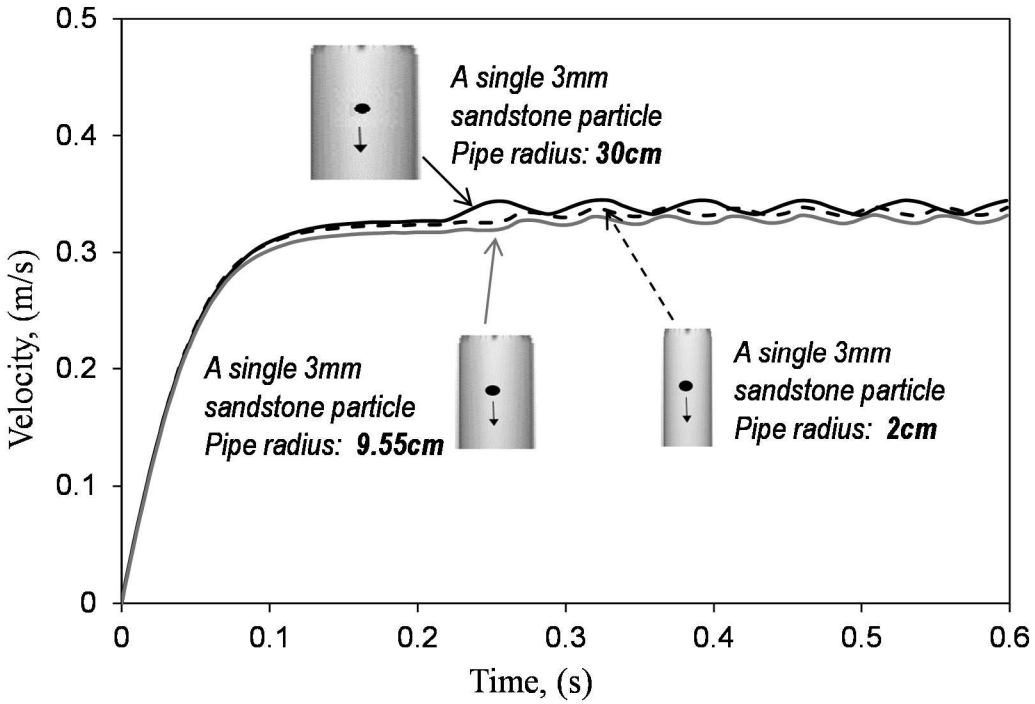

Figure 4.26 – Comparison of simulated settling velocity for a single 3 *mm* sandstone particle in three different pipes of 2.00 *cm*, 9.55 *cm* and 30 *cm* radii.

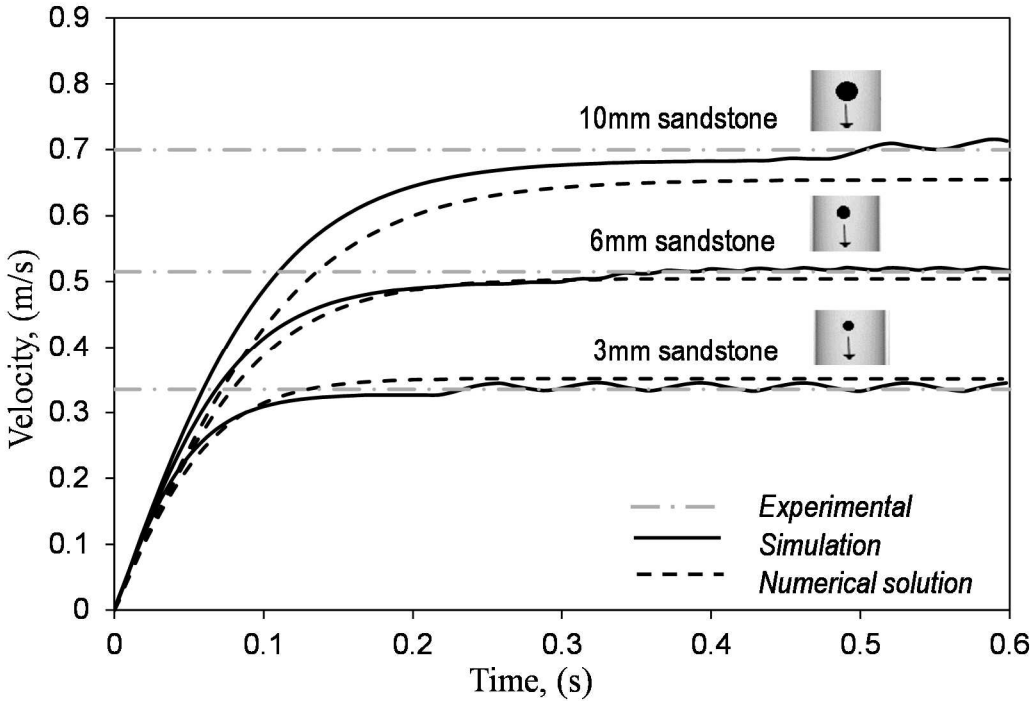

Figure 4.27 – Comparison of settling velocity for 3 different sized single sandstone particles using experimental measurement, numerical model and simulation.

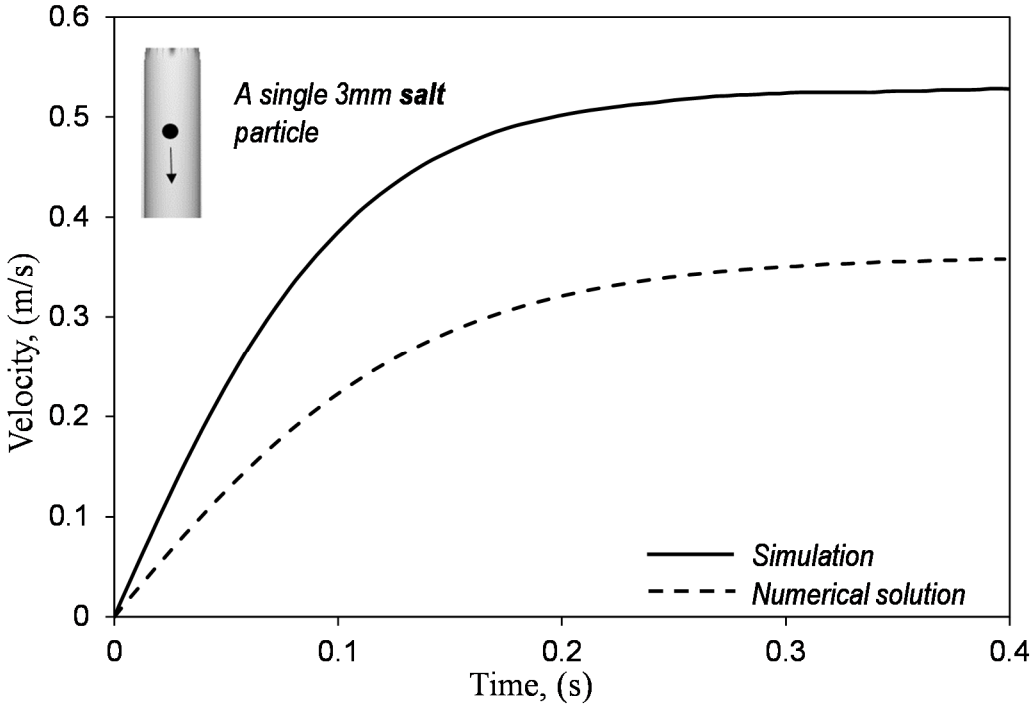

Figure 4.28 – Comparison of settling velocity for a 3 *mm* single salt particle using numerical model and simulation.

The results also show that for very small and heavy particles (i.e. similar to the range defined earlier), the Stokes correlation can be used to predict the settling velocity as well as the particle trajectory with relatively high accuracy.

At very high fluid-to-particle density ratios, the settling velocity increases resulting in the C_D value tends to the upper limit of 0.5 where the stokes correlation becomes very reliable. Even with a fluid-to-particle ratio of 0.375 (i.e. fluid density 3 times higher than water), the BBO numerical solution is still in good agreement with the simulation prediction, as shown in Figure 4.30 (a) and (b). However, the particle size has a significant effect on the accuracy of the numerical solution when one compares the velocity and vertical position of particles with 10 *mm* size shown in Figure 4.31 (a) and (b), with corresponding results of 3 mm particle in Figure 4.29 (a) and (b).

The effect of fluid viscosity and density and particle diameter on reducing the settling rate of particles was also simulated. Figure 4.32 (a) shows the effect of the fluid density and viscosity on the particle settling velocity. The log-log plot in Figure 4.32 (b) shows that the density has a minor effect on the unsteady state behavior of the particle as the slopes of the plots corresponding to different particle's density are the same. However, the effect of the fluid viscosity and particle diameter are more pronounced.

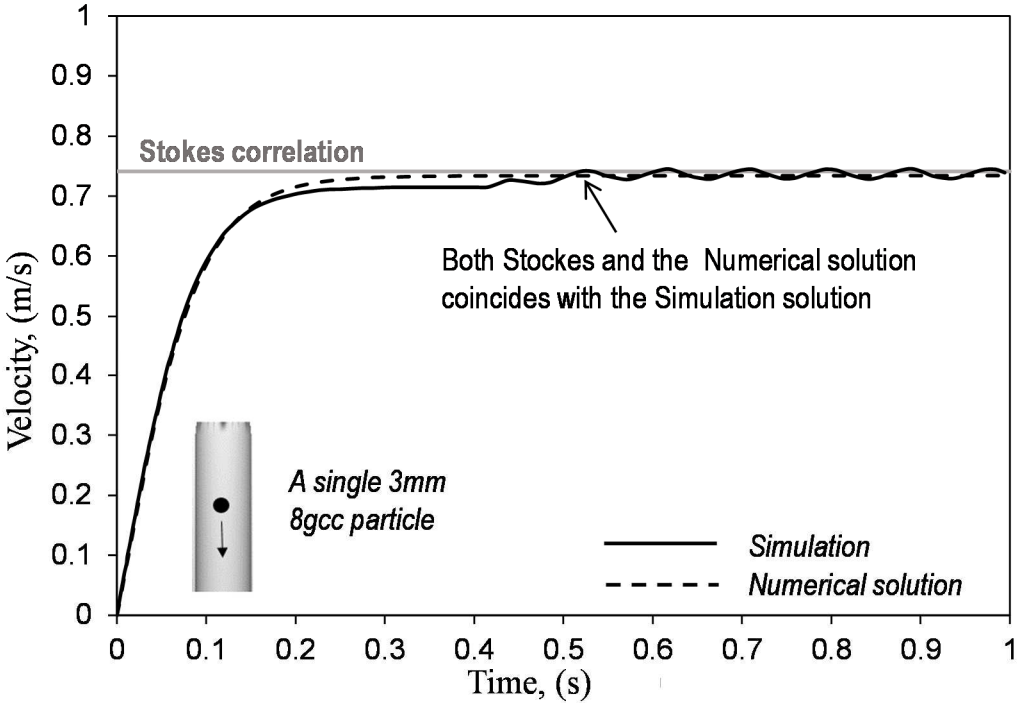

(a)

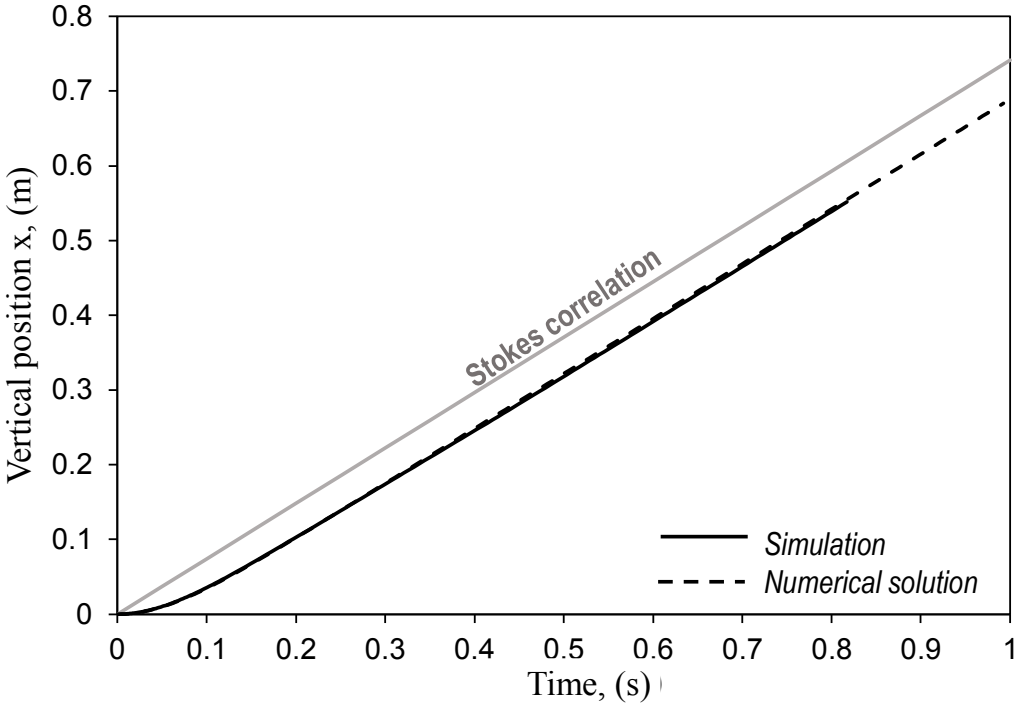

(b)

Figure 4.29 – Comparison of (a) settling velocity (b) particle trajectory (vertical motion) for a single 3 *mm* 8 *gcc* particle in Fluid 1 using Stokes correlation, numerical model and simulation.

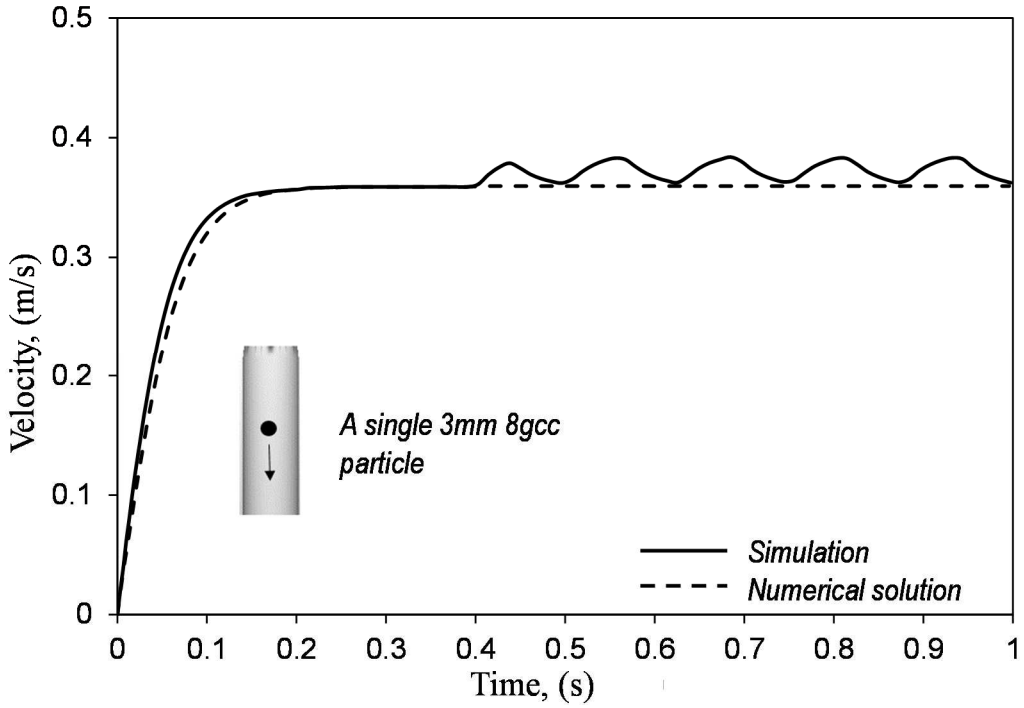

(a)

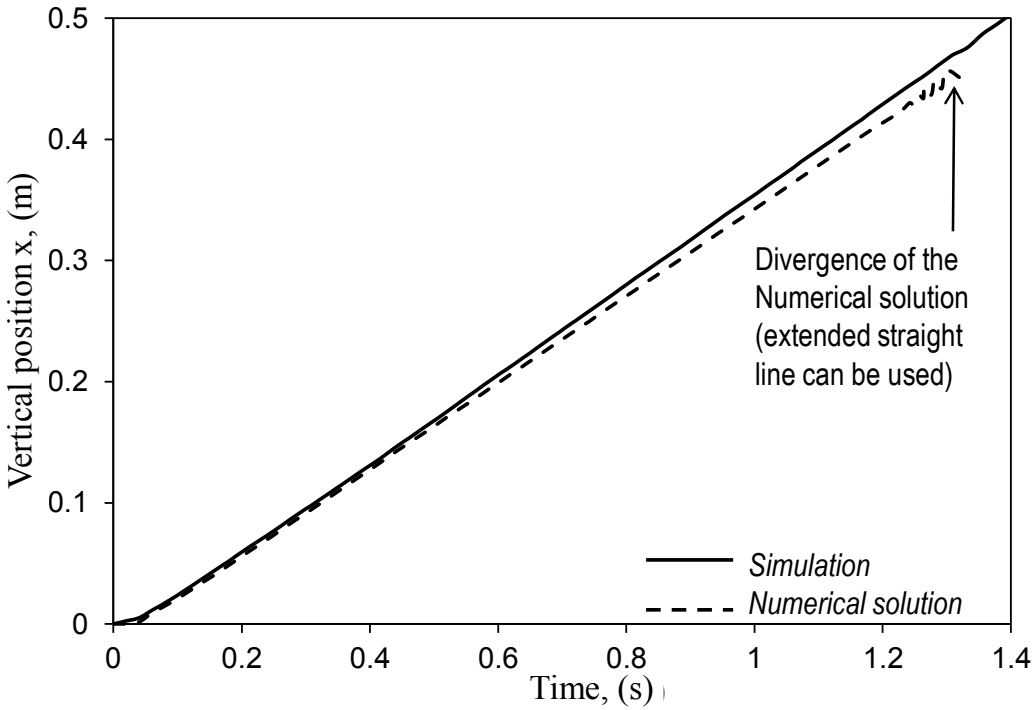

(b)

Figure 4.30 – Comparison of (a) settling velocity (b) particle trajectory (vertical motion) for a single 3 *mm* 8 *gcc* particle in Fluid 2 (3gcc) using Stokes correlation, numerical model and simulation.

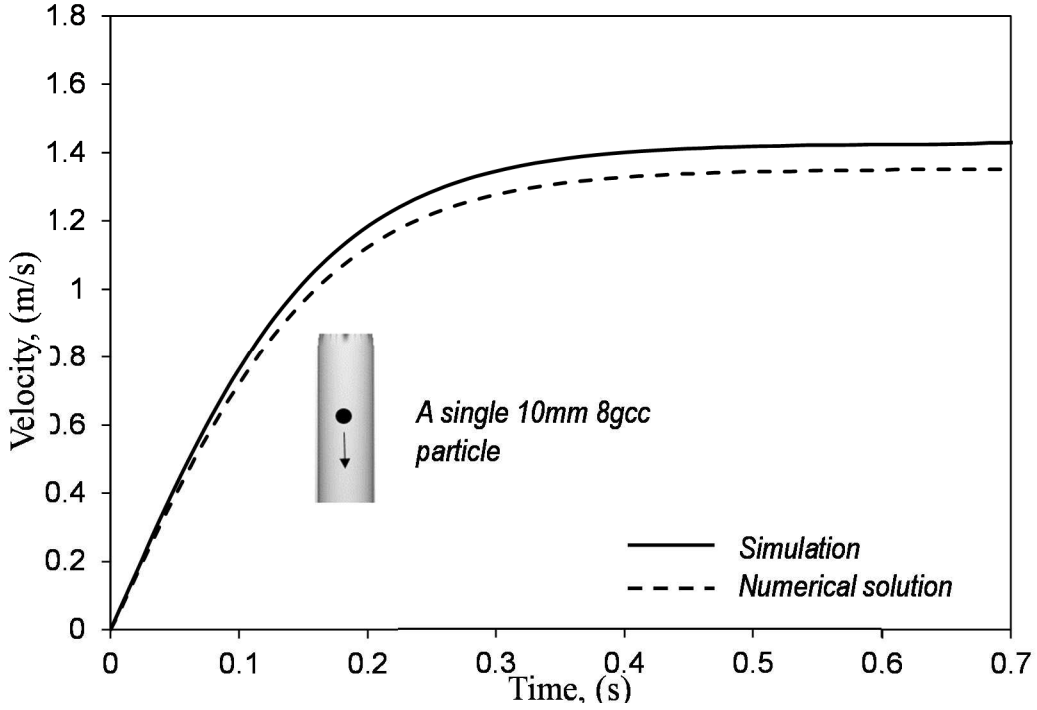

(a)

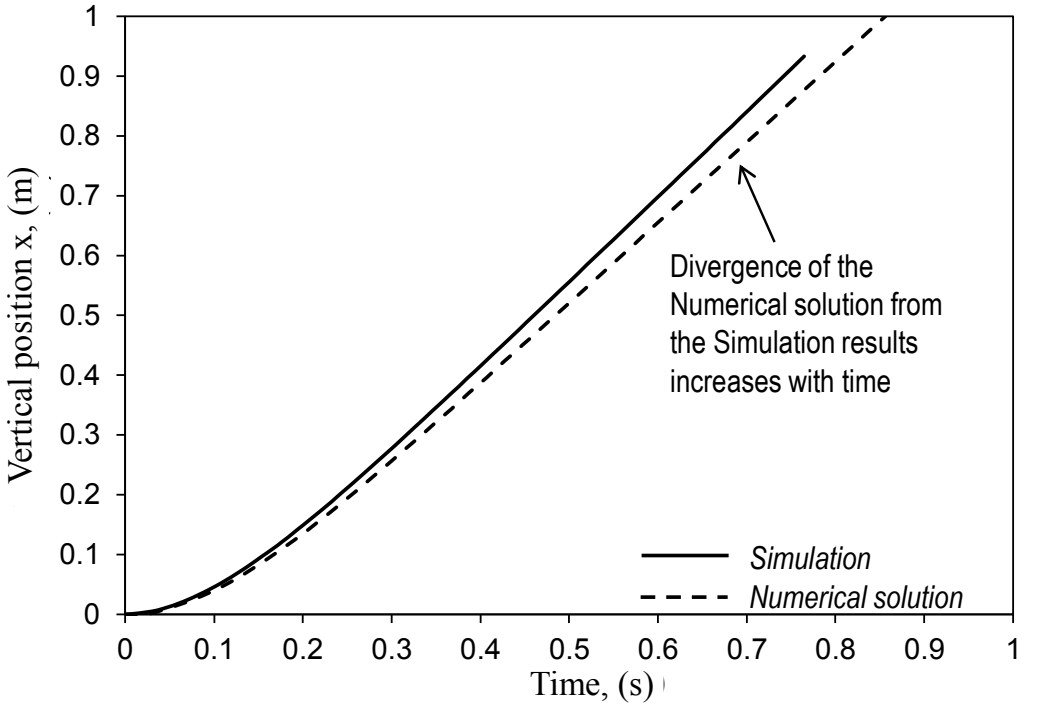

(b)

Figure 4.31 – Comparison of (a) settling velocity (b) particle trajectory (vertical motion) for a single 10 *mm* 8 *gcc* particle in Fluid 1 using Stokes correlation, numerical model and simulation.

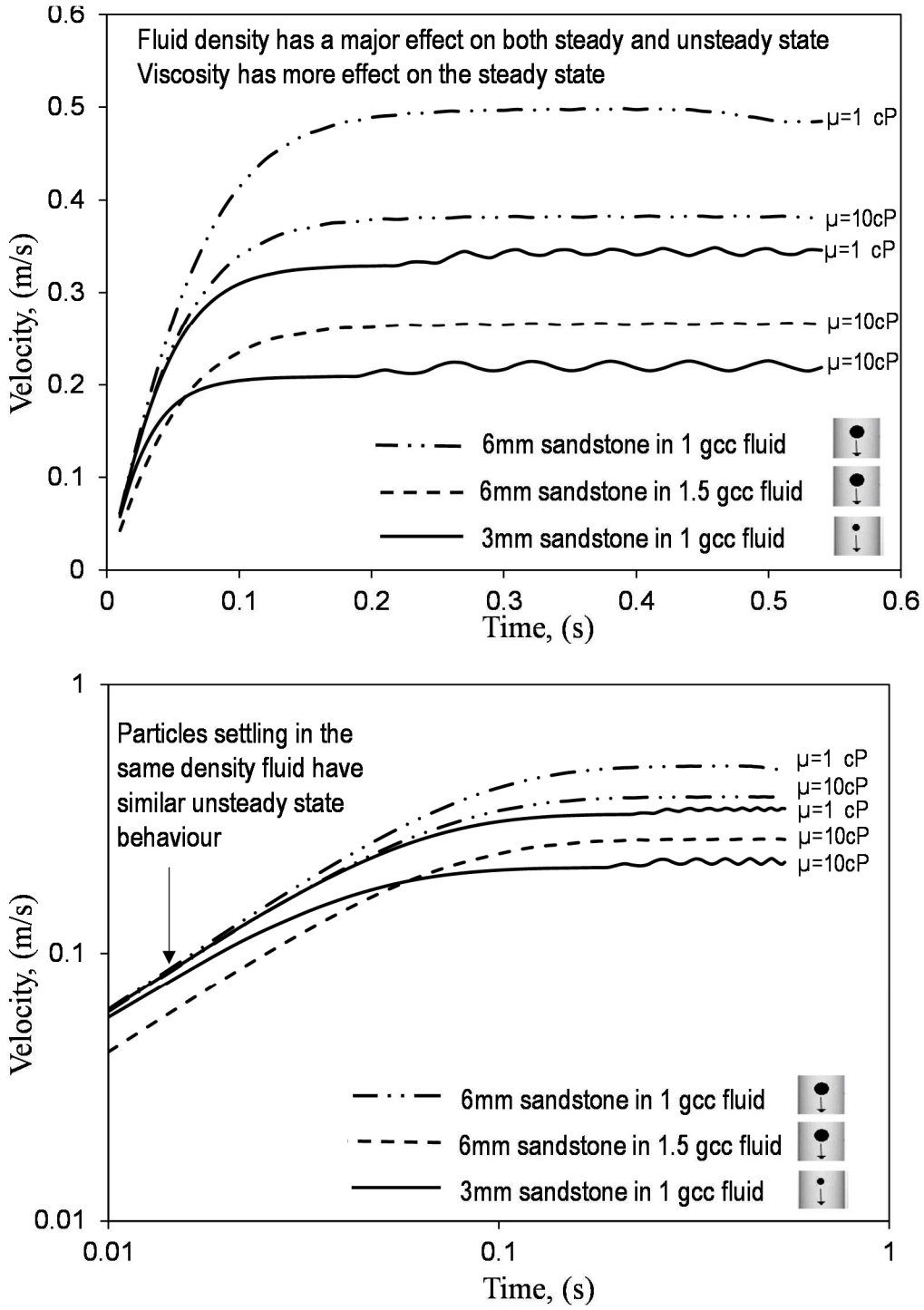

Figure 4.32 – Effect of particle size and fluid density and viscosity on the particle settling velocity using simulation: (a) Cartesian plot (b) log-log plot

4.6 Multiple Particles Analysis

Here, we simulated the motion of a pack of 171 particles of 3 *mm* size and 8 *gcc* density falling in a pipe filled with Fluid 1. From Figure 4.33 which represents different falling stages of the particles pack, clearly shows that the overall shape and height of the pack remains similar with time, however few particles are left behind due to the friction with the wall.

The estimated average velocity of the pack of particles was shown to be very close to the single particle velocity using both simulation and numerical solution of the BBO, even though the simulated velocity was less than that of the single particle, due to the friction particle-to-particle interactions in particle pack model (see Figure 4.34 (a)). Figure 4.34 (b) shows that the trajectory of the pack (the center is the reference point) is also close to the single particle trajectory. Figure 4.35 shows a comparison between the same pack of particles (same concentration) falling in a pipe and in an annulus space. The results show that using the equivalent pipe diameter to simulate the annulus space is a reasonable approach, and the negligible extra friction effect observed is due to additional interaction of the particles with the inner pipe surface of the annulus, which is ignored in the equivalent pipe model.

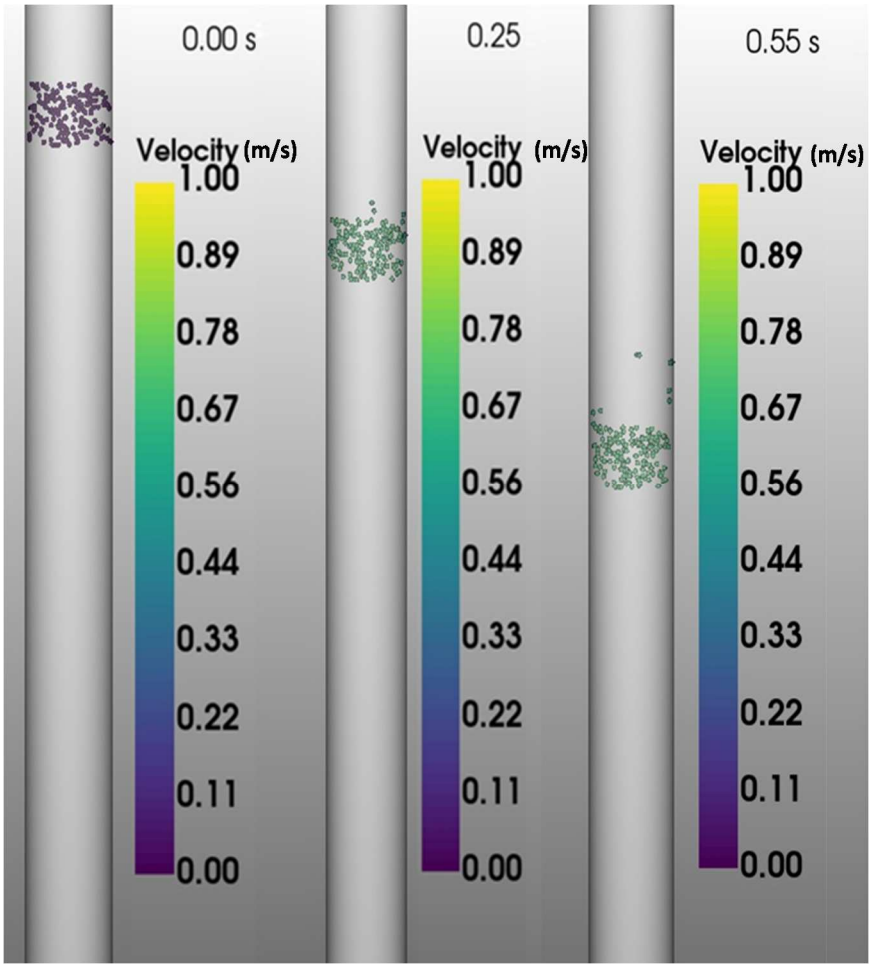

Figure 4.33 – Pack of 3 *mm* 8 *gcc* particles falling in a pipe full with Fluid 1 (total particles in the pack: 171)

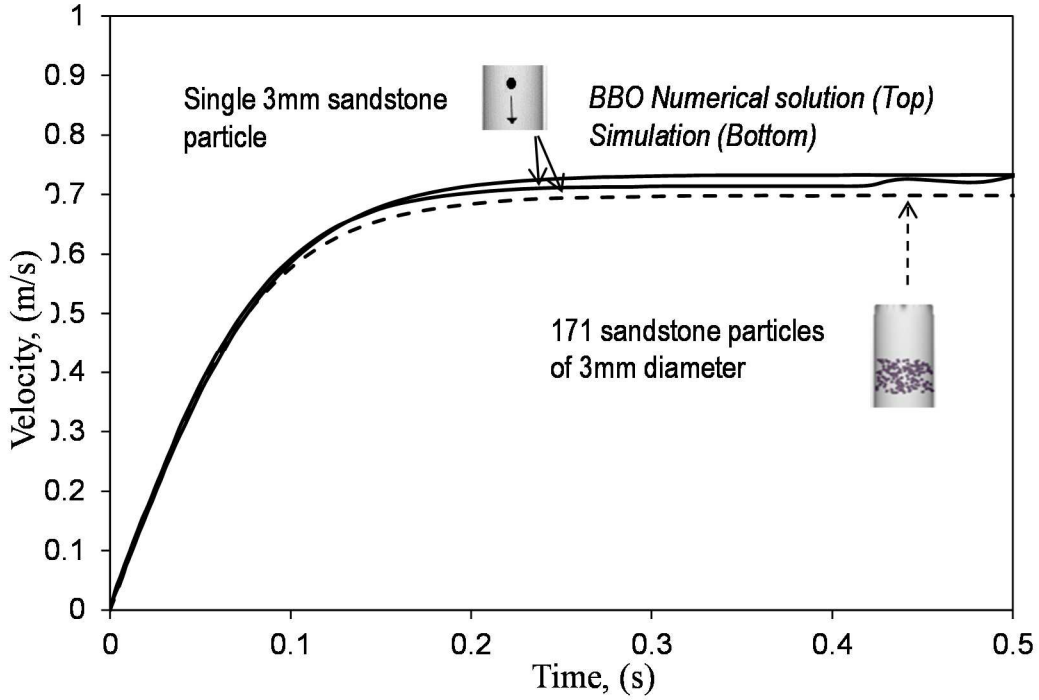

(a)

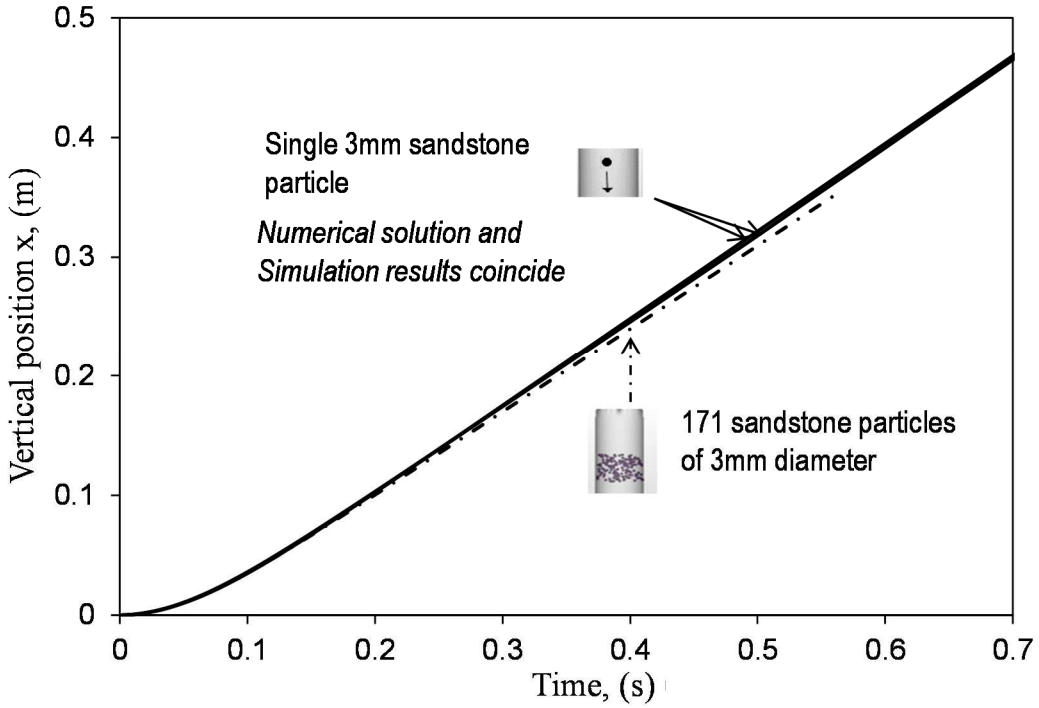

(b)

Figure 4.34 – Comparison of a 3 *mm* 8 *gcc* particles pack (a) average velocity simulation (b) average trajectory simulation with single particle numerical and simulation estimation

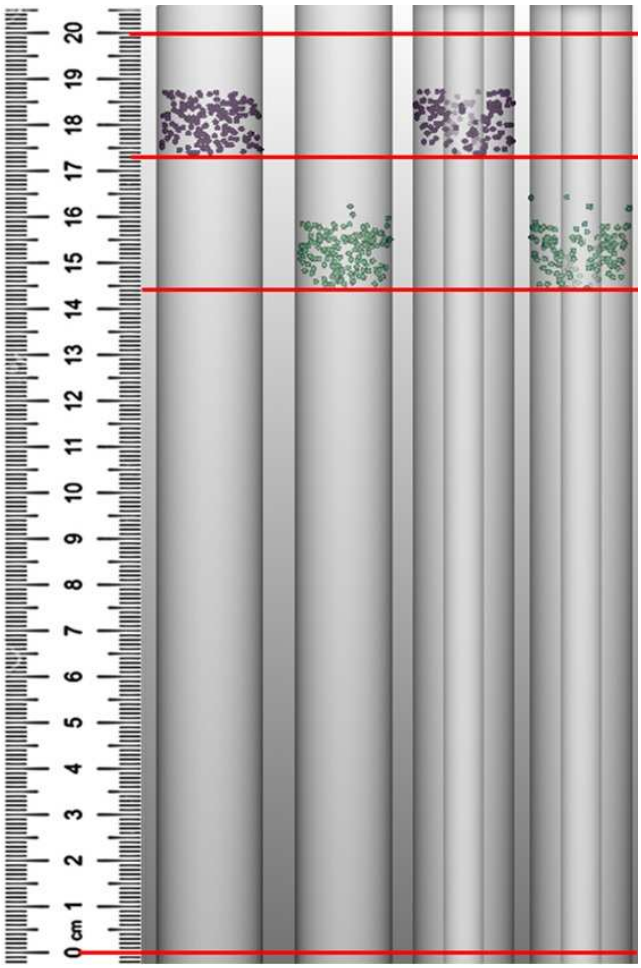

Figure 4.35 – Comparison between the same pack of fluid in Figure 18 (same concentration) falling in a pipe and in an annular space (wellbore while drilling), at t=0.00 s and t=0.25 *s* (scale: 20 *cm* ~ 95 *cm*).

Since the settling velocity tends to stabilize at a constant value after the unsteady state period (terminal settling velocity), the trajectory, which is the differential of the velocity, keeps increasing with a constant slope, therefore we can define the trajectory equation (vertical position x as a function of time t) which is the equation of a straight line. The trajectory equation after reaching the settling velocity is therefore estimated as:

$$x = a \times t + b \tag{4.55}$$

For a single 3 *mm 8 gcc* particle settling in water, the trajectory correlation equation derived from the BBO solution is:

$$x = 0.739 \times t - 0.0511 \quad (4.56)$$

whereas the corresponding results from the simulation is:

$$x = 0.736 \times t - 0.0481 \quad (4.57)$$

For a single 1 *mm 8 gcc* particle settling in water, the trajectory correlation equation derived from the BBO solution is:

$$x = 0.4046 \times t - 0.0145 \quad (4.58)$$

The deposition rate of particles inside an annulus was simulated and compared to the single particle correlations. Figure 4.36 shows a full column of fluid and particles mixture. At t=0 s the system is stationary and at t>0 s, the simulation is run and the particle deposition rate is estimated. The top of the particle pack in the fluid was tracked and the results were compared to the results from correlations (Equation 30 and 31). These results are presented in Table 4.18, which shows that the single particle correlations predict the particles deposition rate (or top of the pack of particles position with time) with good accuracy for a short period of time.

Table 4.18 – Comparison between single particle and multi-particle prediction for 3 *mm* 8 *gcc* particles falling in Fluid 1

	Simulation	Single particle simulation	Single particle BBO solution
Time [s]	0.560	0.560	0.560
Position [m]	0.361	0.36274	0.364
Error [%]	-	0.482	0.827

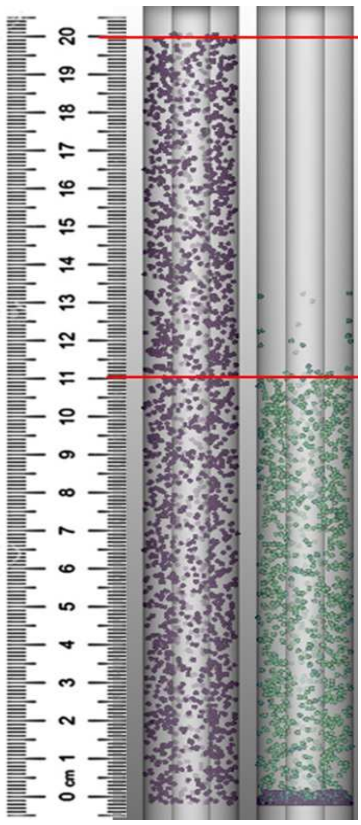

Figure 4.36 – Annulus space of 95 *cm* length filled with 0.5% concentration of 3 *mm* 8 *gcc* particles in Fluid 1, after 0.65 s of simulation, the top of the particles pack is positioned at x=42.75 *cm* (scale: 20*cm*=95 *cm*).

4.7 Heterogeneous Particles Analysis

In this Section, contrary to the previous results presented, we investigate the multi sedimentation process of anhydrite and sandstone particles in a wellbore section. This will help us to better understand the mixing effect of cuttings when we drill different formations and cuttings can be mixed in the wellbore before reaching the surface. This knowledge will help drillers to match the formation mineralogy with correct depths, and geologists to understand the sedimentary rocks' mineralogy mixture during the deposition and basin sedimentation process.

Figure 4.37 shows a combination of similar diameters sandstone and anhydrite particles falling inside an annular space section of 0.95 *m* length. The upper 0.475 *m* section of the wellbore is filled with 1 *mm*, anhydrite particles and the remaining section is filled with 1 *mm*, sandstone particles. The top layers of both sections and the bottom layer of the sandstone particles section

were tracked and their positions were compared to the single particle correlations (Figure 4.38). Also, for simplicity, the single particles dispersed due to the wall friction were not considered in this analysis and only the higher concentration layers were tracked.

Figure 4.39 shows the single particle trajectory prediction for both sandstone and anhydrite for both simulation and BBO numerical model. The results show a disagreement with the single particle prediction based on the BBO numerical model due to particles weight not covered by the BBO assumption. However, the simulation-based prediction predicted the settling time of the layer limits with an error of 0.8%.

The results of arrival times from single particle correlations and simulations are summarized in Table 4.19. Figure 4.40 shows a good correlation between the simulation based single particle settling and the layer limits trajectory (error less than 1%) whereas the prediction based on the BBO numerical solution leads to errors higher than 20% due to the light weight of particles compared to the model assumptions.

Similar study on heavier particles (8gcc) is presented in Appendix A. The results show an amelioration of the application of the single particle BBO numerical model prediction on the multi-particle motion.

Table 4.19 – Multi-particle multi-density sedimentation time comparison with single particle correlations

	Single 1 mm anhydrite		Single 1 mm sandstone		Layers Limit
	Simulation	Numerical	Simulation	Numerical	Simulation
Top Layer 1	5.948	4.649	-	-	5.970
Bottom Layer 1	2.983	2.337	-	-	3.030
Top Layer 2	-	-	3.357	2.598	3.340

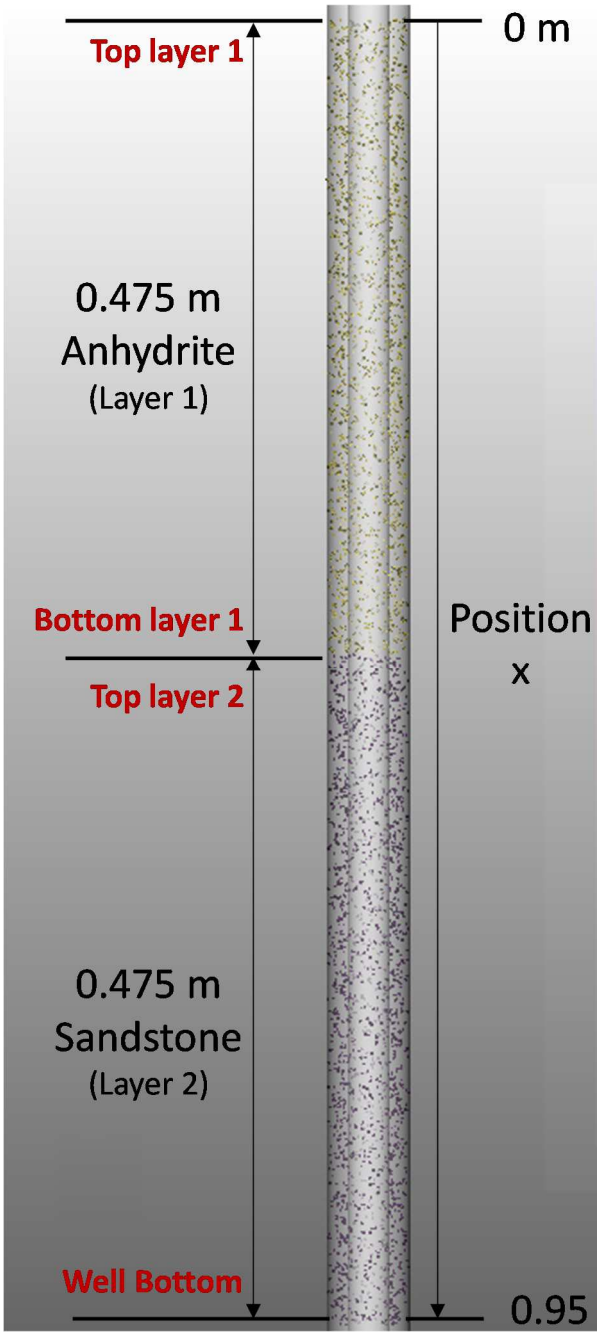

Figure 4.37 – Combination of 1 *mm* sandstone and anhydrite particles falling inside an annulus space section of 0.95 *m* length, anhydrite particles on top with yellow (0.475 *m* section) and sandstone particles at the bottom section in blue (0.475*m* section)

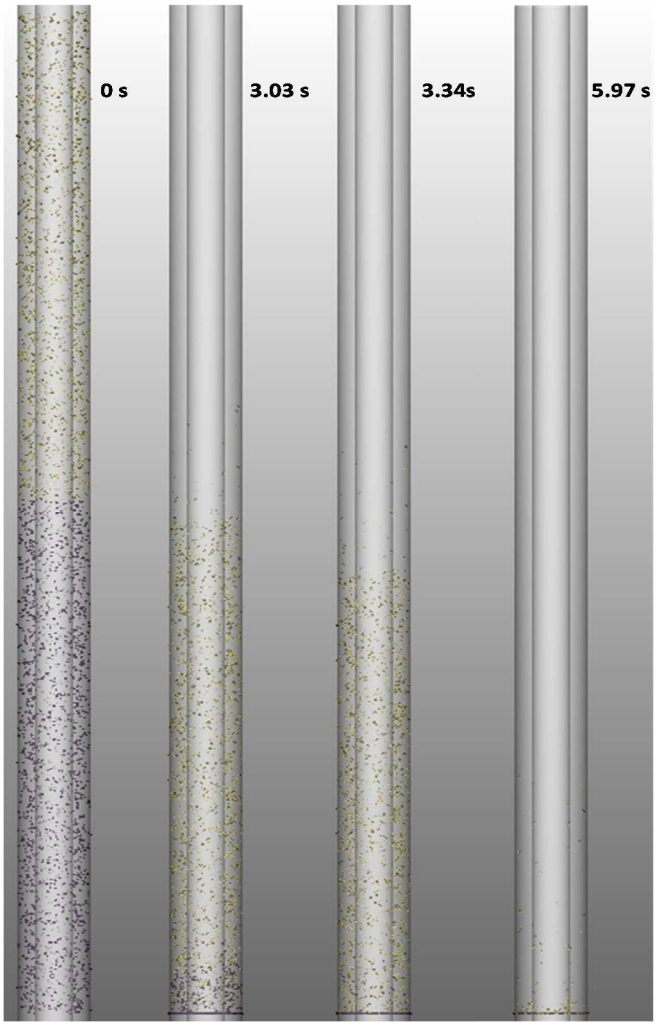

Figure 4.38 – Particles packs limits tracking. From left to right: (1) t=0.00 s, (2) t=3.03 s, the anhydrite particles bottom interface reached the bottom section of the wellbore section, (3) t=3.34 s, the sandstone particles top interface reaches the bottom of the wellbore section, and (4) t=5.97 *s*, the anhydrite particles top interface reaches the bottom of the wellbore section

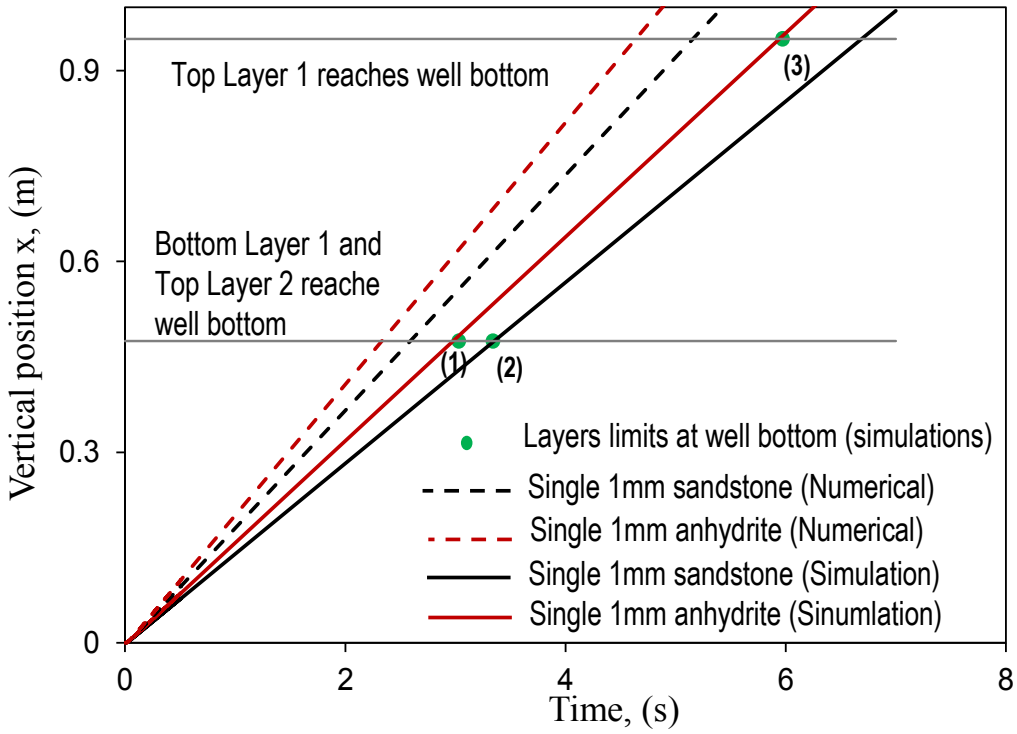

Figure 4.39 – Comparison of a sandstone and anhydrite single particle settling velocity simulation and numerical prediction and multi-particle packs limits motion: (1) anhydrite bottom layer reaches well bottom, (2) sandstone top layer reaches well bottom and (3) anhydrite top layer reaches well bottom

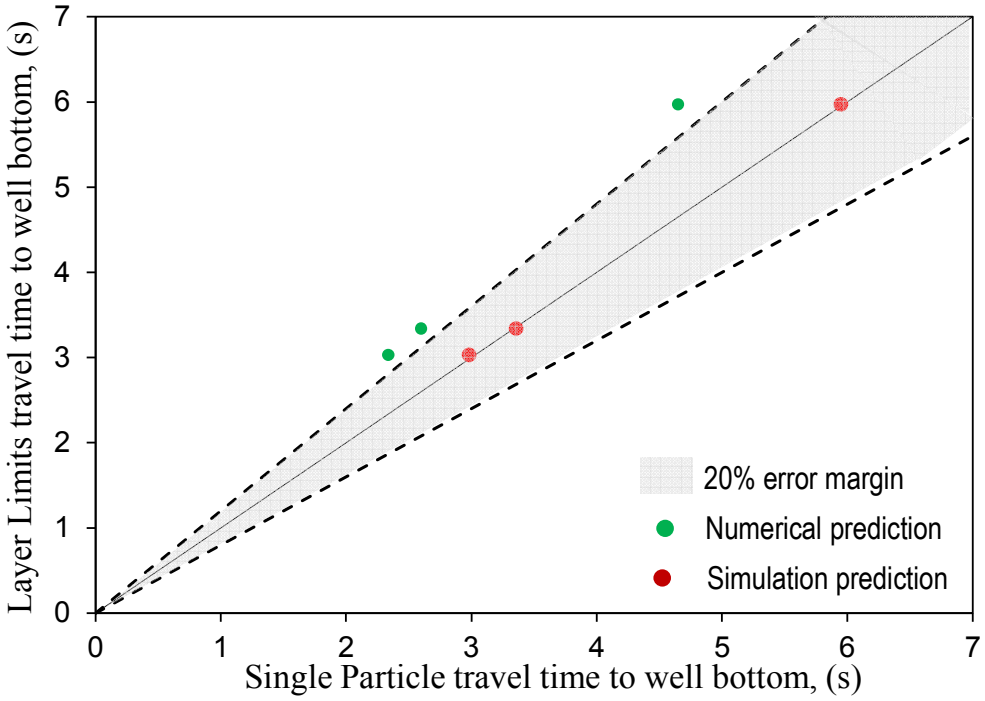

Figure 4.40 – Single particle projection on multi-particles packs limits efficiency

4.8 Summary

In this Chapter analytical models, experiments and numerical simulations were used to estimate the terminal settling velocity of different particles. The results showed that:

1- MFiX software, which works based on Euleurian-Lagrangian model was used in this study as one of the first attempts, to simulate the settling behavior of single particle as well as multiple particles in pipes and wellbore annuli. It was found that this simulator is less time consuming compared to similar software.

2- The BBO numerical solution and the Stokes correlation were found to reasonably predict the particle's motion for particle diameters of less than 3 mm and fluid to particle density ratio higher than 0.38.

3- The simulation results showed that density has a minor effect on the unsteady state behavior of the particles. However, the effect of the fluid viscosity and particle diameter are more pronounced.

4- The prediction correlations obtained from single particle motion models were shown to be able to predict the multi-particle settlement behavior reasonably and present more accurate results than Stokes correlation and BBO equations.

5- The single particle velocity and motion prediction approach can be applied for multiple and mixed sizes particles movement. It is important to understand the mixing phenomena of particles during drilling operation. Single particle settling velocity can be predicted easily using both simulation and analytical mathematical models under certain conditions. The correlations can be projected to real field multiple heterogeneous particles movement prediction.

6- We detect the motion of multi-particles when they are present together. This provides a great knowledge in understanding the cuttings mixing phenomenon when drilling through different formations.

CHAPTER 5

Data Driven Correlations and Graphical Nomograms Developed to Predict Terminal Settling Velocity of Drill Cuttings

5.1 Introduction

Estimation of the terminal settling velocity of solids falling in liquids is critical in many industrial applications such as slurry transportation, mineral processing, oil and gas drilling, and proppants transportation in post-fracking operations. For oil and gas field applications the settling velocity prediction is important for determining the minimum transportation velocity to ensure an optimum cleaning of the drilling cuttings (Ahmed, 2012; Boyou et al., 2019; Busch and Johansen, 2020; Mahmoud et al., 2020; Oseh et al., 2020; Pang et al., 2018; Zhang et al., 2015). The settling velocity allows predicting the profile of cuttings concentration which, in turn, helps to prevent wellbore instabilities and correlate the depth of cuttings as received at the surface (Baldino et al., 2015b). In addition to the lack of enough lifting capacity to transport the drill cuttings to the surface, interruption of the drilling operation causes the cuttings to settle in the drilling mud. Apart from a workover operation to change a drill bit or make a connection, the drilling operation can pause for many other reasons causing the circulation to stop (Agwu et al., 2018; Moreira et al., 2017). If the particle settling in the drilling fluid is not predicted and managed correctly, several operational issues can occur such as stuck pipe, low rate of penetration and wellbore instability

problems (Ahmed and Takach, 2008; Busahmin et al., 2017; Glomstad, 2012; Mohammadsalehi and Malekzadeh, 2011). Another important application of the settling velocity determination in oil and gas industry is to ensure even placement of the proppants in the induced fractures after hydraulic fracturing operations (Bandara et al., 2020; Liu et al., 2021; Wang et al., 2020; Wei et al., 2020b).

Prediction of the settling velocities has been the subject of many past studies, each considered different parameters and presented models with different accuracies and range of applications (Agwu et al., 2018). These models were based on experimental, mathematical, simulation and artificial intelligence approaches (Agwu et al., 2018). The extensive experimental work carried out using cuttings with different shapes resulted in generation of a large data set that can be used for prediction of the particles' velocity in both Newtonian and non-Newtonian fluids (Agarwal and Chhabra, 2007; Agwu et al., 2018; Ahmed, 2012; Baldino et al., 2015b; Buscall et al., 1982; Chhabra et al., 1996; Faitli, 2017; Fidleris and Whitmore, 1961a; Jacobs et al., 2015; Jayaweera and Mason, 1965; Johnsen, 2014; Kelessidis, 2003; Khatmullina and Isachenko, 2016; Nolan, 1970; Peden and Luo, 1987; Sharma and Chhabra, 1991; Wang et al., 2018; Xu et al., 2017). However, the experimental work is time consuming and not cost effective to be repeated for every study, hence, the use of numerical simulations become widespread (Agwu et al., 2018; Blackery and Mitsoulis, 1997; Bush, 1994; Butcher and Jr, 1990; Dazhi and Tanner, 1985; Dhole and Chhabra, 2006; Gavrilov et al., 2017; Ghosh and Stockie, 2015; Gumulya et al., 2014; Missirlis et al., 2001; Prashant and Derksen, 2011; Trofa et al., 2015; Wachs and Frigaard, 2016; Zaidi et al., 2015a). The accuracy of numerical simulations depends on proper calibration of the results with some lab or field data and in many cases their applications are limited to a certain type of particles (e.g. spherical shape) and fluids (Zaidi et al., 2015a). The existence of large data sets offers the

opportunity to apply multiple artificial intelligence (AI) techniques such as artificial neural networks (ANN), support vector machine (SVM) and other generic programming algorithms to predict the settling velocity (Agwu et al., 2020; Barati et al., 2014; Goldstein and Coco, 2014; Kamyab et al., 2016; Li et al., 2014; Rooki et al., 2012; Sadat-Helbar et al., 2009).

Many other studies focused on developing high accuracy correlations (Briens, 1991; Chien, 1994; Kelessidis, 2004; Rushd et al., 2019; Singh, 1969). Majority of these correlations are effective under specific conditions and do not cover all range of Reynolds numbers and different type of particles and fluids and the effect of the wall (see Appendix B). Also, most of the mathematical models available needs an iterative attempt to estimate the settling velocity as both the Reynolds number and the drag coefficient are needed to calculate the settling velocity. This calls the need to develop a new correlation independent of the velocity and applicable in different flow regimes. Also, since wellbores may have different configurations and shapes, the 'hindered' falling velocity (velocity altered due to the presence of wellbore and pipe walls, particle shape or by the presence of other particles) needs to be determined (Kelessidis, 2003; Zaidi et al., 2015b). Several researchers focused on developing wall effect correction factors, but no widely used models have been proposed (see Appendix B)

The graphical nomograms are very convenient, especially for field engineers Nomograms and abaques are two-dimensional diagrams designed to allow or facilitate the approximate graphical calculating (Adams, 1964). A very few researchers tempted to present a simplified graphical procedure for calculating particle settling velocities (Bhargava and Rajagopal, 1992a, 1992b; Cheng, 1997; Rouse, 1938). However, the presented procedures in this trivial literature identify the following shortcomings: 1) limited to a certain type of particles, 2) limited to a certain particle diameters range, 3) some of them are built on a Reynolds dependent (velocity) input, and 4) none

of them consider the hindered velocity. This shows the importance of developing a graphical method with only particle and fluid dependent inputs that predicts the hindered settling velocity.

In this study, we present new correlations and graphical models to predict the terminal settling velocity of solid particles as a function of only the wellbore configuration and the particle and fluid properties. The models are developed based on over 3000 data points collected from the literature and our earlier experimental studies. Comparison of the developed models with numerical simulations presented a good agreement, which shows the applicability of the new models for a wide range of Reynold numbers.

5.2 Materials and Methods

5.2.1 Experimental data

The dataset used for developing the models for spherical particles in this study was obtained from our past laboratory work (see Appendix B) and the work of other researchers (Fidleris and Whitmore, 1961a, 1961b) with a total of over 3000 data points (dataset 1). 55 data points were left for validation purpose. A second dataset from the work of (Song et al., 2017), including a total of 337 data point, was used for developing the model for non-spherical particles, including a total of 337 data point, was used for particle shape correction. 282 data points were used for correlation development and 55 data was left for validation purpose (dataset 2). Dataset 1 experiments were based on spherical particles, however, dataset 2 experiments were based on non-spherical particles.

A third dataset of 50 data was generated using MfiX simulation with random particle and fluid properties to validate both the simulator and the developed models (dataset 3).

Finally, dataset 4 was obtained from the work of (Bourgoyne, 1991), including a total of 688 data point. This dataset was used for developing the model for non-spherical particles settling in infinite medium.

A summary of data statistics for the datasets 1 and 2 is presented in Appendix B.

Dataset 1 and 3 were compiled into two input parameters (a non-dimensional fluid and particle properties dependent parameter and the particle-to-pipe diameter ratio) and one output of Reynolds number.

Dataset 2 was compiled into three input parameters. It does not contain the particle-to-pipe diameter ratio, however, in addition to the non-dimensional fluid and particle properties dependent parameter it includes two new input parameters which are the particle sphericity and shape factor to consider the shape irregularity of the particle. The output parameter is the Reynolds number.

Dataset 4 was compiled into two input parameters (a non-dimensional fluid and particle properties dependent parameter and the particle's sphericity) and one output of Reynolds number.

5.2.2 Numerical Simulation

We used MfiX software in this study. Particle-In-Cell (PIC) multiphase model in MFiX software, is a Lagrangian-Eulerian simulation. The model considers the fluid phase as a continuum while assigning parcels to represent groups of real particles. This approach helps to reduce computational time and cost (Badrouchi and Rasouli, 2020a).

MfiX employs a parcel-based approach. This approach is also known as computational/notional/nominal particles based approach (Strack and Cundall, 1978). Values between Eulerian cell centers, face cell centers, and parcel position are managed through

interpolation operators. MFiX-PIC combines bi-linear operators in each axial direction (Clarke and Musser, 2020).

The fluid–phase governing equations for mass and momentum conservation are similar to those in traditional fluid–phase CFD but with additional coupling terms due to drag from the solids–phase. The solids-phase is modeled using discrete particles.

Physical boundaries are defined by the intersection of the Eulerian grid with a STL (stereolithographic CAD file). Newtonian interaction with boundaries is discretely calculated (Clarke and Musser, 2020).

The simulation serves in this study as a cross-validation. Firstly, to generate a new dataset which is hard to obtain by lab experiments and validate both the correlations and graphical methods. Secondly, to validate the software in drilling applications.

5.2.3 Correlation Models

Fidleris and Whitmore (1961a) used their experimental data to define a wall factor correction equation in the form of two non-dimensional quantities dependent on the terminal velocity:

Reynolds number:

$$Re = \frac{\rho_f v_{sl} d_p}{\eta} \tag{5.59}$$

and a resistance coefficient:

$$\psi = \frac{4g(\rho_p - \rho_f)d_p}{3\rho_f {v_{sl}}^2} \tag{5.60}$$

where g is the acceleration of the gravity, ρ_p and ρ_f are the particle and fluid densities, respectively, d is the particle diameter, v_{sl} is the terminal settling velocity and η is the coefficient of viscosity.

The problem with the reported entities in Eq. (3.1) and (5.60) is that they are both velocity dependent, hence cannot be used for velocity prediction.

The first step is to relate the terminal settling velocity to an entity depending only on the particle and fluid property. A new non-dimensional entity is proposed in this work as:

$$\psi' = \psi . Re^2 = \frac{4g(\rho_p - \rho_f)\rho_f d^3}{3\eta^2} \tag{5.61}$$

If the results of ψ' and Re are plotted logarithmically, to respond to skewness toward large values (since *Re* ranges from less than 0.001 to higher than 10,000), for each particle-to-pipe diameter ratio (d/D), a trend will be observed. A polynomial trend line can illustrate the fluctuations in the data values.

In order to calculate the hindered velocity due to the wall effect, a wall effect factor ($WF = v/v_\infty$) is defined, as the ratio of the hindered velocity v over the velocity in an infinite medium v_∞ when $d/D \to 0$. The velocity can be estimated using either a correlation or a graphical illustration (nomogram) representing the relationship between Re, d/D and WF.

To calculate the hindered velocity due to the particle irregular shape, another correlation was proposed using dataset 2. We define a non-dimensional parameter, ψ'', dependent of the particle shape factors, φ, the sphericity (ratio of the diameter or size length of the particle over the equivalent sphere diameter) and α, the area ratio (ratio of the equivalent sphere area over particle's projected area in the settling direction). $\psi'' = \psi' . \varphi^a . \alpha^b$ and Re are plotted logarithmically and a

polynomial interpolation trend line can be fit to the data. The parameters a and b are two constants to be defined using a solver algorithm to minimize the error.

Besides validation using new experimental and simulation data, the curve fitting criteria for both correlations is to ensure a correlation coefficient R^2 close to 1 and a root mean square error $RMSE$ close to zero. The workflow to calculate the particle's velocity for the spherical and non-spherical particles and the wall effect are summarized here:

For spherical particles (using dataset 1):

1) Calculate ψ' and Re
2) Plot $Log(\psi')$ and $Log(Re)$ for each d/D
3) Identify the trend of data
4) Find the polynomial order matching the fluctuations and bends of the data for $d/D \rightarrow 0$ (infinite medium settling velocity)
5) To find the infinite medium terminal settling velocity, v_∞:
   - Replace ψ' (specific for a particle and fluid) in the correlation obtained in step 4 to find $Log(Re)$ hence, Re
   - Multiply the calculated Re by $\frac{\eta}{\rho_f d_p}$, the infinite medium terminal settling velocity, v_∞

For wall effect correction (using dataset 1):

1) To find the hindered terminal settling velocity (wall effect), v:
   - Plot $WF = f(Log(Re), d/D)$
   - Read the WF for a specific $Log(Re)$ and d/D
   - Multiply v_∞ by WF

For non-spherical particles (using dataset 2):

It is important to note that Song et al. (2017) did not perform a sensitivity analysis on the d/D ratio, hence, the generated correlation is approximate and the wall effect correction cannot be applied.

1) Calculate ψ' and Re
2) Plot $Log(\psi')$ and $Log(Re)$
3) Identify the trend of data
4) Set an initial value of a and b (e.g. 0.5 and 0.5)
5) Find the polynomial order matching the fluctuations and bends of the data
6) Use the polynomial in step 5 and calculate Re^*
7) Calculate the $RMSE(Re, Re^*)$
8) Run the solver algorithm to define a and b until $RMSE(Re, Re^*)$ is minimized to a value close to 0

5.2.4 Graphical Methods

Another objective of this study was to present a graphical nomogram to facilitate the prediction of the hindered settling velocity. As explained in the introduction section, models presented in the literature are either limited to some property and flow regime ranges or needs a tedious iterative calculation to predict the velocity.

Using only the particle and fluid and d/D ratio and the sphericity of the particle φ as input data, the developed charts should be able to predict the hindered terminal settling velocity. Here, we present two methods.

Method 1: calculate the wall effected hindered velocity

1) Plot a nomogram of $Log(\psi')$ and $Log(Re)$ for different d/D ratios

2) Project a new $Log(\psi')$ on a specific d/D line and read $Log(Re)$
3) Multiply Re by $\frac{\eta}{\rho_f d_p}$ to find the hindered terminal settling velocity, v
4) To calculate the wall effect
   - Project $Log(\psi')$ on the reference line ($d/D \sim 0$) and read v_∞
   - Use $WF = v/v_\infty$

Method 2: calculate the wall effect factor and infinite terminal velocity

1) Plot a nomogram of $Log(\psi')$ for $d/D \sim 0$ (reference line: infinite medium settling) on a first vertical axis, $1/WF$ on a second vertical axis for different d/D ratios and $Log(Re_\infty)$ in the horizontal axis
2) Project a new $Log(\psi')$ on the reference line and read $Log(Re_\infty)$
3) Multiply Re_∞ by $\frac{\eta}{\rho_f d_p}$ to find the infinite medium terminal settling velocity, v_∞
4) Project the intersection of $Log(\psi')$ on the Reference Line on the specific $\frac{d}{D}$ line and read $\frac{1}{WF}$
5) Calculate Re using $Log(Re_\infty) = Log(Re.1/WF) \rightarrow Log(Re) = Log(Re_\infty) - Log(1/WF)$
6) Multiply Re by $\frac{\eta}{\rho_f d_p}$ to find the hindered settling velocity, v

Method 3: calculate the sphericity effected infinite medium velocity

It is important to note that Bourgoyne (1991) unlike Song et al. (2017) did their experiments in an infinite medium $d/D \sim 0$. Hence, a nomogram to predict the infinite medium terminal settling velocity for non-spherical particles can be generated.

1) Plot a nomogram of $Log(\psi')$ and $Log(Re)$ for different φ

2) Project a new $Log(\psi')$ on a specific φline and read $Log(Re)$

3) Multiply Re by $\frac{\eta}{\rho_f d_p}$ to find the infinite medium terminal settling velocity, v_∞

4) To consider the wall effect, use the nomogram from method 2 to calculate the wall factor

5) Same process in method 2 steps 3, 4, 5 and 6.

5.3 Results and Discussion

5.3.1 Correlation Models

Following the steps described in the correlation models development section, the experimental results from dataset 1 for a number of d/D ratios, were plotted in the form of two non-dimensional parameters $Log(\psi')$ and $Log(Re)$ as presented in Figure 5.41. It is clear from Figure 5.41 that the retarding wall effect decreases with the Reynolds number from laminar to turbulent regime. This effect has the tendency to reduce at turbulence.

The main step is to relate the settling velocity of the particle (Re), to the non-dimensional fluid-particle parameter (ψ') for an infinite medium ($d/D < 0.05$). The results are plotted in Figure 5.42 and a polynomial interpolation fit is defined with a correlation coefficient $R^2 = 1$ and a Root Mean Square Error $RMSE = 0.01$.

The developed correlation for the Reynolds number as a function of the fluid-particle non-dimensional parameters is:

$$Log_{10}(Re) = 0.0018Log_{10}(\Psi')^3 - 0.0573Log_{10}(\Psi')^2 + 1.0366Log_{10}(\Psi') - 1.3519 \qquad (5.62)$$

From this correlation we can define the infinite medium terminal settling velocity of spherical particles as:

$$v_{sl} = \frac{\eta}{\rho_f d} 10^{0.0018.\, Log_{10}(\psi')^3 - 0.0573 Log_{10}(\psi')^2 + 1.0366 Log_{10}(\psi') - 1.3519} \tag{5.63}$$

Or in a more simplified form as:

$$v_{sl} = 0.04473. \frac{\eta}{\rho_f d}. \psi'^{1.0366}. 10^{0.0018.\, Log_{10}(\psi')^3 - 0.0573 Log_{10}(\psi')^2} \tag{5.64}$$

Applying a similar approach for non-spherical particles and following the steps described in the correlation model development section, the constants in ψ'' equation were found as $a = 0.170$ and $b = 1.062$. Figure 5.43 shows the correlation, with a correlation coefficient $R^2 = 0.9988$ and $RMSE = 0.02$.

The developed correlation for the Reynolds number Re as a function of the fluid-particle shape dependent non-dimensional parameters ψ'' is:

$$Log_{10}(\mathrm{Re}) = -0.0049 Log_{10}(\Psi'')^3 - 0.0281 Log_{10}(\Psi'')^2 + 1.0032 Log_{10}(\Psi'') - 1.353 \tag{5.65}$$

From this correlation we can define the shape corrected settling velocity of non-spherical particles as:

$$v_{sl} = \frac{\eta}{\rho_f d} 10^{-0.0049 Log_{10}(\Psi'')^3 - 0.0281 Log_{10}(\Psi'')^2 + 1.0032 Log_{10}(\Psi'') - 1.353} \tag{5.66}$$

Or in a more simplified form as:

$$v_{sl} = 0.04436. \frac{\eta}{\rho_f d}. \frac{\psi''^{1.0032}}{10^{0.0049 Log_{10}(\Psi'')^3 + 0.0281 Log_{10}(\Psi'')^2}} \tag{5.67}$$

The correlation 1 (see Eq. (5.64)) was used to calculate the terminal settling velocity and the data were compared to the MfiX simulation velocities (dataset 3). Figure 5.44 shows a good agreement between the two methods with a $RMSE = 0.003$.

Similarly, the 55 data points from dataset 2 were used to validate correlation 2 (see Eq. (5.67)). Figure 5.45 shows the correlation between the experimental validation set and correlation 2, with a $RMSE = 0.07$.

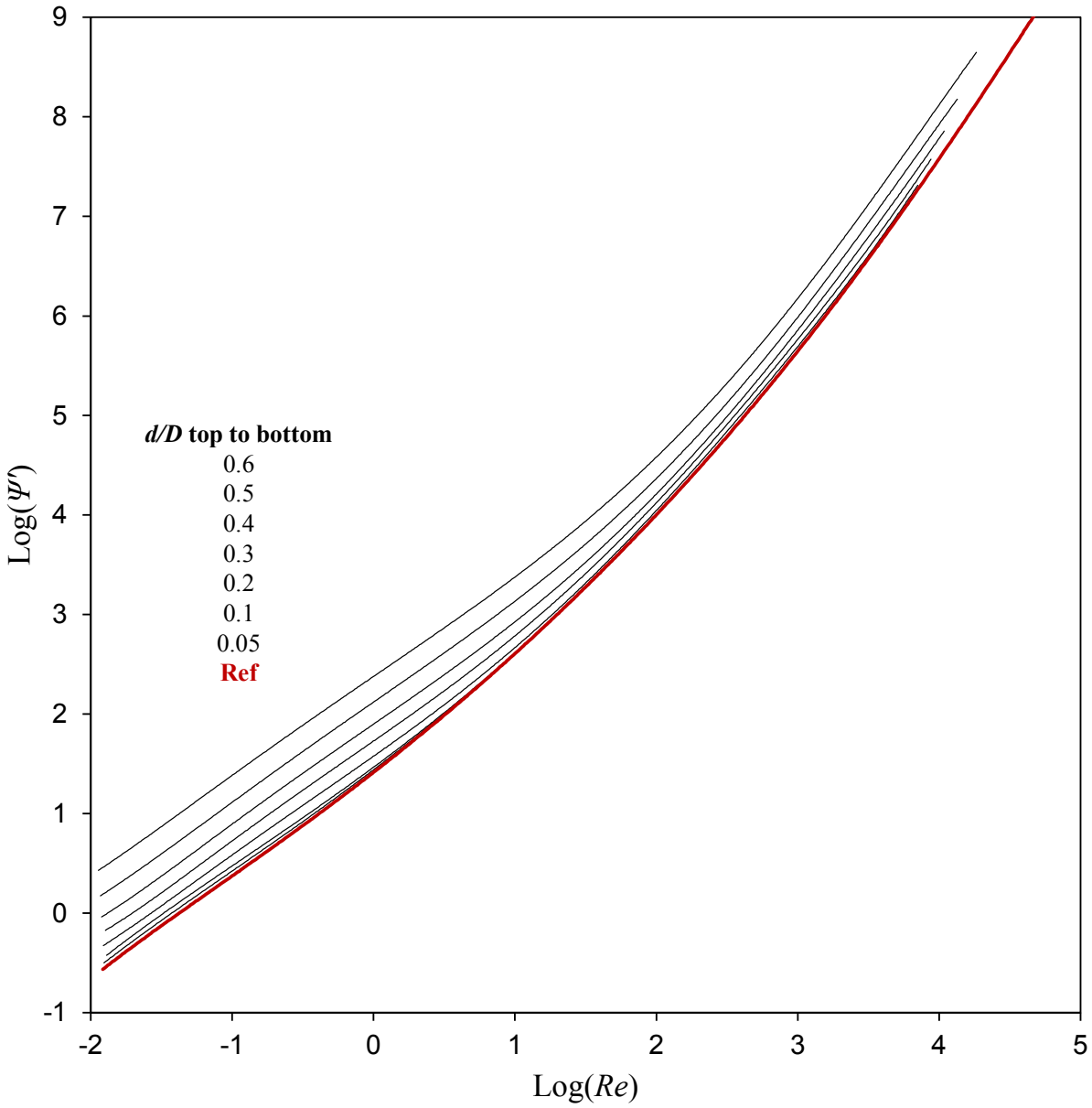

Figure 5.41 – Non-dimensional particle-fluid coefficient versus Reynolds number curves for spheres falling in cylindrical containers

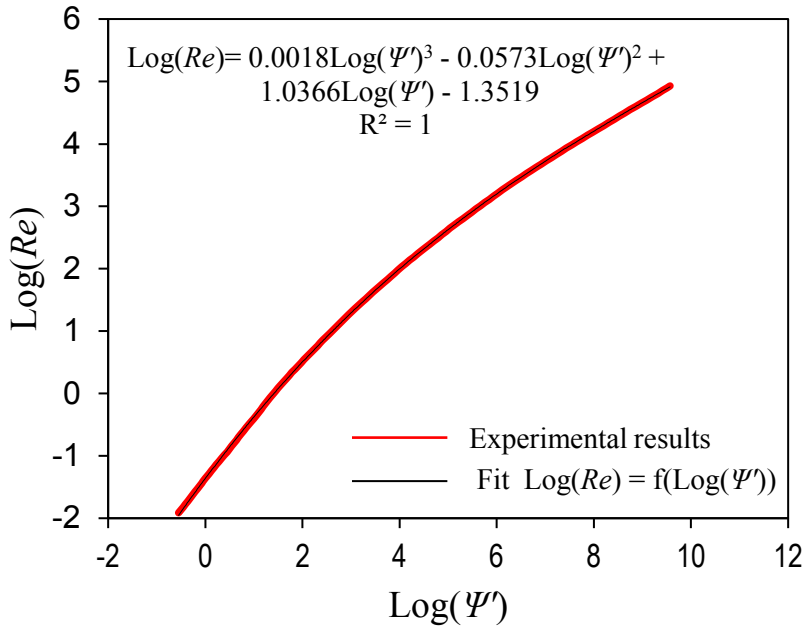

Figure 5.42 – Correlation between ψ' and Re for any spherical particle settling in a random fluid

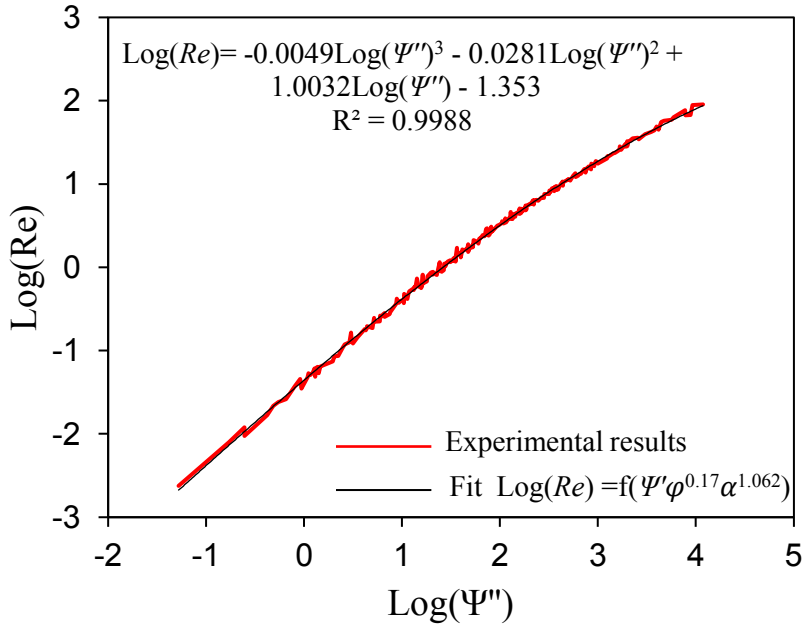

Figure 5.43 – Correlation between $\psi'.\varphi^{a}.\alpha^{b}$ and Re for any irregular shaped particle settling in a random fluid

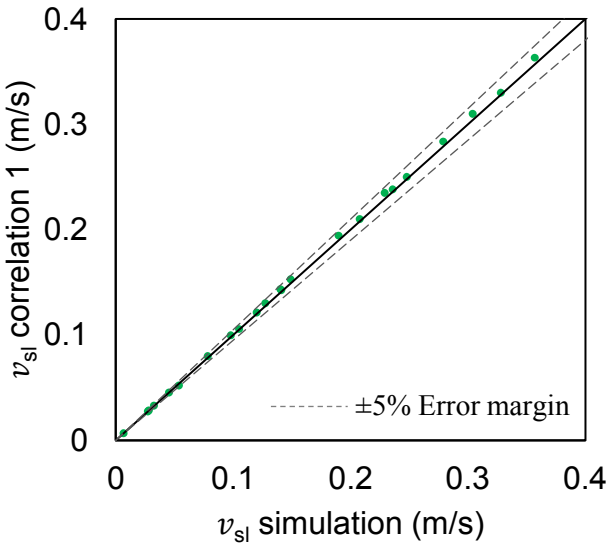

Figure 5.44 – Comparison of the correlation 1 (Eq. (5.64)) and MfiX simulation (dataset 3) of the settling velocity of spherical particles

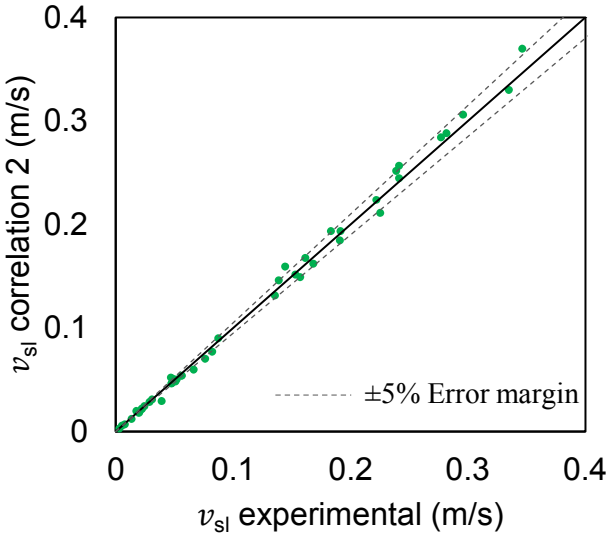

Figure 5.45 – Comparison of the correlation 2 (Eq. (5.67)(5.64)) and the validation experimental data (dataset 2) of the settling velocity of non-spherical particles

5.3.2 Graphical Methods

Spherical Particles

Following the steps described in the graphical methods development section, two nomograms are proposed for spherical particles.

The first nomogram (Nomogram 1), shown in Figure 5.46, allows to directly predict the hindered terminal settling velocity using particle and fluid data (ψ'). The nomogram is divided in two sections depending on the range of the non-dimensional particle-fluid parameter ($-1 < \text{Log}(\psi') < 3$ and $3 < \text{Log}(\psi') < 7$).

The second nomogram (Nomogram 2), shown in Figure 5.47, relates the infinite medium terminal settling velocity to the wall factor.

Both nomograms are straight forward to use (see described steps in the graphical methods development section).

Two illustrative examples for the same particle and fluid properties are presented in Figure 5.48 and Figure 5.49.

For a particle with $Log(\psi') = 4$ falling in pipe with $d/D = 0.3$:

Nomogram 1:

- By projecting $Log(\psi') = 4$ on the $d/D = 0.3$ curve line the read logarithmic of the hindered Reynolds number is 1.93
- By projecting $Log(\psi') = 4$ on the reference curve line the read the logarithmic of the infinite medium Reynolds number is 2.05
- Thus, the wall factor can be calculated as:

  Knowing

$$Log(Re_\infty) = Log(Re.1/WF) \rightarrow Log(Re) = Log(Re_\infty) - Log(1/WF) \quad (5.68)$$

  then,

$$1/WF = 10^{Log(Re)-Log(Re_\infty)} \tag{5.69}$$

- Hence, $1/WF = 10^{2.05-1.93} = 1.31$

Nomogram 2:

- By projecting $\psi' = 4$ on the reference curve line, the read value of the logarithmic of the infinite medium Reynolds number is 2.05
- By projecting vertically the intersection of $Log(\psi') = 4$ and the reference curve line on the $d/D = 0.3$, the read value of the wall effect factor is 1/1.31
- Thus, logarithmic of the hindered Reynolds number can be calculated as:

  From Eq.(5.67), $Log(Re) = 2.05 - Log(1.31) = 1.93$

It is clear from the illustrative examples that the both nomograms provide the same prediction of all infinite and hindered Reynolds number (settling velocity) and wall effect.

Comparison with Simulation and correlation 1:

For a 1 mm particle with density of 1770 kg/m^3 falling in and pipe of diameter $D = 0.023\ m$ filled with water (1000 kg/m^3 density and 0.001 Pa.s), the corresponding logarithmic of the non-dimensional particle-fluid parameter is $Log(\psi')$~4. Since $d/D < 0.05$, we can consider the medium as infinite.

The results show that the monogram is the most accurate method, followed by the simulation and the correlation. As summarized in Table 5.20, all methods were in great agreement with the experimental results.

Table 5.20 – Comparison summary of different prediction methods to experimental results

	ρ_p (kg/m^3)	D (m)	ρ_f (kg/m^3)	η (Pa.s)	$Log(\psi')$ -	Re -	v_{sl} (m/s)	Error -
Experimental	1770	0.001	1000	0.001	4.0031	102.331	0.102	-
Correlation 1					4.0031	99.000	0.099	2.941
Simulation					4.0031	100.000	0.100	1.960
Nomograms 1 and 2					4.000	102.329	0.102	0.001

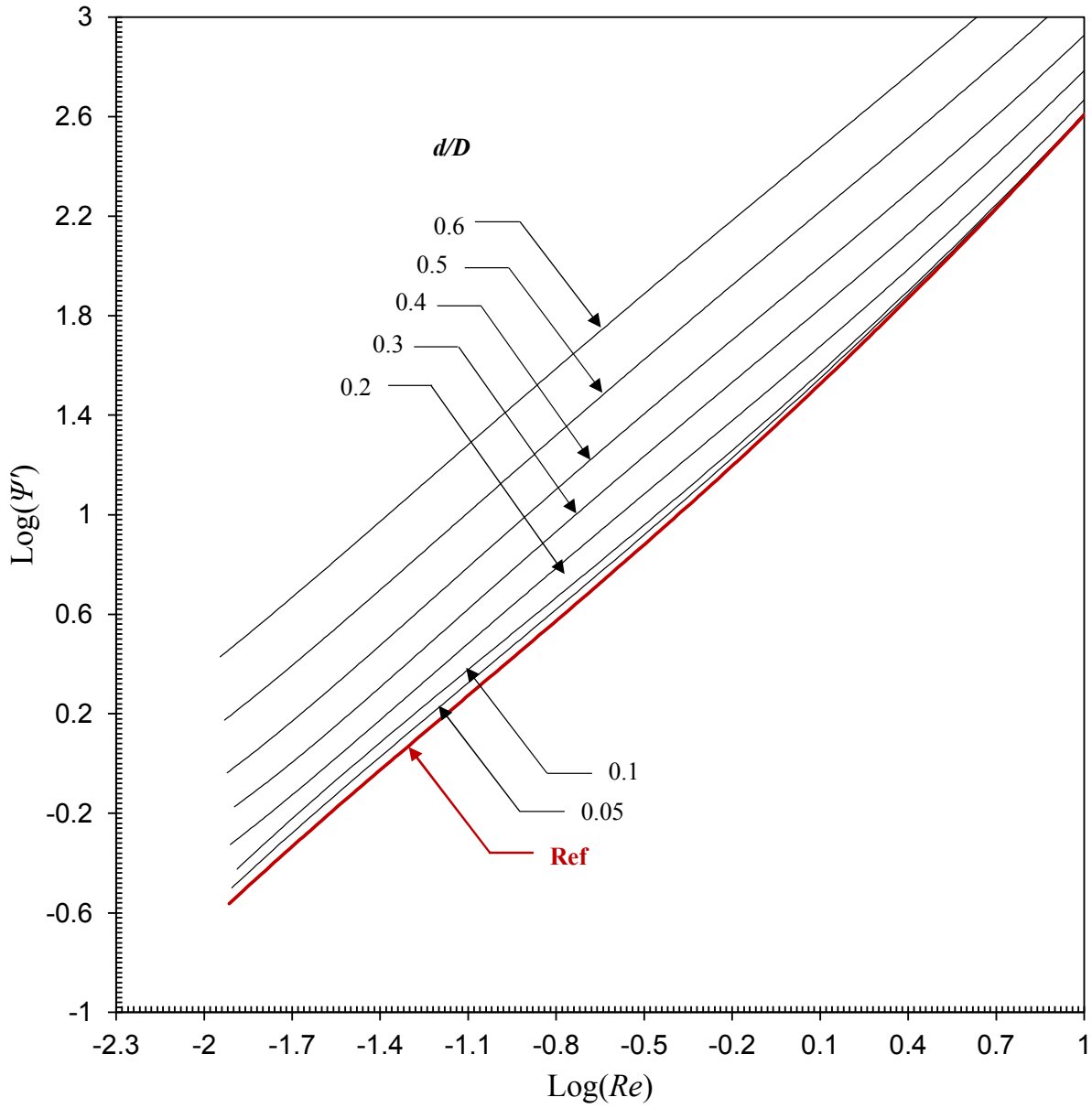

(a)

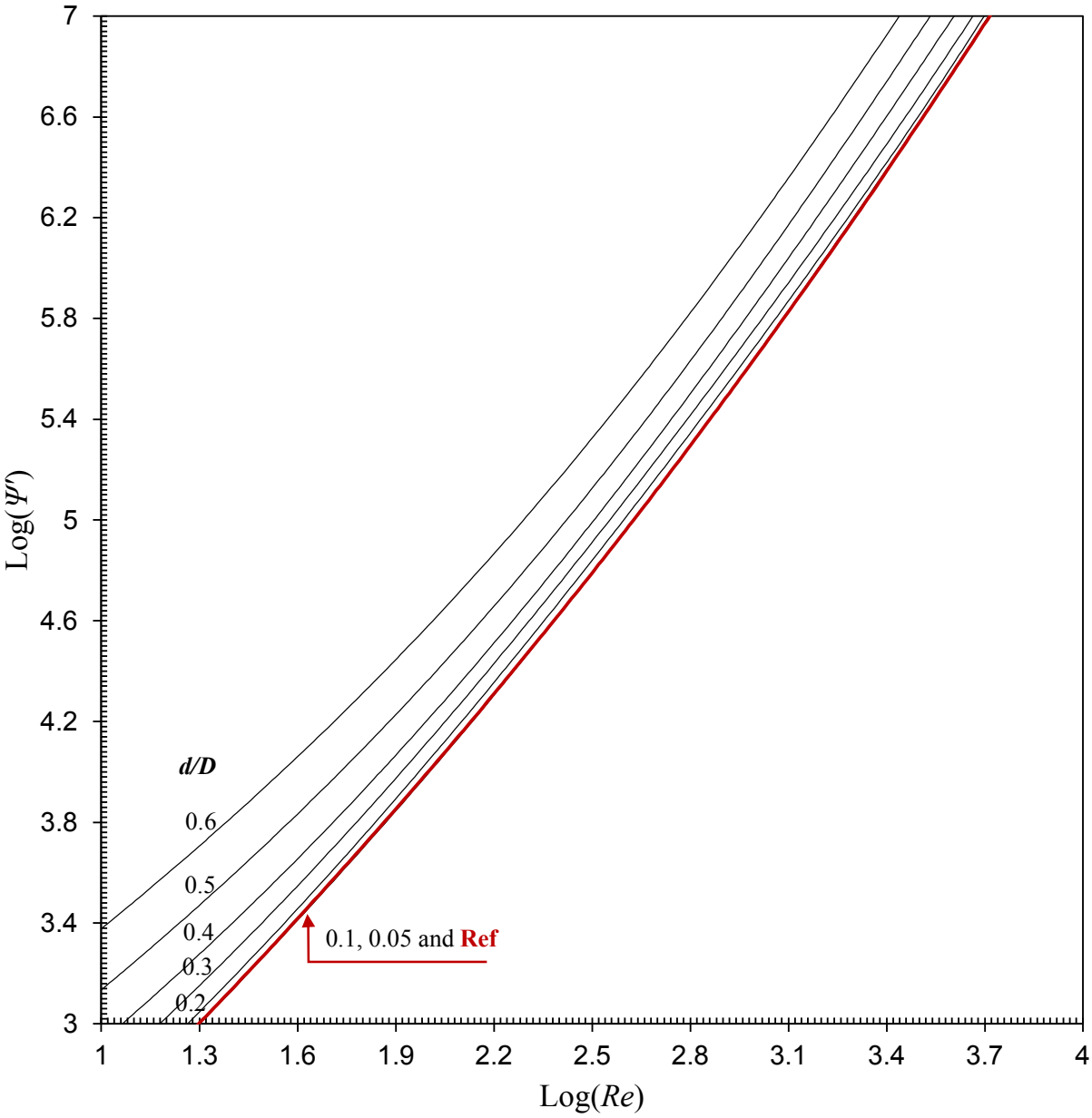

(b)

Figure 5.46 – ψ' - Re nomograms for spherical with (a) $-1 < Log(\psi') < 3$ and (b) $3 < Log(\psi') < 7$

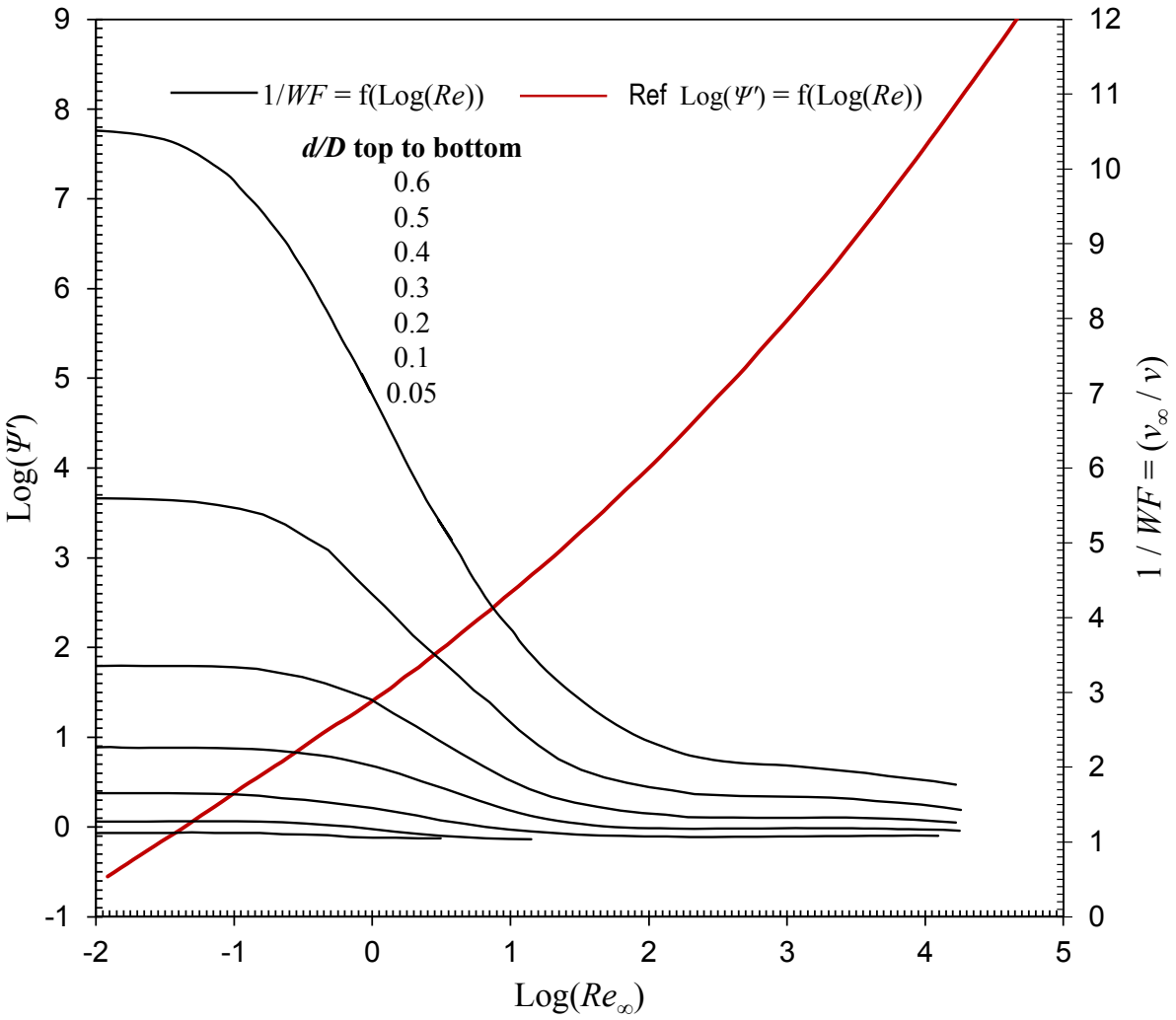

Figure 5.47 – ψ' - Re - WF nomogram

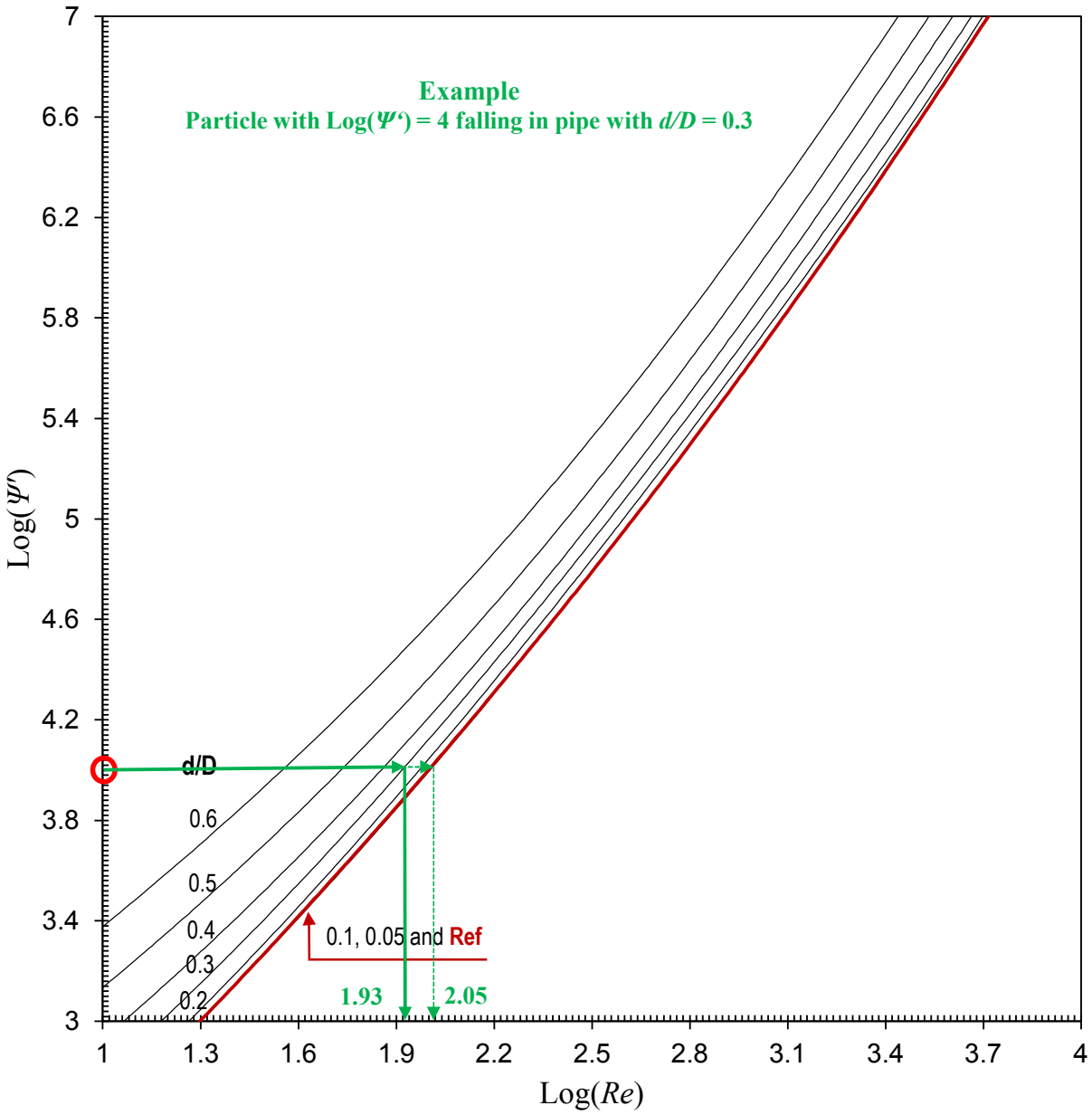

Figure 5.48 – Illustrative use example of ψ' - Re nomograms

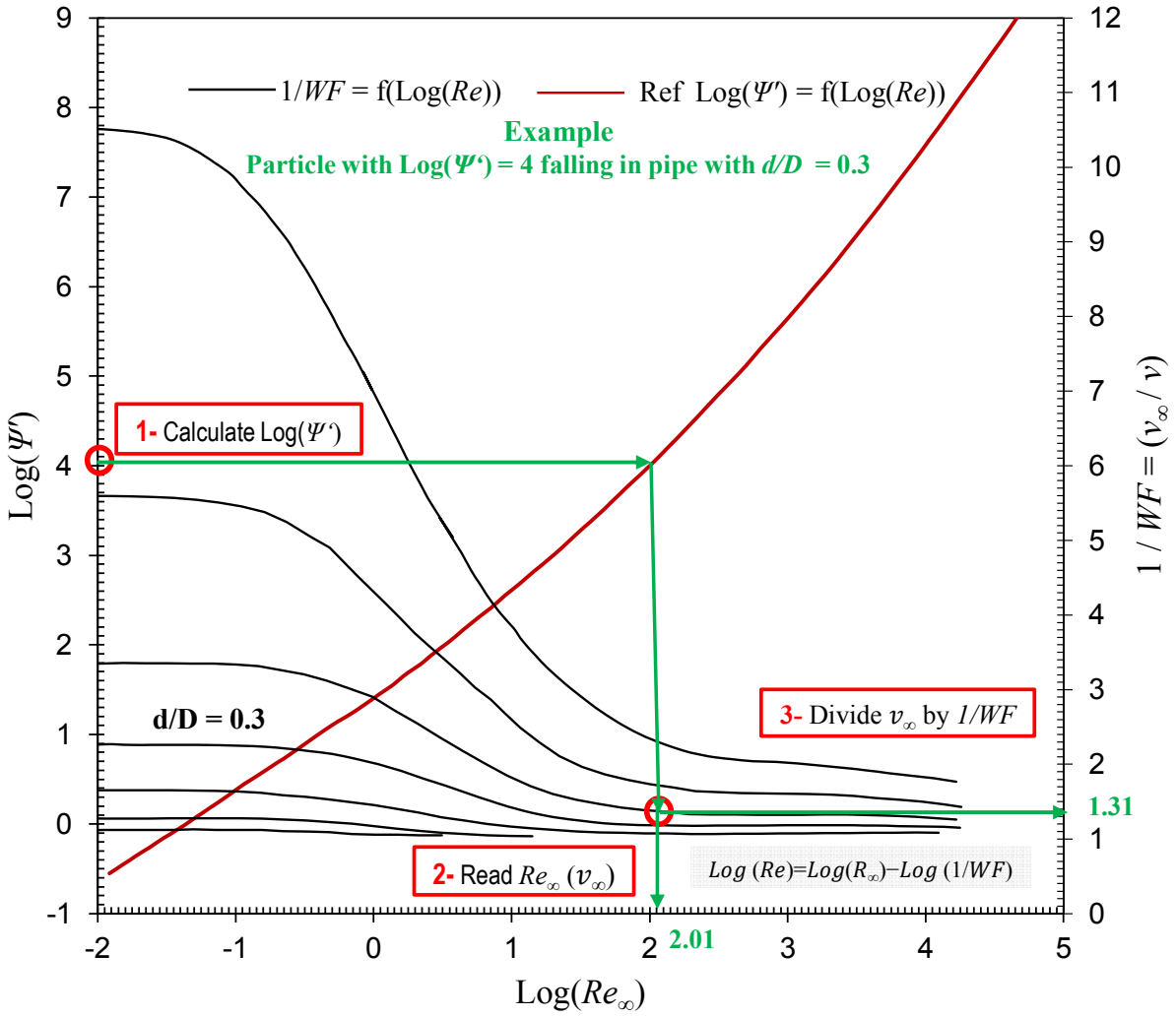

Figure 5.49 – Illustrative use example of ψ' - Re - WF nomogram

Non-spherical Particles

Experimental results from dataset 4 for a number of φ, were plotted in the form of two non-dimensional parameters $Log(\psi')$ and $Log(Re)$ as presented in Figure 5.50. It is clear from Figure 5.50 that the retarding shape irregularity effect increases with the Reynolds number from laminar to turbulent regime. This effect has the tendency to reduce at laminar regime.

Similar to Nomogram 1, a third nomogram (Nomogram 3) shown in Figure 5.51, allows to directly predict the hindered terminal settling velocity using particle and fluid data (ψ'). The nomogram is

divided in two sections depending on the range of the non-dimensional particle-fluid parameter ($-1 < \mathrm{Log}(\psi') < 3$ and $3 < \mathrm{Log}(\psi') < 7$).

Similar to Nomogram 1 and 2, Nomogram 3 is straight forward to use (see described steps in the graphical methods development section).

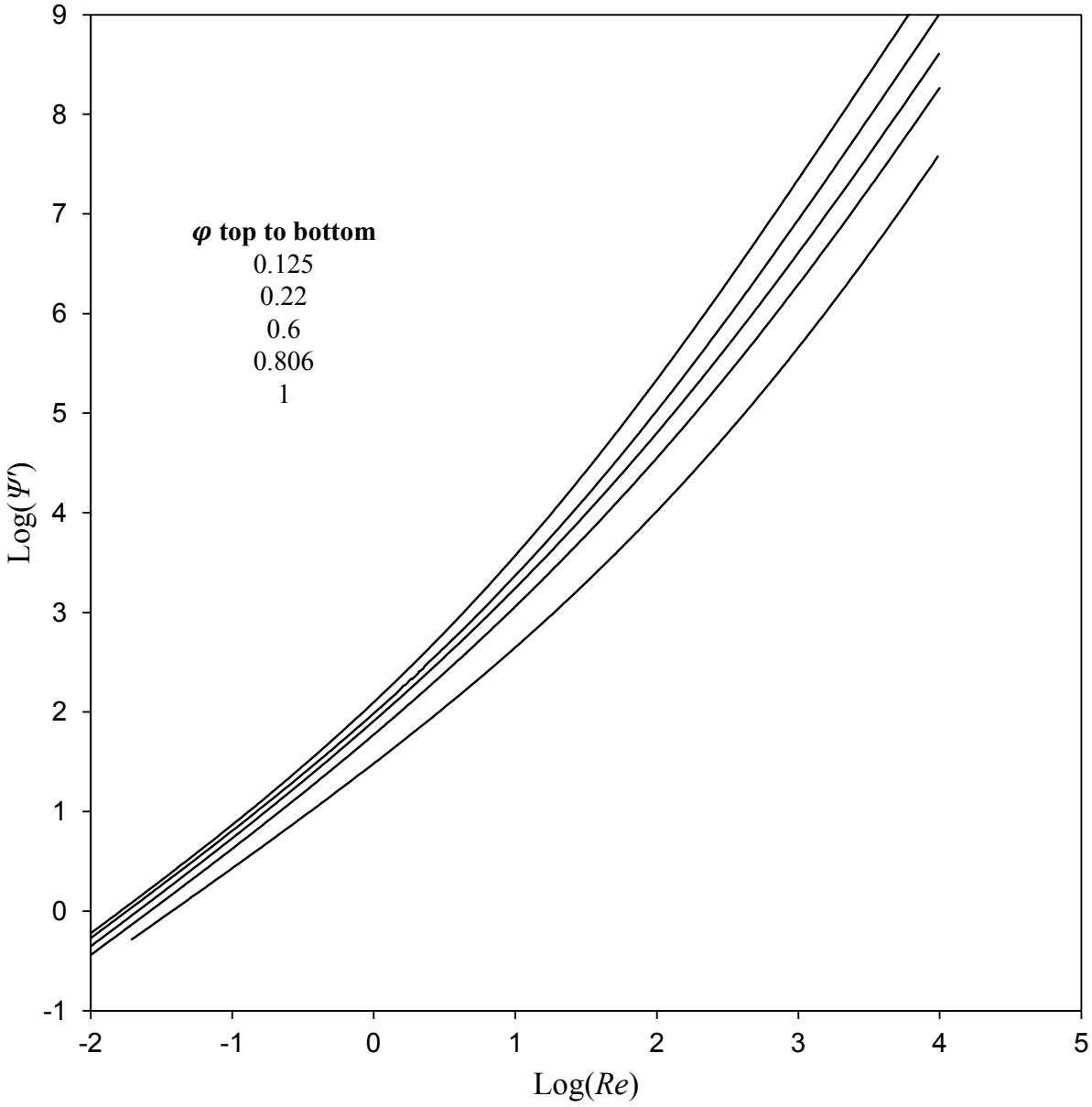

Figure 5.50 – Non-dimensional particle-fluid coefficient versus Reynolds number curves for spheres falling in cylindrical containers

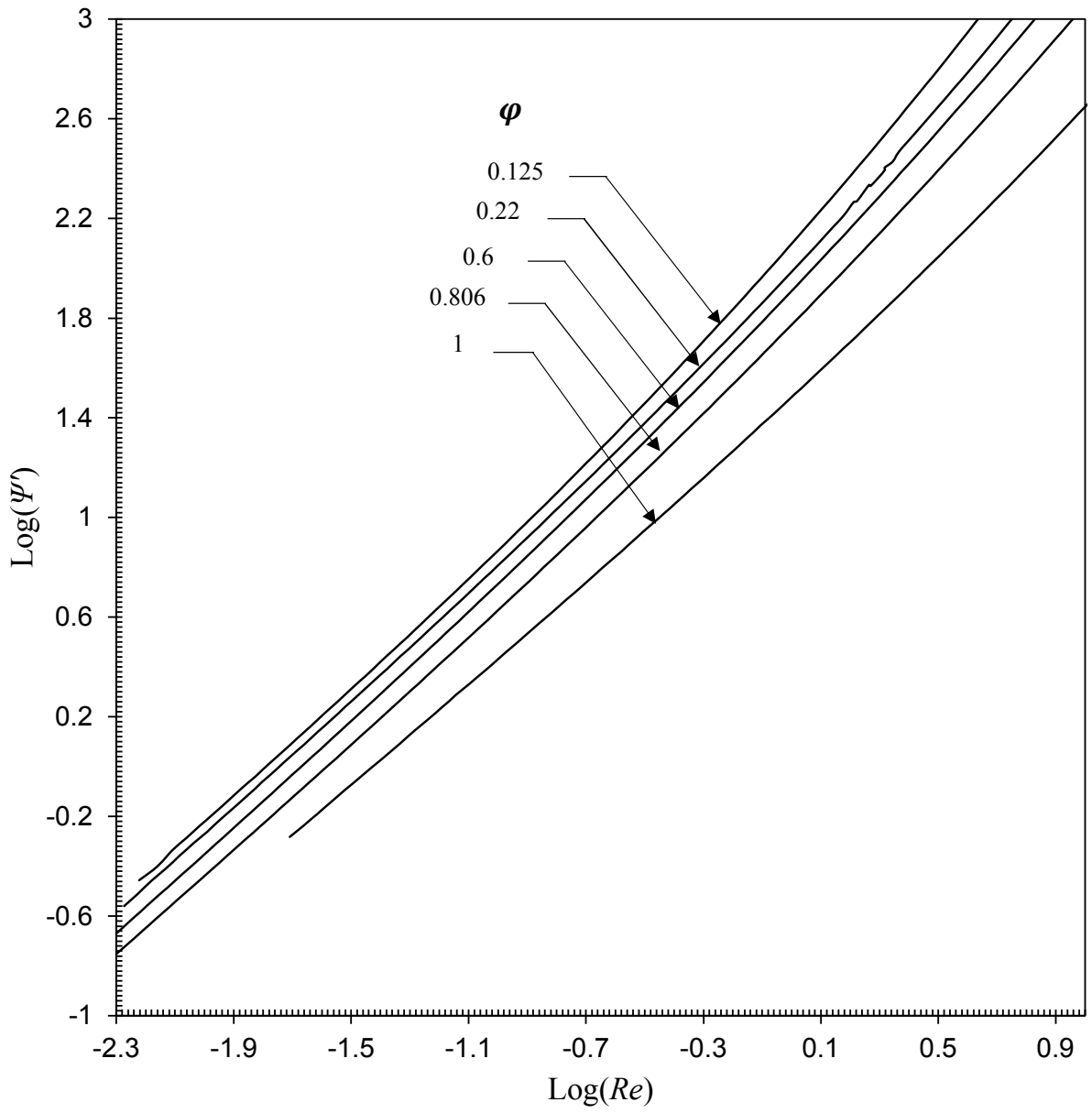

(a)

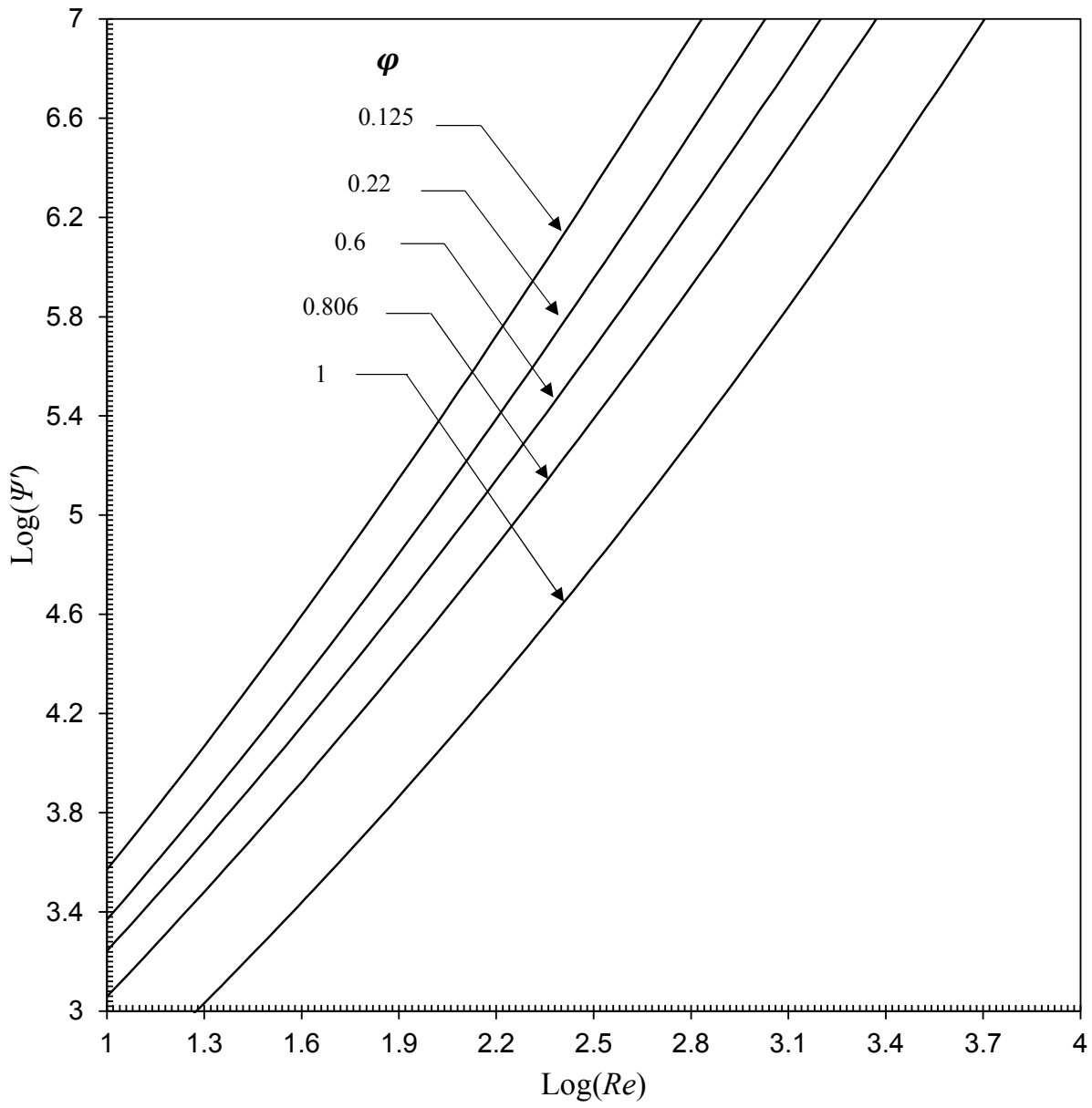

(b)

Figure 5.51 – ψ' - Re nomograms for non-spherical with (a) $-1 < Log(\psi') < 3$ and (b) $3 < Log(\psi') < 7$

5.4 Summary

In this Chapter, correlations and nomograms were developed for direct prediction of the hindered settling velocities of the various particles and fluids. The results showed that:

1. From the developed correlations and graphical models, a field engineer will be able to predict the terminal settling velocity using only the particle and fluid properties considering the retarding wall and particle shape effect.
2. The developed models in this work are robust and reliable while they are simple to use. Also, the models are applicable in a wide range of particle and fluid parameters and Reynolds number.
3. The prediction capability of the proposed correlations and nomograms was compared to experimental data and MfiX numerical simulation and good agreement was observed with corresponding experimental data.
4. MfiX, which demonstrated its ability to simulate the particle settling process close to the experimental work may be used to account for the effects of the wall and the particle shape simultaneously.
5. Implementing the Artificial Intelligence techniques such as ANN when such large volume of data exists will be the next step to estimate the minimum required mud flow rate to ensure an efficient hole cleaning.

CHAPTER 6

Artificial Neural Network Models to Predict Terminal Settling Velocity of Drill Cuttings

6.1 Introduction

Efficient cuttings transportation is very important to ensure an effective hole cleaning. If the drilling mud fails to transport the cuttings to the surface, problems such as wellbore instabilities, bit balling and stuck pipe can occur leading to equipment and time loss (Lin et al., 2018; Mkuyi, 2016; Pašić et al., 2007). When the drilling fluid is stagnant, the buoyancy and gravity force vectors are acting in the same line but in opposite directions, and since cuttings density is always higher than the mud density, the resultant force leads the cuttings to settle toward the bottom of the wall. To ensure the upward movement of the cuttings, the fluid lifting force (velocity) should conquest the buoyancy and gravity resultant force, this critical fluid velocity is so-called minimum transport velocity (Shadizadeh and Zoveidavianpoor, 2012). Consequently, the cuttings are lifted toward the surface, however, with a velocity slower than the fluid velocity. The difference between the fluid and particle velocities is often called slip velocity. For practical purposes, slip velocity of a solid particle can be considered as the terminal settling velocity (Baldino et al., 2015b; Kamyab et al., 2016). Hence, theoretically, the velocity of the drilling fluid must be higher than the settling velocity of the cuttings for an efficient hole cleaning (Agwu et al., 2018; Graham and Jones, 1994). Therefore, predicting the settling velocity of the cuttings is crucial to determine the minimum

transport velocity for an efficient hole cleaning (Aswad and Rashid, 2014). Also, settling velocity prediction is important to ensure even placement of the proppants in the induced fractures after hydraulic fracturing operations (Bandara et al., 2020; Liu et al., 2021; Wang et al., 2020; Wei et al., 2020b).

The settling velocity is an intrinsic property of a specific particle falling in a specific fluid. Hence, the settling velocity prediction has been the subject of many past studies and many models have been developed ranging from experimental, mathematical, simulation and artificial intelligence approaches. However, the developed models accuracy is limited to certain particle and fluid properties and flow regime application ranges (Agwu et al., 2018). The interest in finding predictive models for the settling velocity led to an extensive experimental work resulted in generation of a large data set that can be used for prediction of the particles' velocity in both Newtonian and non-Newtonian fluids (Agarwal and Chhabra, 2007; Agwu et al., 2018; Ahmed, 2012; Baldino et al., 2015b; Buscall et al., 1982; Chhabra et al., 1996; Faitli, 2017; Fidleris and Whitmore, 1961a; Jacobs et al., 2015; Jayaweera and Mason, 1965; Johnsen, 2014; Kelessidis, 2003; Khatmullina and Isachenko, 2016; Nolan, 1970; Peden and Luo, 1987; Sharma and Chhabra, 1991; Wang et al., 2018; Xu et al., 2017). Despite its importance and accuracy, experimental work is time consuming and not cost effective and cannot cover all possible scenarios, hence, numerical simulation was used as an alternative by many researchers (Agwu et al., 2018; Blackery and Mitsoulis, 1997; Bush, 1994; Butcher and Jr, 1990; Dazhi and Tanner, 1985; Dhole and Chhabra, 2006; Gavrilov et al., 2017; Ghosh and Stockie, 2015; Gumulya et al., 2014; Missirlis et al., 2001; Prashant and Derksen, 2011; Trofa et al., 2015; Wachs and Frigaard, 2016; Zaidi et al., 2015a). The limitations of numerical simulation based predictions lay on their dependency on the proper calibration and validation of the results with some lab or field data and that it is limited to some

application (e.g. particle shape, fluid models) (Zaidi et al., 2015a). Also, most of the mathematical models and correlations relate the drag coefficient of drag to the Reynolds number which implies a tedious iterative work as both input and output are velocity related parameters. Furthermore, majority of these models are flow regime dependent and does not consider the irregularity of the particles shape or the retarding effect of the wellbore and pipe walls (Agwu et al., 2020). This calls the need to propose new models to predict the 'hindered' settling velocity, independent of the velocity and applicable in different flow regimes and for different particles and wellbore configurations. The hindered velocity is the velocity altered due to the presence of wellbore and pipe walls, particle shape or by the presence of other particles (Kelessidis, 2003; Zaidi et al., 2015b).

Another alternative, considering the existing large experimental data available in the area of the settling velocity, is the Artificial Intelligence (AI) and Machine Learning (ML) techniques. Since its inception, technology has driven the development and transformation of the oil and gas industry. AI and ML allow computers to assess large volumes of data and make decisions to solve problems in a manner that is similar to how the human brain does it (Badrouchi et al., 2019; Mitchell, 2006). Recently, some researchers focused on using AI techniques such as Artificial Neural Networks (ANN), support vector machine (SVM) and other generic programming algorithms to predict the settling velocity (Agwu et al., 2020; Barati et al., 2014; Goldstein and Coco, 2014; Kamyab et al., 2016; Li et al., 2014; Rooki et al., 2012; Sadat-Helbar et al., 2009). A summary on the previous application of AI techniques in the prediction of the terminal settling velocity can be found in Table 6.21. It is important to note that ANN and other AI techniques, do not take into consideration the physics of the process, however, they allow the machine to learn from field or experimental data (Alnuaim, 2019; Osborne, 1977).

Table 6.21 – Previous AI application in terminal settling velocity prediction

Technique	Structure	Inputs			Outputs	Reference
		Fluid	Particle	Other		
ANN	6-12-1	ρ_f, k, n	ρ_P, d_P	g	v_{sl}	(Rooki et al., 2012)
ANN	7-12-1	ρ_f, k, n	ρ_P, d_P	$d_P/D, d_P/L_P$	WF	(Li et al., 2014)
ANN	2-5-1	φ	-	$Log(Re)$	f	(Kamyab et al., 2016)
ANN	4-4-1	d_n	υ	$\rho_f/\rho_f, S_f$	v_{sl}	(Sadat-Helbar et al., 2009)
SVM	-	ρ_f, k, n	ρ_P, d_P	$d_P/D, d_P/L_P$	WF	(Li et al., 2014)
GP	-	d_n	υ	ρ_f/ρ_f	v_{sl}	(Goldstein and Coco, 2014)
MGGP	-	-	-	Re	C_D	(Barati et al., 2014)

S_f= Corey's shape factor

Considering the existence of a large database in the literature and our laboratory data using the Slurry Loop unit (see Appendix B), applications of AI techniques such as Artificial Neural Networks (ANN) appears to be useful to build a velocity predictive model relating all the non-velocity dependent parameters of the particle, fluid and wellbore configuration. The objective of this work is to develop efficient data-driven ANN models for predicting the hindered settling velocity. To achieve this objective, a new non-dimensional parameter relating the fluid and particle properties (diameter, density, viscosity) was developed and two models proposed. The first model is for spherical particles considering the wall effect. However, the second model is for non-spherical particles. The results are presented and discussed.

6.2 Materials and Methods

6.2.1 ANN overview

The models presented in this work are developed using Artificial Neural Network (ANN). This is an intelligent mathematical algorithm that simulates the human nervous system (Sivanandam et al., 2006). This network is set of interconnected neurons which consist of several input signals with synaptic weights (Kamyab et al., 2010).

These networks are good at mimicking functions and recognizing patterns hard to recognize by just plotting the data or even using mathematical pattern detection tools such as chi-squared test, correlation coefficient or root square mean error (Sivanandam et al., 2006). Indeed, ANNs can be proved to fairly fit any practical function (Demuth, Howard; Beale, 2015). The processing ability of the network is stored in the inter-nodes connection strengths (weights $\omega_{i,j}$), obtained by a process of adaptation to, or learning from, a set of training patterns (Gharbi and Mansoori, 2005). Each artificial neuron has inputs and produce a single output using a transfer function, which translates the input signals to output signals between 0 and 1 (e.g. sigmoid), which can be sent to multiple other neurons (Demuth, Howard; Beale, 2015). Figure 6.52 shows how the nodes of the ANN are connected and transfer the signal using a sigmoid function. While training the model, the weights ($\omega_{i,j}$) are changed until the final signal in the output layer reproduces the output from the experimental data. This is why, each ANN is defined by its intrinsic weights and number of layers and nodes.

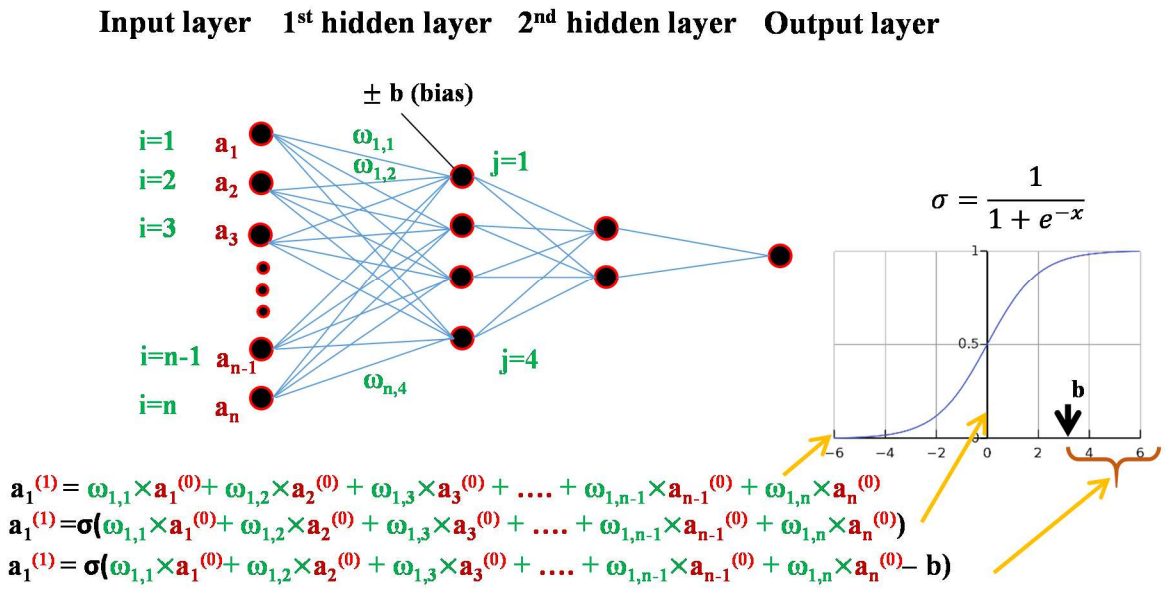

Figure 6.52 – ANN architecture and mathematical procedure illustration

6.2.2 Experimental data

Mainly, two datasets were used to develop the ANN models.

Dataset 1 was obtained from our past laboratory work (see Appendix B) and the work of other researchers (Fidleris and Whitmore, 1961a, 1961b) with a total of over 3000 data points. 55 data points were left for validation purpose. This dataset was used to develop a model for prediction the settling velocity of spherical particles with considering the wall retarding effect.

Dataset 2 was obtained from the work of Bourgoyne (1991), including a total of 688 data point. 47 data were left for validation purpose. This dataset was used for developing the model for non-spherical particles.

A summary of data statistics for the datasets 1 and 2 is presented in Appendix B.

Data preparation

The datasets were summarized and the input data compiled into a few non-dimensional entities.

For dataset 1, the input parameters were summarized as:

- particle-to-pipe ratio: d/D
- non-dimensional parameter ψ':

$$\psi' = \psi . Re^2 = \frac{4g(\rho_p - \rho_f)\rho_f d^3}{3\eta^2} \tag{6.70}$$

For dataset 2, the input parameters were summarized as:

- non-dimensional parameter: ψ'
- sphericity: φ

where g is the acceleration of the gravity, ρ_p and ρ_f are the particle and fluid densities, respectively, d is the particle diameter, v_{sl} is the terminal settling velocity, η is the coefficient of viscosity and φ is the sphericity of the particle.

For both datasets, Reynold number was considered as the output parameter:

$$Re = \frac{\rho_f v_{sl} d_p}{\eta} \tag{6.71}$$

A summary on the inputs and outputs used in the ANN models can be found in Table 6.22.

Table 6.22 – Dataset 1 and 2 inputs and outputs summary

Dataset	Inputs	Outputs
1	ψ'	Re
	d/D	
2	ψ'	
	φ	

6.2.3 ANN models

Model 1: Spherical Particles and Wall Effect

This model was developed for predicting the hindered settling velocity of spherical particles with considering the wall effect. Dataset 1 was used for the training of this model. The dataset was compiled into two input parameters: ψ', and d/D and one output, Re.

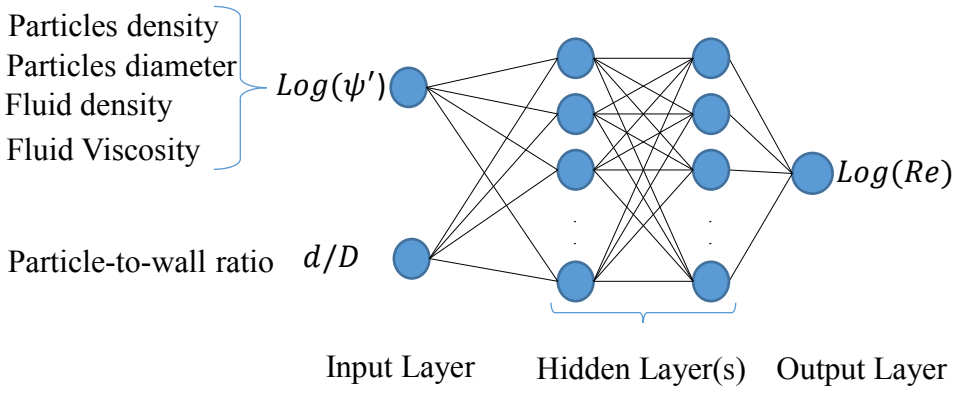

Figure 6.53 – ANN model for spherical particles settling velocity prediction

Model 2: Non-Spherical Particles

This model is developed for predicting the hindered settling velocity of spherical particles with considering the shape irregularity effect. Dataset 2 was compiled into two input parameters. It does not contain the particle-to-pipe diameter ratio, however, in addition to ψ', it includes the particle sphericity φ. The output parameter is Re.

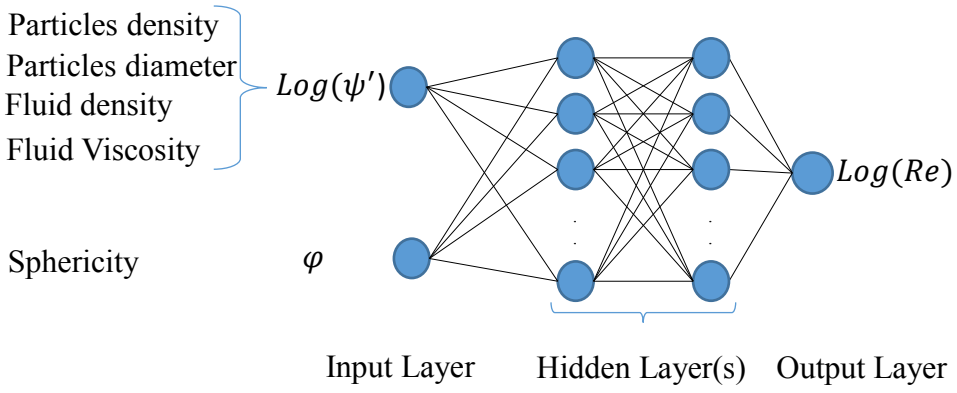

Figure 6.54 – ANN model for non-spherical particles settling velocity prediction

6.3 Results and Discussion

ANN Models

To determine the optimal ANN architectures, a trial-and-error approach was used to select the optimum number of neurons in the hidden layer. A sensitivity on the number of the hidden layer neurons was performed. A data set different that the training data set was used to check the validity and the performance of the model to predict unseen data. The selection criteria was based on low Root Mean Square Error ($RMSE$) and a high correlation coefficient (R^2).

Figure 6.55 shows that 7 or 9 nodes network architecture present a good fit to the data for both Model 1 (for spherical particles considering the wall effect) and Model 2 (for non-spherical particles). The inputs for Model 1 were the non-dimensional particle-fluid coefficient versus (ψ') and the particle-to-wall ratio (d/D). A 6 nodes model is presented in Appendix C.

From Figure 5.41, one can clearly observe a non-arbitrary trends of the non-dimensional particle-fluid coefficient (ψ') versus the Reynolds number (Re) for different particle-to-wall ratios (d/D) . Hence, the choice of inputs will help the ANN model to better understand the relationship between ψ' and Re. This was confirmed by the performance plots of the ANN model (Model 1)

shown in Figure 6.57 and Figure 6.58. The model has a relatively low Mean Square Error $RMSE = 0.0003$ and a correlation coefficient R^2 close to 1. A validation test on a new unseen dataset of 55 points was performed. The model was able to predict the Reynolds number (settling velocity) with high accuracy with $RMSE = 0.018$ and this can be seen in Figure 5.44. The model weights and biases were presented in Table 6.23 for work replicability.

An important use of the developed model is to generate more data for cases not available in experimental work. The ANN Model 1 was used to generate new ψ' vs Re curves for new d/D ratios (0.7, 0.6, 0.55, 0.45, 0.35, 0.25 and 0.15) not considered in the experimental work.

It can be seen from Figure 6.60, that the ANN predicted curved (red lines) are accurately interpolated.

The experimental data (curve with black lines) are those lines used to train the network.

Similar to Model 1 selection, non-spherical particles in Model 2 were selected with a single hidden layer composed of 9 nodes. The inputs for this model are the non-dimensional particle-fluid coefficient (ψ') and particle sphericity (φ). From Figure 6.61, one can recognize the non-arbitrary trends of the non-dimensional particle-fluid coefficient (ψ') versus the Reynolds number (Re) for different particle sphericities (φ). Model weights and biases for replicability reasons are displayed in

Table 6.*24*.

The model showed a strong knowledge gain from training and high prediction capabilities. A validation test on a new unseen dataset of 47 points was performed. The model was able to predict the Reynolds number (settling velocity) with high accuracy with $RMSE = 0.0106$.

Similarly, the ANN Model 2 was used to generate new ψ' versus Re curves for new sphericity values φ (0.3, 0.7 and 0.9) not considered in the experimental work. It can also be seen from Figure 6.62, that the ANN predicted curved (red lines) are accurately interpolated.

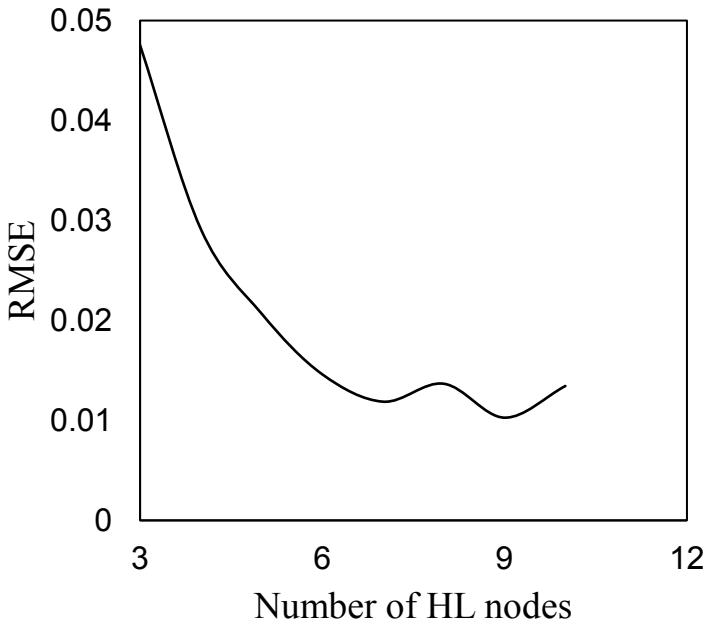

Figure 6.55 – Hidden layer node number sensitivity analysis

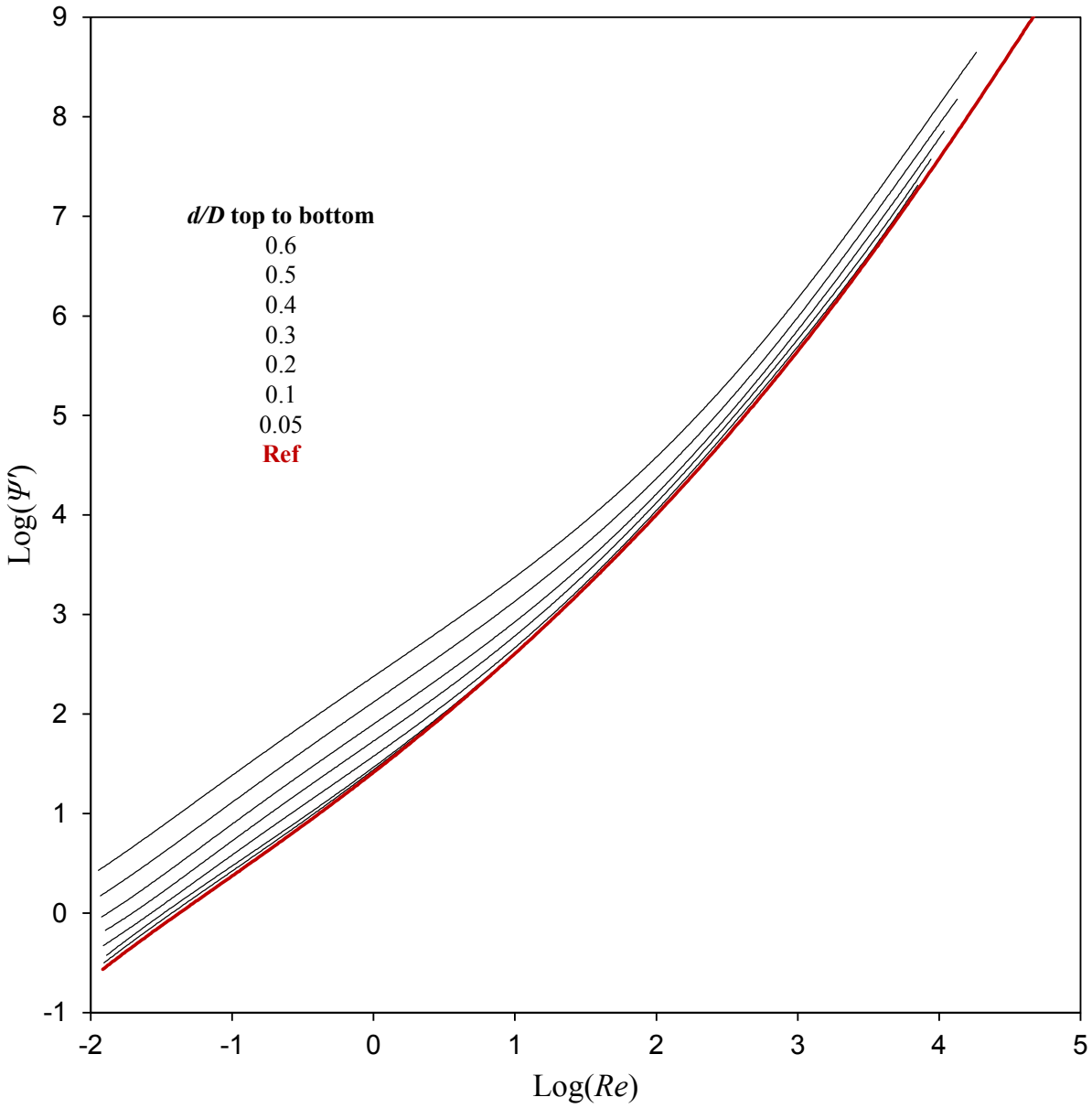

Figure 6.56 – Non-dimensional particle-fluid coefficient versus Reynolds number curves for spheres falling in cylindrical containers (the reference line corresponds to $d/D \rightarrow 0$)

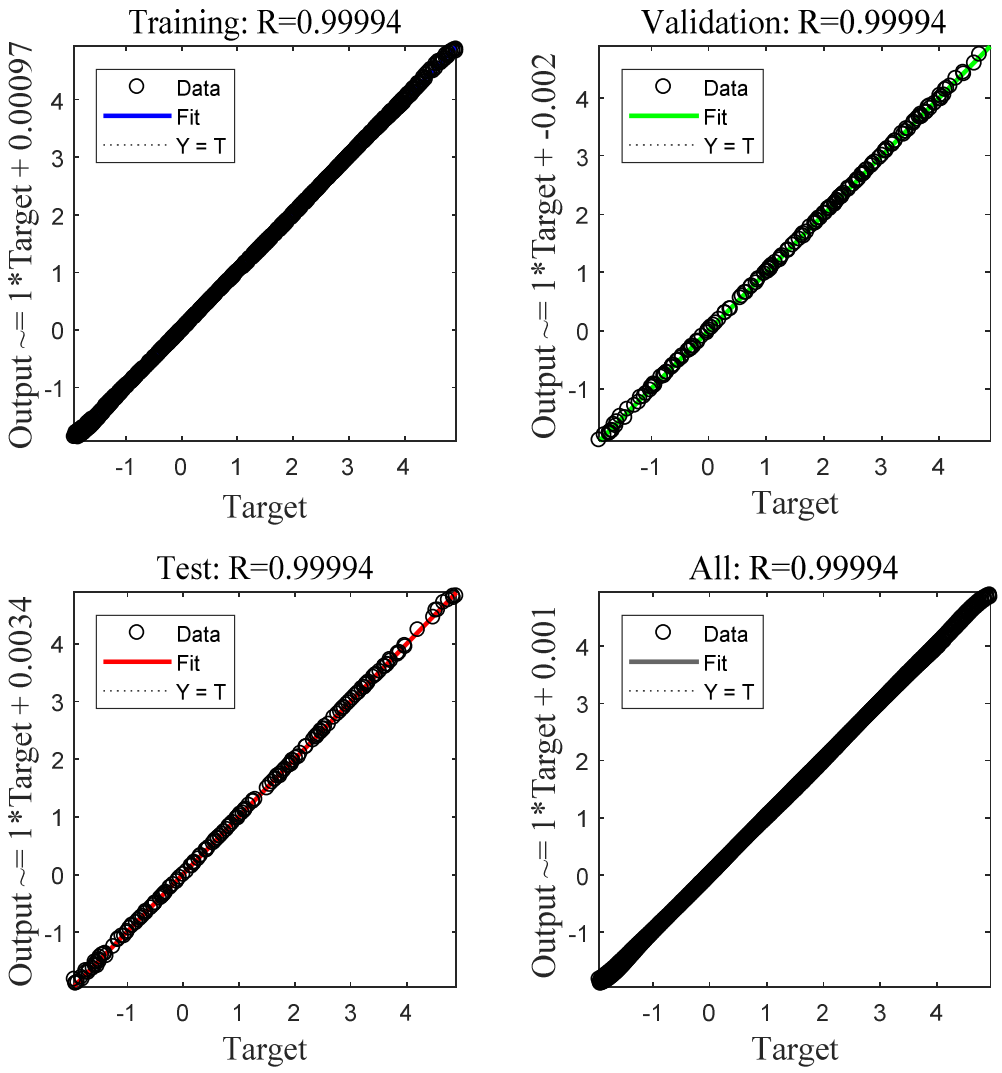

Figure 6.57 – Scatter plots of a single hidden layer with 7 nodes ANN model

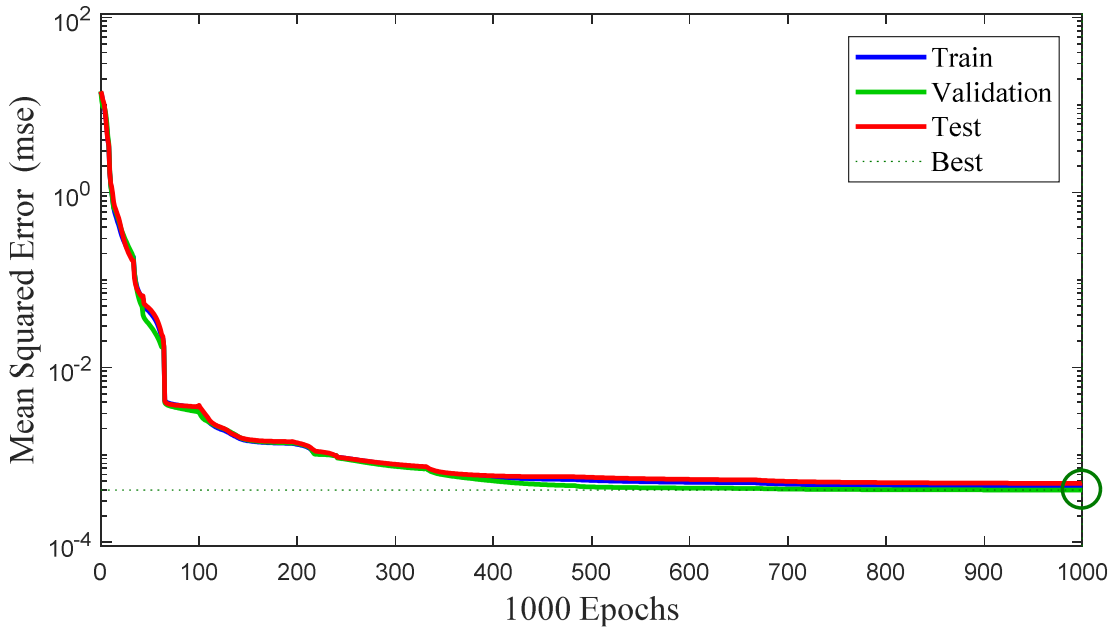

Figure 6.58 – Single hidden layer with 7 nodes ANN model performance

Table 6.23 – Model 1 weights and biases

Hidden Layer						Output Layer			
$\omega_{1,1}$	4.8145	$\omega_{2,1}$	-22.7153	b_1	-25.129	$\omega_{1,1}$	-7.199		
$\omega_{1,2}$	-1.375	$\omega_{2,2}$	3.2481	b_2	3.8361	$\omega_{1,2}$	1.1148		
$\omega_{1,3}$	-0.59882	$\omega_{2,3}$	1.4085	b_3	-3.336	$\omega_{1,3}$	-7.6945		
$\omega_{1,4}$	0.39894	$\omega_{2,4}$	-11.6927	b_4	14.0651	$\omega_{1,4}$	-10.0308	b_1	9.1989
$\omega_{1,5}$	0.031421	$\omega_{2,5}$	-2.0084	b_5	-3.9149	$\omega_{1,5}$	-11.6444		
$\omega_{1,6}$	-0.38072	$\omega_{2,6}$	1.8855	b_6	-2.6444	$\omega_{1,6}$	7.0014		
$\omega_{1,7}$	0.72705	$\omega_{2,7}$	-15.2175	b_7	-17.0241	$\omega_{1,7}$	-11.9668		

Table 6.24 – Model 2 weights and biases

Hidden Layer						Output Layer			
$\omega_{1,1}$	-8.6598	$\omega_{2,1}$	-2.5593	b_1	13.9509	$\omega_{1,1}$	-11.2903		
$\omega_{1,2}$	0.7458	$\omega_{2,2}$	2.0458	b_2	-3.565	$\omega_{1,2}$	29.9057		
$\omega_{1,3}$	1.5044	$\omega_{2,3}$	3.0992	b_3	-3.1765	$\omega_{1,3}$	-5.5778		
$\omega_{1,4}$	13.2959	$\omega_{2,4}$	2.4175	b_4	1.8824	$\omega_{1,4}$	-0.13455	b_1	-11.8463
$\omega_{1,5}$	21.642	$\omega_{2,5}$	-11.9893	b_5	-4.6129	$\omega_{1,5}$	-0.0247		
$\omega_{1,6}$	10.2524	$\omega_{2,6}$	5.8575	b_6	-1.9114	$\omega_{1,6}$	-0.06311		
$\omega_{1,7}$	-0.48683	$\omega_{2,7}$	1.6796	b_7	-12.6939	$\omega_{1,7}$	4.3906		
$\omega_{1,8}$	0.15376	$\omega_{2,8}$	3.677	b_8	6.1789	$\omega_{1,8}$	23.0444		
$\omega_{1,9}$	13.1925	$\omega_{2,9}$	-17.1946	b_9	8.9051	$\omega_{1,9}$	-0.06306		

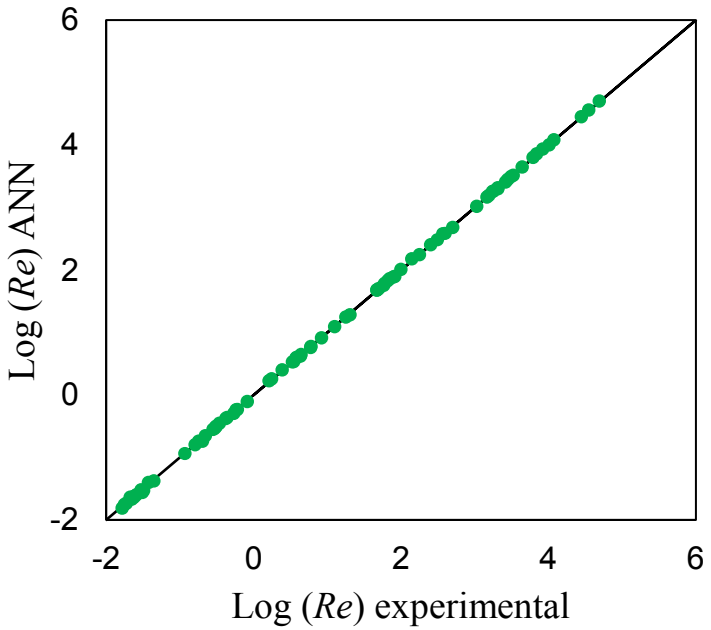

Figure 6.59 – Comparison of the ANN Model 1 prediction and experimental measurement of the settling velocity of spherical particles

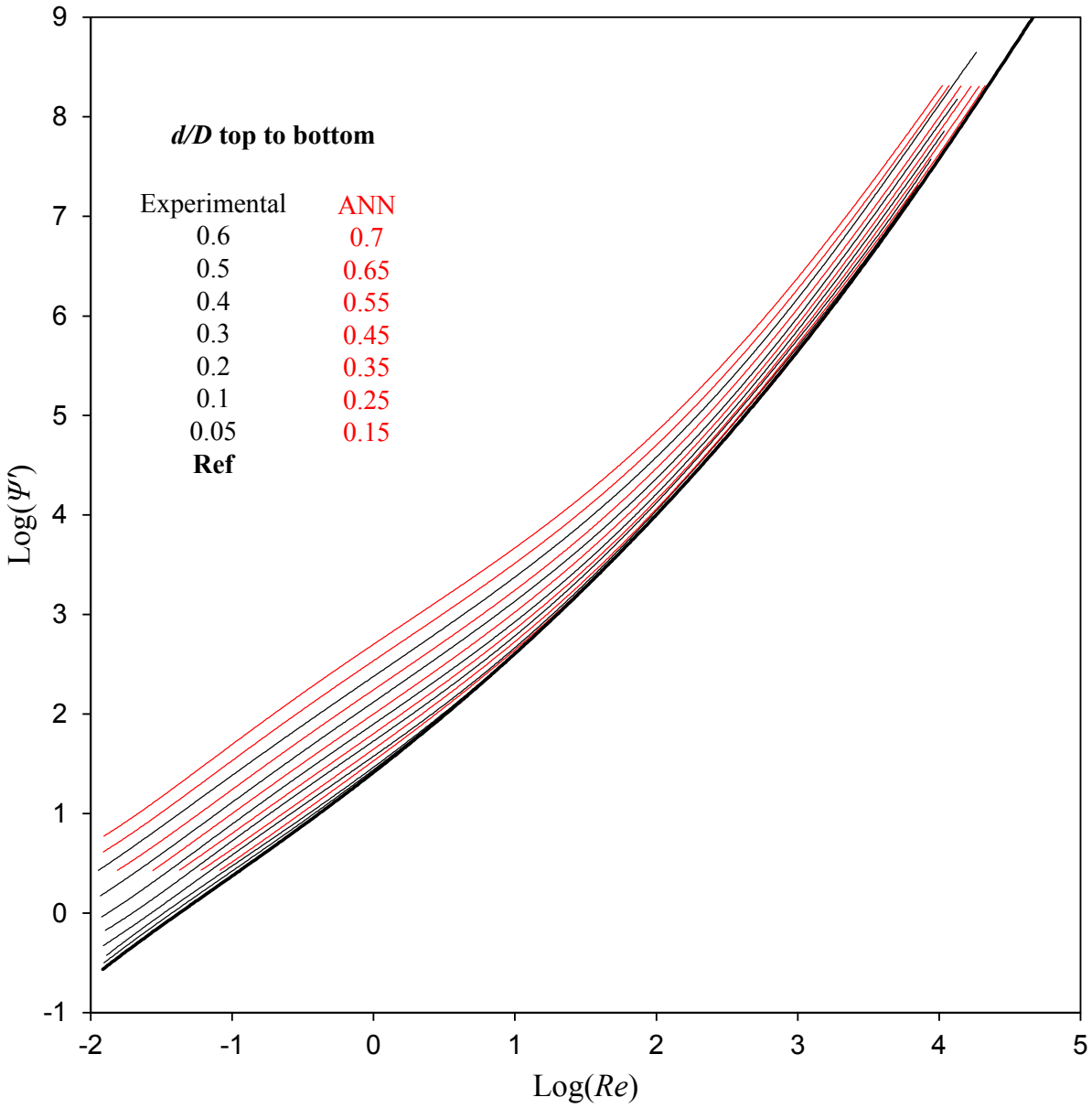

Figure 6.60 – The results from the ANN Model 1 could predict the unseen data for d/D of 0.7, 0.6, 0.55, 0.45, 0.35, 0.25 and 0.15

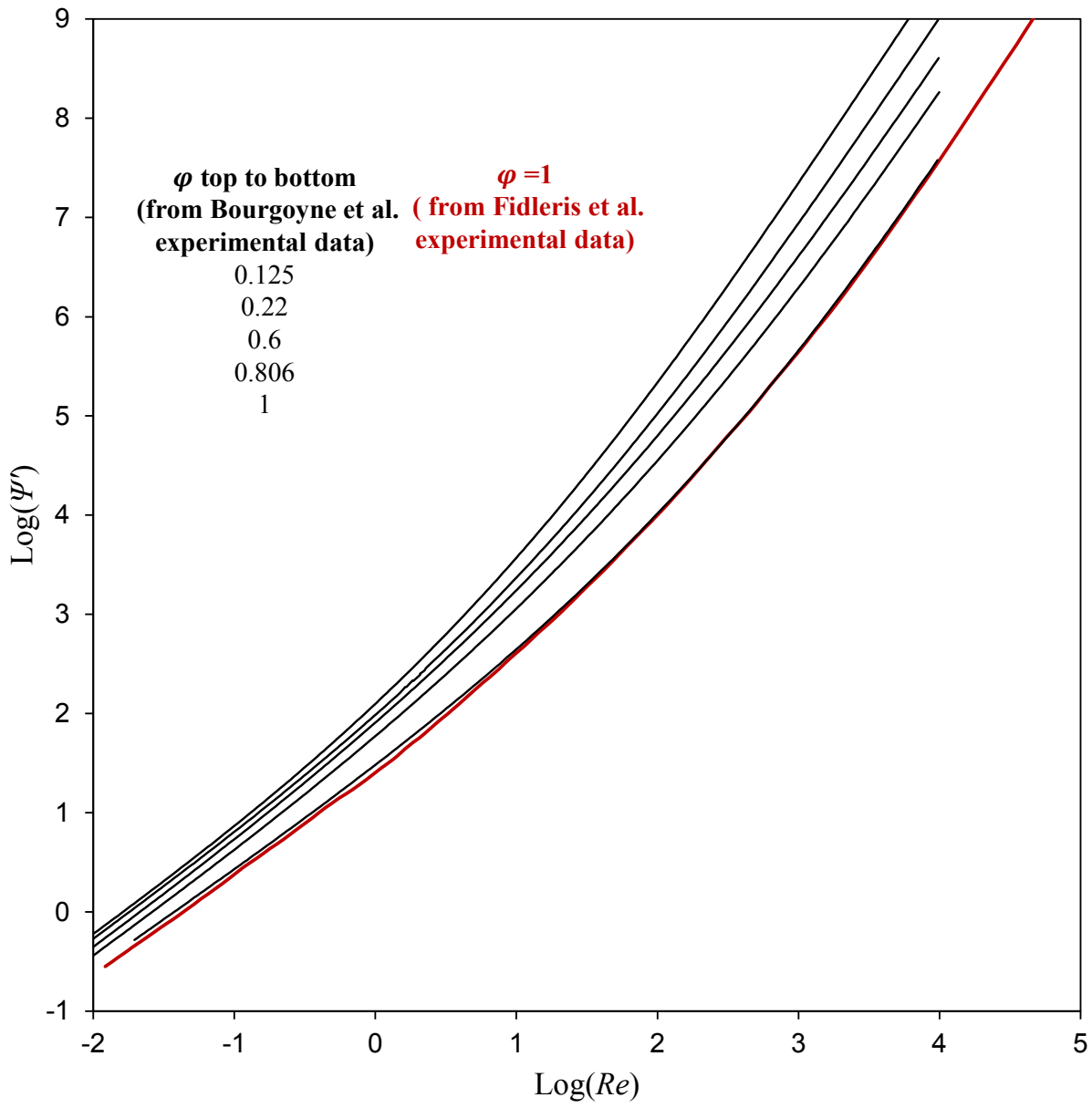

Figure 6.61 – Non-dimensional particle-fluid coefficient versus Reynolds number curves for non-spherical particles falling in infinite medium container ($d/D \rightarrow 0$)

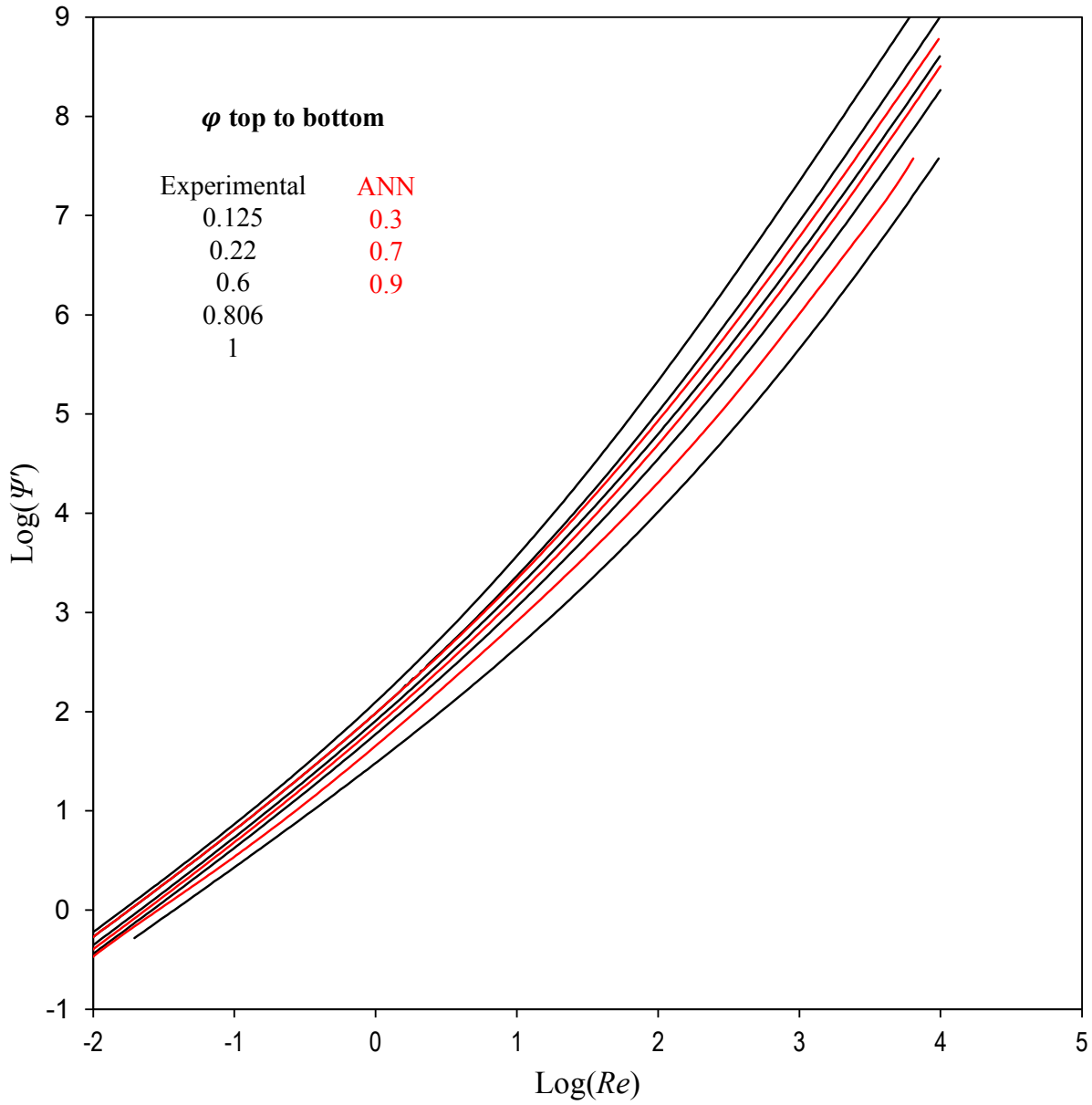

Figure 6.62 – The results from the ANN Model 2 could predict the unseen data for φ of 0., 0.7 and 0.9

New Settling Velocity Nomograms

Using both experimental and ANN generated data, a new set of nomograms was developed. The proposed nomograms are simple and straightforward to use. They allow the prediction of the settling velocity with only using the particle and fluid properties. Based on the two ANN models discussed earlier, two nomograms were proposed.

The first nomogram is to predict the settling velocity of a spherical particle considering the wall effect (Figure 5.46). The second nomogram allows the prediction of the settling velocity of non-spherical particles (Figure 6.64). Both nomograms, allow the direct prediction of the hindered terminal settling velocity using particle and fluid data (ψ'). The nomograms are divided in two sections depending on the range of the non-dimensional particle-fluid parameter ($-1 < \mathrm{Log}(\psi') < 3$ and $-1 < \mathrm{Log}(\psi') < 3$).

An illustrative example for non-spherical particles settling velocity prediction using nomograms is presented in Figure 5.48.

For a particle with $Log(\psi') = 4$ with a sphericity of $\varphi = 0.9$, to calculate the settling velocity:

- Project $Log(\psi') = 4$ on the $\varphi = 0.9$ curve line the read logarithmic of the Reynolds number is 1.75, hence the settling velocity is calculated using $v_{sl} = \frac{\eta}{\rho_f d_p} Log(Re)$.

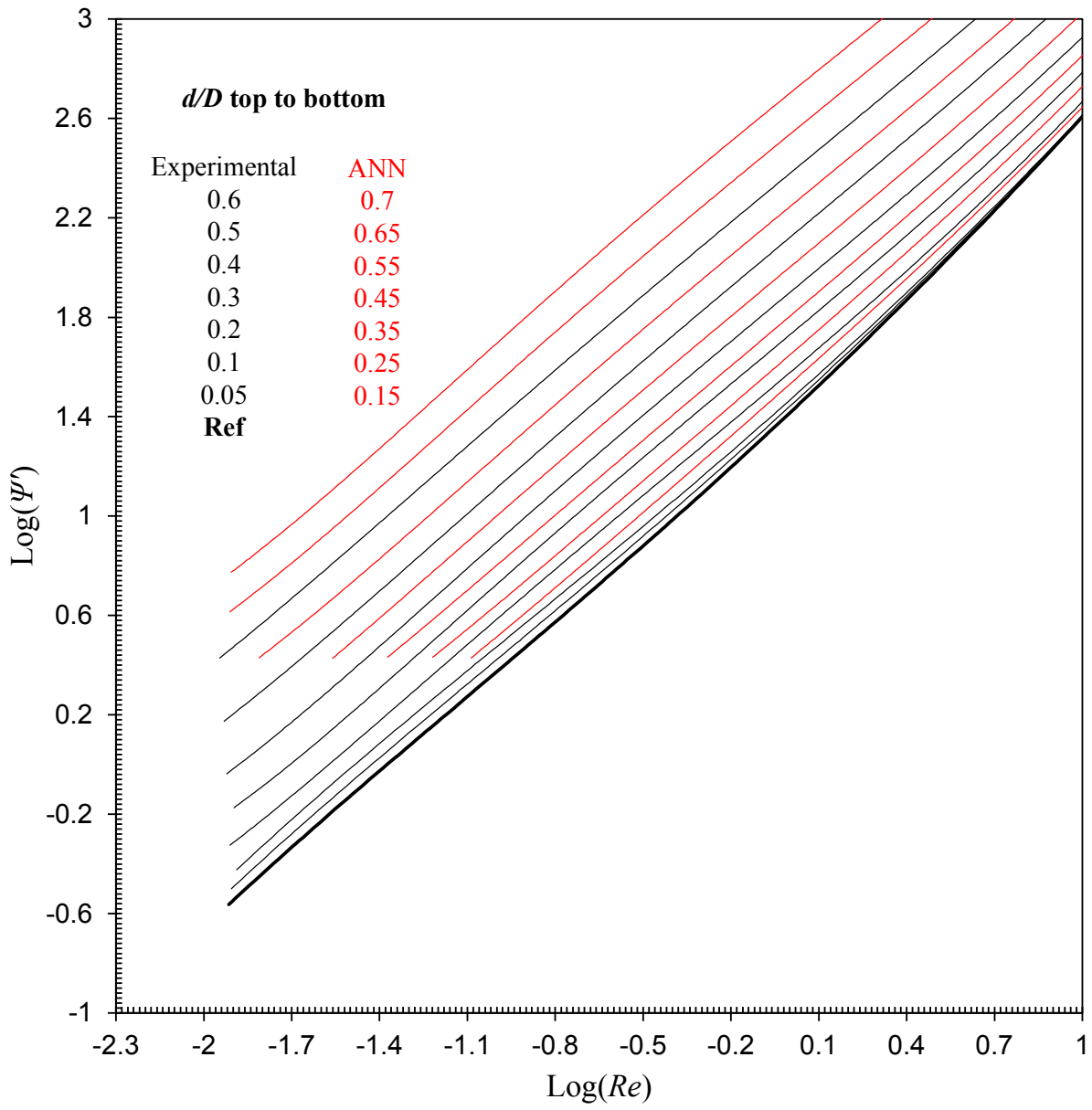

(a)

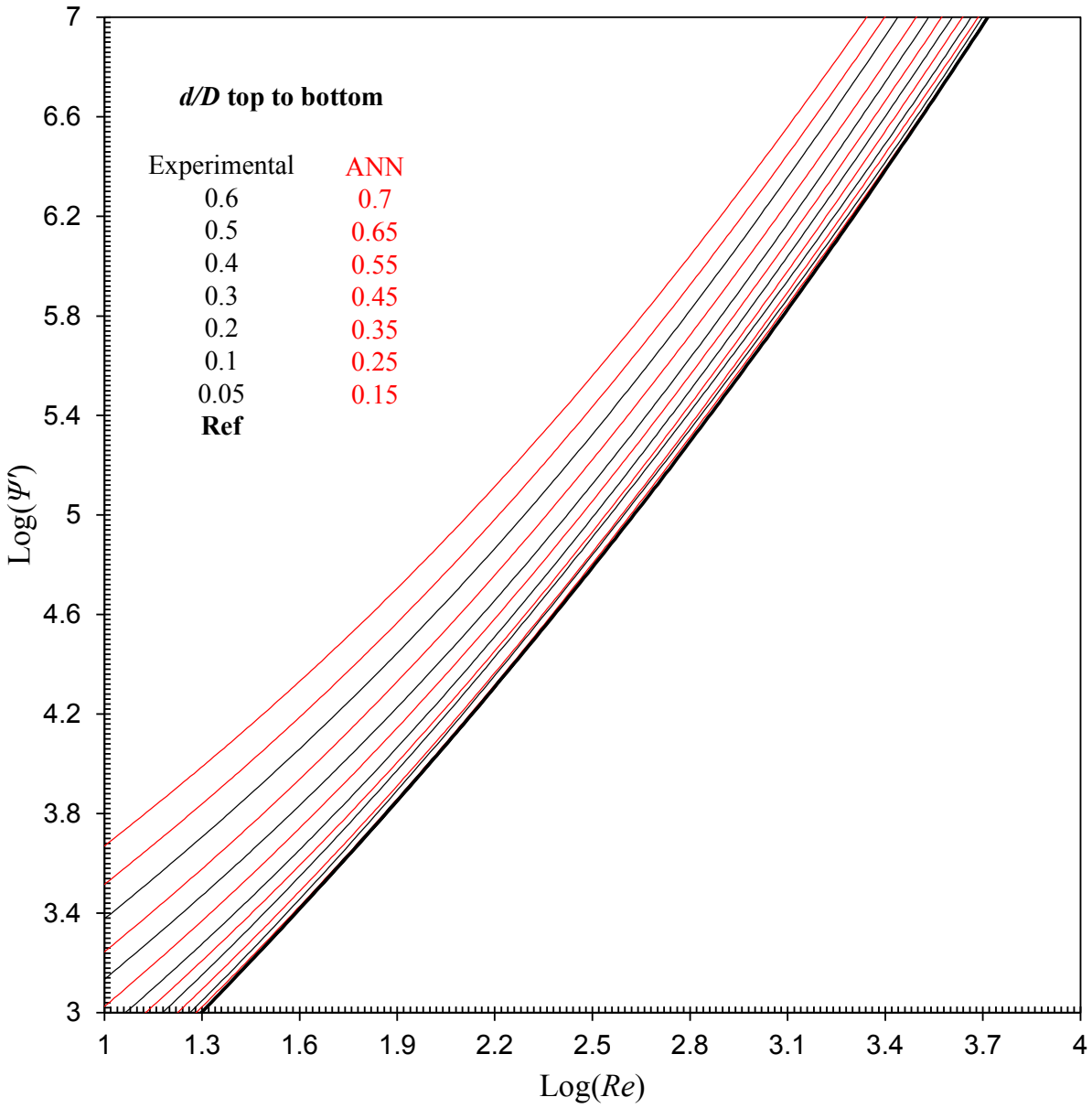

(b)

Figure 6.63 – ψ' - Re nomograms for particle-fluids with (a) $-1 < Log(\psi') < 3$ (b) $3 < Log(\psi') < 7$

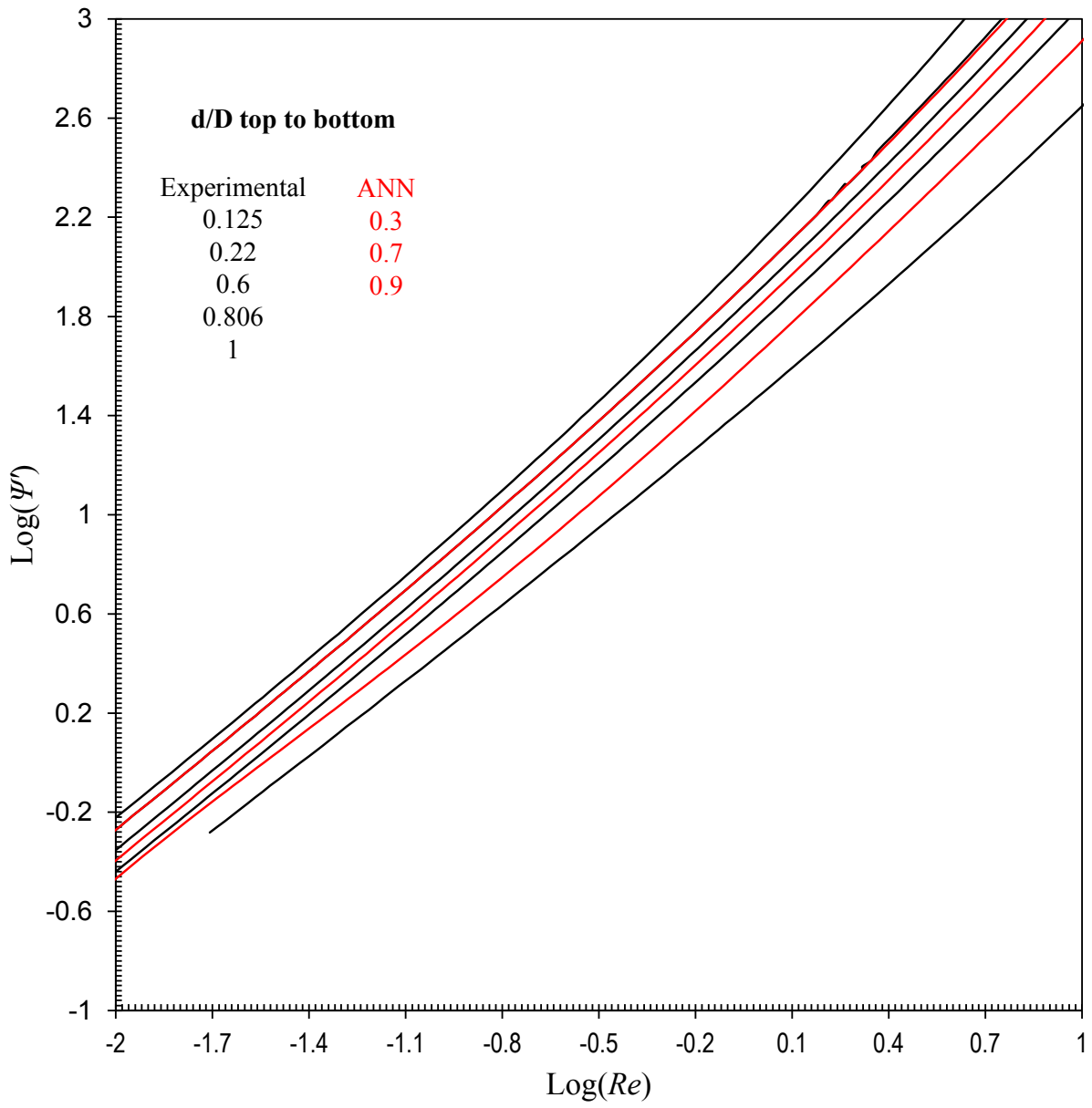

(a)

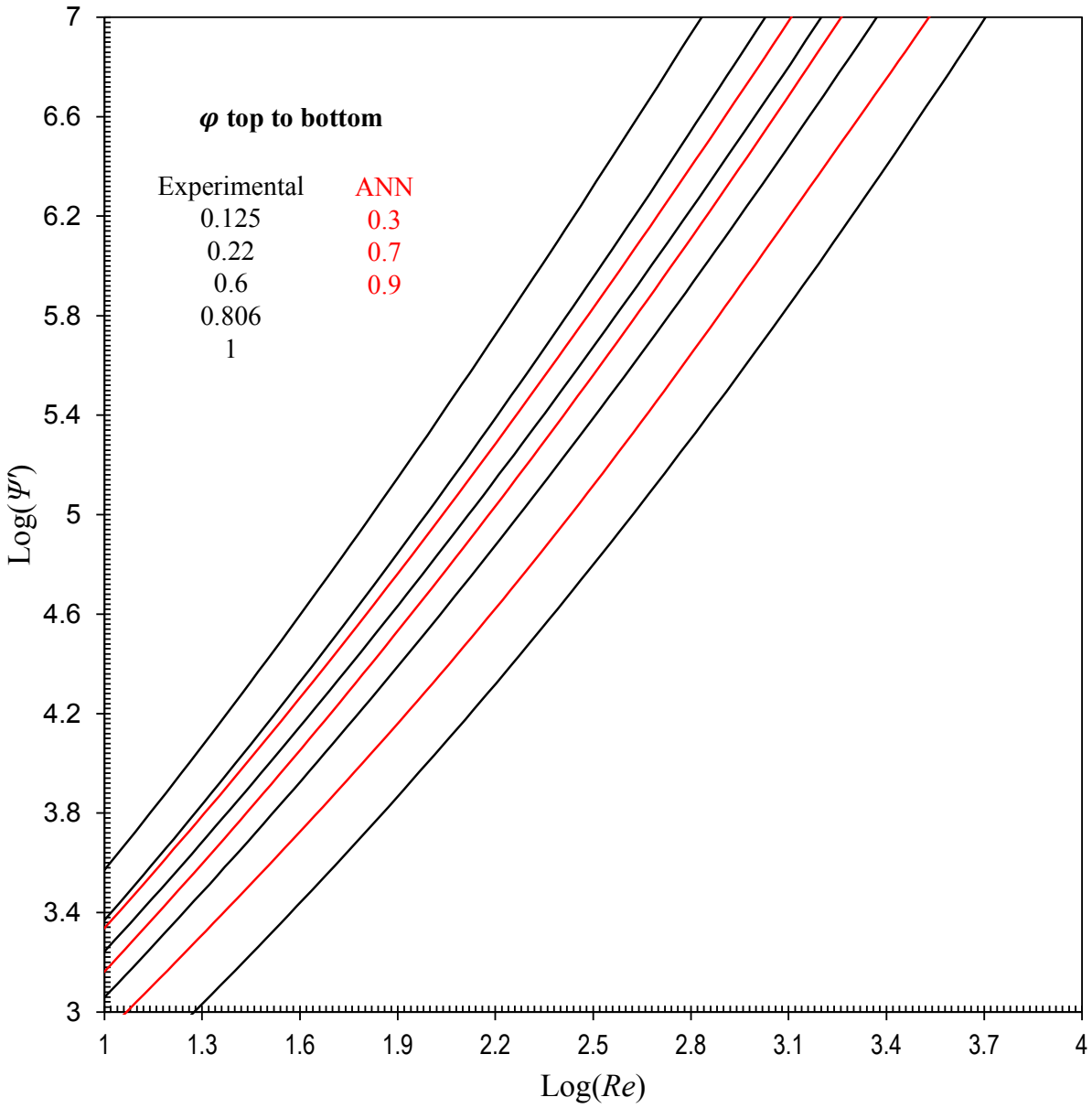

(b)

Figure 6.64 – ψ' - Re nomograms for particle-fluids with (a) $-1 < Log(\psi') < 3$ and (b) $3 < Log(\psi') < 7$

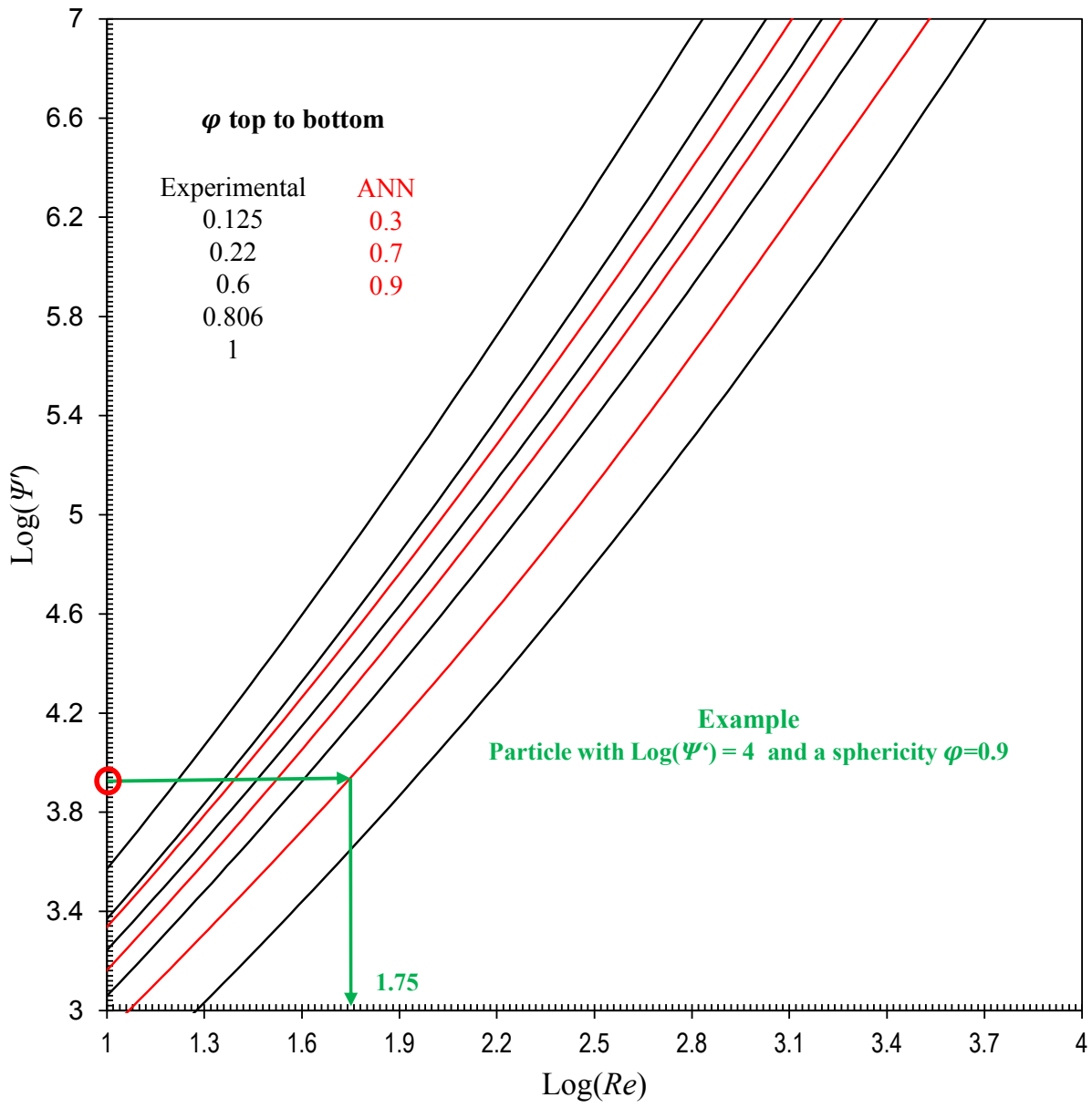

Figure 6.65 – Illustrative use example of ψ' - Re nomograms (non-spherical particle)

Comparison with existing AI models

Some studies in the field of the settling velocity prediction focused on applying AI techniques. Table 6.25 presents some of them with a comparison of results in term of accuracy based on the factors considered, dataset volume and R^2, $RMSE$ and MSE accuracy factors. It is clearly seen that

the dataset used in this study is larger and the proposed models present higher accuracy due to the large dataset used and the choice of inputs.

Table 6.25 – Comparison of our developed model with existing AI models

Technique	Structure	Data points	Nbr. inputs	Sphericity / Wall effect	R^2	$RMSE$	MSE	Ref.
ANN	6-12-1	88	6	/	0.947	0.038 0.26	0.0014	(Rooki et al., 2012)
GP	-	935	6	/	0.94	0.0274	0.0676	(Goldstein and Coco, 2014)
ANN	5-5-1	336	5	Sphericity	0.978	0.038 0.26	0.0007	(Agwu et al., 2020)
ANN	2-7-1	3000	2	Wall effect	0.999	0.0118	0.0003	This work
ANN	2-9-1	688	2	Sphericity	0.999	0.0106	0.0003	

6.4 Summary

In this Chapter, two Artificial Neural Network models were developed for predicting the hindered settling velocity of the particles. The results showed that:

1- The developed models in this work are robust and reliable due to their accuracy and simplicity using two input parameters.

2- Also, unlike other studies, the models are also replicable since the weights and biases required for re-developing the ANN model are provided.

3- The prediction capability of the proposed ANN models has been tested with unseen datasets and was able to predict the settling velocity with high accuracy as well as it was compared to the existing AI models.

4- The developed models helped to generate new dataset for cases not covered in the experimental work and allowed us to establish new nomograms for predicting the hindered settling velocity.

5- From the developed graphical models (nomograms), a field engineer will be able to predict the terminal settling velocity using only the particle and fluid properties considering the retarding wall and particle shape effect.

It is also important to note that it is believed that the choice of the non-dimensional particle-fluid coefficient versus, ψ', helped the algorithm to better learn from the training set rather than using different fluid and particle properties that requires more complex architecture of the ANN in order to understand the relationship between them. Implementing wellbore inclination and pipe rotation to estimate the minimum required mud flow rate to ensure an efficient hole cleaning will be another future work to consider.

CHAPTER 7

Impact of Hole Cleaning and Drilling Performance on the Equivalent Circulating Density

7.1 Introduction

In drilling operation weighting materials such as Barite are used to increase the bottom hole pressure in order to prevent the influx of formation fluids into the wellbore. However, this increase in density, can cause circulation losses of mud when drilling into unstable or naturally fractured formations unless the pressure is kept below the formation fracture pressure. This introduces a range for the appropriate mud density for the drilling operation known as safe mud weight windows (Bourgoyne, 1991). During the drilling operation as the mud circulates, the pressure required to circulate the mud and overcome the pressure losses in the annulus is added into the hydrostatic pressure of the mud leading to an increase of the bottom hole pressure. The new circulating mud gradient is known as the equivalent circulating density (ECD). Most of the researchers consider only the effect of pressure loss on the ECD, however, the impact of the cuttings concentration on the ECD, especially at low flow rates, and/or high rates of penetration (ROP) needs to be studied.

Several literatures report on modelling of the cuttings transportation in the annular space including the settling velocity. These studies focused on both experimental investigations (Agarwal and

Chhabra, 2007; Ahmed, 2012; Badrouchi et al., 2020; Badrouchi and Rasouli, 2020b; Baldino et al., 2015b; Buscall et al., 1982; Chhabra et al., 1996; Faitli, 2017; Fidleris and Whitmore, 1961a; Jacobs et al., 2015; Jayaweera and Mason, 1965; Johnsen, 2014; Kelessidis, 2003; Khatmullina and Isachenko, 2016; Nolan, 1970; Peden and Luo, 1987; Sharma and Chhabra, 1991; Wang et al., 2018; Xu et al., 2017) and numerical simulations (Badrouchi et al., 2020; Badrouchi and Rasouli, 2020b; Blackery and Mitsoulis, 1997; Bush, 1994; Butcher and Jr, 1990; Dazhi and Tanner, 1985; Dhole and Chhabra, 2006; Gavrilov et al., 2017; Ghosh and Stockie, 2015; Gumulya et al., 2014; Missirlis et al., 2001; Prashant and Derksen, 2011; Trofa et al., 2015; Wachs and Frigaard, 2016; Zaidi et al., 2015a)

Accurate determination of ECD requires correct modelling of the wellbore system and understanding the various sources of pressure increase in the annulus (Xiang et al., 2012). Attempts has been made to model the ECD based on the pressure losses but neglecting the cuttings effect (Al-Hameedi et al., 2019; Elzenary et al., 2018; Han et al., 2019; Kulkarni et al., 2014; Vajargah et al., 2014). Other researchers attempted to include the effect of the cuttings on ECD (Abdelgawad et al., 2019; Kerunwa, 2020; Xiang et al., 2012), however, most of these studies are limited by the range of particles and drilling fluids considered in their models. Also, no work has been reported to relate the ECD to the fluid and formation properties as well as drilling operational parameters.

Xiang et al. (2012) studied the effect of cuttings concentration on ECD while drilling. They performed a comparison between the ECD predicted with and without cuttings concentration effect and concluded that the cuttings concentration affects the ECD in the annulus and is important to avoid losses, pipe sticking and other problems causing non-productive times (NPT). However, in their work, the model they used to predict the cuttings concentration was limited to fluid model. Kerunwa (2020) showed that ECD will increase with increasing ROP and decrease with increasing

mud flowrate. They mentioned that high mud flowrate decreases the effect of the cuttings in the mud. Thus, the effective mud weight due to cuttings decreases with increased mud flowrate. However, high mud flow rates cause an increase in pressure losses leading to higher ECD.

Maximizing the rate of penetration (ROP) to reduce drilling cost in oil and gas development is the permanent objective of drilling researchers (Chen et al., 2018, 2016a, 2016b, 2014c; Chen and Gao, 2017). Many parameters help to increase ROP and the rotary speed (RPM) is one of the most important ones (Chen et al., 2018). However, increasing RPM may cause extra frictional pressure losses.

The process of optimizing drilling parameters, such us the ROP, should be not only drilling system specific but also formation specific (Chen et al., 2018). Mechanical Specific Energy (MSE) is defined as the mechanical work done to excavate a unit volume of rock, and it could provide an objective assessment of the drilling efficiency. Teale (1965) presented the first MSE model for rotary drilling system. His model, which was based on the surface measurements of drilling parameters, led into large sources of error due to the indirect measurements of bottom hole data at surface. Thereafter, numerous researchers attempted to develop more accurate models based on bottom hole data from logging while drilling (LWD) and more accurate measurement of the WOB and torque (Armenta, 2008; Chen et al., 2018; Dupriest and Koederitz, 2005a; Hammoutene and Bits, 2012a; Mohan et al., 2014a, 2009a; Pessier and Fear, 1992a).

MSE models have been widely used in bit selection, drilling efficiency quantification, drilling performance monitoring, drilling performance optimization and ROP improvement. In this work, it was attempted to employ MSE in optimizing hole cleaning and controlling ECD. No comprehensive study is available in the literature concerning the effect of different drilling parameters on ECD. In this work we present a new model for predicting the ECD in vertical and

deviated wellbores that considers 1) the fluid properties, 2) formation properties, 3) wellbore and drill string structure and 4) drilling operational parameters. The developed model was used to study the effect of different drilling parameters on ECD and help engineers to optimize their operational parameters.

The importance of integrating the drilling operational parameters is to provide a more controlling options to drillers in monitoring ECD values and maintaining it inside the safe margin as well as optimizing the drilling job.

7.2 ECD Calculation Workflow

Figure 5.41 shows the workflow to estimate the ECD. Starting from the formation properties, MSE optimal can be estimated, then, ROP can be calculated based on NSE and drilling properties. Cuttings feeding rate can be predicted based on the ROP, porosity and fluid flow rate. Once the feeding rate is known, based on the fluid type and wellbore configuration, both cuttings concentration and pressure losses can be estimated therefore, ECD can be predicted. The ECD value is then used to adjust the MSE and a number of iteration are performed until ECD value stability.

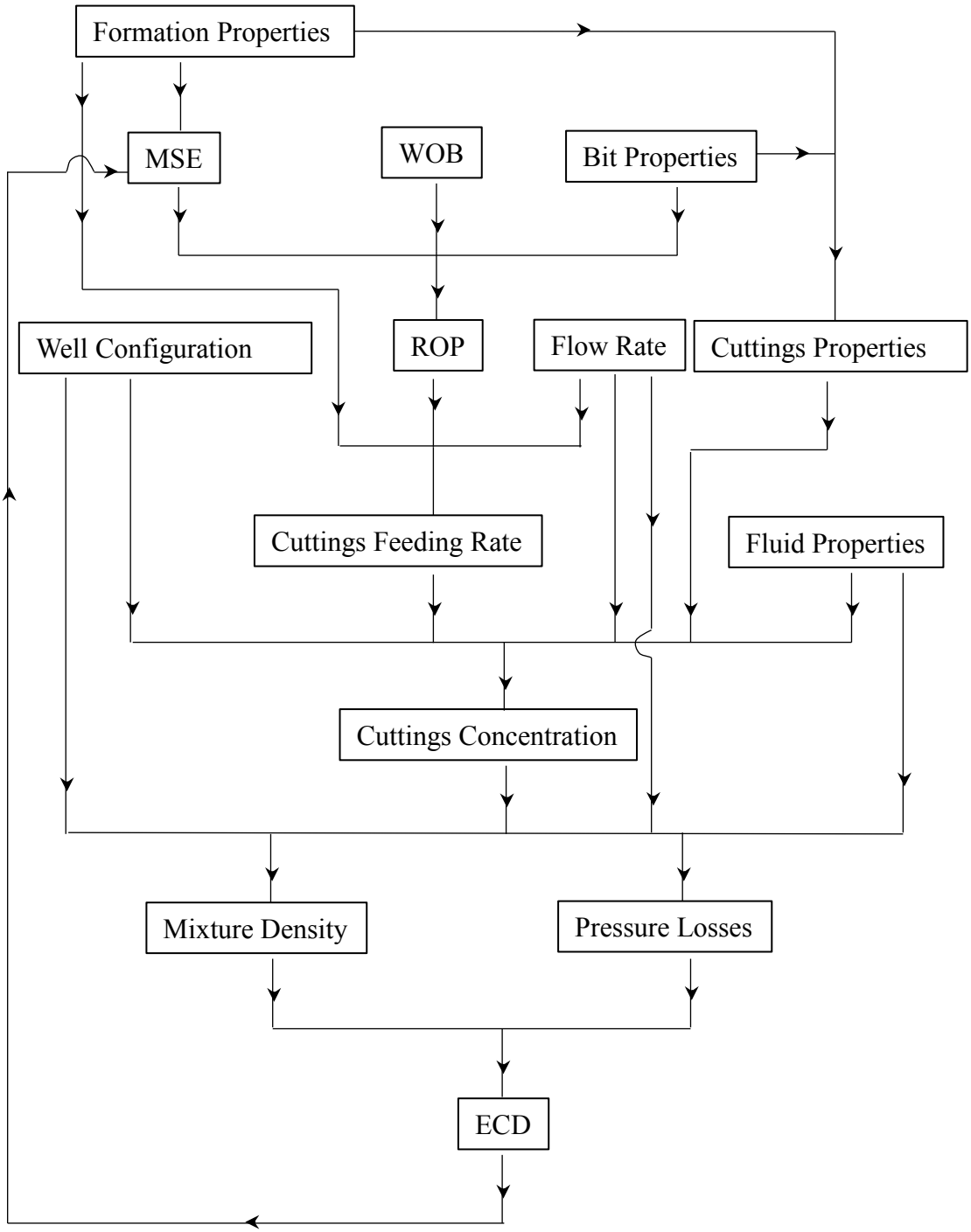

Figure 7.66 – ECD calculation workflow

7.3 Drilling Mechanical Specific Energy

7.3.1 Vertical Drilling

Defined as the mechanical work done to drill a unit volume of rock, Teale (1965) initially proposed the first MSE model for rotating drilling system as:

$$MSE = \frac{WOB}{A_b} + \frac{120.\pi.RPM.T}{D_b.ROP} \tag{7.72}$$

where, WOB is the weight on bit, A_b and D_b are the bit area and diameter, respectively; RPM is the rotary speed, T is the torque at bit and ROP is the rate of penetration.

The main problem with Teale's model is regarding the torque measurement (Chen et al., 2018). In the absence of reliable torque measurements at the bit, the calculation of MSE based on this model contains even large sources of error. Therefore, it is only used qualitatively as a trending tool. Pessier and Fear (1992) proposed a simple and more accurate method to calculate the torque at the bit based on WOB in absence of reliable torque measurement (Chen et al., 2014a). Their model's parameters are easy to obtain in the field and therefore, it has been commonly used in the drilling industry (Chen et al., 2018). The modified form of MSE proposed is as following.

$$MSE = WOB\left(\frac{1}{A_b} + \frac{13.33.\mu_b.RPM}{D_b.ROP}\right)$$
$$\mu_b = 36\frac{T}{D_b.WOB} \tag{7.73}$$

In the above equations, μ_b is the bit-specific coefficient of sliding friction, which is usually assumed to be of an average value of 0.3 and 0.85 for roller-cone and PDC bits, respectively (B. Rashidi et al., 2010).

The mechanical efficiency E_m is applied to adjust the bit performance in the actual drilling process and it reduces the drilling efficiency MSE (Amadi and Iyalla, 2012; Dupriest and Koederitz, 2005b; Hammoutene and Bits, 2012b). The mechanical efficiency E_m can be obtained from core sampling in the lab or derived from adjacent drilled well logs. The relationship between the MSE and drilling parameters are defined as (Chen et al., 2018):

$$MSE = E_m \,.WOB\left(\frac{1}{A_b} + \frac{13.33.\mu_b.RPM}{D_b.ROP}\right) \tag{7.74}$$

7.3.2 MSE model of directional and horizontal drilling

The drag force is greatly reduced in directional or horizontal sections of the wellbore due to the friction of the drill string and the wellbore wall. This results in a great difference between the surface measured WOB and the measurement of the WOB at the bottom hole (WOB_b) near the bit. The relationships between WOB and WOB_b have been presented for the bend and straight (inclined and horizontal) sections of the wellbore (Chen et al., 2014b) as:

$$WOB_b = WOB.e^{-\mu_s.\gamma_b} \tag{7.75}$$

where, γ_s is the section inclination differential and μ_d is the drill string sliding coefficient and assumed to be between 0.25 to 0.4, usually the value of 0.35 is commonly used (Caicedo et al., 2005; Chen et al., 2018).

For rotary drilling with positive displacement motor (PDM), the MSE model is as following (Chen et al., 2016c):

$$MSE = E_m \,.\left[WOB.e^{-\mu_s.\gamma_b}\left(\frac{1}{A_b} + \frac{13.33.\mu_b.RPM_s}{D_b.ROP}\right) + \frac{1155.2.\eta.\Delta P_m Q}{A_b ROP}\right] \tag{7.76}$$

Here, that RPM_s is drill pipe rotary speed, ΔP_m is the pressure drop across the PDM, Q is the fluid flow rate and η is the efficiency of PDM but not the bit. The last term of the equation represents the hydraulic energy at the bottom, some researchers believe that the hydraulic energy aids in drilling certain formations, hence they add the hydraulic term to the MSE (Mohan et al., 2014b, 2009b).

For sliding drilling, where the bit is rotating with a mud motor downhole (PDM) without rotating the drillstring from the surface. and the drilling fluid is pumped through the drill string, the MSE equation member depending on the pipe RPM vanishes (Maidla and Haci, 2004). In this case, the MSE can be estimated as (Chen et al., 2016d):

$$MSE = E_m \cdot \left(WOB.e^{-\mu_s \cdot \gamma_b} . \frac{1}{A_b} + \frac{1155.2.\eta.\Delta P_m Q}{A_b ROP} \right) \tag{7.77}$$

7.3.3 ROP model Based on MSE

In his experimental work in laboratory, Teale (1965) observed that at maximum drilling efficiency (optimal condition) MSE value is close to the formation uniaxial compressive strength (UCS). However, since his experimental tests were performed at atmospheric condition, in field operation MSE should be close to the confined compressive strength (CCS) to achieve an optimal drilling efficiency (Chen et al., 2018). A widely practiced and accepted CCS prediction method was proposed by Caicedo et al. (2005) as:

$$CCS = UCS + P_c + 2P_c \frac{\sin\phi}{1 - \sin\phi} \tag{7.78}$$

where, ϕ is the angle of internal friction and P_c is the confining pressure and defined as:

$$P_c = ECD - P_p \tag{7.79}$$

Assuming the minimum value of the MSE for optimal drilling efficiency, ROP can be defined by combining Equations (7.75), (7.78) and (7.79) in (7.74) or (7.76) or (7.77). ROP can be expressed as (Chen et al., 2014b):

$$ROP = \frac{13.33.\mu_b.RPM}{D_b\left(\frac{CCS}{WOB.e^{-\mu_s.\gamma_b}} - \frac{1}{A_b}\right)} \tag{7.80}$$

The above ROP model is relatively simple. By using this model, ROP can be predicted with reasonable accuracy for all of the bit types, based on formation properties and the drilling environment (Chen et al., 2018, 2014b).

7.3.4 Cuttings Settling Velocity

Different models for different fluid types were used to accurately predict the settling velocity. In this work, correlations were used for simple calculations and an Artificial Neural Network (ANN) was implemented in the MATLAB code to predict the settling velocity. The settling velocity prediction using ψ' vs Re correlation for Newtonian fluids are detailed in Chapter 5.

Similarly, for Bingham Plastic fluids, ψ' vs Re relation is presented in Figure 7.67.

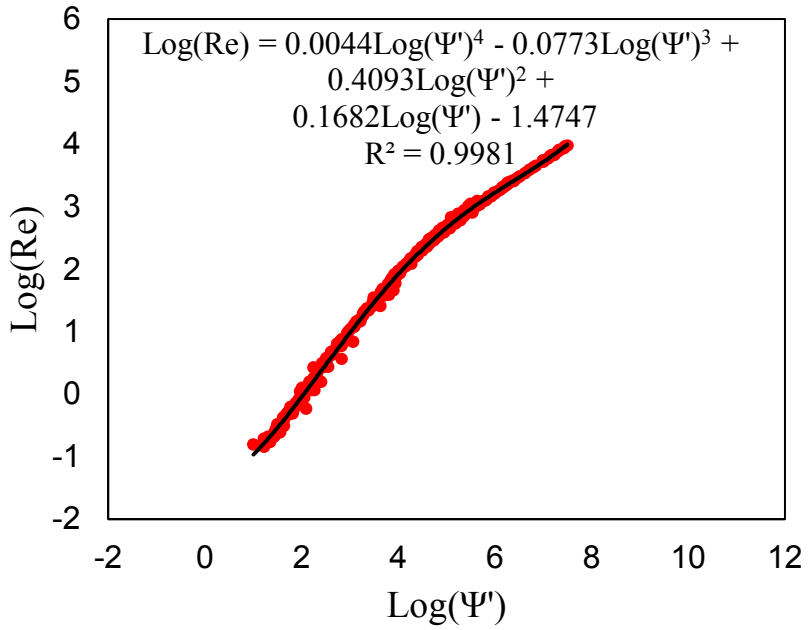

Figure 7.67 – Correlation between ψ' and Re for any spherical particle settling in a Bingham Plastic Fluid

The settling velocity of a spherical particle in Bingham Plastic fluid requires an iterative work and is expressed as:

$$Re = 10^{0.0044Log_{10}(\psi')^4 \ - 0.0773Log_{10}(\psi')^4 \ + 0.4093Log_{10}(\psi')^4 \ + 0.1682Log_{10}(\psi') - 1.4747} \tag{7.81}$$

where,

$$\psi' = \frac{4g(\rho_p - \rho_f)\rho_f d^3}{3\left(\tau_y + \frac{\eta_{PV}V_{sl}}{d}\right)^2} \tag{7.82}$$

and

$$Re = \frac{\rho_f v_{sl} d_p}{\tau_y + \frac{\eta_{PV}V_{sl}}{d_p}} \tag{7.83}$$

where, τ_y and η_{PV} are the yield point and the plastic viscosity, respectively.

For Power Law fluids, ψ' vs Re relation is presented in Figure 7.68.

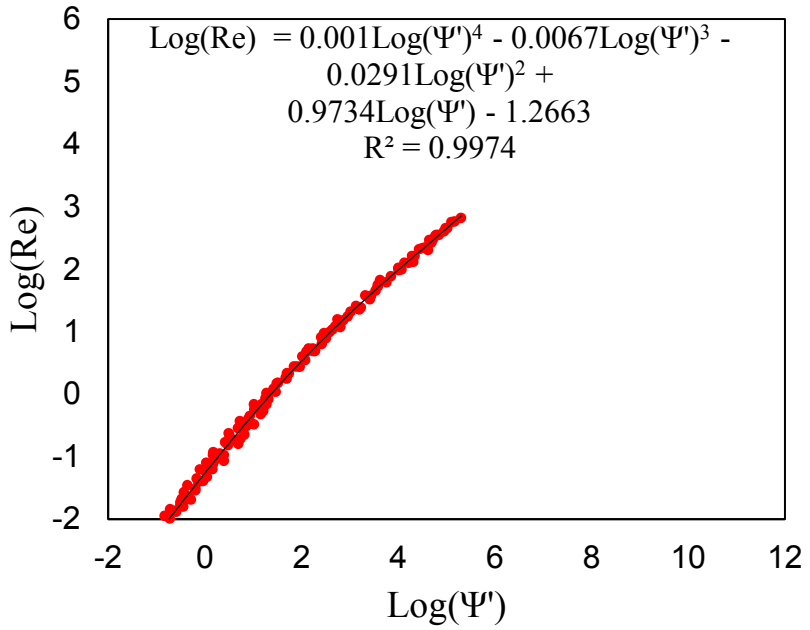

Figure 7.68 – Correlation between ψ' and Re for any spherical particle settling in a Power Law Fluid

The settling velocity of spherical particle in a Power Law fluid, similar to the settling in Bingham Plastic fluid, requires an iterative work and is expressed as:

$$Re = 10^{0.001\,Log_{10}(\psi')^4 - 0.0067\,Log_{10}(\psi')^3 - 0.0291\,Log_{10}(\psi')^2 + 0.9734 Log_{10}(\psi') - 1.2663} \tag{7.84}$$

where,

$$\psi' = \frac{4g(\rho_p - \rho_f)\rho_f d^{2n+1} {V_{sl}}^{2-2n}}{3(2^{n-1}K)^2} \tag{7.85}$$

and

$$Re = \frac{\rho_f {v_{sl}}^{2-n} {d_p}^n}{2^{n-1}K} \tag{7.86}$$

where, n and K are the flow behavior and consistency indexes, respectively.

7.3.5 Cuttings Concentration in Annular

Knowing the rate of penetration (ROP), the formation properties, drilling fluid properties and the well configuration (see Figure 7.69), cuttings concentration in the well can be calculated with respect to the drilling fluid flow rate.

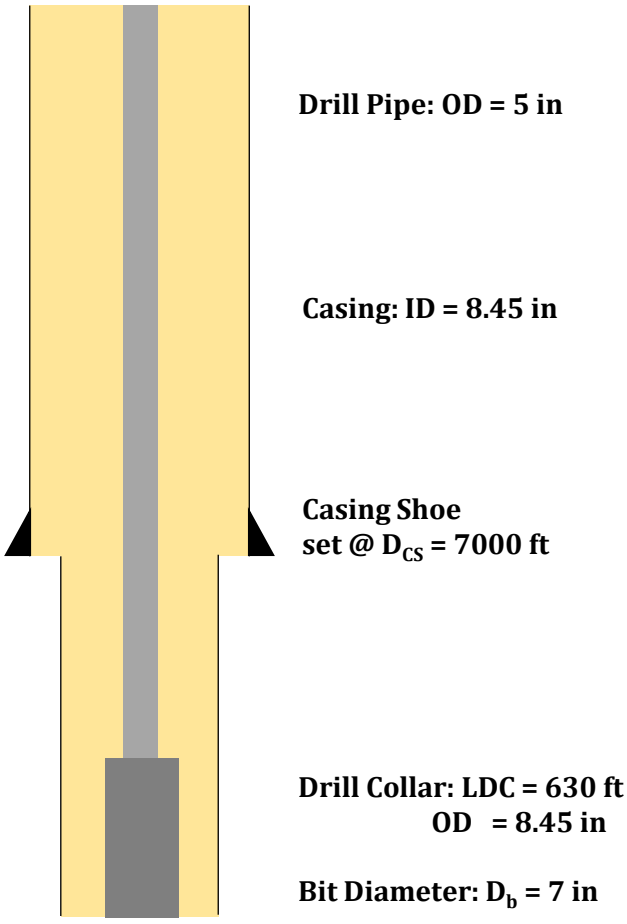

Figure 7.69 – Vertical wellbore geometry

We define the following parameters to calculate the ECD.

1- Cuttings feed rate: This is the volume of solids excavated from the bottom per unit time and defined as:

$$Q_c = A_b . ROP . (1 - \phi) \tag{7.87}$$

where, Q_c is the cuttings feeding rate and ϕ is the formation porosity.

2- Time for particles to reach surface: This is the time required the particles to reach the surface from the bottom of the well

For vertical wells the particle velocity is considered as the settling velocity of the particle stated as:

$$t_{csurf} = \frac{(V_{fDC} - V_{sl})}{L_{DC}} + \frac{(V_{fOH} - V_{sl})}{(TVD - L_{Cs} - L_{DC})} + \frac{(V_{fCs} - V_{sl})}{L_{Cs}} \tag{7.88}$$

Here, t_{csurf} is the time for particles to reach surface, V_{sl} is the particle settling velocity, V_{fDC}, V_{fOH} and V_{fCs} are the fluid velocities in the annular spaces between drill collar – open hole, drill pipe – open hole and drill pipe – casing, respectively; TVD is the true vertical depth and L_{Cs} and L_{DC} are the lengths of the casing and the drill collar, respectively.

For deviated wells the fluid velocity should be higher than the critical lift fluid velocity described by Badrouchi et al. (2020). Here, the particle velocity is considered as the settling velocity of the particle. The particle velocity is defined as:

$$V_s = (V_f - V_{sl}) . \cos(\alpha) \tag{7.89}$$

where, V_s is the solid particle velocity, V_f is the fluid velocity and α is the inclination angle from the horizontal.

Note that the measured depth (MD) is used to calculate t_{csurf} in deviated wells and not TVD.

3- Cuttings volume: This is the volume of the cuttings left in the annular space mixed with fluid during the drilling operation.

$$V_c = Q_c . t_{csurf} \tag{7.90}$$

4- **Volume of Annular Space:** This is the volume between the drillstring and the open hole as well as the cased hole.

$$V_T = \frac{\pi}{576}[(HD^2 - {OD_{DC}}^2).(L_{DC}) + (HD^2 - {OD_{DP}}^2).(TVD - L_{cs} - L_{DC}) + ({ID_{Cs}}^2 - {OD_{DP}}^2).L_{cs}] \tag{7.91}$$

where, V_T is the volume of the annular space, HD is the hole diameter (can be replaced by the bit diameter D_b), OD_{DC} and OD_{DP} are the outer diameters of the drill collar and the drill pipe respectively and ID_{Cs} is the casing inner diameter.

5- **Cuttings concentration:** This the ratio of the cuttings volume left in the annular space to the total volume of annular space.

$$C_{c\%} = \frac{V_c}{V_T} \tag{7.92}$$

6- **Density of the fluid-cuttings mixture:** This is the density of the mixture of drilling mud and cuttings in the annular space.

$$\rho_{mix} = \rho_f(1 - C_{c\%}) + \frac{\rho_p}{0.12}.C_{c\%} \tag{7.93}$$

where, ρ_f, ρ_p and ρ_{mix} are the densities of the fluid, cuttings and the mixture in the annular space respectively.

7.3.6. Pressure Losses

There are two types of pressure losses that contribute to the ECD:1) Frictional pressure losses and 2) Pipe rotational pressure losses in rotary drilling.

For frictional pressure losses ΔP_f over a certain length ΔL of the annular space, an equivalent diameter D_{eq} should be determined based on the pipe inner ID and outer OD diameters. The friction coefficient is calculated using Colebrook implicit formulation that requires iterative calculations.

Frictional pressure losses ΔP_f and pipe rotation pressure losses ΔP_{rpm} are calculated for each annular section (i.e. drill collar/open hole, drill pipe/open hole and drill pipe/casing) and then summed up. The calculation steps are presented in Appendix D.

For pipe rotation pressure losses, the correlation proposed by (Hemphill et al., 2008) was adopted in this work to calculate the frictional pressure losses due to the pipe rotation.

$$\Delta P_{rpm} = \left(-1.0792\left(\frac{ID}{OD}\right) + 17.982\left(\frac{ID}{OD}\right)^2\right).L.RPM.10^{-5} \tag{7.94}$$

7.3.6 Equivalent Circulation Density

The equivalent circulation density ECD is the apparent fluid density which results from adding annular friction to the density of the mud in the annular space. Knowing the pressure losses and the cuttings concentration, the ECD can be expressed as the following.

$$ECD = \rho_f + \frac{P_{back} + \Delta P_f + \Delta P_{rpm}}{0.052.TVD} + C_{c\%}(\rho_p - \rho_f) \tag{7.95}$$

Here, P_{back} is the back pressure at surface, for open surface it is usually the atmospheric pressure and is higher when drilling with managed pressure drilling (MPD).

7.4 Results and Discussions

A parametric sensitivity study was performed on the effect of different parameters (e.g. fluid, formation and drilling properties and parameters) on cuttings concentration and ECD in the wellbore annular as function of flow rate. The data used in this study are presented in

Table 4.16,

Table 7.27 and Table 7.28, respectively.

Table 7.26 – Well data summary

Property	Symbol	Value	Unit
Drillpipe Outer Diameter	OD_{DP}	5	in
Drillpipe Inner Diameter	ID_{DP}	4.5	in
Casing Inner Diameter	ID_{Cs}	8.45	in
Casing Outer Diameter	OD_{Cs}	9.625	in
Drill Collar Diameter	OD_{DC}	5.5	in
Drill Collar length	L_{DC}	360	ft
Casing Shoe Depth	L_{Cs}	7000	ft
Total Depth	TVD	14000	ft

Table 7.27 – Cuttings and fluid properties summary

Property		Symbol	Value	Unit
Particle Density		ρ_p	2.65	gcc
Particle Diameter		d_p	10	mm
Fluid Density		ρ_f	8.34	ppg
gravity		g	980.665	cm/s2
Newtonian	Fluid Viscosity	μ	0.021	Pa.s
Bingham Plastic	Yield Point	τ_y	0.1	lb/100ft2
	Plastic Viscosity	η_{PV}	3.5	lb/100ft2

Power Law	Behavior index	n	0.76	-
	Consistency index	K	0.0651	-

Table 7.28 – Drilling and Formation properties summary

Property	Symbol	Value	Unit
Weight on Bit	WOB	18600	lbf
Rotary Speed	RPM	100	rpm
Uniaxial Compressive Strength	UCS	16000	psi
Torque	T	762.5	ft.lbf
Bit Diameter	D_b	7	in
Friction Angle	$\emptyset$	5	(°)
Pore Pressure	P_p	2000	in
Porosity	φ	0.1	N/A

7.4.1 Fluid Properties Effect

Fluid properties have major effect on both cuttings velocity and pressure losses. Figure 7.70 (a) and b shows the effect of the fluid viscosity on the cuttings concentration in the wellbore as well as the equivalent circulation density. From Figure 7.70 (a), it is observed that increasing the fluid viscosity decreases the cuttings concentration in the wellbore and reduces the minimum required flow rate to bring the cuttings concentration below 5% the maximum acceptable value for the hole cleaning (Xiang et al., 2012). As the flow rate increases, fluid viscosity effect on cuttings concentration reduces and different fluid viscosities have similar effect on the cuttings percentage. However, for the ECD, increasing the viscosity leads to a significant increase of the ECD due to the increase of pressure losses that becomes more pronounced at higher viscosities (Figure 7.70 (b)). It is worth to mention that the same minimum value of ECD can be obtained for different fluid viscosity at different optimal rates. Therefore, the viscosity has no effect on the minimum

ECD that can be obtained. For example, if the ECD needs to be maintained below 9.2 ppg, using a 1 cP fluid requires a flow rate of 370 gpm and using a 25cP fluid requires a flow rate of 245 gpm. For 586% increase of fluid viscosity (from 6.859 to 24.761 cP), the minimum ECD increases by less than 1% (from 9.08 to 9.16 ppg).

Figure 7.71 (a) and (b) show the effect of the fluid density on the cuttings concentration in the wellbore as well as the equivalent circulation density. From Figure 7.71 (a), the decreasing effect of the minimum required flow rate to ensure cuttings concentration less than 5% is observed. It implies that the fluid density has a less pronounced effect on the minimum flow rate required to clean the cuttings as compared to viscosity. Also, as the flow rate increases, the effect of the fluid density on cuttings concentration vanishes more rapidly than that of viscosity. However, it seen from Figure 7.71 (b) that the fluid density has a more pronounced effect on the ECD as it is expected from Equation (7.95). As the flow rate increases, the effect of the fluid density becomes more pronounced. Also, as the density of the fluid increases, the minimum value of the ECD presents a sharp increase. For example, if the ECD needs to be maintained below 9.2 ppg, using an 8.34 ppg fluid requires a flow rate of 270 gpm, however when increasing the fluid density, regardless of the flow rate, the minimum value of ECD will be higher than 9.2ppg (for an 8.84 ppg mud, the minimum ECD that can be obtained is 9.64 at 260 gpm). For 60% increase of fluid density (from 8.34 to 13.34 ppg), the minimum ECD increases by more than 50% (from 9.16 to 13.95 ppg).

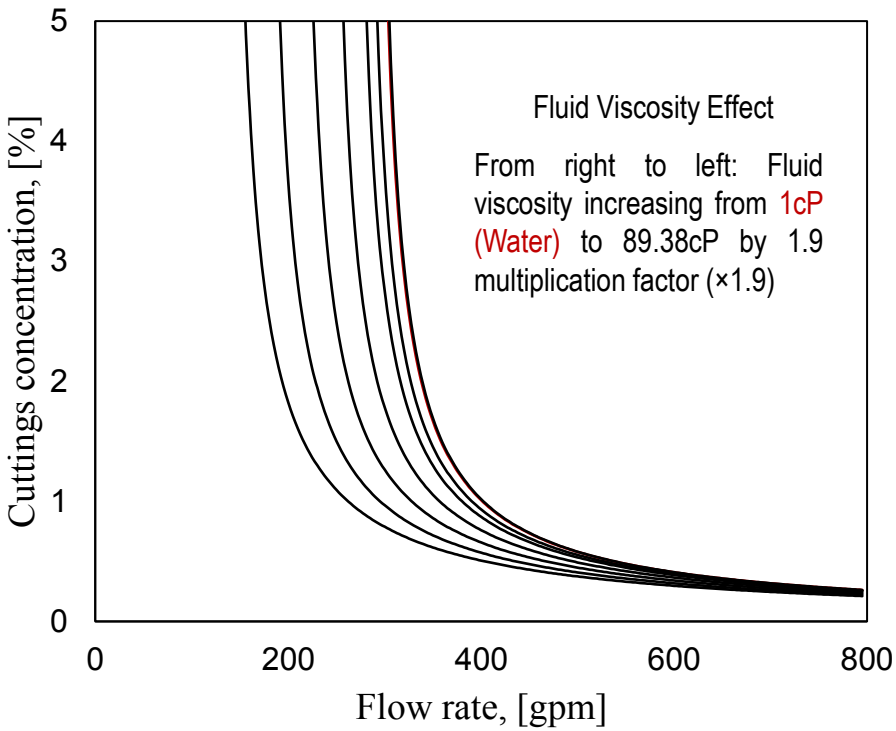

(a)

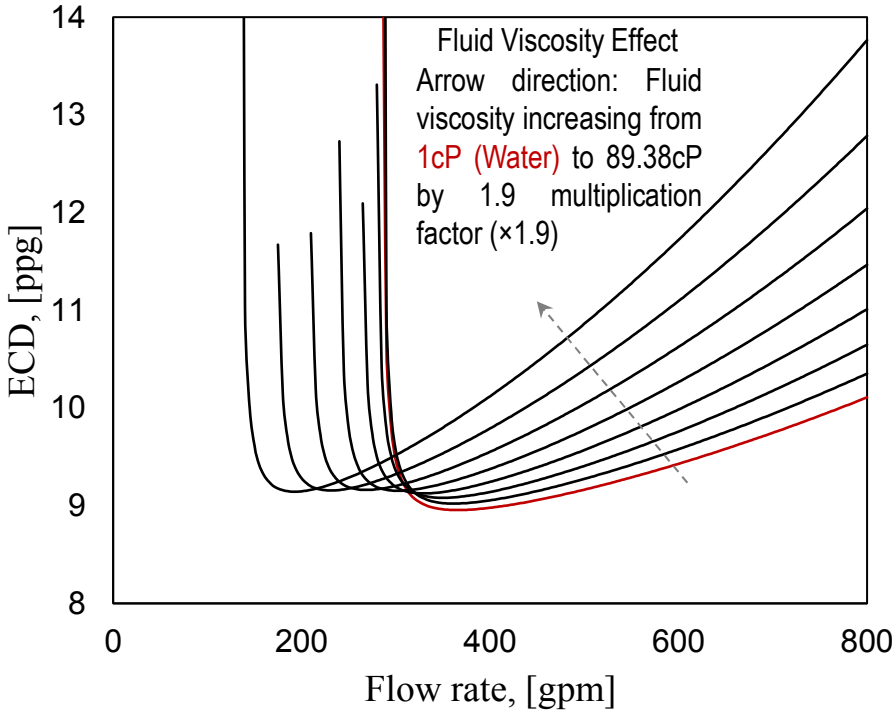

(b)

Figure 7.70 – Fluid viscosity effect as function of flow rate on (a) cuttings concentration (b) equivalent circulation density

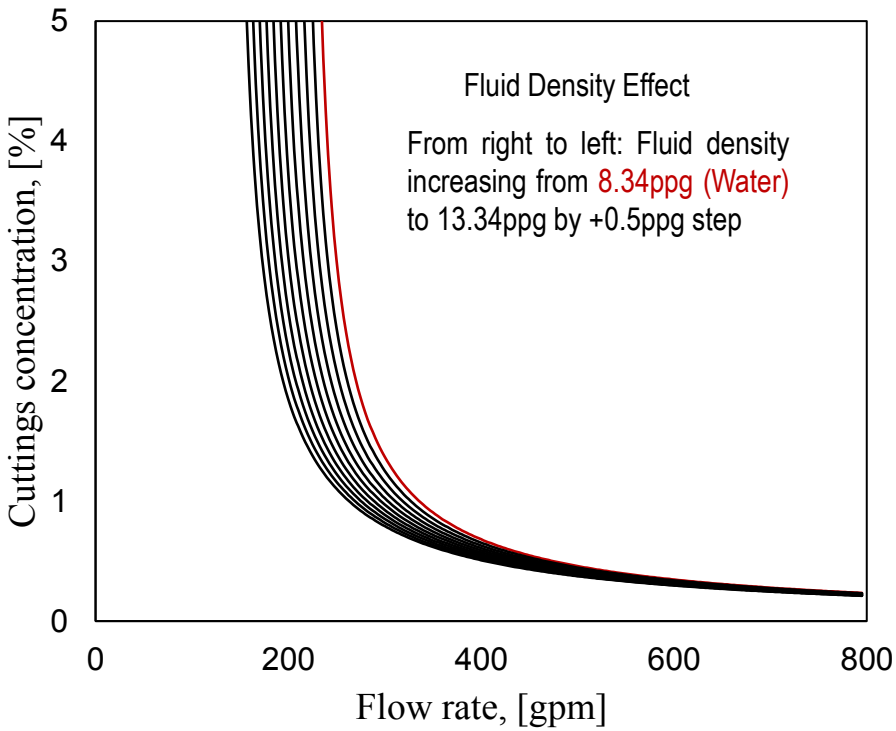

(a)

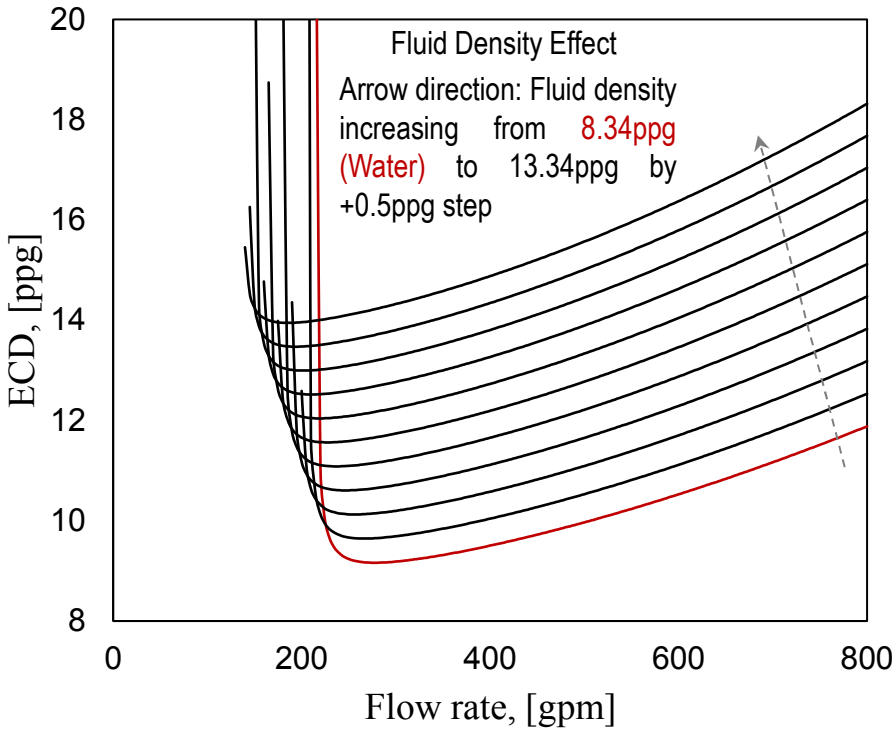

(b)

Figure 7.71 – Fluid density effect as function of flow rate on (a) cuttings concentration (b) equivalent circulation density

7.4.2 Cuttings Properties Effect

Cuttings density and size have significant effect on the settling velocity and the velocity of the particles which directly affect the cuttings concentration in the wellbore annular space. Particles density is an intrinsic property related to the formation, however, the size is both related to the formation type and composition as well as the drilling properties such us the bit type, cutters type and the rotary speed of the bit. Figure 7.72 (a) shows that the increase of particles density increases remarkably the minimum required flow rate to ensure cuttings concentration less than 5%. As the flow rate increases, particles density effect on cuttings concentration vanishes and different particles density show similar effect on the cuttings percentage. From Figure 7.72 (b), it is observed that increasing the particles density has no effect on the ECD at high flow rates as particles concentration is approaching 0% due to the high fluid velocity compared to the particles settling velocity. Also, as the density of the particles increases, the minimum value of ECD is moderately increasing. For 120% increase of particles density (from 1.5 to 3.3 gcc), the minimum ECD increases by 6% (from 8.834 to 9.36 Ppg).

Similar effect but more pronounced on both cuttings concentration and ECD is observed when increasing particle diameter. Since the size also has a major effect on the particles velocity, the minimum required flow rate to achieve less than 5% of cuttings concentration in the wellbore annular increases noticeably with the increase of the particle size (Figure 7.73 (a)). Similarly, the increase of the particles' diameter will slightly increase the minimum achievable ECD (Figure 7.73 (b)). As the flow rate increases, the cuttings present in the annular is reduced to the point where they have no significant effect on the ECD. For 125% increase of particles diameter (from 1.14 to 2.56 mm), the minimum ECD increases by 1.3% (from 8.865 to 8.797 ppg).

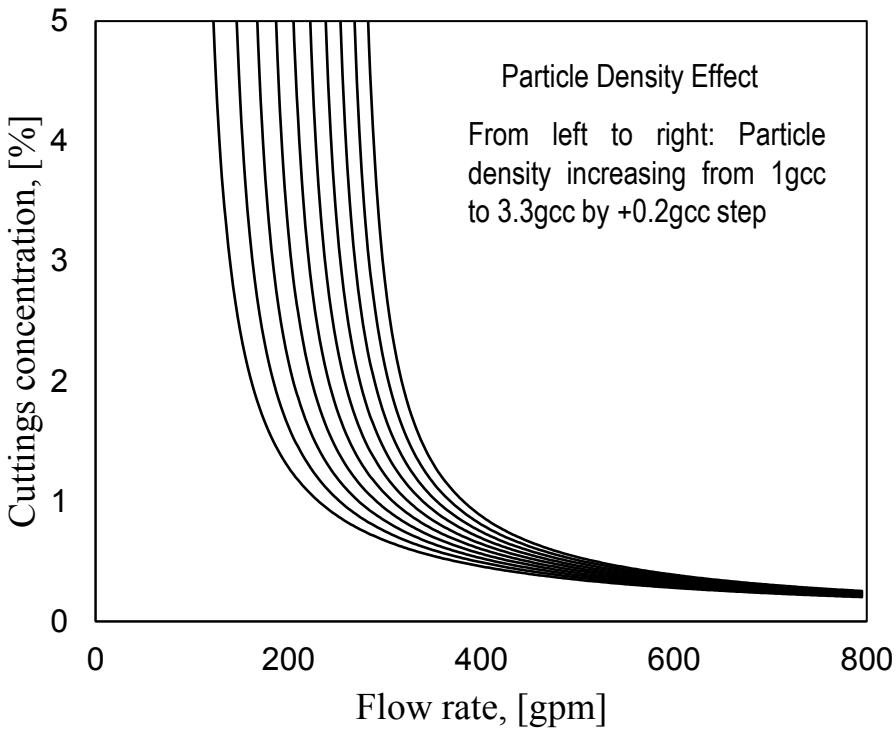

(a)

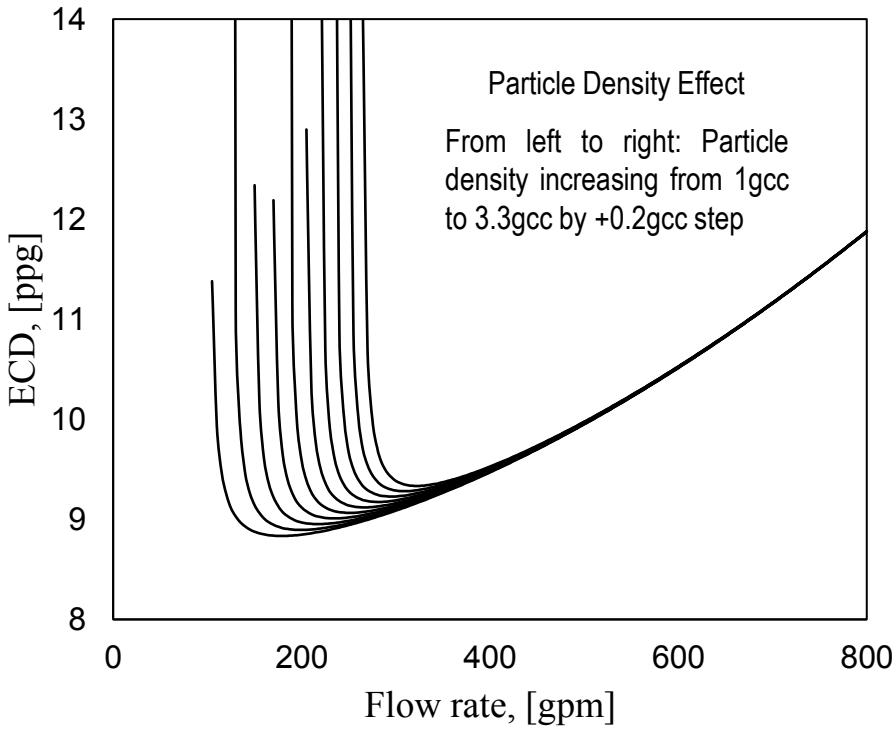

(b)

Figure 7.72 – Particles density effect as function of flow rate on (a) cuttings concentration (b) equivalent circulation density

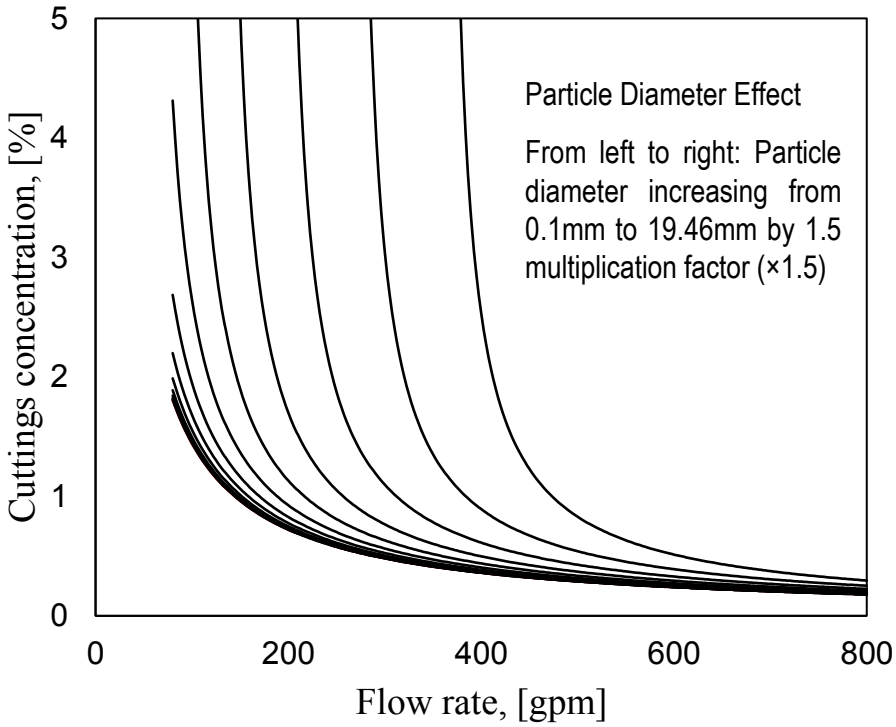

(a)

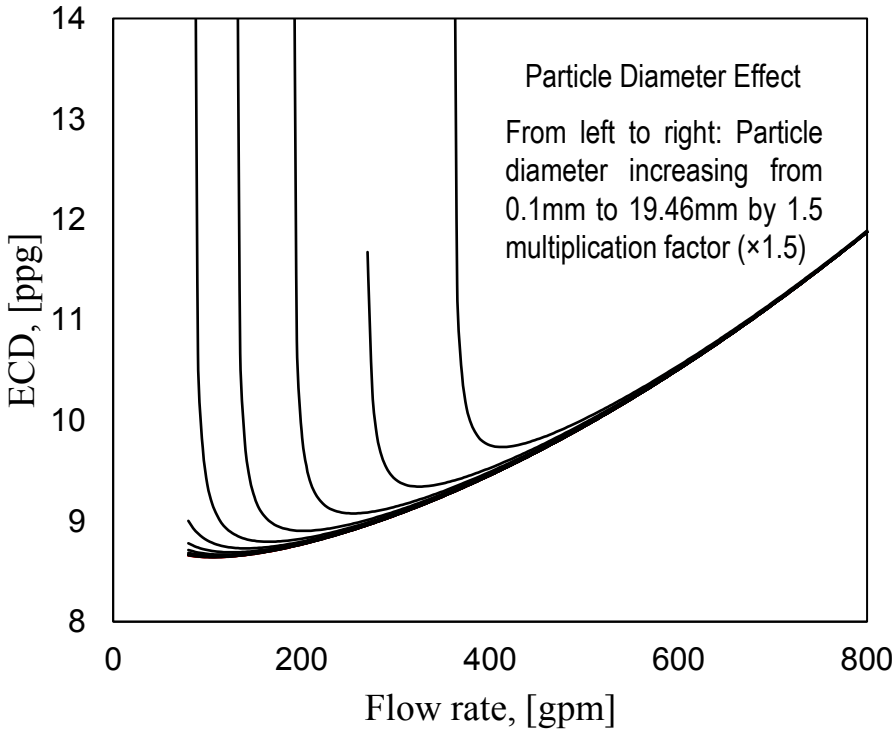

(b)

Figure 7.73 – Particles diameter effect as function of flow rate on (a) cuttings concentration (b) equivalent circulation density

7.4.3 Drill Pipe Size Effect

Drill pipe size affects mainly the fluid velocity in the annular space. As the drill pipe diameter increases, the annular fluid velocity increases it enhances the cleaning process (less cuttings left in the wellbore) therefore less flow rate is required to obtain a maximum of 5% of cuttings trapped in the annular (Figure 7.74 (a)). However, this increase in the annular fluid velocity leads to a major increase in the pressure losses due to friction leading to higher ECD values (Figure 7.74 (b)). Also, it is seen from the results of Figure 7.74 (b) that the increase of the pipe diameter leads to a small margin of low ECD values (ECD curves becomes more concave).

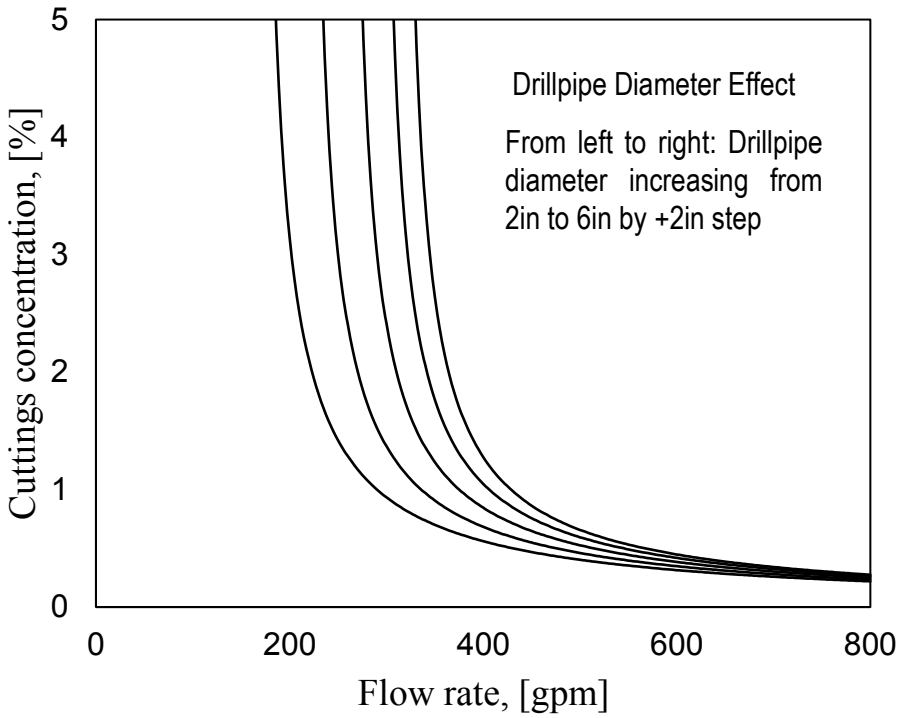

(a)

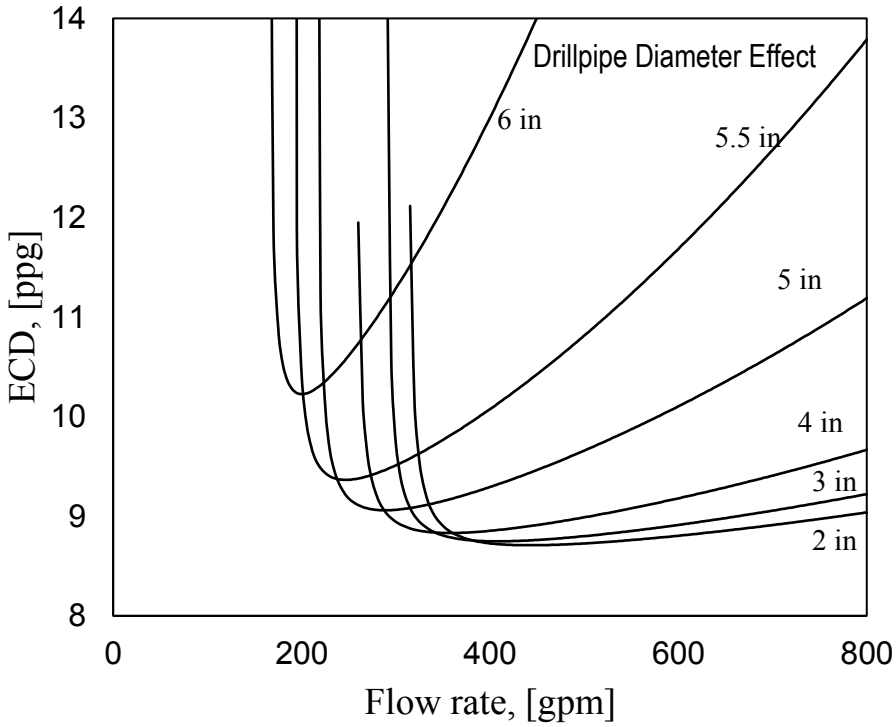

(b)

Figure 7.74 – Drill Pipe outer diameter effect as function of flow rate on (a) cuttings concentration (b) equivalent circulation density

7.4.4 Formation UCS Effect

Formation UCS is the determining factor of the value of the minimal MSE to achieve an efficient drilling and rate of penetration. As the formation strength increases, the ROP decreases leading to a reduction in the cuttings concentration in the wellbore, which means better hole cleaning leaving with minimal flow rates (Figure 7.75 (a)). However, the effect of the UCS in the ECD is minimal and slightly affects the minimum ECD value that can be obtained as shown in Figure 7.75 (a). For 600% increase of UCS (from 5000 to 35000 psi), the minimum ECD increases by 7% (from 9.018 to 9.658 ppg).

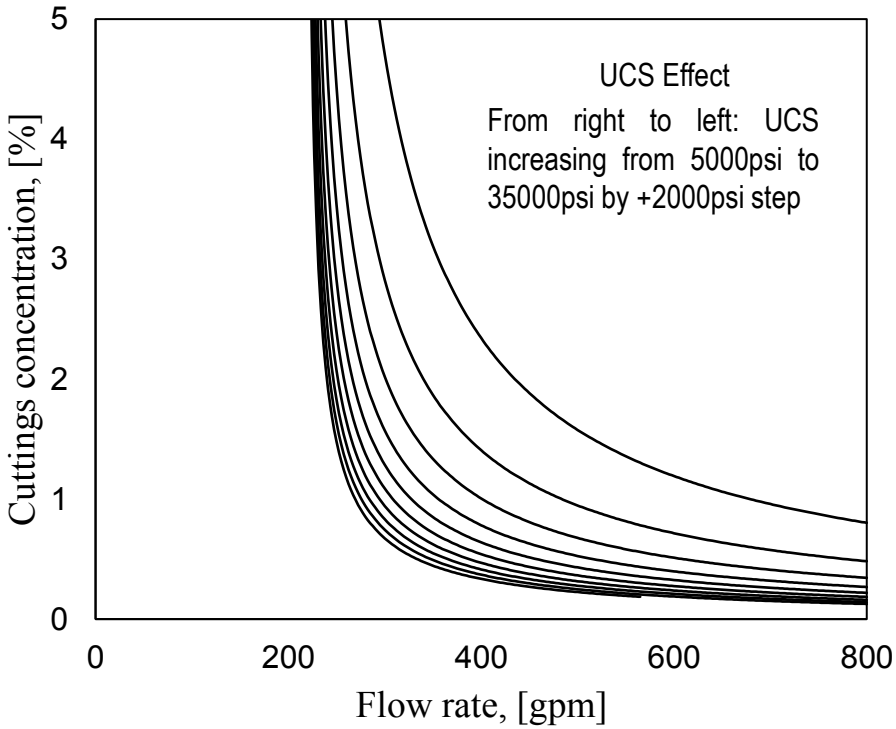

(a)

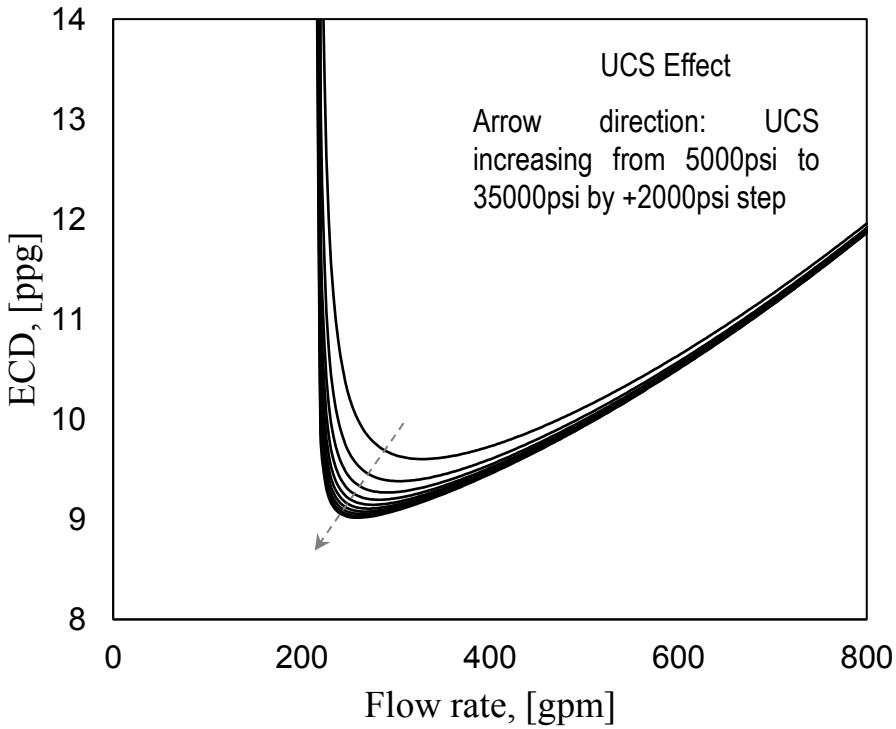

(b)

Figure 7.75 – UCS effect as function of flow rate on (a) cuttings concentration (b) equivalent circulation density

7.4.5 Drilling Parameters Effect

Pipe rotation is a parameter affecting both the ROP and the pressure losses. For similar formation and drilling fluid and same drilling parameters, the effect of RPM on the cuttings concentration is more critical when lower cuttings percentage is required, however to obtain a minimum of 5% cuttings concentration moderate effect of the RPM is observed (Figure 7.76 (a)). Similarly, the effect of RPM on the minimum ECD value that can be achieved is moderate when the pressure losses due to the pipe rotation are considered (Figure 7.76 (b)). This effect is minimized when the pipe rotation pressure losses are not considered (Figure 7.76 (c)). The effect of the pressure losses due to the pipe rotation increases significantly at high rates as presented in Figure 7.77.

The Torque and WOB have inverse effect on the cuttings concentration and ECD compared to the UCS effect. As torque and WOB increase, the cuttings concentration increases. However, similar to the UCS effect, their effect on ECD is minor, especially at high rates, as they increase the rate of penetration without affecting the pressure losses due to friction (Figure 7.78).

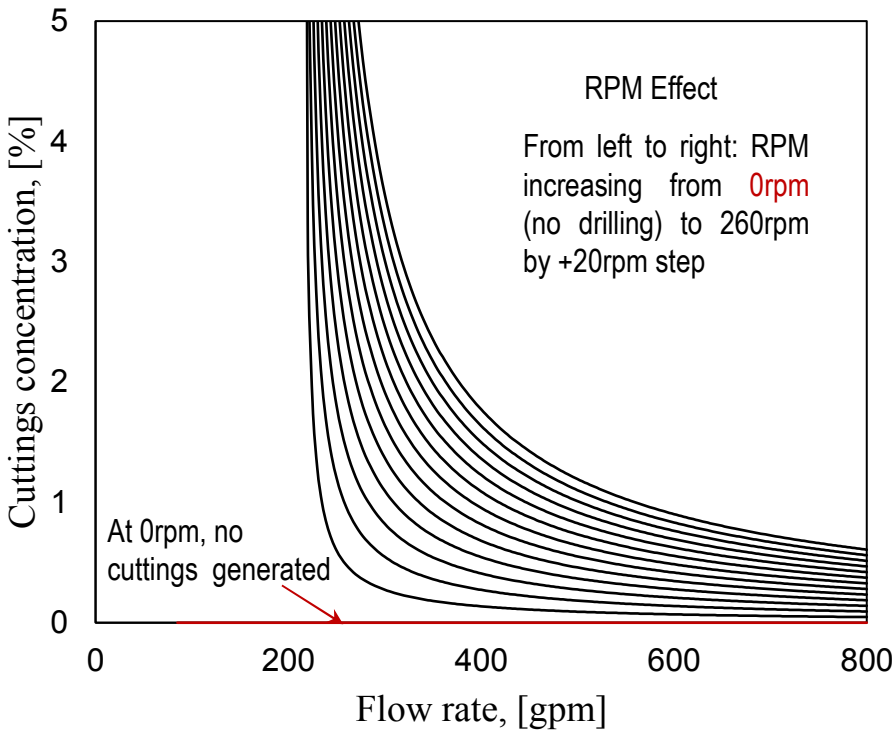

(a)

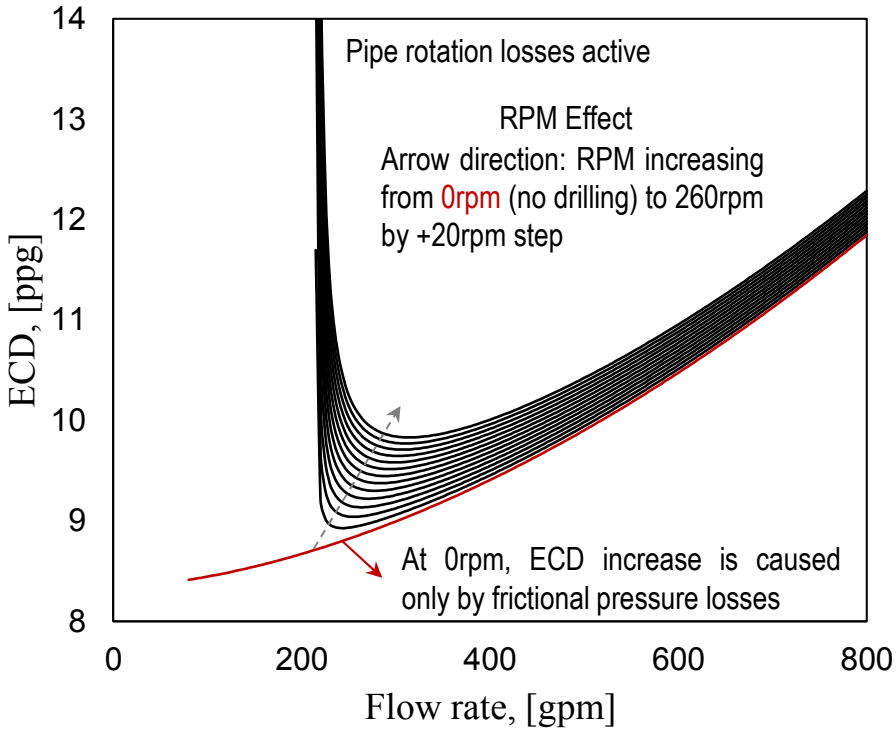

(b)

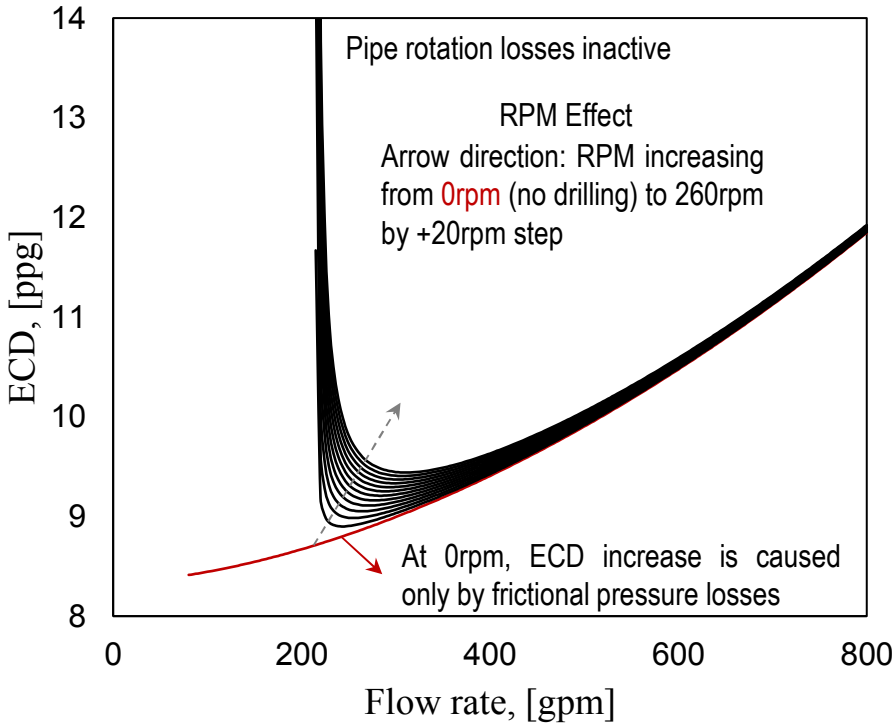

(c)

Figure 7.76 – RPM effect as function of flow rate on (a) cuttings concentration (b) equivalent circulation density with pipe rotation losses (c) equivalent circulation density without pipe rotation losses

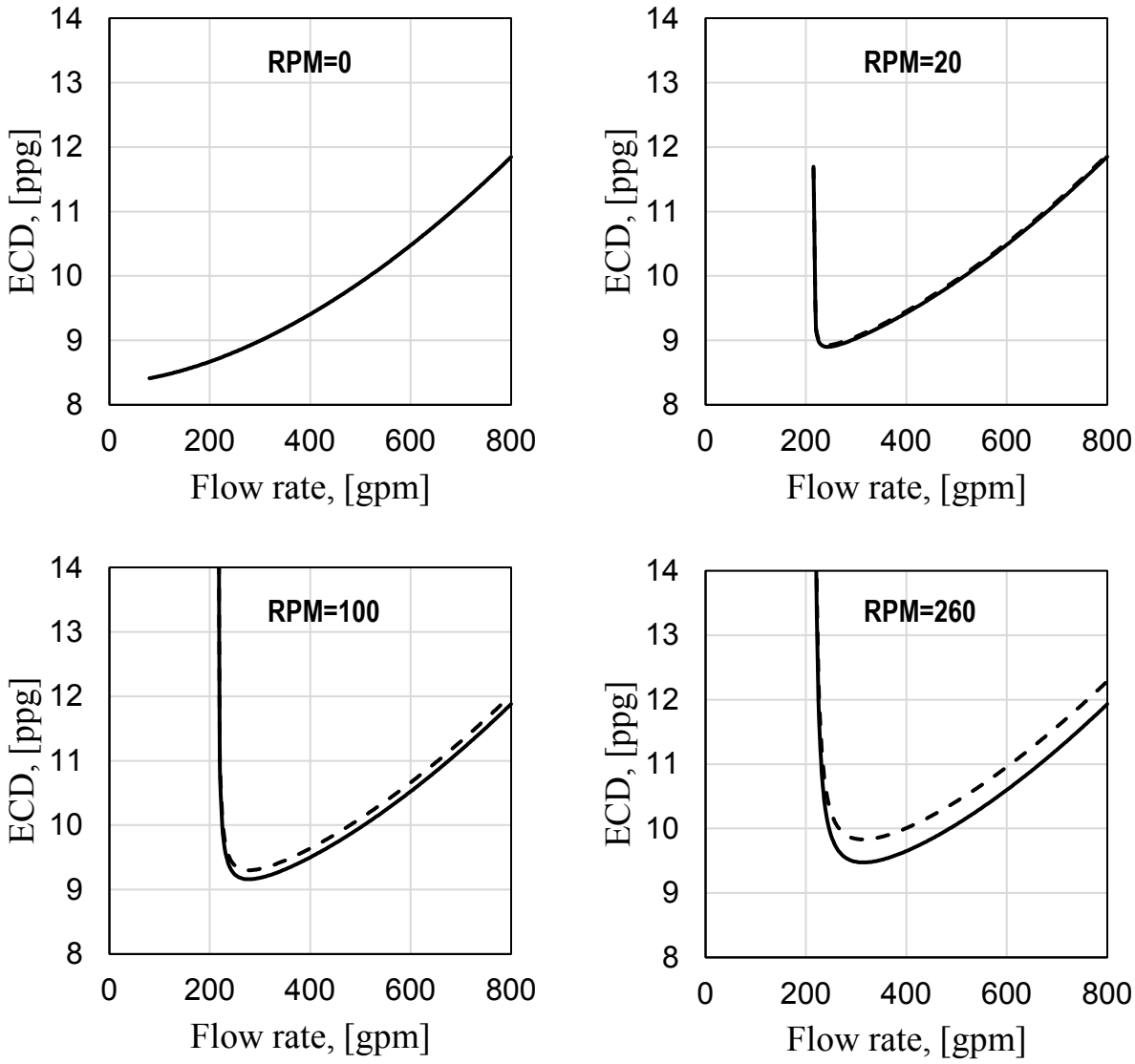

Figure 7.77 – Pipe rotation pressure losses effect on ECD

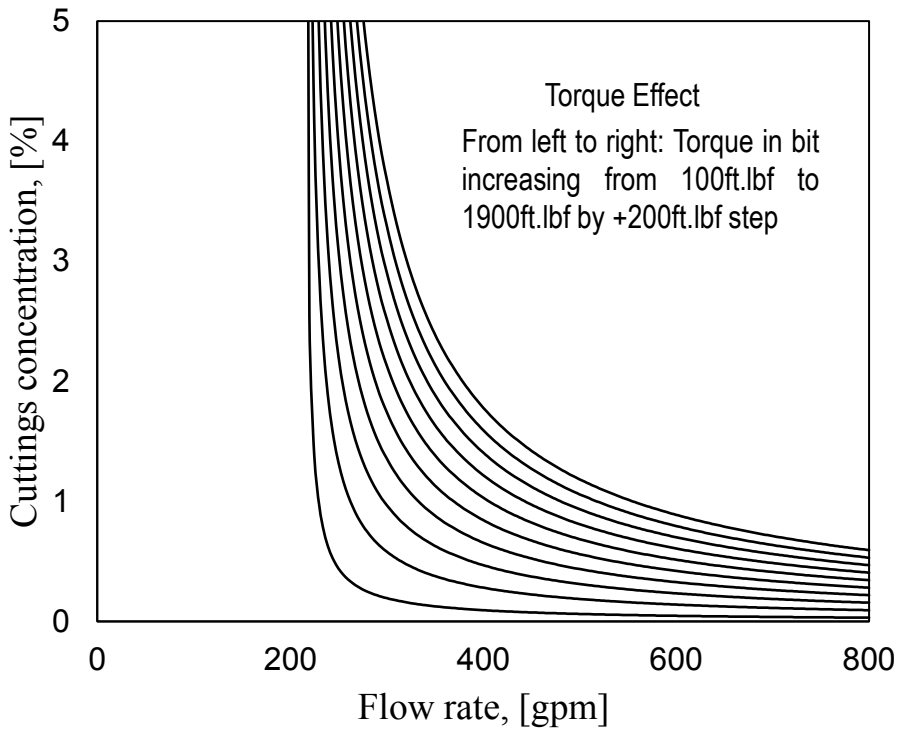

(a)

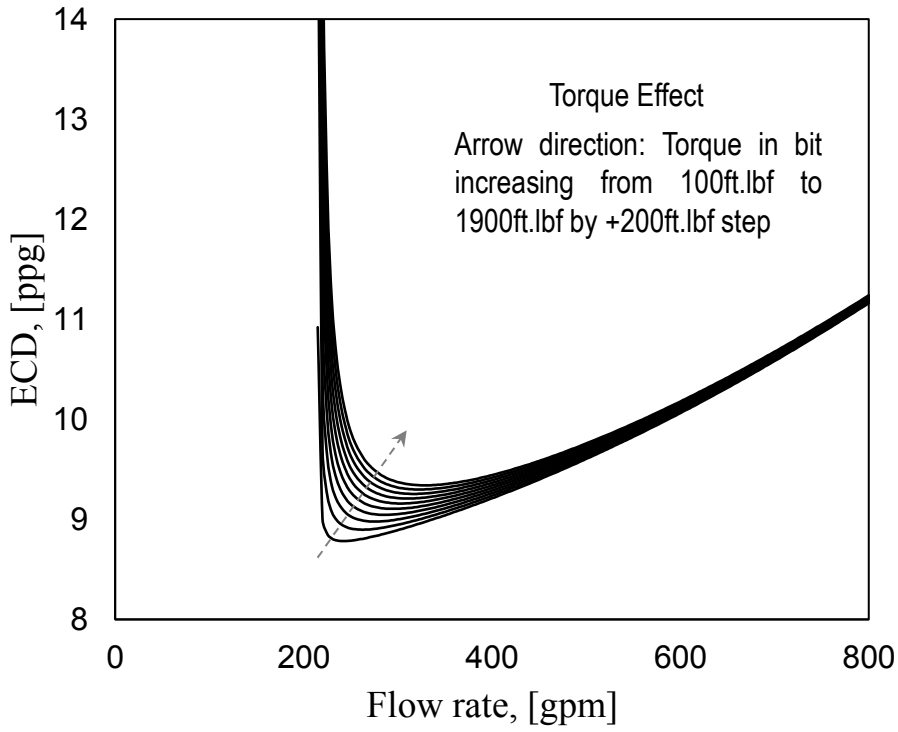

(b)

Figure 7.78 – Torque effect as function of flow rate on (a) cuttings concentration (b) equivalent circulation density

7.5 Summary

In this Chapter, settling and critical velocity models of the previous Chapters were coupled with the mechanical specific energy (MSE) model and pressure losses to predict the equivalent circulating density as well as the cuttings concentration in the wellbore annular during drilling operation. The results of the parametric studies were showed that:

1. From the developed ECD model, a reservoir and drilling engineer can optimize drilling parameters and injection flow rate to avoid any wellbore instability and mud losses.
2. The developed model is applicable fora wide range of particle, fluid and drilling parameters as well as valid for most types of drilling fluids.
3. Pipe rotation has an enhancing effect on the rate of penetration but also increases of the pressure losses and cuttings concentration leading to higher ECD values. WOB and torque can be two alternatives to increase the ROP without causing more frictional losses.
4. The wellbore geometry and mainly the drill pipe size has major effect on the hole cleaning and the ECD. Larger pipe sizes present a better hole cleaning but in expense of higher pressure losses. The presented model can be used as the optimization tool to better select the right drilling string.
5. Fluid properties such us density and viscosity have a dominant effect on the ECD. In case of field limitations, the presented provides a guide on what parameter to change and what flow rate to use to prevent losses and wellbore instabilities.
6. This model allows engineers to optimize their drilling operation not based on the MSE only but also with considering the ECD and cuttings concentration effect.

Field logging while drilling data as well as experimental measurements are needed for better validation of the model. Also, a study on the effect of drilling parameters and formation properties on the cuttings size is a future work that needs to be considered.

CHAPTER 8

The Impact of Stabilizers Geometry on Hole Cleaning Efficiency

8.1 Introduction

Effective hole cleaning is one of the major factors affecting the design of the hydraulic parameters during the drilling operation. A poor hole cleaning can lead to serious problems during and after the drilling operation such as lost circulation, bit balling, high rotary torque, high equivalent circulation density, bit wearing, pipe sticking, low rate of penetration and can hinder the placement of the casing (Chen et al., 2002; Dupriest et al., 2011; Gaynor et al., 2001; Hopkin, 1967; Mason and Chen, 2006; Mkuyi, 2016; Skalle, 2011).

Hole cleaning is often assessed in relation to flow rate, fluid properties, cuttings properties, wellbore inclination and some drilling parameters such us rate of penetration and rotary speed (Badrouchi et al., 2020; Badrouchi and Rasouli, 2020a; Bilgesu et al., 2007; Gavignet and Sobey, 1989; Iyoho, 1980; Kenny et al., 1996; Martins et al., 1999; Menegbo et al., 2019; Mohammadsalehi and Malekzadeh, 2011; Nazari et al., 2010; Pilehvari et al., 1996; Saasen and Løklingholm, 2002; Saeid and Busahmin, 2016; Sanchez et al., 1997b; van Oort et al., 1996; Zeidler, 1972). The existence of wellbore hardware, such as stabilizer may present a large disturbance to the cuttings movement along the annulus space and ultimately result in poor hole

cleaning. This concept has not been adequately studied in the past (Xiaofeng et al., 2013). Stabilizer selection was often based on mechanical stability under harsh downhole environment (Pastusek, 2018; Woods and Lubinski, 1955). Stabilizer is a drillstring sub mounted on the top of the bit to mechanically stabilize the bottom hole assembly (BHA) in the borehole in order to avoid unintentional sidetracking, vibrations, and ensure the quality of the hole geometry (Woods and Lubinski, 1955). It ensures the drilling string to be concentric in the wellbore by keeping its outside diameter close to wellbore wall (Chen and Guan, 2000).

In field applications, mix successes have been reported in terms of the effectiveness of the stabilizers for what they are intended to do (Woods and Lubinski, 1955). However, even for wellbore stability, Woods and Lubinski (1955) mentioned that the problem of selecting appropriate stabilizers is so complex that it seems impossible from field experiences to establish rules for the successful use of them. Since field tests are expensive and can cause damage to the wellbore, simulation is important to evaluate the selection criteria of stabilizers and the impact of different parameters in their performance.

Straight, straight with offset and helical blades are the three general types of stabilizers that are used in drilling operations. Helical blade stabilizer has larger surface area to make sure there is enough contact with borehole wall. Few researches are available in the literature considering the effect of stabilizers on hole cleaning (Anayo et al., 2012; Chen and Xiong, 2010; Shu, 2005; Shu and Liu, 2006, 2005; Xiaofeng et al., 2013). Some researches on helical centralizers showed that for deviated to horizontal holes, helices in the helical centralizers help to enhance cuttings transport efficiency to some extent by generating eddies (Anayo et al., 2012; Chen and Xiong, 2010; Shu, 2005; Shu and Liu, 2006, 2005). However, these studies do not present a comparison between different blade geometries. Xiaofeng et al. (2013) compared two models of straight and helical

blades stabilizers and showed that the straight blade ones are better in terms of hole cleaning without presenting a sensitivity analysis or a wide comparison between different types. Other researchers investigated the use of hole cleaning devices, similar geometries to stabilizer, to cleanout deviated wellbores (Nwagu et al., 2014; Yan et al., 2019). However, all these studies do not present a comprehensive comparative study of the effect on hole cleaning.

Very few studies focused on the effect of the stabilizers blade geometry effect on hole cleaning. In this work we investigate this in vertical wells. Also, the well inclination may also have an impact on choosing the optimum stabilizer geometry, and this also needs separate investigation.

8.2 Stabilizers

Drilling stabilizers are downhole equipment incorporated to the drilling string to increase rate of penetration and prevent undesired hole deviation problems.

Stabilizers can be categorized in two families, welded and integral blades. The welded Blade Stabilizers used in the B.H.A for drilling soft to medium hard formation holes are available in three types of straight, straight-offset or spiral design. However, the integral blade stabilizers are made from high-strength alloy steel as a single piece tool and suited for use in most formations from soft and sticky to hard and abrasive. They are rolled and machined to provide the blades to minimize down hole torque, reduce damage to the hole wall and ensure maximum fluid circulation, but are more expensive (Choudhary, 2011).

Stabilizers blades are available in the following three configurations:

1- Straight blade:

The blades are straight and their axes are parallel to the axis of the stabilizer body. Figure 8.79 shows the design parameters for a straight blade stabilizer. Where W is the width of the blades, L

is the length of the stabilizer, and *D* is the diameter of the circle contouring the blades centered with the axis of the stabilizer.

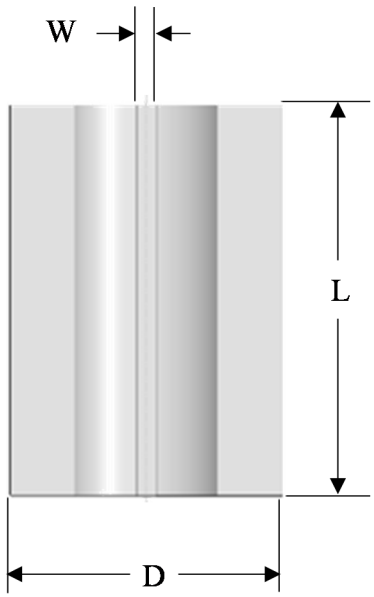

Figure 8.79 – Straight blade stabilizer geometry

2- Straight blade with offset:

The blades are straight and its axis is deviated (counterclockwise) from the axis of the stabilizer body with a certain angle called offset. Figure 8.80 shows the design parameters for a straight blade with offset stabilizer.

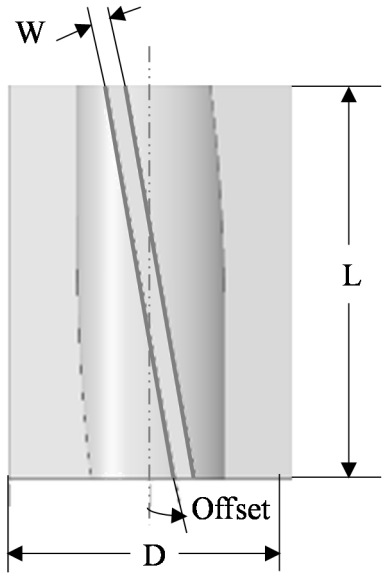

Figure 8.80 – Straight blade with offset stabilizer geometry

3- Helical/spiral blade:

The blades are helices with consistent height from the stabilizer body. A specific design parameter for the helices is the pitch. The helices pitch is the distance in between a helical blade adjacent coils along the central axis of the stabilizer body (i.e. if the pitch is equal to the stabilizer length, the helices will complete a hole tour on the stabilizer body). Figure 8.81 shows the design parameters for a helical blade stabilizer.

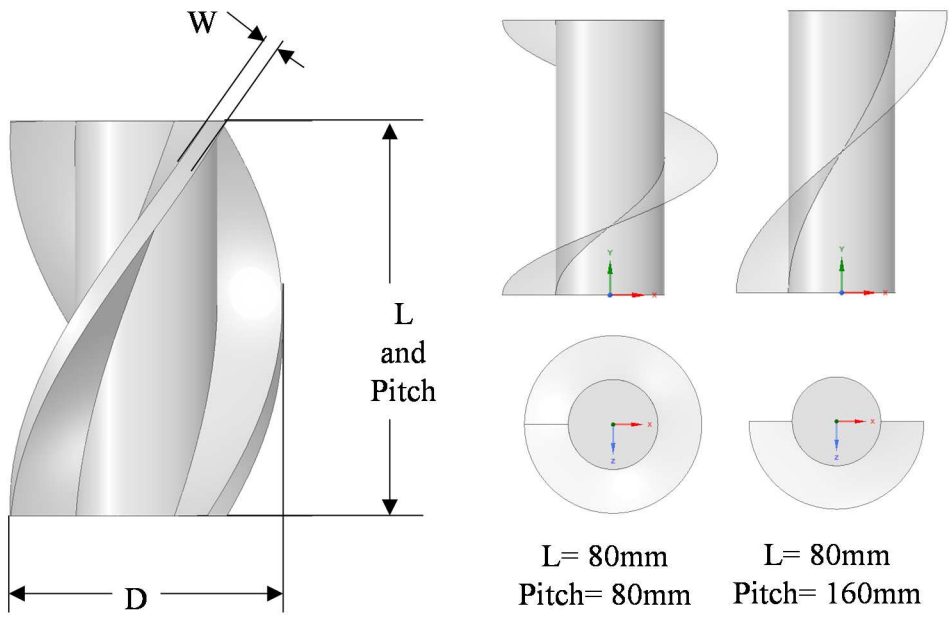

Figure 8.81 – Helical blade stabilizer geometry

8.2.1 Use of stabilizers in coiled tubing

Stabilizers are also used in coiled tubing operations where the coiled tubing string and BHA is not subjected to a rotational force (Livescu and Craig, 2018; Pereira et al., 2019). The stabilizers are designed to be included as part of the coiled tubing work string to assist in providing centralization of the coiled tubing BHA, allowing easier location of tools during fishing and/or to provide general stability in the tubing.

8.2.2 Stabilizer Blade Shape Effect

When the particles reach the stabilizer at a velocity u, some are blocked by the bottom section of the blades causing a velocity loss. For straight blades with offset (θ) and helical blades, the particles encounters partial plastic collisions ($0<e_t<1$) to a reflected velocity v. An illustration of partial plastic collision of a spherical cuttings particle on an oblique blade wall is presented in Figure 8.82. For the MfiX simulation model used in this study, the restitution coefficient vector is $\binom{0.85}{1}$. For

a case of a spherical particle with an initial velocity $u = 0.5\ m/s$ hitting an oblique smooth blade (tangential restitution coefficient $e_{tT} = 1$) of an angle θ, the effect of the normal restitution coefficient which depends on the wall and particle properties is presented in Figure 8.83.

Normal restitution coefficient: $e_{tN} = 0.85$

Tangential restitution coefficient: $e_{tT} = 1$

The forces equilibrium equations along the line of impact is:

$$v.cos(\varphi) = e_{tN}.u.\cos(\theta) \tag{8.96}$$

and along the smooth surface is:

$$v.sin(\varphi) = e_{tT}.u.\sin(\theta) \tag{8.97}$$

Combining the square root of both Equations (3.1) and (8.97), we can estimated the hindered velocity due to the collision with the blade as:

$$v = u.\sqrt{{e_{tT}}^2.sin^2(\theta) + {e_{tN}}^2.cos^2(\theta)} \tag{8.98}$$

and dividing Equation (3.1) by Equation (8.97), we obtain the deflection angle as:

$$\varphi = Atan\left(\frac{e_{tN}}{e_{tT}}.tan(\theta)\right) \tag{8.99}$$

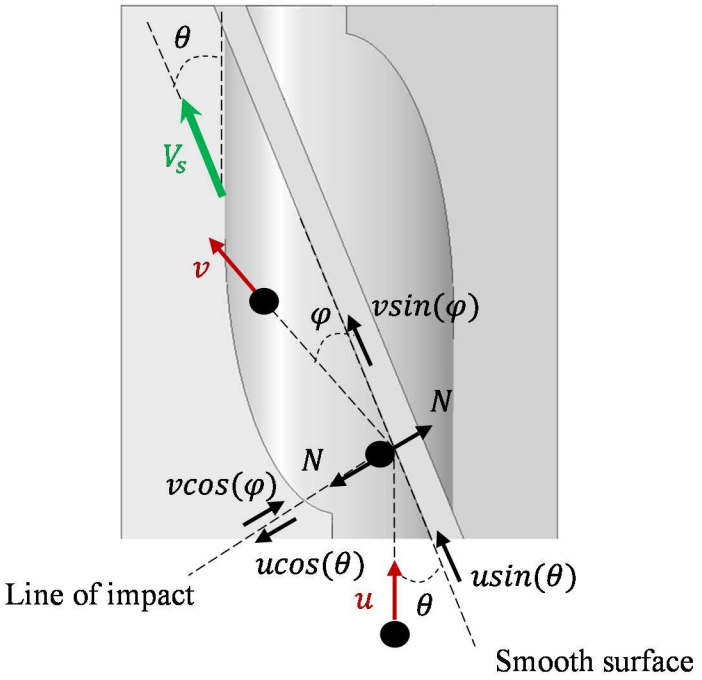

Figure 8.82 – Oblique collision of spherical cuttings on a stabilizer blade

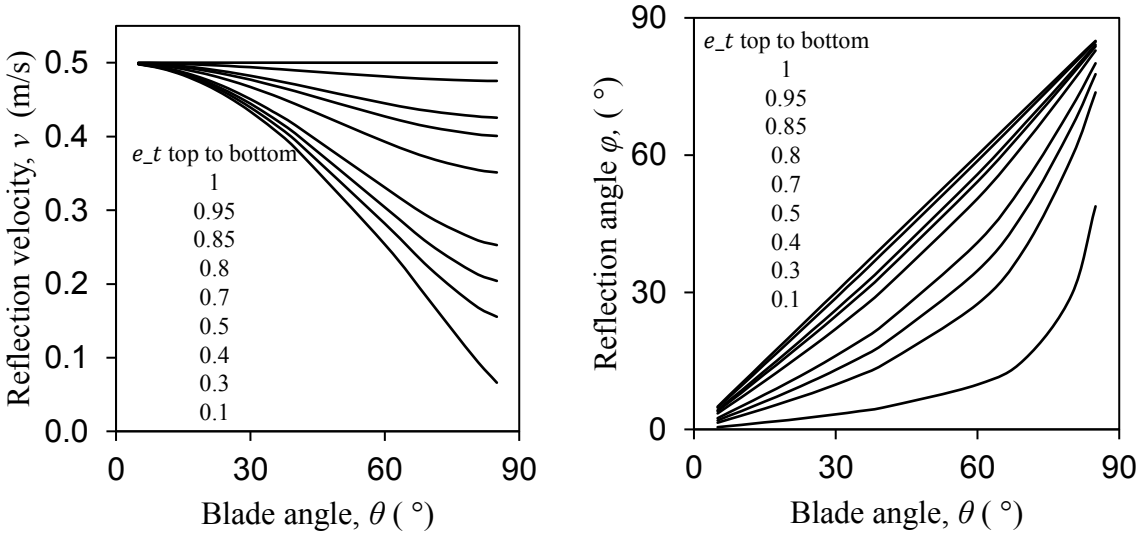

Figure 8.83 – Oblique collision of spherical cuttings on a stabilizer blade

8.3 Numerical Simulation

To study the effect of stabilizers on the hole cleaning process, two assessment criteria were opted in this work, the average particles velocity and concentration in the whole system after a steady state regime is observed (Figure 8.84 (a) and (b)). These properties were selected because the particles velocity and concentration in the wellbore are the key properties defining the cleaning state of the hole.

As cuttings start entering the wellbore, the particles velocity increases to reach a steady state motion. As soon as the particles arrives at the stabilizer, some particles are blocked by the bottom section (Figure 8.84 (c)) and walls of the blades, and due to the decrease of the section open to flow, an increase of velocity is observed followed by a decrease of the velocity due to exiting the stabilizer section. After some time, the system reaches an equilibrium steady state in the average velocity and cuttings concentration in the wellbore.

A better design is the one leaving less particles in the wellbore, in other words, less average cuttings concentration at steady state. From Figure 8.84 (b), it is clear that the hole cleaning in a wellbore with a 4 mm width - 4 blades stabilizer leaves less cuttings in the wellbore than a 7 mm width and even enhances the cleaning comparing to a wellbore without stabilizer. Similarly, different stabilizer designs will be compared to evaluate the effect on the hole cleaning process.

More than 30 stabilizer design were used in this study (see Appendix E).

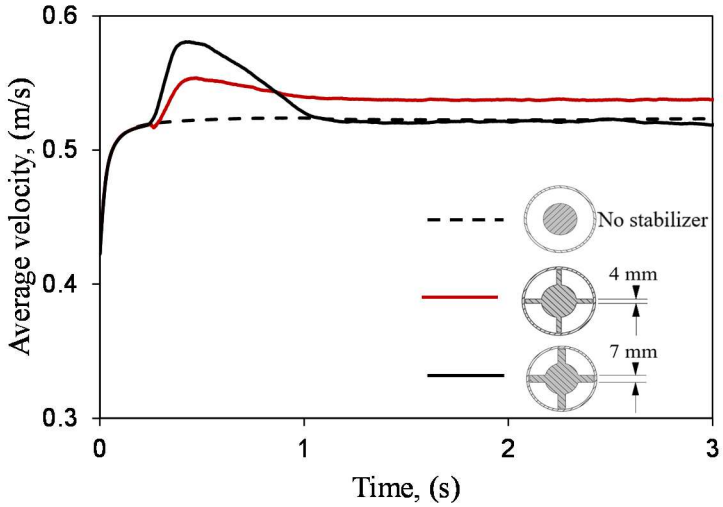

(a)

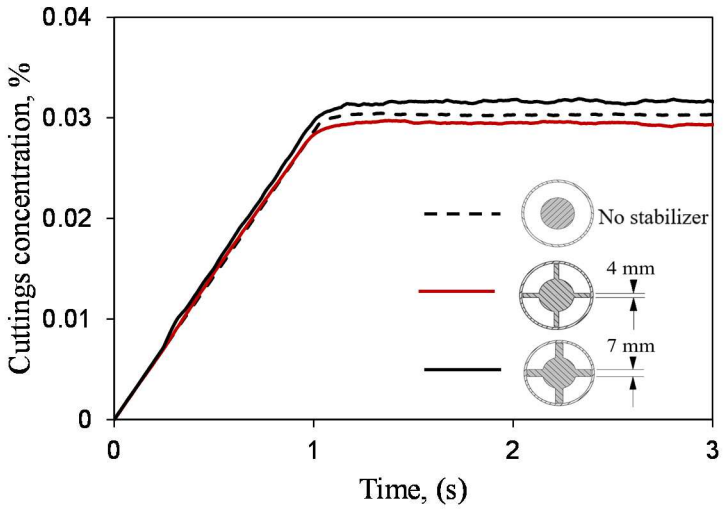

(b)

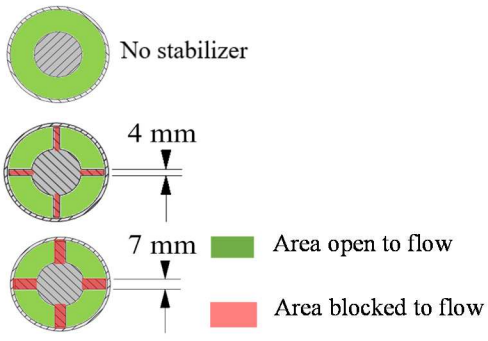

(c)

Figure 8.84 – Average cuttings (a) velocity and (b) concentration in clear wellbore (no stabilizer) and wellbores with 4 blades straight stabilizers of W=4 mm and W=7 mm. (c) shows the increase of the area blocked to flow due to the blades base surface increase with width.

Numerical Simulations

Particle-In-Cell (PIC) multiphase model in MFiX software, was used to perform the numerical simulations of the hole cleaning of vertical wells with stabilizers. PIC model is a Lagrangian-Eulerian simulation that considers the fluid phase as a continuum while assigning parcels to represent groups of real particles to reduce computational time and cost ("MFiX - Multiphase Flow Science Group at NETL," n.d.).

MfiX employs a parcel-based approach also known as nominal particles based approach (Strack and Cundall, 1978). PIC uses interpolation operators to manage the position of parcels, cell centers and face cell centers (Clarke and Musser, 2020).

Governing equations such us mass and momentum conservations are similar to those in traditional fluid–phase CFD. However, solids-phase is modeled using discrete particles and additional coupling terms due to drag from the solids–phase are added to the governing equations.

Physical boundaries are defined by the intersection of the Eulerian grid with a STL (stereolithographic CAD file). Newtonian interaction with boundaries is discretely calculated (Clarke and Musser, 2020). The stabilizers geometries are created in Ansys spaceclaim as STL files and exported to MFIX as STM boundaries (Corporation, 2007). Also, the restitution coefficient, e_t, is defined with normal and tangential components $\binom{e_{tN}}{e_{tT}}$.

MfiX reliability in simulation hole cleaning process was discussed in the work of (Badrouchi and Rasouli, 2020a).

Since the main objective of this study is to investigate the effect of stabilizers blade shape and design, any well configuration and particle and fluid properties can be used. Sandstone spherical particles as cuttings and water as the drilling fluid were considered for this study. The input data

used for simulation in this study are summarized in Table 8.29, and a schematic of the well configuration can be found in the Appendix E.

Table 8.29 – Simulation inputs

Properties	value	unit
Pipe length	550	mm
Inner pipe diameter	29.8	mm
Outer pipe diameter	60	mm
Fluid Density	1×10^{3}	kg/m^3
Fluid viscosity	1×10^{-3}	Pa.s
Particles density	2.65×10^{-3}	kg/m^3
Particles diameter	1.5	mm
Particles concentration	4	%
Particles rate	6×10^{-5}	m^3/s
Fluid flow rate	1.5×10^{-3}	m^3/s

8.4 Results and Discussion

8.4.1 Straight blade stabilizers

Straight blade stabilizers come in different blade numbers and blade widths. To study the effect of the blades width on hole cleaning, a set of different blades width of 4 blades stabilizers (Figure 8.85 (a)) were simulated and their cleaning efficiencies were compared. Figure 8.85 (b) shows that a 4 mm blade thickness enhances the hole cleaning. It is also seen that the increase of the fluid velocity caused by the reduction of the area open to flow against the stabilizer resulted in increasing the average velocity of particles hence enhancing the cleaning efficiency. However, this holds to be the case to a certain extent since the metal area of the bottom sections of the blades, as shown in Figure 8.84 (c), block the cuttings reducing the velocity and increase the amount of particles

trapped in the well (Figure 8.85 (c)). Figure 8.86 (a) and (b) confirms the effect of the area blocked to flow on the particles velocity and concentration in the well. The blocked area has both a positive effect (increase of the velocity of some particles due to the fluid velocity increase) and a negative effect (decrease of the velocity of some particles due to hitting the bottom section of the blades) on the hole cleaning.

To study the effect of the number of blades, stabilizers with 4 mm blades width and 2, 3, 4, 6 and 8 blades (see Figure 8.87 (a)) were simulated and their results were compared. The results show that increase of the number of blades improves hole cleaning (Figure 8.87 (b)) up to 6 blades but the trend reverses beyond that. The increase of blades number helps decrease the area open to flow causing a fluid velocity increase resulting in an increase of the particles velocity. However, after 6 blades, the area open to flow becomes very narrow and the rapid increase of the particles friction with the blades walls reduces the velocity of the particles with detrimental impact on hole cleaning (Figure 8.87 (b) and (c)).

Even with higher cuttings flow rate (increased by 2.5 times) straight blades stabilizer with 4 mm wall thickness ensures a better cleaning compared to a wellbore without a stabilizer (Appendix E).

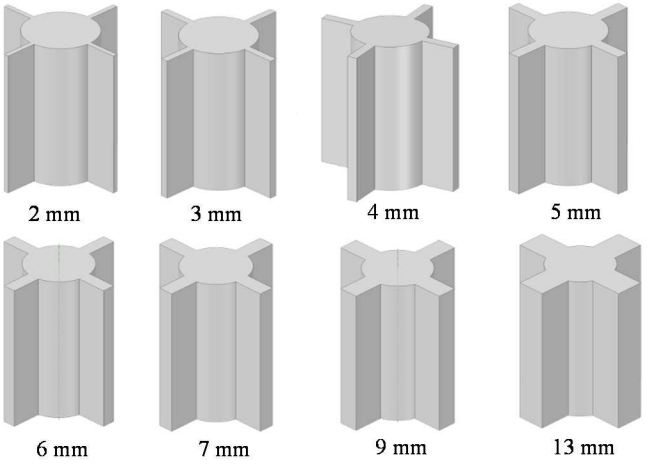

(a)

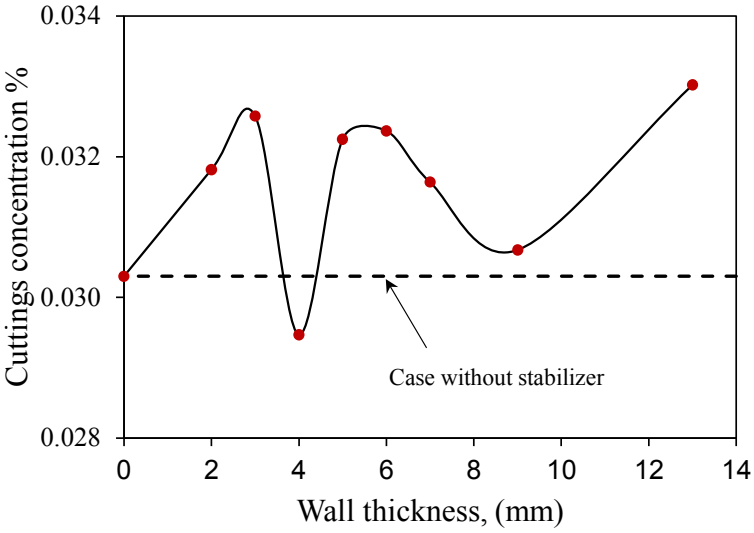

(b)

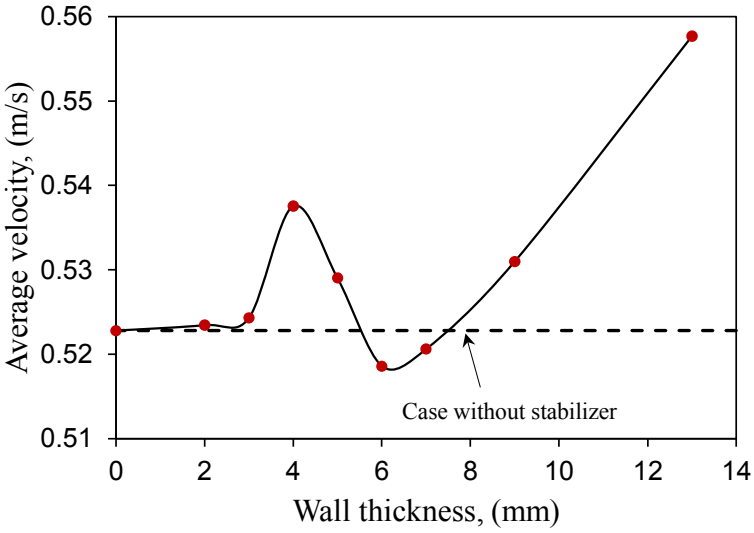

(c)

Figure 8.85 – Effect of wall thickness of a 4 blades stabilizer (a) designs used, (b) Effect on concentration, and (c) effect on velocity

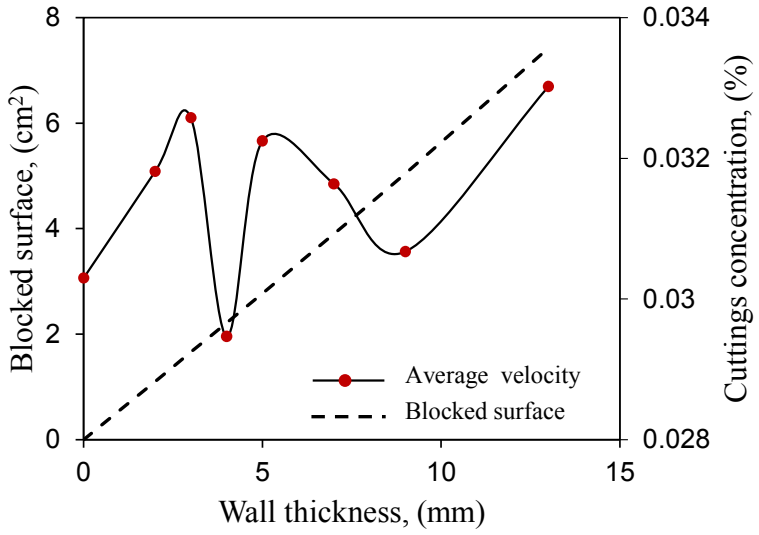

(a)

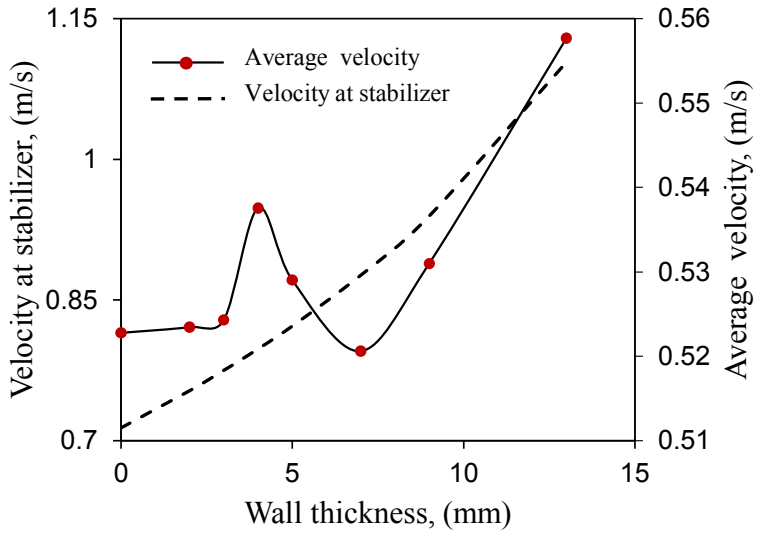

(b)

Figure 8.86 – Effect of wall thickness of a 4 blades stabilizer (a) comparison of the blades blocked to flow area and cuttings concentration, (b) comparison of the fluid velocity at the stabilizer level and the particles average velocity

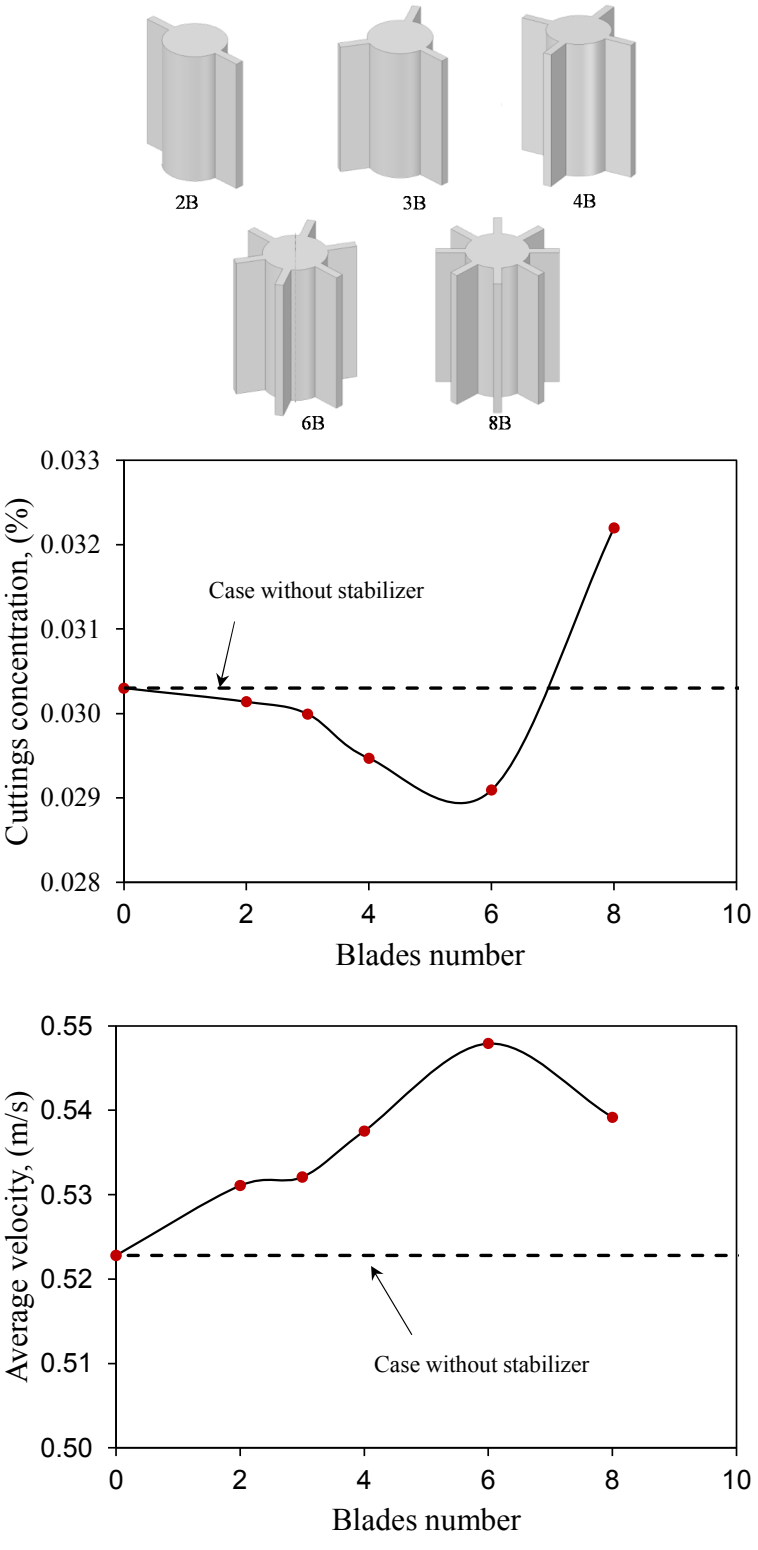

Figure 8.87 – Effect of blades number of a 4mm width stabilizer (a) designs used, (b) Effect on concentration, and (c) effect on velocity

8.4.2 Straight Blade Stabilizers with Offset

Some straight blade stabilizers come in different blades offset angles and numbers. To study the effect of the number of blades in hole cleaning, stabilizers with 10° offset blade and 2, 4 and 6 blades (Figure 8.88 (a)) were modeled and their cleaning efficiencies were compared. The results of Figure 8.88 (b) show that the increase of the number of blades reduces the hole cleaning efficiency. While in this case also the increase of the fluid velocity is observed across the stabilizer section due to the decrease of the area open to flow, the average particle velocity reduces as the friction of the particles with the blades wall increases (see Figure 8.88 (c)). This observation is expected as explained in the Stabilizer Blade Shape Effect section (Figure 8.82 and Figure 8.83).

A similar detrimental effect is observed when the offset angle of the blades is increased. Simulations were carried out for 4 blades stabilizers with different offset angles of 5°, 10°, 15°, and 20°, respectively, as depicted in Figure 8.89 (a). The increase of the offset angle results in a decrease of the average velocity of particles hence less hole cleaning efficiency (Figure 8.89 (b)). The negative effect of the offset angle on the particles motion to the surface is expected as presented in Figure 8.82 and Figure 8.83.

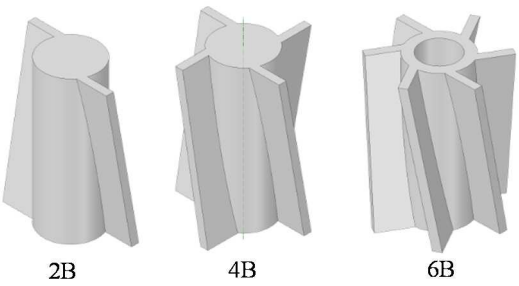

(a)

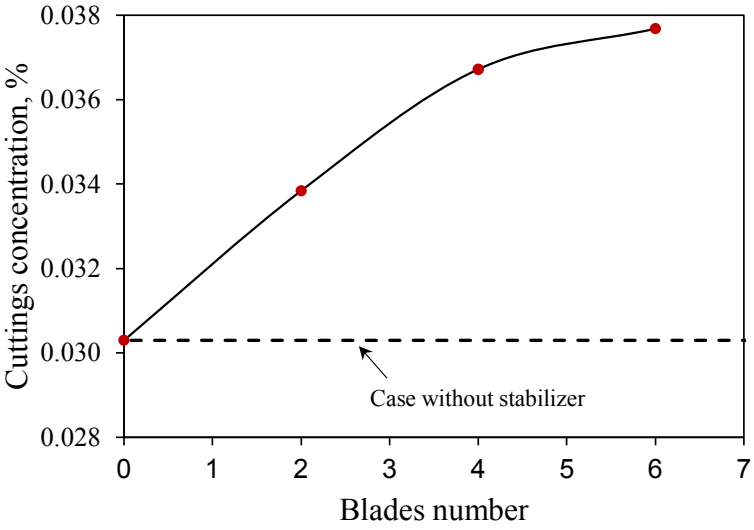

(b)

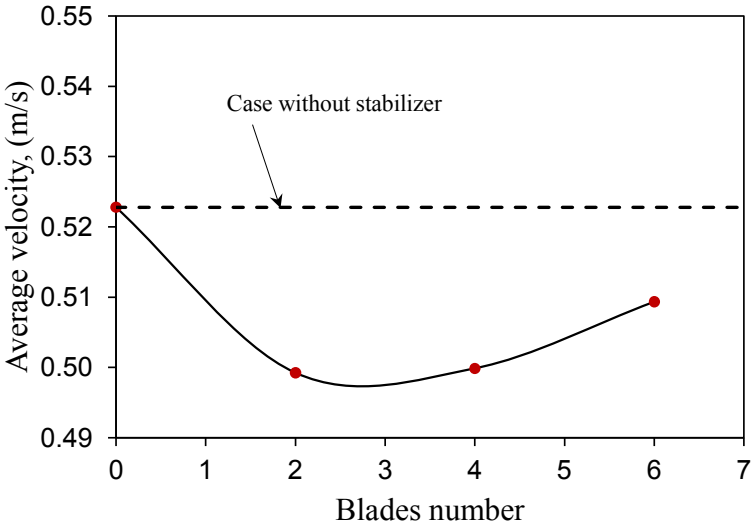

(c)

Figure 8.88 – Effect of blades number of a 4mm width stabilizer (a) designs used, (b) Effect on concentration, and (c) effect on velocity

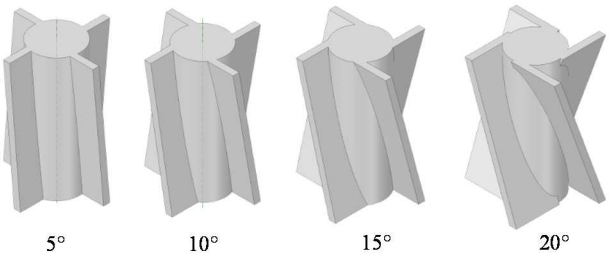

(a)

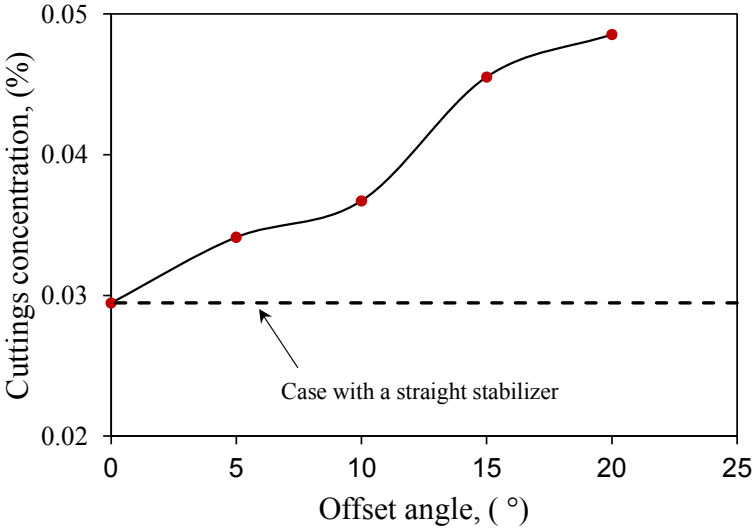

(b)

Figure 8.89 – Effect of blades offset angle of a 4mm width -4blades stabilizer (a) designs used, and (b) Effect on concentration

8.4.3 Helical Stabilizers

Helical blades are expected to have more blocking effect on the particles motion in the annulus space. Stabilizers with straight, straight with offset and helical blades with similar design properties (i.e. the blades width and the number of blades), as shown in Figure 8.90 (a), were modeled and the results were compared. For accurate comparison reasons, as shown in Figure 8.90 (a), the offset angle of the straight stabilizer with offset was 10° which is equivalent to the helical blades. The results show that stabilizers with straight blade geometry are more efficient in hole cleaning compared to those with straight blade with offset and helical blades (Figure 8.90 (b)).

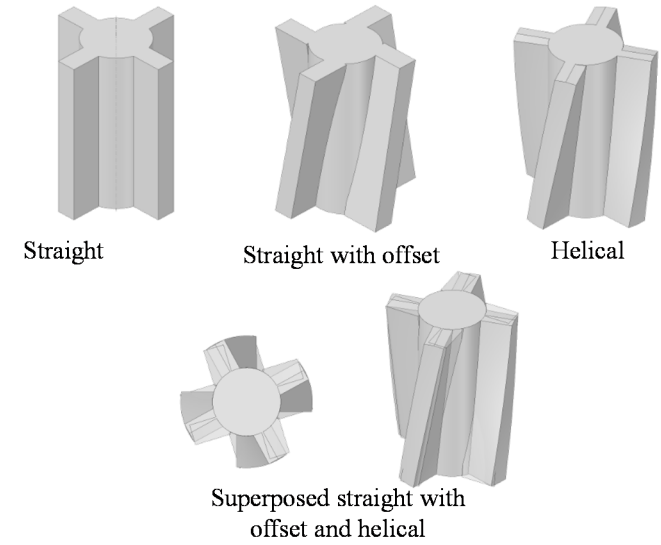

(a)

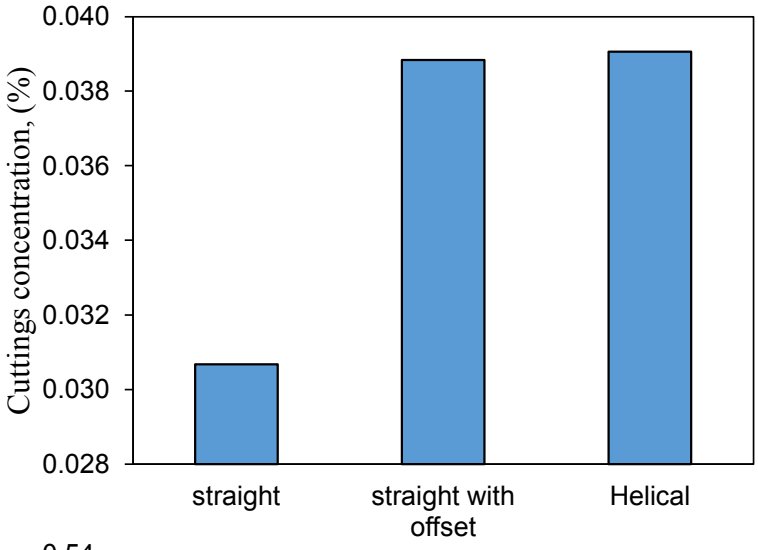

(b)

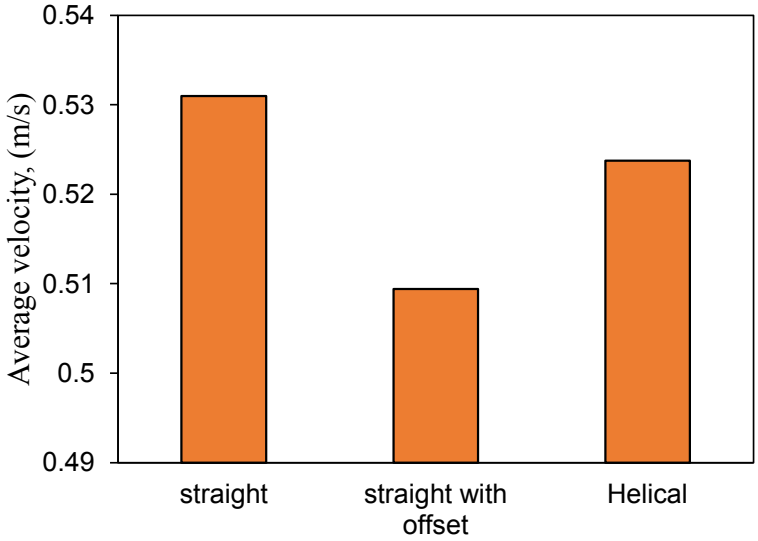

(c)

Figure 8.90 – Comparison between a straight, straight with offset and helical 9mm width- 4 blades stabilizer (a) designs used, and (b) Effect on concentration, and (c) effect on velocity

8.4.4 An Example Case Study

The data in this section were taken from the work of Xiaofeng et al. (2013). Field tests were conducted in four medium deep vertical wells drilled in a block of Daqing Oil Field, in China in 2010 in members 4 and 3 of the Quantou Formation (Quan 4 and Quan 3) as shown in Figure 8.91. The formation is a tight shaley sandstone with moderate difficulty in drilling (Figure 8.92) (Ryder et al., 2003).

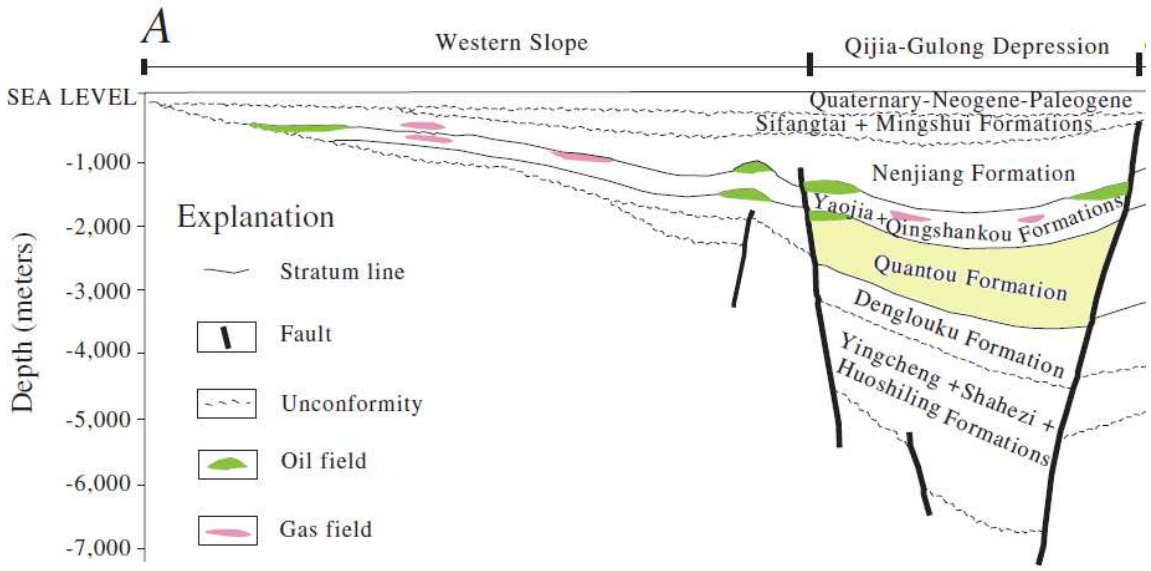

Figure 8.91 – Cross section through the Songliao Basin, China. The Quantou Formation is highlighted in yellow (modified from (Ryder et al., 2003))

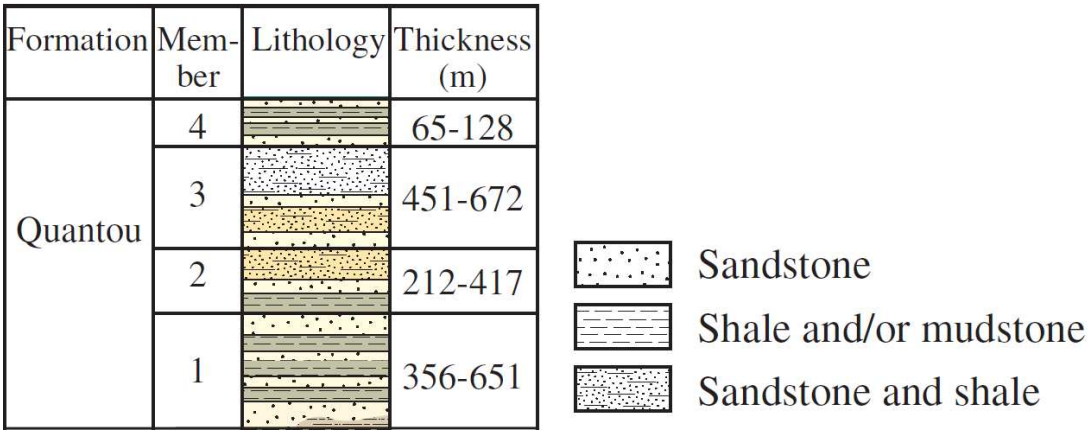

Figure 8.92 – Stratigraphic column for the Quantou Formation, Songliao Basin, China (modified from (Ryder et al., 2003))

The four field tests were subdivided into two pairs of tests in Quan 3 and Quan 4 respectively using straight and helical stabilizers. The layers have a similar depth and lithology and drilling parameters are quest the same to a maximum extent. Table 8.30 presents a summary of the main drilling parameters and the rate of penetration (ROP) for each case. The field observation reported a better cleaning (less balling and pipe sticking in the case with straight stabilizer) and therefore better ROP is observed in the wells drilled with Straight blade stabilizers (Wang 1 and Pu 2). It is seen from Table 8.30 that for the two wells drilled in Quan 3, straight blade stabilizers enhanced the rate of penetration by more than 45%. Similarly, for the wells drilled in Quan 4, an improvement of the ROP by more than 15% is observed.

These field observations show the advantage of using straight blade stabilizer in cleaning the well from cuttings observed on surface and in the drilling parameters which endorses the simulation results obtained in previous sections.

Table 8.30 – Field data in Daqing medium-deep wells (obtained from Xiaofeng et al. (2013))

Stabilizer	Wells	Formation	WOB (klbf)	Depth (ft)	RPM	Drilling time (hr)	ROP (ft/hr)
Helical	Pu 1	Quantou 3	11.2404	935.0394	180	9.3575	99.92406
Straight	Wang 1	Quantou 3	13.4885	738.189	120	4.0125	183.9723
Helical	Pu 1	Quantou 4	11.2404	836.6142	180	10.965	76.2986
Straight	Pu 2	Quantou 4	8.99236	754.5932	120	8.395	89.88602

8.5 Summary

In this Chapter, more than 30 different stabilizers with varied blade geometries were modeled for their effect on hole cleaning. The main conclusions drawn from this study are summarized as below:

1- It was observed that straight blade stabilizers offer a better hole cleaning efficiency comparing to straight blades with offset and helical stabilizers, respectively.

2- The blades type, width and the number of blades significantly affect the cuttings transportation process. Helical and straight with offset blades create a large deflection angle path lines causing the reduction in the upward velocity of the particles.

3- The selection of the stabilizer design to be used in the field should be based on the hole cleaning efficiency alongside with the wellbore stability and hole deviation.

4- Optimum design of the blades is needed to maximize the rate of penetration.

5- A field case study show that the use of straight blade geometry maximizes the hole cleaning efficiency and enhances the rate of penetration compared to helical blade geometry.

It is important to note that more field tests and experiments are needed to study the effect of stabilizers blades geometry on hole cleaning.

CHAPTER 9

Conclusions and Recommendations

In this study, the motion of solid particles was studied and modeled to optimize the cuttings transportation and hole cleaning. The first Section of this Chapter lists the main conclusions made from this work and the second Section presents some of the future work that is recommended as continuation of this study.

9.1 Conclusions

From this study the following conclusions are drawn:

- The analytical models for lifting and rolling provided good estimates of cleaning critical velocities when the results compared to experimental measurements. Also, the lift velocity is the limiting velocity needed to start cleaning a bed deposited at the wellbore. This value is not the optimum velocity for cleaning; however, it is the limit where the cuttings start to be transported out of the well.
- The repose angle of the solid dry cuttings was shown to be an important parameter in hole cleaning efficiency. This assumption was confirmed analytically and experimentally. The cuttings transportation becomes more difficult when the wellbore angle exceeds the complementary of the repose angle (from the horizontal plane); above this angle, the cleaning becomes easier.

- MfiX software showed to be capable for the simulations of cuttings transportation. It works based on Euleurian-Lagrangian model was used in this study as one of the first attempts, to simulate the settling behavior of single particle as well as multiple particles in pipes and wellbore annuli. Quicker processing time is perhaps one of the main advantages of the MfiX comparing to other similar software under the same computational facility.
- The simulation results showed that density has a minor effect on the unsteady state behavior of the particles. However, the effect of the fluid viscosity and particle diameter are more pronounced. Also, the prediction correlations obtained from single particle motion simulation models showed to be able to predict the multi-particle settlement behavior reasonably and present more accurate results than analytical and semi-analytical models.
- The single particle velocity and motion prediction approach can be applied for multiple and mixed sizes particles movement. It is important to understand the mixing phenomena of particles during drilling operation. Single particle settling velocity can be predicted easily using both simulation and analytical mathematical models under certain conditions. The correlations can be projected to real field multiple heterogeneous particles movement prediction. We detected the motion of multi-particles when they are present together. This provided a great knowledge in understanding the cuttings mixing phenomenon when drilling through different formations.
- The developed correlations and nomograms models to predict the settling velocity of drill cuttings in this work are robust and reliable while they are simple to use. Also, the models are applicable in a wide range of particle and fluid parameters and Reynolds number. The prediction capability of the proposed correlations and nomograms was compared to

experimental data and MfiX numerical simulation and good agreement was observed with corresponding experimental data.

- Artificial Neural Network was used to generate new dataset for cases not covered in the experimental work and allowed us to establish new nomograms for predicting the hindered settling velocity. The models were developed for predicting the hindered settling velocity of the particles. The developed models in this work are robust and reliable due to their accuracy and simplicity using two input parameters.
- From the developed graphical models (nomograms) in this work, a field engineer will be able to predict the terminal settling velocity using only the particle and fluid properties considering the retarding wall and particle shape effect.
- Cuttings concentration has a noticeable effect on the pressure and ECD in annulus. At the design stage, cuttings concentration should be calculated to predict the actual ECD at bottom to prevent the loss of circulation, differential sticking and other hazard damage of the wellbore.
- The relationship between the MSE (ROP, RPM, WOB and bit properties), rock properties (UCS, angle of internal friction, porosity and), ECD (pressure loss, fluid properties) and cuttings properties need to be investigated in order for complete evaluation of the effect of drilling parameters on hole cleaning. Bad hole cleaning can cause an increase of more than 0.7 ppg in ECD, which can lead to fluid loss and instability issues for wells with a narrow margin between the pore and fracture pressure gradients.
- Simulating more than 30 different stabilizers with varied blade geometries modeled, it was observed that the blades type, width and the number significantly affect the cuttings transportation efficiency. Straight blade stabilizers offer a better hole cleaning efficiency comparing to straight blades with offset and helical stabilizers, respectively. Helical and

straight with offset blades create a large deflection angle path lines causing the reduction in the upward velocity of the particles.

9.2 Recommendations

Several ideas and potential ameliorations were mentioned throughout this study, which require further investigations. Here, some of these ideas are recommended as continuation of this study:

- Expanding the analytical models in 3D will add value for comparison with the simulations results and more realistic analysis.
- Further investigation on the motion of multi-particles is important to better model the cuttings mixing phenomenon when drilling through different formations.
- Developing new datasets for the simultaneous effect of particle shape and annular size on particles motion will carry a great prediction tools useful for cuttings transportation modelling and optimization.
- Implementing wellbore inclination and pipe rotation to an easy and straight forward analytical models to estimation the minimum required mud flow rate to ensure an efficient hole cleaning is another future work to consider.
- Implementing the Artificial Intelligence techniques should be another future work to consider to estimate the minimum required mud flow rate for efficient hole cleaning.
- Studying the hole cleaning with colloidal suspensions or nonofluids is a novel area of interest in drilling that will provide a crucial knowledge especially when drilling geothermal wells.
- The MSE-ECD relationship proposed in this work is more applicable for vertical and slightly deviated wellbore (higher than 60°). For inclined well, it is more difficult to transport the cuttings to the surface, hole cleaning is more complicate and important. Further study on inclined wells is recommended.

- Experimental and quantitative investigation on the effect of stabilizers and centralizers on hole cleaning is needed to provide a better guidance in drilling subs selection for efficient hole cleaning.

Appendix A. Settling Wall Effect and Simulation

• Wall Effect

The Effect of pipe walls on the settling velocity of particles is assessed with great difficulty. Comprehensive equations were proposed based on an extensive study of the wall effect for both Newtonian and non-Newtonian fluids (Fidleris and Whitmore, 2002, 1961b; Kelessidis, 2004).

The retarding wall effect on spherical particles is expressed as a correction factor defined as the ratio of the particle velocity in the vessel v to the velocity of the particle in an infinite medium v_∞. This factor depends on the particle-to-pipe diameter ratio d/D.

The widely used equations of the correction factor are:

For laminar flow region

- Ladenburg (Ladenburg, 1907)

$$f = \frac{v}{v_\infty} = \frac{1}{1 - 2.1\, d/D} \tag{A.1}$$

- Faxen (Faxén, 1921)

$$f = \frac{v}{v_\infty} = 1 - 2.104\, d/D + 2.09(d/D)^3 - 0.95(d/D)^5 \tag{A.2}$$

- Francis (Francis, 1933)

$$f = \frac{v}{v_\infty} = \left[\frac{1 - d/D}{1 - 0.475\, d/D}\right]^4 \tag{A.3}$$

- Mott considered the wall-effects to be negligible below a d/D ratio of 0.15 (Mott, 1951).

It is clearly seen from Table A.1 and Figure A.1 that the agreement is good in the case of the Francis and Faxen equation with experimental results and rather poorer using the Landenburg equation.

Table A.1 - Comparison of wall-correction equations in the laminar region of flow at $Re = 0.1$ (Fidleris and Whitmore, 2002)

d/D	Experimental	Ladenburgh	Faxen	Francis
0.1	0.788	0.826	0.792	0.797
0.2	0.61	0.704	0.596	0.611
0.3	0.446	0.613	0.423	0.444
0.4	0.3	0.543	0.283	0.301
0.5	0.18	0.488	0.179	0.185
0.6	0.094	0.442	0.115	0.098

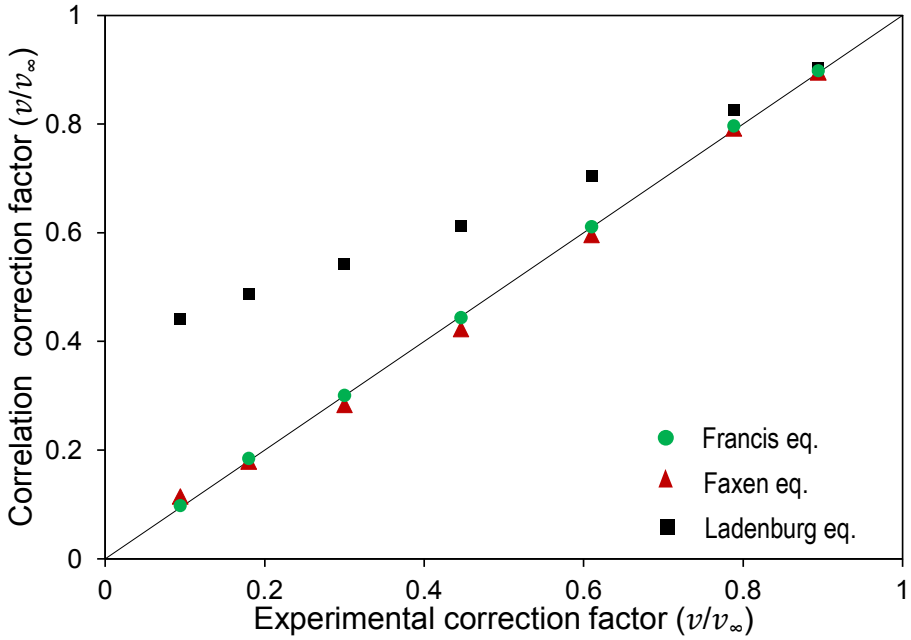

Figure A.1 – Comparison of different wall-effect correction factor correlation to experimental values at Turbulent Flow Region

For turbulent flow region

- Newton (Barr, 1931)

$$f = \frac{v}{v_\infty} = \frac{(D^2 - d^2)\sqrt{D^2 - \frac{d^2}{2}}}{D^3} \tag{A.4}$$

- Munroe (Munroe, 1889)

$$f = \frac{v}{v_\infty} = 1 - (d/D)^{3/2} \quad \text{(A.5)}$$

- Lunnon (Lunnon, 1928)

$$f = \frac{v}{v_\infty} = 1 - 0.23(d/D) \quad \text{(A.6)}$$

- Mott (Mott, 1951)

For values of d/D from 0.2 to 0.5 he obtained the equation:

$$f = \frac{v}{v_\infty} = \frac{1}{1 - A(d/D)^4} \quad \text{(A.7 a)}$$

where A is a constant varying from 1.8 to 3.2, and for values of d/D from 0.5 to 0.7 the equation:

$$f = \frac{v}{v_\infty} = \frac{1}{1 - (2\,d/D)^4} \quad \text{(A.8 b)}$$

It is clearly seen from Table A.2 and Figure A.2 that the degree of correspondence of the given wall correction factor equations varies to some extent with Reynolds number, although not always in the same way.

Thus the agreement with Mott's and Newton's equations is within 2% up to a d/D ratio of 0.3, but worsens considerably at higher ratios. Munroe's correction shows best agreement with experimental results between Reynolds numbers of 1000 and 3000, whereas Newton's is most reliable at Reynolds numbers near 13000. The least satisfactory formula is that of Lurmon.

Table A.2 – Comparison of wall-correction equations in the Turbulent region of flow at $Re = 3000$ (Fidleris and Whitmore, 2002)

d/D	Experimental	Newton	Munroe	Lunnon	Mott
0.1	0.987	0.968	0.982	0.977	0.982
0.2	0.960	0.950	0.911	0.954	0.933
0.3	0.875	0.889	0.836	0.931	0.860
0.4	0.779	0.806	0.747	0.908	0.776
0.5	0.651	0.702	0.646	0.885	0.689
0.6	0.524	0.543	0.535	0.862	0.607

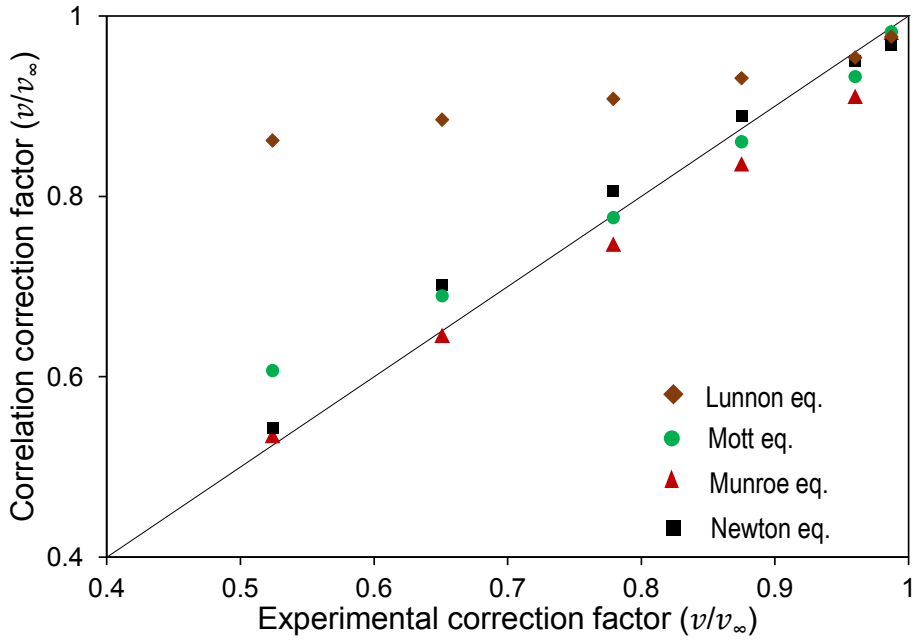

Figure A.2 – Comparison of different wall-effect correction factor correlation to experimental values at Turbulent Flow Region

- **Heterogeneous Heavy Particles Settling**

Figure A.3 shows a combination of different diameters particles with a constant density of 8gcc falling inside an annular space section of 0.95 *m* length. The upper 0.437 *m* section of the wellbore is filled with 3 *mm*, 8 *gcc* particles and the remaining section is filled with 1 *mm*, 8 *gcc* particles. The top layers of both sections and the bottom layer of the 3 *mm* particles section were tracked and their positions were compared to the single particle correlations (Figure A.4). Also, for simplicity, the single particles dispersed due to the wall friction were not considered in this analysis and only the higher concentration layers were tracked.

The 3 *mm* and 1 *mm* particles at the interface of x=0.437 *m* reach the bottom section after traveling a distance of 0.513 *m*.

The results of arrival times from single particle correlations and simulations are summarized in Table A.3 and Figure A.5. The results show a good agreement for 3 *mm* size particles, whereas for 1 *mm* particles the error margin was close to 10% which is due to the excessive particles collision and wall friction.

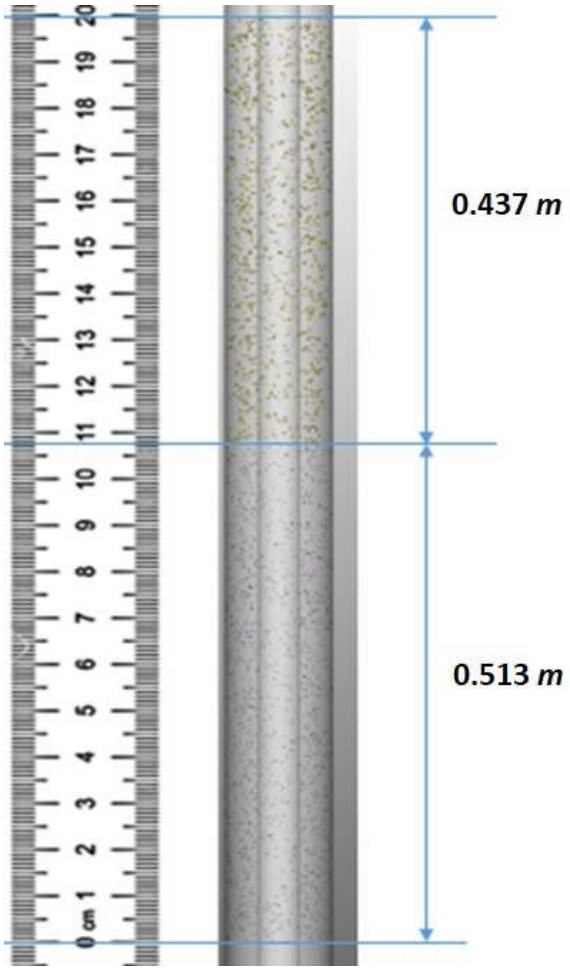

Figure A.3 – Combination of different diameters 8 gcc particles falling inside an annulus space section of 0.950 m length, 3mm particles on top with yellow (0.437 m section) and 1mm particles at the bottom section in blue (0.513m section)

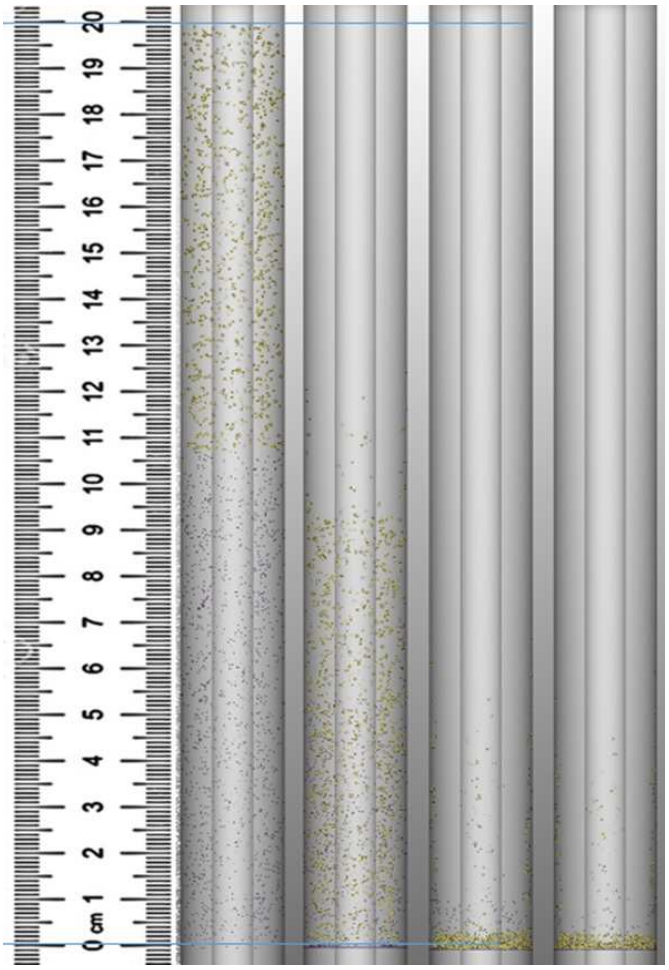

Figure A.4 – Particles packs limits tracking. From left to right: (1) t=0.00 s, (2) t=0.77 s, the 3 mm particles bottom interface reached the bottom section of the wellbore section, (3) t=1.36 s, the 3mm particles top interface reaches the bottom of the wellbore section, and (4) t=1.45 s, the 1 mm particles top interface reaches the bottom of the wellbore section

Table A.3 – Multi-particle multi-diameter sedimentation time comparison with single particle correlations

	Single particle BBO [s]	Single particle simulation [s]	Simulation [s]	Error P1 [%]	Error P2 [%]
$t_{3mm-Bottom}$	0.763	0.762	0.77	0.91	1.04
$t_{3mm-Top}$	1.354	1.356	1.36	0.44	0.294
$t_{1mm-Top}$	1.308	1.442	1.45	9.79	0.55

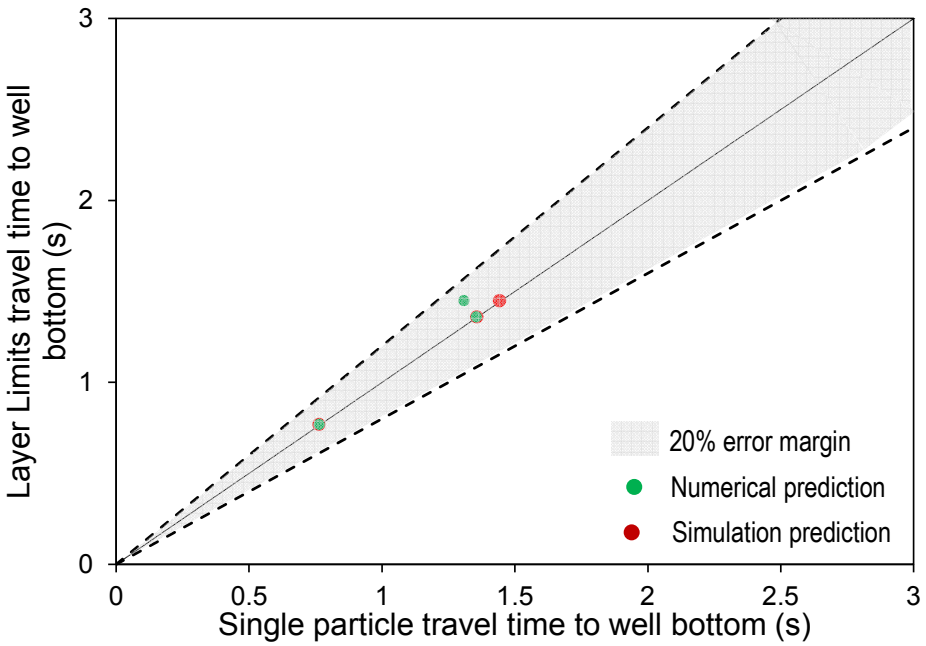

Figure A.5 – Single particle projection on multi-particles packs limits efficiency

Appendix B. Datasets Summary

Dataset 1 includes the data from the work of Fidleris and Whitmore (1961a, 1961b) and our previous laboratory work performed using the Slurry Loop Unit using particles with different densities and sizes, including sand, proppants and other heavy and light materials. The flow rate was changed until the particles remained in the same vertical position inside the annulus. At this point the settling velocity is nearly equal to the annular fluid velocity. The settling velocity was also estimated from the video of particle settlement taken during their settlement after the flow rate was brought down to zero.

The experimental results obtained from the Slurry Loop Unit lays perfectly with the trend of the data obtained by (Fidleris and Whitmore, 1961a, 1961b) (see Figure B.1).

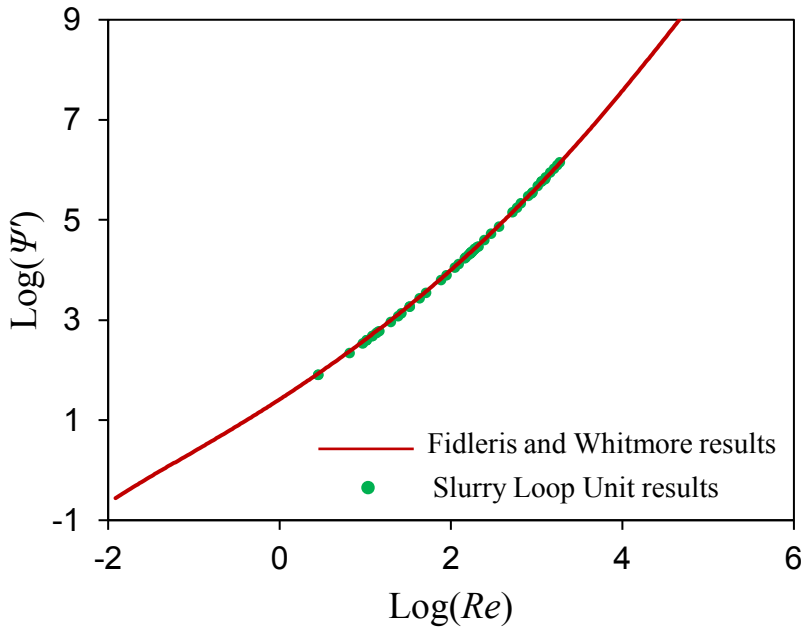

Figure B.1 – Comparison of experimental results from the Slurry Loop Unit experimental work and the work of (Fidleris and Whitmore, 1961a, 1961b).

Table B.1 – Dataset 1 statistical summary

	d/D	Log(Re)	Log(ψ')
Mean	0.245889	1.224302	3.514942
Median	0.2	1.165653	3.100431
Mode	0	#N/A	#N/A
Standard Deviation	0.209712	1.909398	2.62342
Range	0.6	6.878107	10.13453
Minimum	0	-1.94602	-0.55068
Maximum	0.6	4.932087	9.583848
Count	3000	3000	3000

Table B.2 – Dataset 2 statistical summary

	Sphericity	Particle density (kg/m3)	Fluid density (kg/m3)	Fluid viscosity (Pa·s)	Settling velocity (m/s)
Mean	0.783	5009.018	1237.000	0.364	0.160
Median	0.779	4450.000	1237.000	0.289	0.117
Mode	1.000	2680.000	1250.000	0.669	0.156
Standard Deviation	0.143	2198.834	10.630	0.225	0.150
Range	0.529	5280.000	26.000	0.534	0.784
Minimum	0.471	2680.000	1224.000	0.135	0.001
Maximum	1.000	7960.000	1250.000	0.669	0.785
Count	336	336	336	336	336

Table B.3- Dataset 4 statistical summary

	φ	Log(Re)	Log(ψ')
Mean	0.552598	0.805	3.263696
Median	0.6	0.788361	2.85367

Mode	1	-0.130155	1.926138
Standard Deviation	0.335486	1.851469	2.721364
Range	0.875	6.555881	10.59862
Minimum	0.125	-2.556873	-1.132105
Maximum	1	3.999008	9.466521
Count	688	688	688

Appendix C. ANN Supplementary

For a 2-6-1 ANN model using dataset 1 (for spherical particles), for comparison purposes, one can compare the accuracy parameters in Figure C.1 and Figure C.2 to the ones in Figure 6.57 and Figure 6.58.

The models can also be replicated and compared by using the weights and biases presented in Table 6.23 and Table C.1.

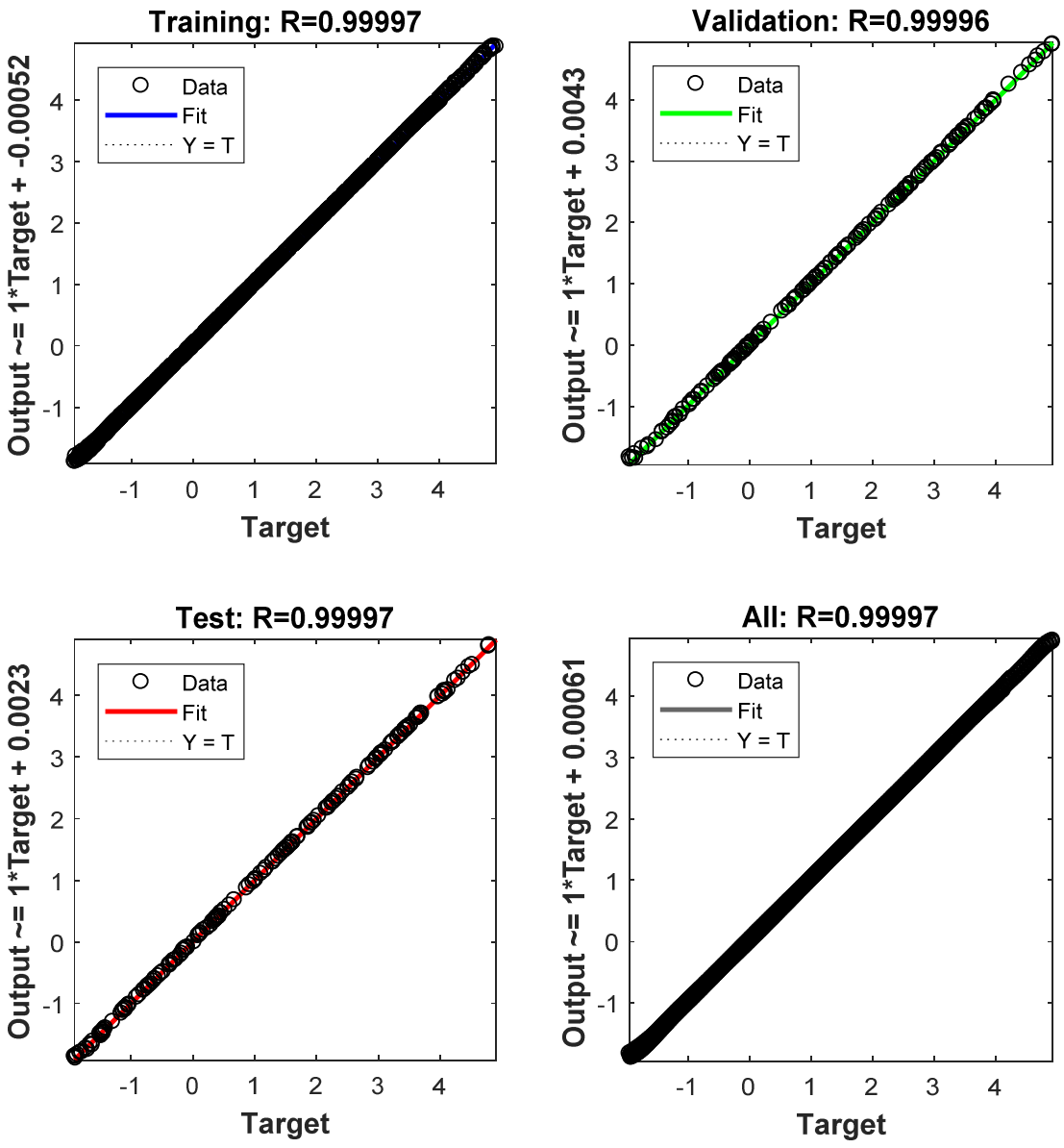

Figure C.1 – Scatter plots of a single hidden layer with 6 nodes ANN model

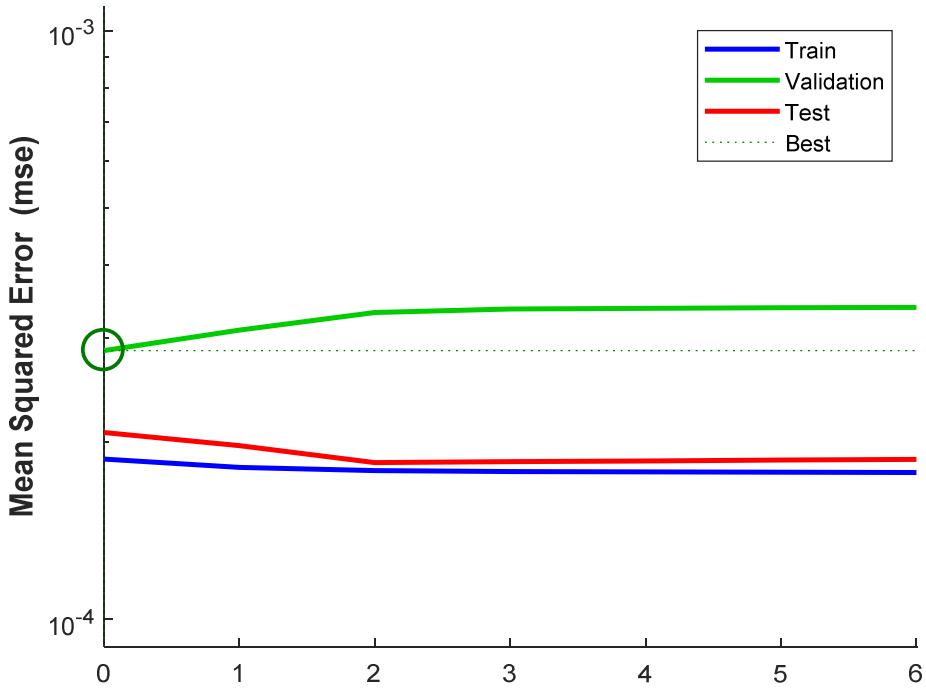

Figure C.2 – Single hidden layer with 6 nodes ANN model performance

Table C.1 – Model 1 weights and biases (6 nodes)

Hidden Layer						Output Layer			
$\omega_{1,1}$	-1.4838	b_1	19.4251	$\omega_{2,1}$	18.0652	$\omega_{1,1}$	14.1798		
$\omega_{1,2}$	1.1811	b_2	-6.4077	$\omega_{2,2}$	-2.4836	$\omega_{1,2}$	-17.2306		
$\omega_{1,3}$	0.059165	b_3	-4.8852	$\omega_{2,3}$	-2.1633	$\omega_{1,3}$	-25.0971	b_1	-11.538
$\omega_{1,4}$	0.30282	b_4	3.1667	$\omega_{2,4}$	-1.4827	$\omega_{1,4}$	-16.0065		
$\omega_{1,5}$	0.5131	b_5	3.6006	$\omega_{2,5}$	-1.1683	$\omega_{1,5}$	13.5254		
$\omega_{1,6}$	-0.1894	b_6	-15.4728	$\omega_{2,6}$	13.0358	$\omega_{1,6}$	11.8542		

Appendix D. Frictional Pressure Loss Calculations

- Equivalent diameter:
  - Exact approximation:

$$D_{eq} = \sqrt{OD^2 + ID^2 - \frac{OD^2 - ID^2}{\ln(\frac{OD}{ID})}} \quad \text{(D.100)}$$

  - Slot approximation:

$$D_{eq} = \sqrt{\frac{2}{3}}.(OD - ID) \quad \text{(D.101)}$$

- Newtonian fluid:
  - Laminar:

$$\frac{\Delta P_f}{\Delta L} = \frac{\mu.V_f}{1500{D_{eq}}^2} \quad \text{(D.102)}$$

  - Turbulent:

$$Re = 928\frac{\rho.V_f.D_{eq}}{\mu} \quad \text{(D.103)}$$

$$\frac{1}{\sqrt{f}} = -4Log\left(\frac{1.255}{Re}\frac{1}{\sqrt{f}}\right) \quad \text{(D.104)}$$

$$\frac{\Delta P_f}{\Delta L} = f.\frac{\rho.{V_f}^2}{25.8D_{eq}} \quad \text{(D.105)}$$

- Bingham Plastic fluid (slot approximation):
  - Laminar:

$$\frac{\Delta P_f}{\Delta L} = \frac{\eta_{PV}.V_f}{1000(OD-ID)^2} + \frac{\tau_y}{200(OD-ID)} \quad \text{(D.106)}$$

- Turbulent:

Apparent viscosity:

$$\mu_a = \eta_{PV} + 5\frac{\tau_y(OD-ID)}{V_f} \quad \text{(D.107)}$$

$$Re = 928\frac{\rho.V_f.D_{eq}}{\mu_a} \quad \text{(D.108)}$$

$$\frac{1}{\sqrt{f}} = -4Log\left(\frac{1.255}{Re}\frac{1}{\sqrt{f}}\right) \quad \text{(D.109)}$$

$$\frac{\Delta P_f}{\Delta L} = f.\frac{\rho.{V_f}^2}{25.8D_{eq}} \quad \text{(D.110)}$$

- Power Law fluid (slot approximation):

  - Laminar:

$$\frac{\Delta P_f}{\Delta L} = \frac{K.{V_f}^{-n}}{143.640(OD-ID)^{n+1}}\left(48\frac{2n+1}{n}\right)^n \quad \text{(D.111)}$$

  - Turbulent:

$$\mu_a = \frac{K.{V_f}^{n-1}}{143.9(OD-ID)^{n-1}}\left(48\frac{2n+1}{n}\right)^n \quad \text{(D.112)}$$

$$Re = 928\frac{\rho.V_f.D_{eq}}{\mu_a} \quad \text{(D.113)}$$

$$\frac{1}{\sqrt{f}} = -4Log\left(\frac{1.255}{Re}\frac{1}{\sqrt{f}}\right) \quad \text{(D.114)}$$

$$\frac{\Delta P_f}{\Delta L} = f.\frac{\rho.{V_f}^2}{25.8D_{eq}} \quad \text{(D.115)}$$

Appendix E. Stabilizers

- **3D Designs**

- Well configuration

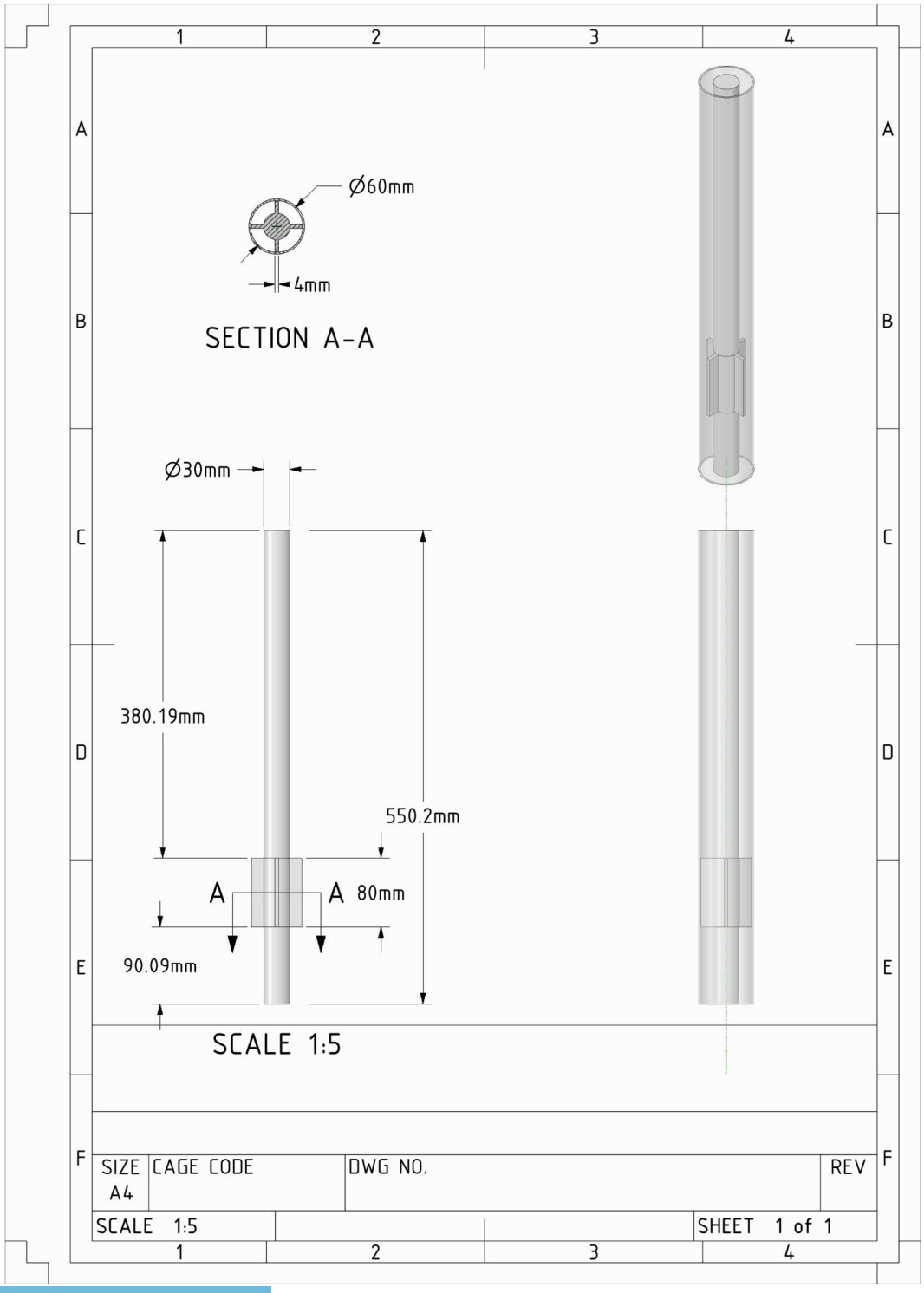

Figure E.1 – Well configuration used in the simulation.

- Straight stabilizer's designs

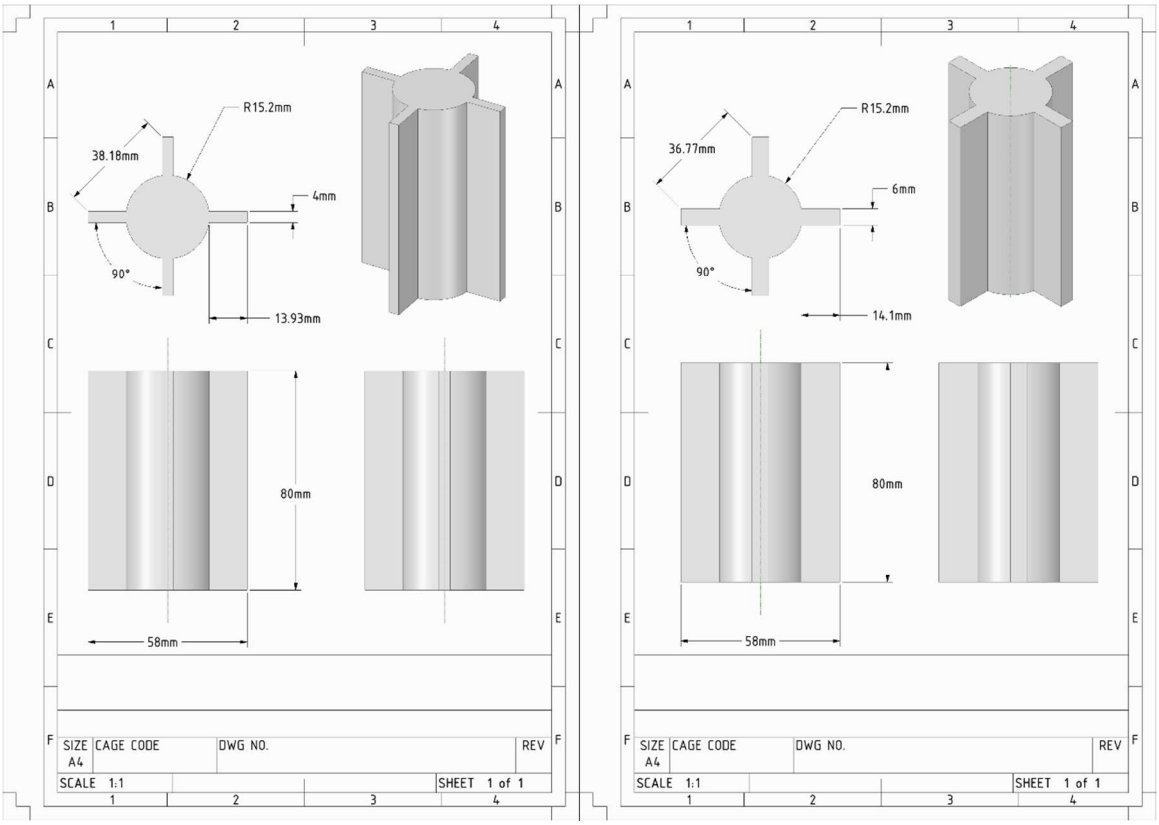

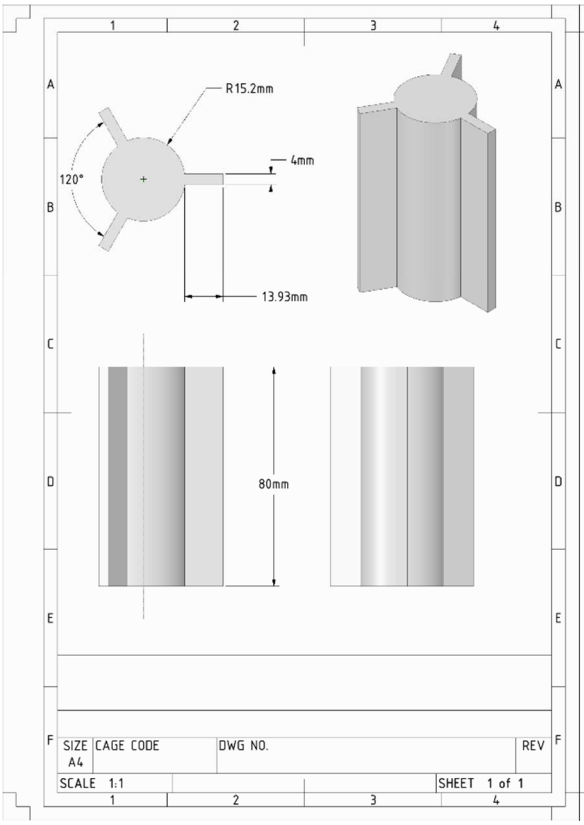

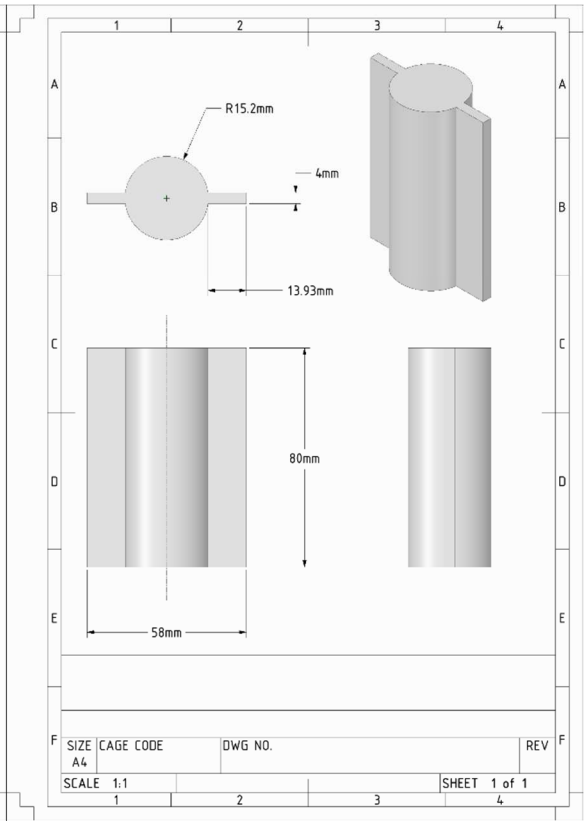

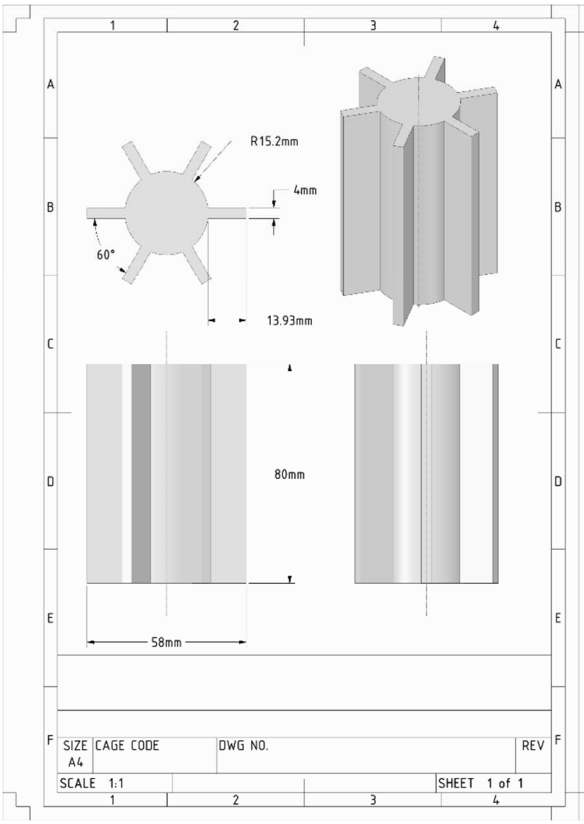

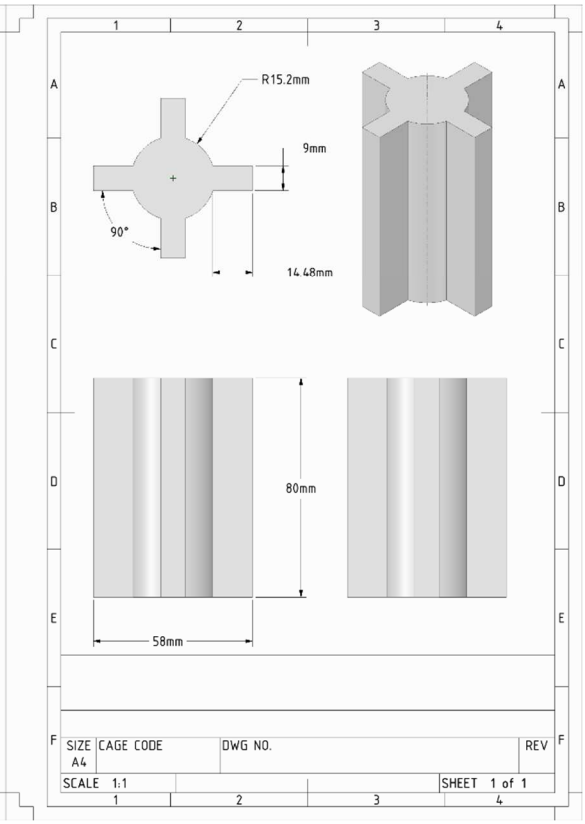

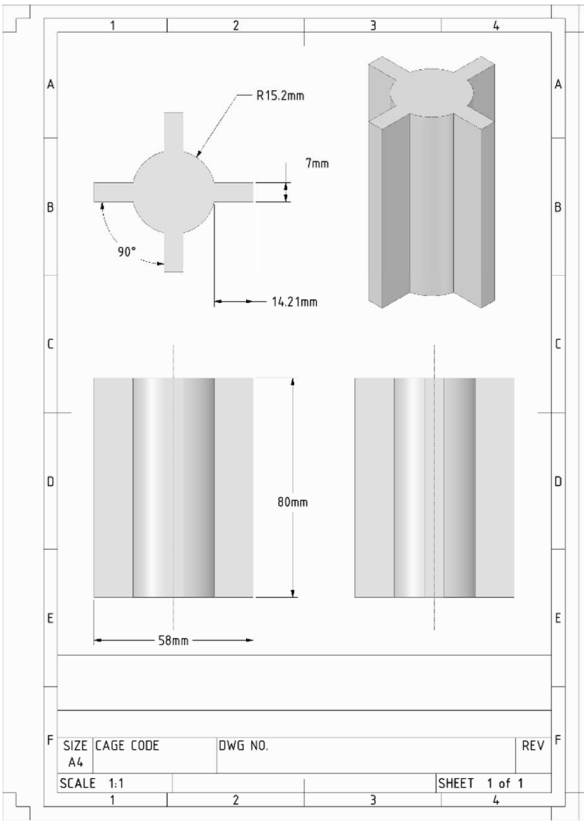

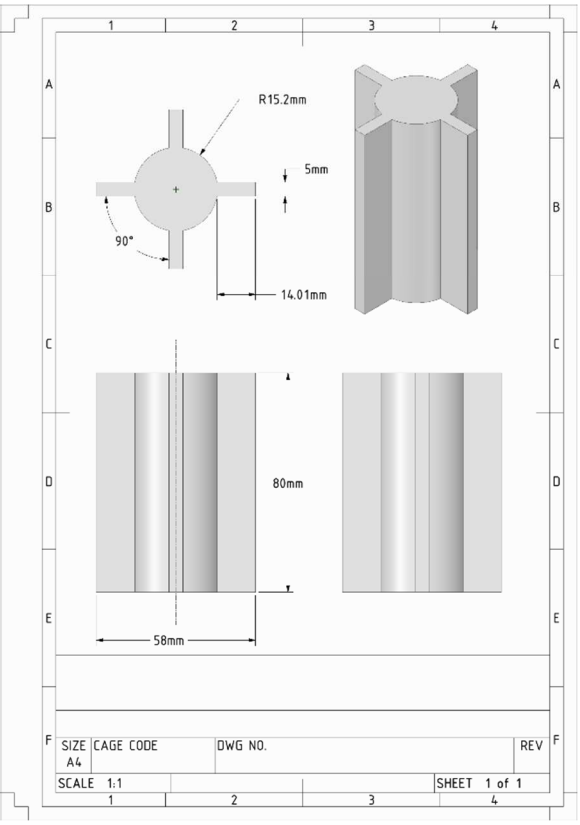

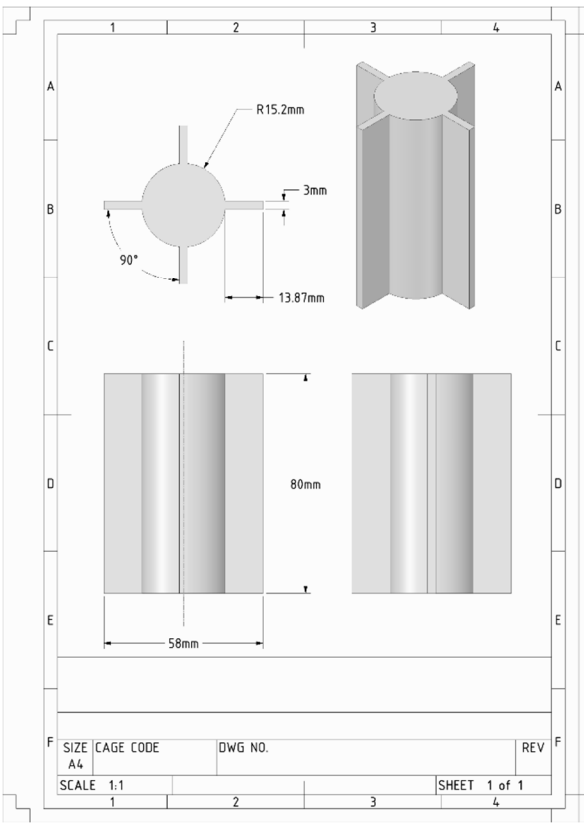

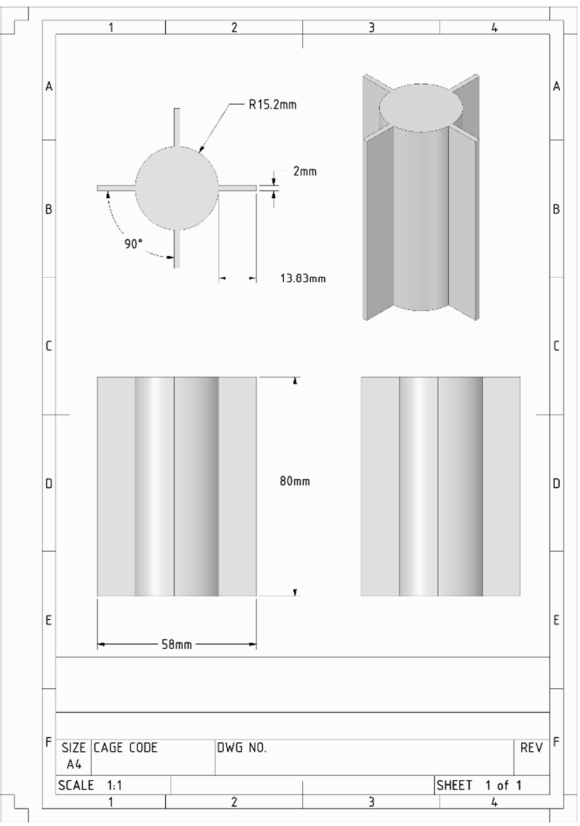

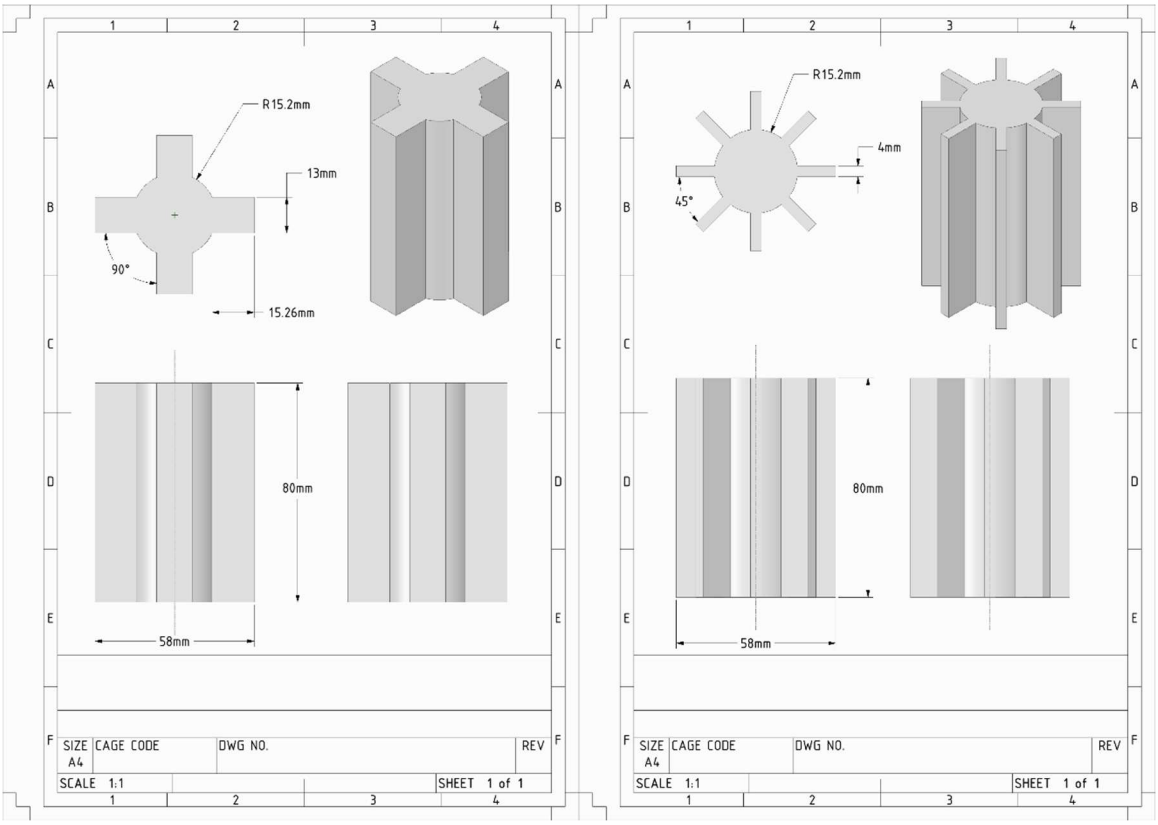

Figure E.2 – Straight blade stabilizers designs used in the simulations

- Straight with offset stabilizer's designs

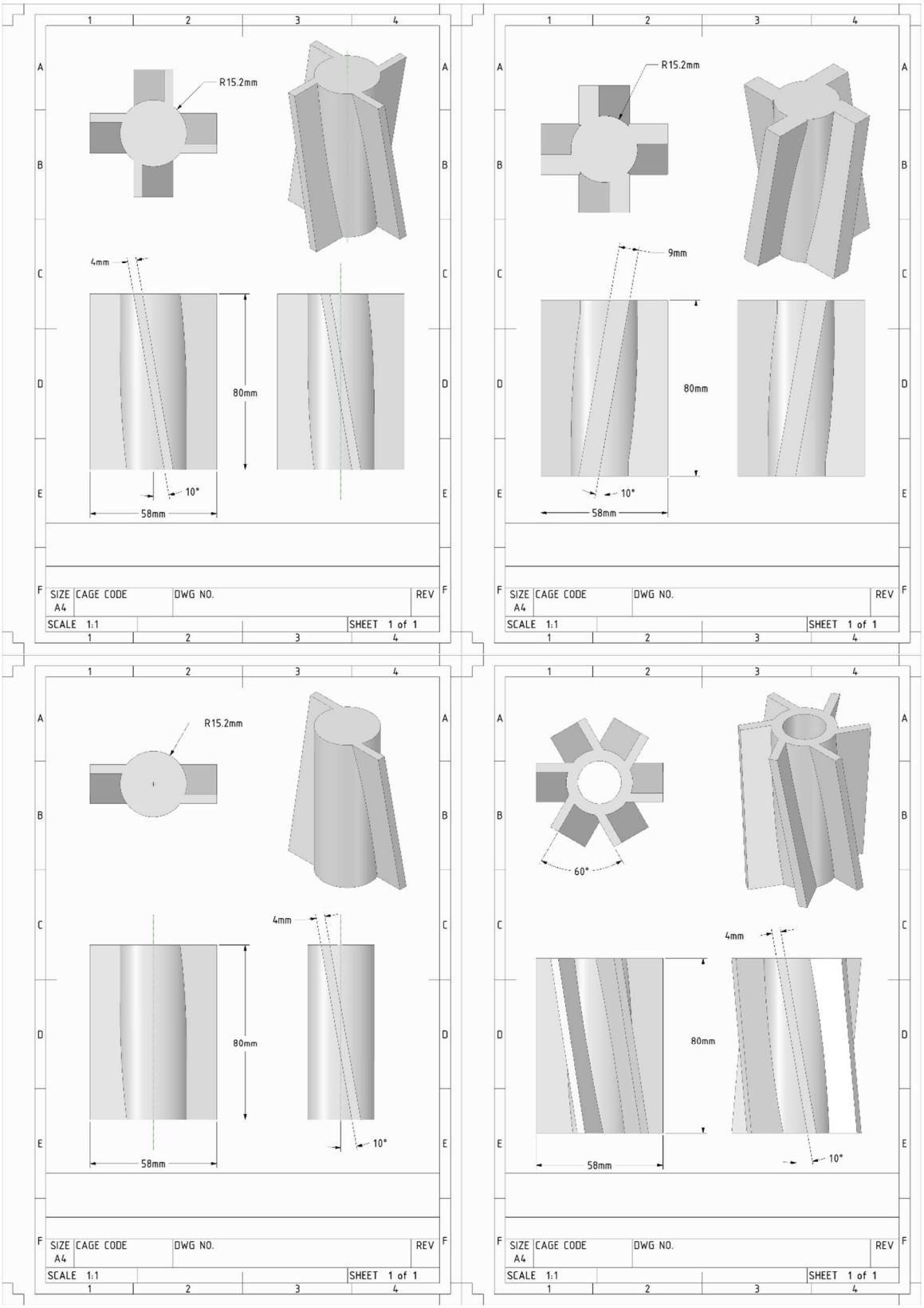

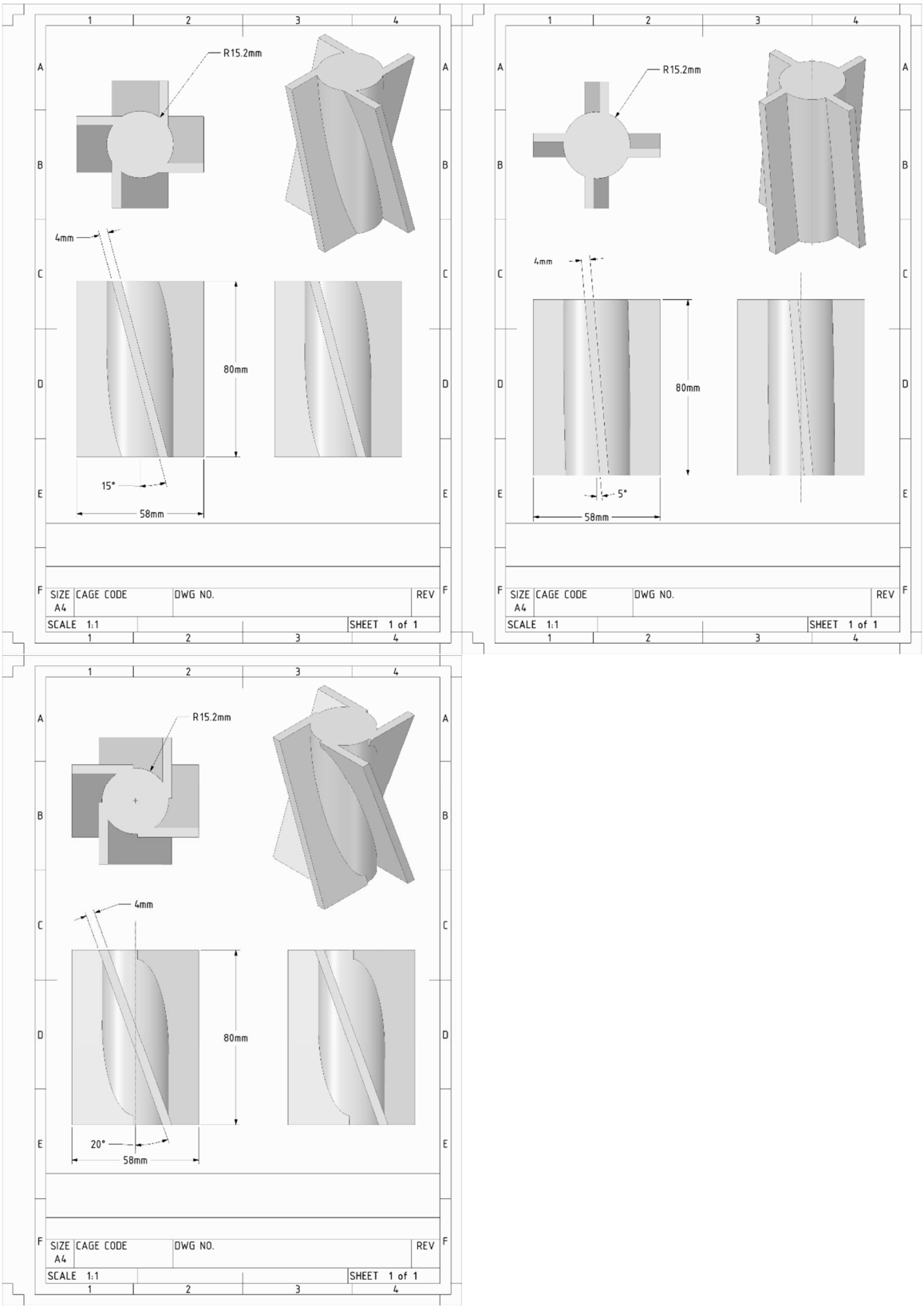

Figure E.3 – Straight blade with offset stabilizers designs used in the simulations

- Helical stabilizer's designs

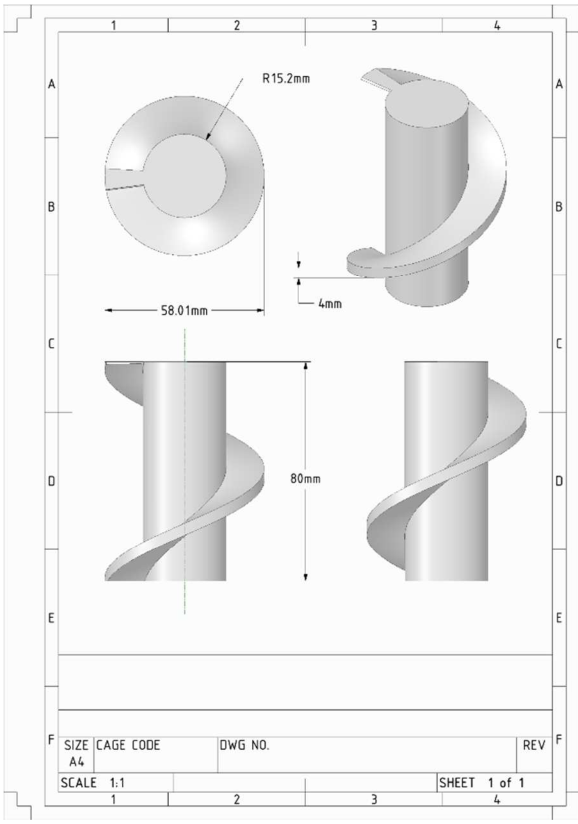

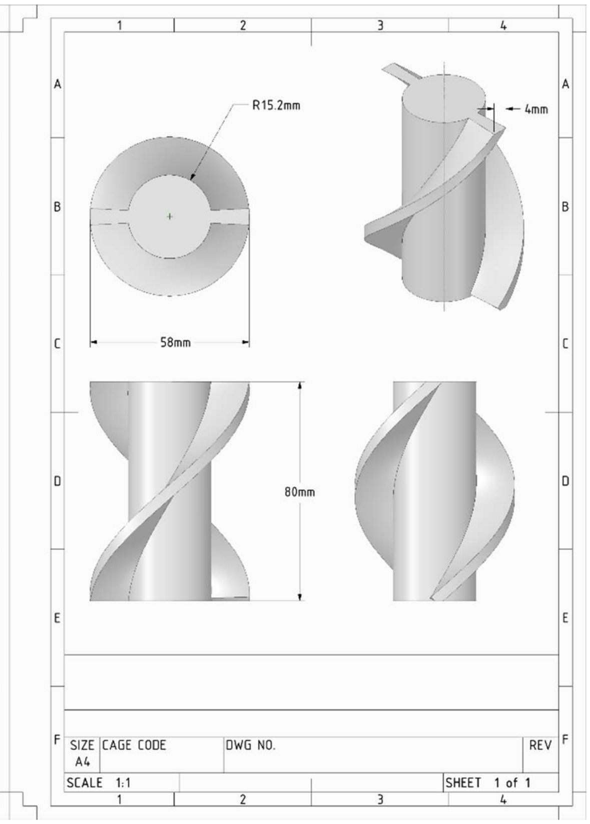

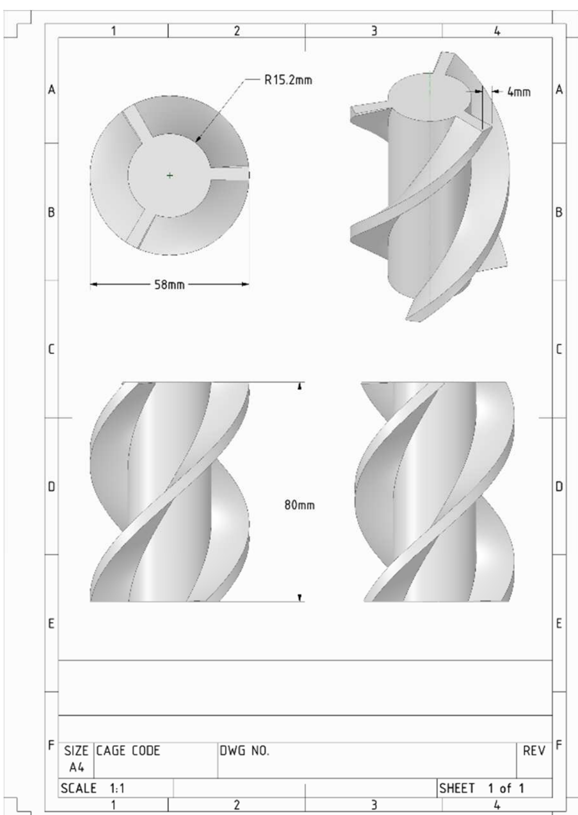

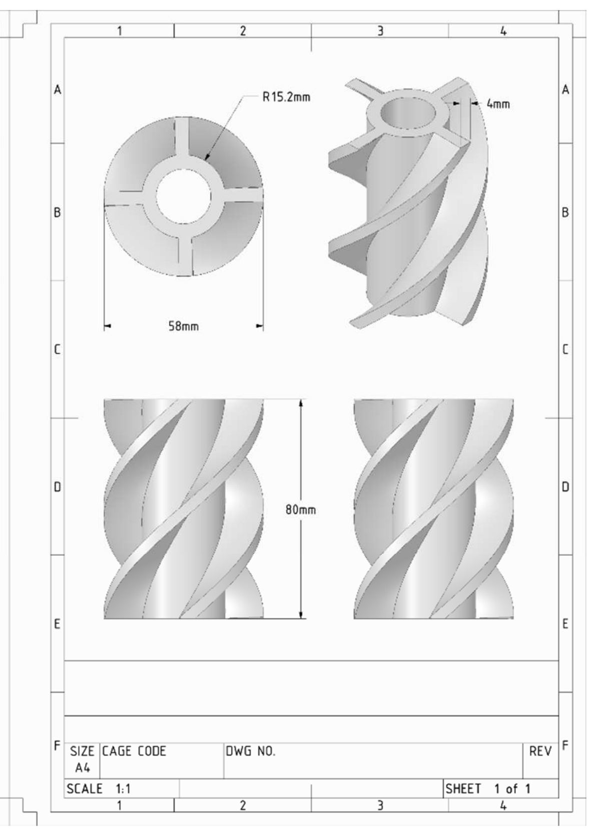

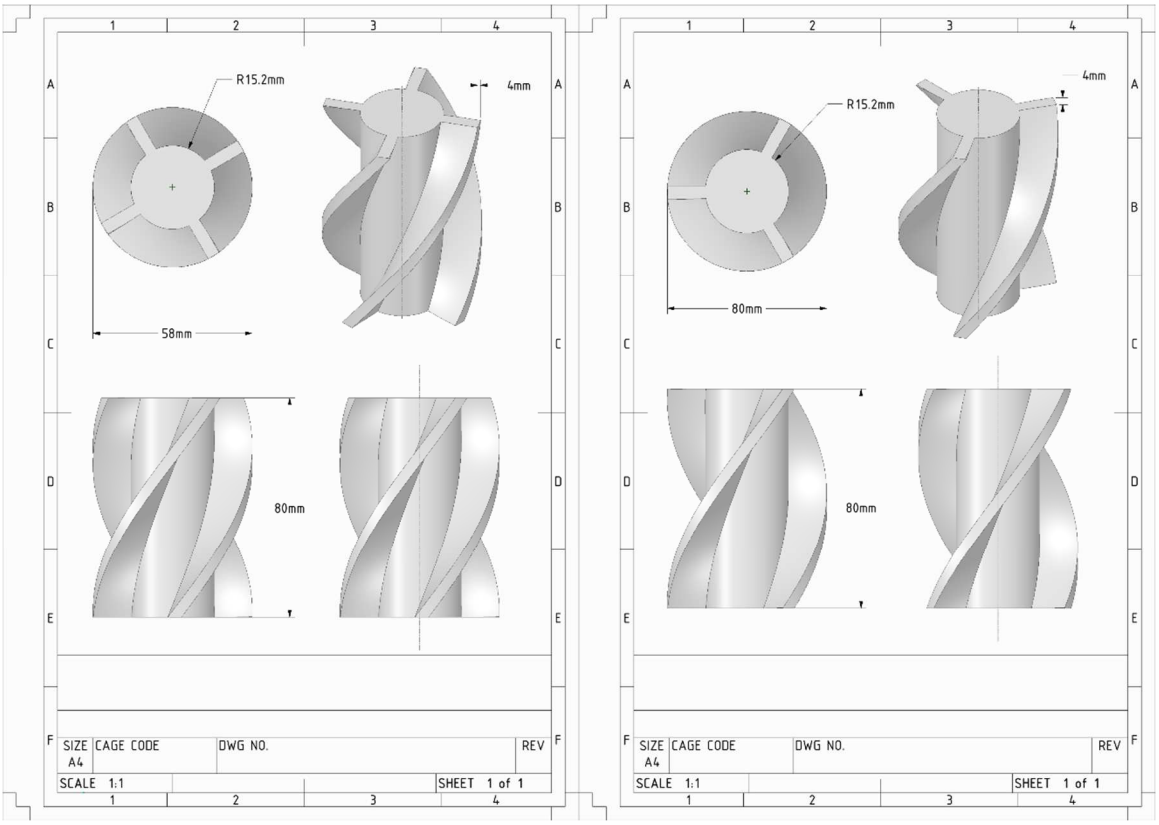

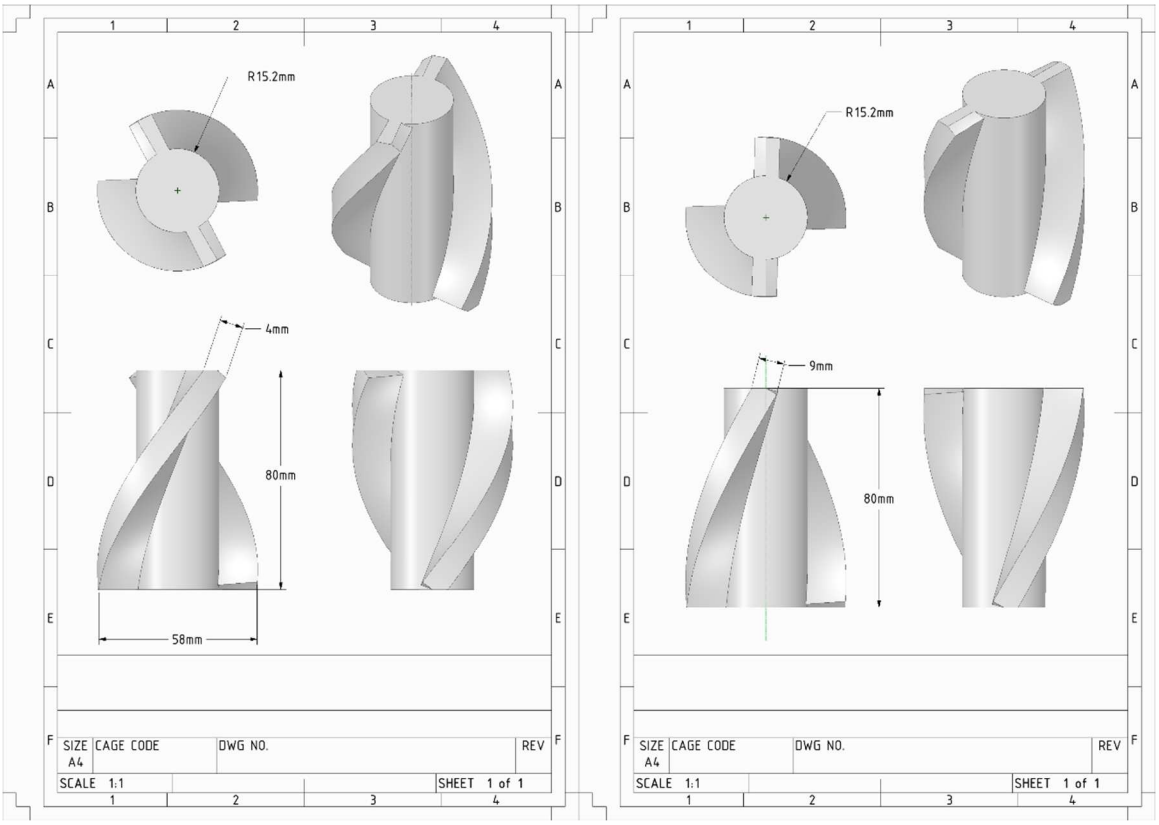

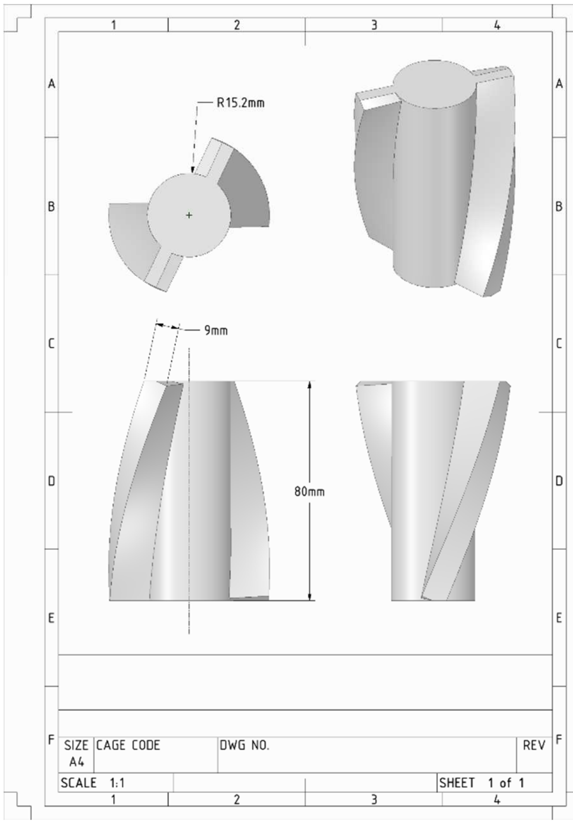

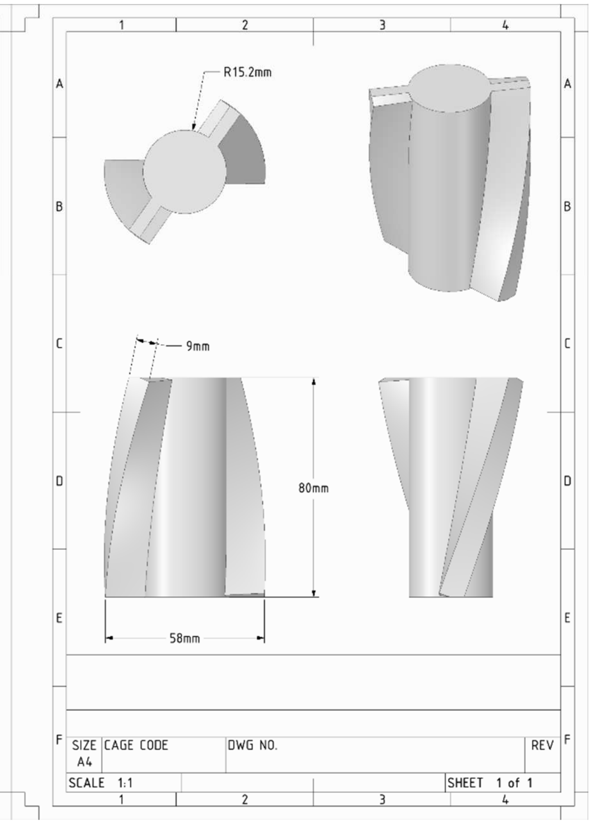

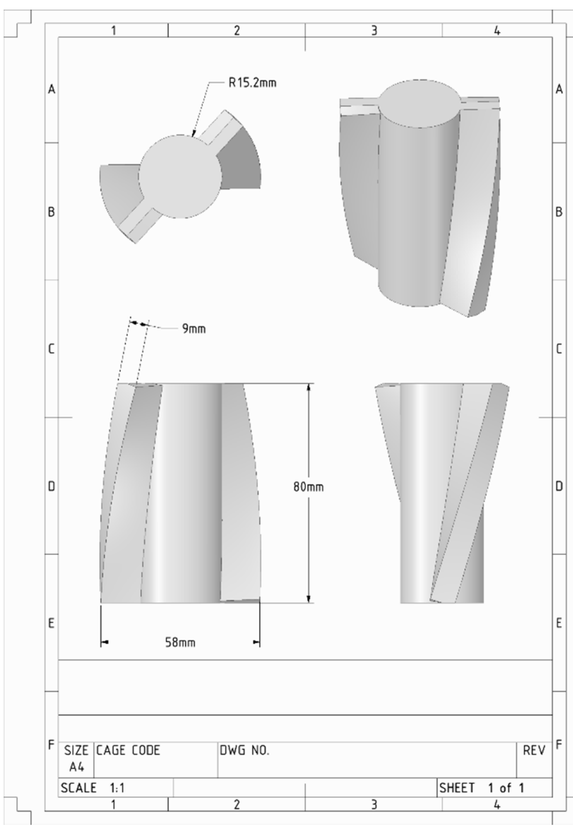

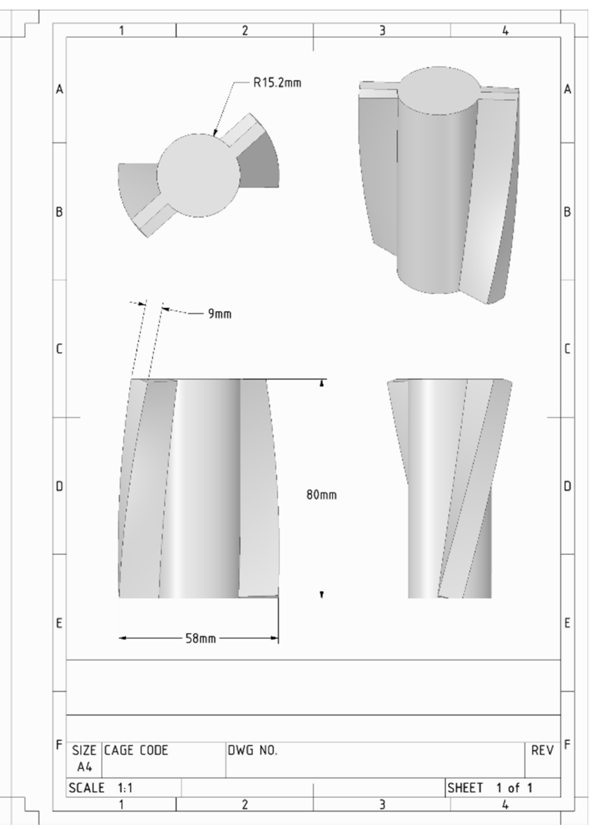

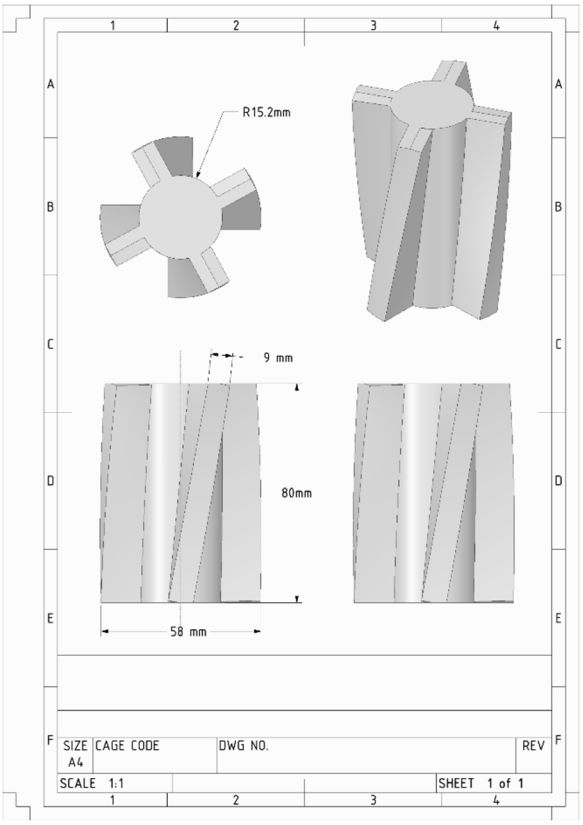

Figure E.4 – Helical blade stabilizers designs used in the simulations

- **Supplementary**

By Increasing the particles feeding rate by 2.5 folds (feeding concentration 10% / particles rate 15×10^{-3}), the 4 mm width blades straight stabilizer still enhances the hole cleaning as shown in Table E.1.

Table E.1 - Model 1 weights and biases (6 nodes)

	Cuttings concentration in wellbore (%)	Average velocity (m/s)
No stabilizer	7.713	0.544032
Straight stabilizer	7.6105	0.561367

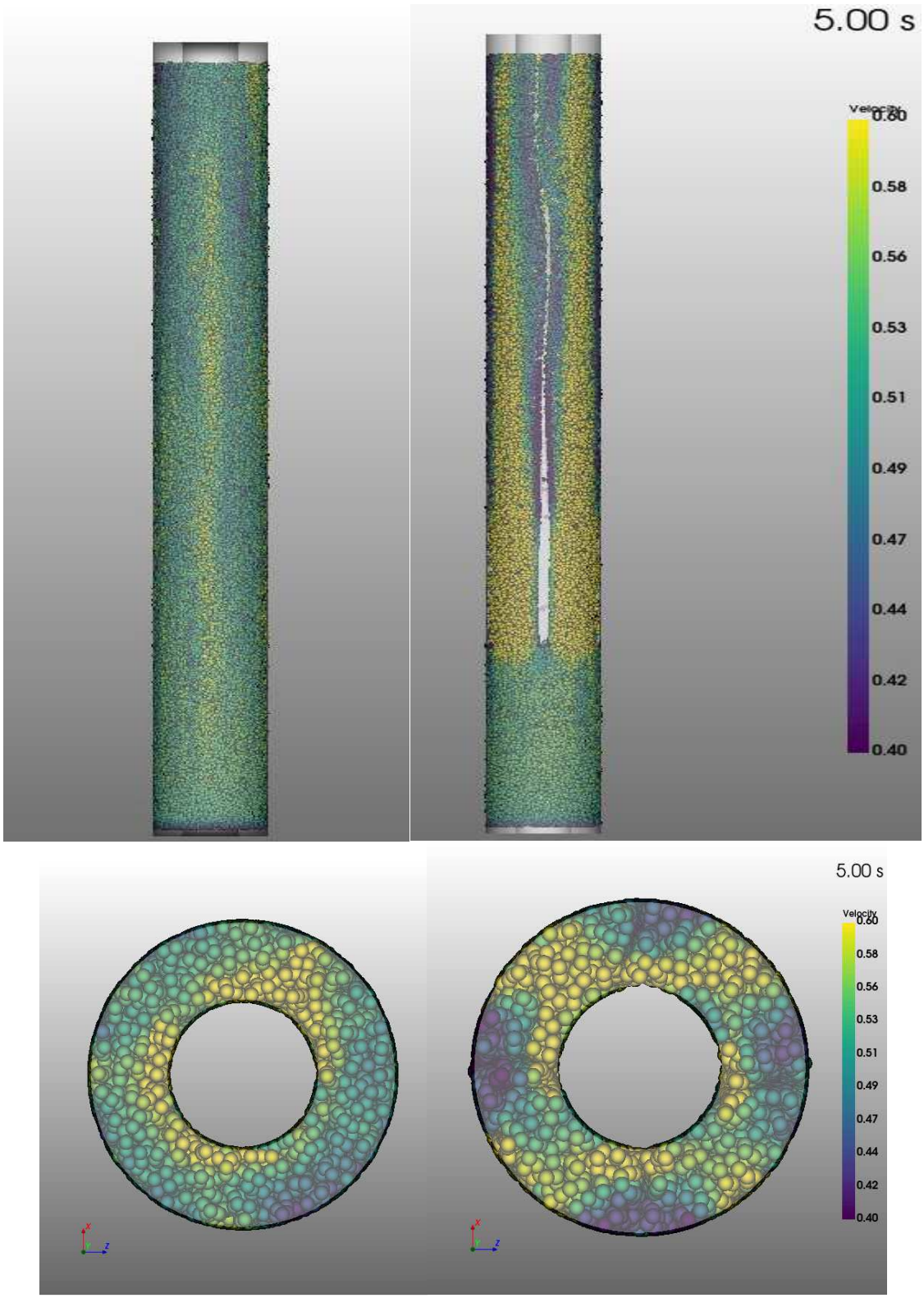

Figure E.5 – Comparison between a pipe without stabilizer (left) and a pipe with 4mm width straight blade stabilizer with a cuttings feeding rate of 4%

References

Abdelgawad, K.Z., Elzenary, M., Elkatatny, S., Mahmoud, M., Abdulraheem, A., Patil, S., 2019. New approach to evaluate the equivalent circulating density (ECD) using artificial intelligence techniques. J. Pet. Explor. Prod. Technol. 9, 1569–1578. https://doi.org/10.1007/s13202-018-0572-y

Acrivos, A., Davis, R.H., Herbolzheimer, E., 1983. Enhanced Sedimentation in Vessels Having Inclined Walls. The Boycott Effect, in: MEYER, R.E.B.T.-T. of D.M.F. (Ed.), . Academic Press, pp. 81–95. https://doi.org/https://doi.org/10.1016/B978-0-12-493120-6.50010-6

Adams, D.P., 1964. Nomography: Theory and Application. Shoe String Pr Inc.

Agarwal, N., Chhabra, R., 2007. Settling velocity of cubes in Newtonian and power law liquids. Powder Technol. - POWDER TECHNOL 178, 17–21. https://doi.org/10.1016/j.powtec.2007.04.002

Agwu, O., Akpabio, J., Alabi, S., Dosunmu, A., 2018. Settling velocity of drill cuttings in drilling fluids: A review of experimental, numerical simulations and artificial intelligence studies. Powder Technol. 339. https://doi.org/10.1016/j.powtec.2018.08.064

Agwu, O.E., Akpabio, J.U., Dosunmu, A., 2020. Artificial neural network model for predicting drill cuttings settling velocity. Petroleum 1–13. https://doi.org/10.1016/j.petlm.2019.12.003

Ahmed, R., 2012. Fiber-containing Sweep Fluids for Ultra Deepwater D rilling Applications. Rep. Prep. by Univ. Oklahoma Spons. by Res. Partnersh. to Secur. Energy Am.

Ahmed, R.M., Takach, N.E., 2008. Fiber Sweeps for Hole Cleaning. SPE/ICoTA Coiled Tubing Well Interv. Conf. Exhib. https://doi.org/10.2118/113746-MS

Akhshik, S., Behzad, M., Rajabi, M., 2015a. CFD–DEM approach to investigate the effect of drill pipe rotation on cuttings transport behavior. J. Pet. Sci. Eng. 127, 229–244.

Akhshik, S., Behzad, M., Rajabi, M., 2015b. CFD-DEM approach to investigate the effect of drill pipe rotation on cuttings transport behavior. J. Pet. Sci. Eng. 127, 229–244. https://doi.org/10.1016/j.petrol.2015.01.017

Al-Hameedi, A.T., Alkinani, H.H., Dunn-Norman, S., Al-Alwani, M.A., Lian, D., 2019. Equivalent Circulation Density Optimization: Can Flow Regimes Significantly Affect the Relationship Between Equivalent Circulation Density and Flow Rate? . https://doi.org/10.2118/196571-MS

Ali, M.W., 2002. A parametric study of cutting transport in vertical and horizontal well using computational fluid dynamics (CFD).

Alnuaim, S., 2019. The Technology Arm of Sustainability. J. Pet. Technol. 71.

Altindal, M.C., Ozbayoglu, E., Miska, S., Yu, M., Takach, N., May, R., 2017. Impact of Viscoelastic Characteristics of Oil Based Muds/Synthetic Based Muds on Cuttings Settling Velocities, in: Volume 8: Polar and Arctic Sciences and Technology; Petroleum Technology. American Society of Mechanical Engineers. https://doi.org/10.1115/OMAE2017-62129

Amadi, K., Iyalla, I., 2012. Application of Mechanical Specific Energy Techniques in Reducing Drilling Cost in Deepwater Development . https://doi.org/10.2118/156370-MS

Anayo, O., Timothy, I., Friday, O., 2012. Combination of spirolizers and spring centralizers reduces the risk of differential sticking: Case study of wells in Shell Petroleum Development Company (SPDC), Nigeria. Soc. Pet. Eng. - North Africa Tech. Conf. Exhib. 2012, NATC 2012 Manag. Hydrocarb. Resour. a Chang. Environ. 1, 513–523. https://doi.org/10.2118/150687-ms

Armenta, M., 2008. Identifying Inefficient Drilling Conditions Using Drilling-Specific Energy .

https://doi.org/10.2118/116667-MS

Aswad, Z.A.R., Rashid, A., 2014. The combined effect of irregular shape particles and fluid rheology on settling velocity measurement. 10th Int. Conf. Heat Transf. Fluid Mech. Thermodyn. 309–314.

Aydemir, K., Mukhtarov, O., 2015. α-Parameterized Differential Transform Method.

Badrouchi, F., Badrouchi, N., Rabiei, M., Rasouli, V., 2019. Estimation of Elastic Properties of Bakken Formation Using an Artificial Neural Network Model. 53rd U.S. Rock Mech. Symp.

Badrouchi, F., Rasouli, V., 2020a. Simulation of Settling Velocity and Motion of Particles in Drilling Operation. J. Pet. Sci. Eng.

Badrouchi, F., Rasouli, V., 2020b. Simulation of settling velocity and motion of particles in drilling operation. J. Pet. Sci. Eng. 107971. https://doi.org/10.1016/j.petrol.2020.107971

Badrouchi, F., Scott, N., Feilen, H., Badrouchi, N., Tomomewo, O.S., Benouadah, N., Rasouli, V., 2020. Analytical and Experimental Analysis of the Rolling and Lifting of Cuttings in Deviated Wellbores. 54th U.S. Rock Mech. Symp.

Baldino, S., Osgouei, R.E., Miska, S., Takach, N., May, R., Clapper, D., 2015a. Cuttings Settling and Slip Velocity Evaluation in Synthetic Drilling Fluids, in: 12th Offshore Mediterranean Conference and Exhibition Held in Ravenna, Italy from 25th – 27th March 2015.

Baldino, S., Osgouei, R.E., Miska, S., Takach, N., May, R., Clapper, D., 2015b. Cuttings Settling and Slip Velocity Evaluation in Synthetic Drilling Fluids, in: 12th Offshore Mediterranean Conference and Exhibition. Ravenna, Italy.

Bandara, K.M.A.S., Ranjith, P.G., Rathnaweera, T.D., 2020. Extensive analysis of single ceramic proppant fracture mechanism and the influence of realistic extreme reservoir

conditions on proppant mechanical performance. J. Pet. Sci. Eng. 195, 107586. https://doi.org/10.1016/j.petrol.2020.107586

Barati, R., Neyshabouri, S.A.A.S., Ahmadi, G., 2014. Development of empirical models with high accuracy for estimation of drag coefficient of flow around a smooth sphere: An evolutionary approach. Powder Technol. 257, 11–19. https://doi.org/10.1016/j.powtec.2014.02.045

Barr, G., 1931. Monograph of viscometry. By G. Barr, B. A., D.Sc. Pp. xiv + 318. London: Humphrey Milford, Oxford University Press, 1931. 30s. J. Soc. Chem. Ind. 50, 729–729. https://doi.org/10.1002/jctb.5000503509

Bassal, A.A., 1995. Study Of The Effect Of Drill Pipe Rotation On Cuttings. University of Tulsa.

Basset, A.B., 1888. Treatise on Hydrodynamics, George Bell and Sons. London. https://doi.org/10.1038/040412a0

Becker, T., 1982. The effects of mud weight and hole geometry variations on cuttings transport in directional drilling. University of Tulsa.

Becker, T.E., 1987. Correlations for drill cuttings transport in directional well drilling. Tulsa Univ., OK (USA).

Becker, T.E., Azar, J.J., Okrajni, S.S., 1991. Correlations of Mud Rheological Properties With Cuttings-Transport Performance in Directional Drilling. SPE Drill. Eng. 6, 16–24. https://doi.org/10.2118/19535-PA

Bhargava, D., Rajagopal, K., 1992a. An integrated expression for settling velocity of particles in water. Water Res. 26, 1005–1008. https://doi.org/10.1016/0043-1354(92)90208-L

Bhargava, D., Rajagopal, K., 1992b. Simplified procedure for calculating particle settling velocities. Proc. Inst. Civ. Eng. - Water, Marit. Energy 96, 55–57.

https://doi.org/10.1680/iwtme.1992.00567

Bilgesu, H.I., Mishra, N., Ameri, S., 2007. Understanding the Effect of Drilling Parameters on Hole Cleaning in Horizontal and Deviated Wellbores Using Computational Fluid Dynamics. East. Reg. Meet. https://doi.org/10.2118/111208-MS

Blackery, J., Mitsoulis, E., 1997. Creeping motion of a sphere in tubes filled with a Bingham plastic material. J. Nonnewton. Fluid Mech. 70, 59–77. https://doi.org/10.1016/S0377-0257(96)01536-4

Blevins, R.D., 1984. Applied fluid dynamics handbook, New York.

Bourgoyne, A.T., 1991. Applied drilling engineering. Society of Petroleum Engineers, Richardson, TX.

Boussinesq, J., 1885. Application des potentiels à l'étude de l'équilibre et du mouvement des solides élastiques. Gauthier-Villars, Paris.

Boycott, A.E., 1920. Sedimentation of Blood Corpuscles. Nature 104, 532. https://doi.org/10.1038/104532b0

Boyou, N.V., Ismail, I., Wan Sulaiman, W.R., Sharifi Haddad, A., Husein, N., Hui, H.T., Nadaraja, K., 2019. Experimental investigation of hole cleaning in directional drilling by using nano-enhanced water-based drilling fluids. J. Pet. Sci. Eng. 176, 220–231. https://doi.org/10.1016/j.petrol.2019.01.063

Briens, C.L., 1991. Correlation for the direct calculation of the terminal velocity of spherical particles in newtonian and pseudoplastic (power-law) fluids. Powder Technol. 67, 87–91. https://doi.org/10.1016/0032-5910(91)80030-M

Brown, N.P., Bern, P.A., Weaver, A., 1989. Cleaning Deviated Holes: New Experimental and Theoretical Studies. SPE/IADC Drill. Conf. https://doi.org/10.2118/18636-MS

Busahmin, B., N.H, S., Alusta, G., 2017. Analysis of Hole Cleaning for a Vertical Well. Open Access Libr. J. volume 4, 10. https://doi.org/10.4236/oalib

Buscall, R., Goodwin, J.W., Ottewill, R.H., Tadros, T., 1982. The Settling of Particles Through Newtonian and Non-Newtonian Media. J. Colloid Interface Sci. 85, 78–86. https://doi.org/10.1016/0021-9797(82)90237-5

Busch, A., Johansen, S.T., 2020. Cuttings transport: On the effect of drill pipe rotation and lateral motion on the cuttings bed. J. Pet. Sci. Eng. 191, 107136. https://doi.org/10.1016/j.petrol.2020.107136

Bush, M.B., 1994. On the stagnation flow behind a sphere in a shear-thinning viscoelastic liquid. J. Nonnewton. Fluid Mech. 55, 229–247. https://doi.org/10.1016/0377-0257(94)80072-3

Butcher, T., Jr, T., 1990. Use of the falling ball viscometer to obtain flow curves for inelastic, non-Newtonian fluids. J. Non-newtonian Fluid Mech. - J NON-NEWTONIAN FLUID MECH 36, 51–70. https://doi.org/10.1016/0377-0257(90)85003-H

Caicedo, H.U., Calhoun, W.M., Ewy, R.T., 2005. Unique ROP Predictor Using Bit-specific Coefficient of Sliding Friction and Mechanical Efficiency as a Function of Confined Compressive Strength Impacts Drilling Performance . https://doi.org/10.2118/92576-MS

Cerny, L.C., Cerny, C.L., Cerny, E.L., 1988. The sedimentation potential and the boycott effect. Biorheology 25, 503–516. https://doi.org/10.3233/BIR-1988-25310

Chen, D.C.-K., Gaynor, T., Comeaux, B., 2002. Hole Quality: Why It Matters. SPE Int. Pet. Conf. Exhib. Mex. https://doi.org/10.2118/74403-MS

Chen, T.G., Guan, Z.C., 2000. Drilling engineering theory and technology. Dongying Univ. Pet. Press.

Chen, X., Fan, H., Guo, B., Gao, D., Wei, H., Ye, Z., 2014a. Real-Time Prediction and

Optimization of Drilling Performance Based on a New Mechanical Specific Energy Model. Arab. J. Sci. Eng. 39, 8221–8231. https://doi.org/10.1007/s13369-014-1376-0

Chen, X., Fan, H., Guo, B., Gao, D., Wei, H., Ye, Z., 2014b. Real-Time Prediction and Optimization of Drilling Performance Based on a New Mechanical Specific Energy Model. Arab. J. Sci. Eng. 39, 8221–8231. https://doi.org/10.1007/s13369-014-1376-0

Chen, X., Gao, D., 2017. The Maximum-Allowable Well Depth While Performing Ultra-Extended-Reach Drilling From Shallow Water to Deepwater Target. SPE J. 23, 224–236. https://doi.org/10.2118/183025-PA

Chen, X., Gao, D., Guo, B., 2016a. Optimal design of jet mill bit for jet comminuting cuttings in horizontal gas drilling hard formations. J. Nat. Gas Sci. Eng. 28, 587–593. https://doi.org/https://doi.org/10.1016/j.jngse.2015.12.033

Chen, X., Gao, D., Guo, B., 2016b. A Method for Optimizing Jet-Mill-Bit Hydraulics in Horizontal Drilling. SPE J. 21, 416–422. https://doi.org/10.2118/178436-PA

Chen, X., Gao, D., Guo, B., Feng, Y., 2016c. Real-time optimization of drilling parameters based on mechanical specific energy for rotating drilling with positive displacement motor in the hard formation. J. Nat. Gas Sci. Eng. 35, 686–694. https://doi.org/https://doi.org/10.1016/j.jngse.2016.09.019

Chen, X., Gao, D., Guo, B., Feng, Y., 2016d. Real-time optimization of drilling parameters based on mechanical specific energy for rotating drilling with positive displacement motor in the hard formation. J. Nat. Gas Sci. Eng. 35, 686–694. https://doi.org/https://doi.org/10.1016/j.jngse.2016.09.019

Chen, X., Gao, D., Guo, B., Luo, L., Liu, X., Zhang, X., 2014c. A new method for determining the minimum gas injection rate required for hole cleaning in horizontal gas drilling. J. Nat.

Gas Sci. Eng. 21, 1084–1090. https://doi.org/https://doi.org/10.1016/j.jngse.2014.11.009

Chen, X., Yang, J., Gao, D., 2018. Drilling Performance Optimization Based on Mechanical Specific Energy Technologies. Drilling. https://doi.org/10.5772/intechopen.75827

Chen, Z., Xiong, J., 2010. Numerical Calculation for Carrying-cutting Lifting of Spiral Centralizer in Conventional Drilling. Nat. Gas Technol. 4, 44–46.

Cheng, N.-S., 1997. Simplified Settling Velocity Formula for Sediment Particle. J. Hydraul. Eng. 123, 149–152. https://doi.org/10.1061/(ASCE)0733-9429(1997)123:2(149)

Chepil, W.S., 1958. The use of evenly spaced hemispheres to evaluate aerodynamic forces on a soil surface. Trans. Am. Geophys. Union 39, 397. https://doi.org/10.1029/TR039i003p00397

Chhabra, R.., 2007. Bubbles, drops and particles in non-newtonian fluids, 2nd ed, CRC Press. Taylor & Francis Group, LLC. https://doi.org/10.1016/0377-0257(95)90008-x

Chhabra, R.P., McKay, A., Wong, P., 1996. Drag on discs and square plates in pseudoplastic polymer solutions. Chem. Eng. Sci. 51, 5353–5356. https://doi.org/https://doi.org/10.1016/S0009-2509(96)00369-7

Chien, S.F., 1994. Settling velocity of irregularly shaped particles. https://doi.org/10.2118/26121-PA

Cho, H., Shah, S.N., Osisanya, S.O., 2000. A Three-Layer Modeling for Cuttings Transport with Coiled Tubing Horizontal Drilling. SPE Annu. Tech. Conf. Exhib. https://doi.org/10.2118/63269-MS

Choudhary, D., 2011. DIRECTIONAL DRILLING TECHNOLOGY: 18. STABILIZERS [WWW Document].

Clark, R.K., Bickham, K.L., 1994. A Mechanistic Model for Cuttings Transport. SPE Annu.

Tech. Conf. Exhib. https://doi.org/10.2118/28306-MS

Clarke, M., Musser, J., 2020. The MFiX Particle-in-Cell Method (MFiX-PIC) Theory Guide. https://doi.org/10.2172/1630414

Clift, R., Grace, J.R., Weber, M.E., 1978. Bubbles, drops, and particles, Acadimic Press. New York. https://doi.org/10.1017/S0022112079221290

Corporation, S., 2007. SpaceClaim User's Guide: ASpaceClaim Document.

Crowe, C., Schwarzkopf, J., Sommerfeld, M., Tsuji, Y., 2011. Multiphase flows with droplets and particles.

D. Nguyen, B.., 1997. MATHEMA TICAL MODELS OF CUTTINGS TRANSPOR T & DRILLING FLUID DISPLACEM ENT BY CEMENT SLURRY IN HORIZONT AL WELLS by. The University of New South Wales.

Dazhi, G., Tanner, R.I., 1985. The drag on a sphere in a power-law fluid. J. Nonnewton. Fluid Mech. 17, 1–12. https://doi.org/10.1016/0377-0257(85)80001-X

Demuth, Howard; Beale, M., 2015. MATLAB Neural Network Toolbox: User's Manual, Mathworks Inc. Natick, Massachusetts, USA.

Dhole, S., Chhabra, R., 2006. Flow of Power-Law Fluids Past a Sphere at Intermediate Reynolds Numbers. Ind. Eng. Chem. Res. - IND ENG CHEM RES 45. https://doi.org/10.1021/ie0512744

Domiri Ganji, D., 2012. A semi-Analytical technique for non-linear settling particle equation of Motion. J. Hydro-environment Res. 6, 323–327. https://doi.org/10.1016/j.jher.2012.04.002

Doron, P., Granica, D., Barnea, D., 1987. Slurry flow in horizontal pipes—experimental and modeling. Int. J. Multiph. Flow 13, 535–547. https://doi.org/10.1016/0301-9322(87)90020-6

Duan, M., Miska, S., Yu, M., Takach, N., Ahmed, R., Zettner, C., 2007. Critical conditions for effective sand-sized solids transport in horizontal and high-angle wells. SPE Prod. Oper. Symp. Proc. 327–337. https://doi.org/10.2118/106707-ms

Duan, M., Miska, S., Yu, M., Takach, N.E., Ahmed, R.M., Hallman, J.H., 2010. Experimental Study and Modeling of Cuttings Transport Using Foam With Drillpipe Rotation. SPE Drill. Complet. 25, 352–362. https://doi.org/10.2118/116300-PA

Duan, M., Miska, S.Z., Yu, M., Takach, N.E., Ahmed, R.M., Zettner, C.M., 2009. Critical Conditions for Effective Sand-Sized Solids Transport in Horizontal and High-Angle Wells. SPE Drill. Complet. 24, 229–238. https://doi.org/10.2118/106707-PA

Duan, M., Miska, S.Z., Yu, M., Takach, N.E., Ahmed, R.M., Zettner, C.M., 2008. Transport of Small Cuttings in Extended-Reach Drilling. SPE Drill. Complet. 23, 258–265. https://doi.org/10.2118/104192-PA

Dupriest, F.E., Elks, W.C., Ottesen, S., Pastusek, P.E., Zook, J.R., Aphale, C.R., 2011. Borehole-Quality Design and Practices To Maximize Drill-Rate Performance. SPE Drill. Complet. 26, 303–316. https://doi.org/10.2118/134580-PA

Dupriest, F.E., Koederitz, W.L., 2005a. Maximizing Drill Rates with Real-Time Surveillance of Mechanical Specific Energy . https://doi.org/10.2118/92194-MS

Dupriest, F.E., Koederitz, W.L., 2005b. Maximizing Drill Rates with Real-Time Surveillance of Mechanical Specific Energy . https://doi.org/10.2118/92194-MS

Einstein, H.A., El-Samni, E.-S.A., 1949. Hydrodynamic Forces on a Rough Wall. Rev. Mod. Phys. 21, 520–524. https://doi.org/10.1103/RevModPhys.21.520

Elgaddafi, R., Ahmed, R., George, M., Growcock, F., 2012. Settling behavior of spherical particles in fiber-containing drilling fluids. J. Pet. Sci. Eng. 84–85, 20–28.

https://doi.org/https://doi.org/10.1016/j.petrol.2012.01.020

Elgaddafi, R., Ahmed, R., Growcock, F., 2016. Settling behavior of particles in fiber-containing Herschel Bulkley fluid. Powder Technol. 301, 782–793. https://doi.org/10.1016/j.powtec.2016.07.006

Elzenary, M., Elkatatny, S., Abdelgawad, K.Z., Abdulraheem, A., Mahmoud, M., Al-Shehri, D., 2018. New Technology to Evaluate Equivalent Circulating Density While Drilling Using Artificial Intelligence . https://doi.org/10.2118/192282-MS

Faitli, J., 2017. Continuity theory and settling model for spheres falling in non-Newtonian one- and two-phase media. Int. J. Miner. Process. 169. https://doi.org/10.1016/j.minpro.2017.09.010

Faxén, H., 1921. Einwirkung der Gefasswande auf den Widerstand gegen die Bewegung einer kleinen Kugel in einer zahen Flussigkeit. University of Uppsala.

Ferreira, J., Duarte Naia, M., Chhabra, R., 1998. An Analytical Study of the Transient Motion of a Dense Rigid Sphere in an Incompressible Newtonian Fluid. Chem. Eng. Commun. 168, 45–58. https://doi.org/10.1080/00986449808912706

Fidleris, V., Whitmore, R., 2002. Experimental Determination of Wall Effect for Spheres Falling Axially in Cylindrical Vessels. Br. J. Appl. Phys. 12, 490. https://doi.org/10.1088/0508-3443/12/9/311

Fidleris, V., Whitmore, R., 1961a. Experimental Determination of Wall Effect for Spheres Falling Axially in Cylindrical Vessels. Br. J. Appl. Phys. 12, 490. https://doi.org/10.1088/0508-3443/12/9/311

Fidleris, V., Whitmore, R., 1961b. The physical interaction of spherical particles in suspensions. Rheol. acta 1, 573–580. https://doi.org/10.1007/BF01989126

Ford, J., 1993. Development of mathematical models describing drilled cuttings transport in deviated wells, in: Proceedings of the CADE/CAODC Spring Drilling Conference, Calgary, AB.

Ford, J.T., Peden, J.M., Oyeneyin, M.B., Gao, E., Zarrough, R., 1990. Experimental Investigation of Drilled Cuttings Transport in Inclined Boreholes. SPE Annu. Tech. Conf. Exhib. https://doi.org/10.2118/20421-MS

Francis, A.W., 1933. Wall Effect in Falling Ball Method for Viscosity. Physics (College. Park. Md). 4, 403–406. https://doi.org/10.1063/1.1745151

Gavignet, A.A., Sobey, I.J., 1989. Model Aids Cuttings Transport Prediction. J. Pet. Technol. 41, 916–921. https://doi.org/10.2118/15417-PA

Gavrilov, A., Finnikov, K., Podryabinkin, E., 2017. Modeling of steady Herschel–Bulkley fluid flow over a sphere. J. Eng. Thermophys. 26, 197–215. https://doi.org/10.1134/S1810232817020060

Gaynor, T.M., Chen, D.C.-K., Stuart, D., Comeaux, B., 2001. Tortuosity versus Micro-Tortuosity - Why Little Things Mean a Lot. SPE/IADC Drill. Conf. https://doi.org/10.2118/67818-MS

Gharbi, R.B.C., Mansoori, G.A., 2005. An introduction to artificial intelligence applications in petroleum exploration and production. J. Pet. Sci. Eng. 49, 93–96. https://doi.org/https://doi.org/10.1016/j.petrol.2005.09.001

Ghosh, S., Stockie, J., 2015. Numerical Simulations of Particle Sedimentation Using the Immersed Boundary Method. Commun. Comput. Phys. 18, 380–416. https://doi.org/10.4208/cicp.061113.050115a

Glomstad, T.S., 2012. Analysis of Hook load Signal to reveal the Causes of Restrictions.

Norwegian University of Science and Technology.

Goldstein, E.B., Coco, G., 2014. A machine learning approach for the prediction of settling velocity. Water Resour. Res. 50, 3595–3601. https://doi.org/10.1002/2013WR015116

Govier, G.W., Khalid, A., 1972. The Flow of Complex Mixtures in Pipes. Van Nostrand Reinhold Company.

Graham, D.I., Jones, T.E.R., 1994. Settling and transport of spherical particles in power-law fluids at finite Reynolds number. J. Nonnewton. Fluid Mech. 54, 465–488. https://doi.org/10.1016/0377-0257(94)80037-5

Gumulya, M., Horsley, R., Pareek, V., 2014. Numerical simulation of the settling behaviour of particles in thixotropic fluids. Phys. Fluids 26. https://doi.org/10.1063/1.4866320

Guo, J., 2011. Motion of Spheres Falling Through Fluids. J. Hydraul. Res. - J Hydraul RES 49, 32–41. https://doi.org/10.1080/00221686.2010.538572

Haider, A., Levenspiel, O., 1989. Drag Coefficient and Terminal Velocity of Spherical and Non-Spherical Particles. Powder Technol. - POWDER TECHNOL 58, 63–70. https://doi.org/10.1016/0032-5910(89)80008-7

Hajipour, M., 2020. CFD simulation of turbulent flow of drill cuttings and parametric studies in a horizontal annulus. SN Appl. Sci. 2, 1146. https://doi.org/10.1007/s42452-020-2970-2

Hammoutene, C., Bits, S., 2012a. FEA Modelled MSE/UCS Values Optimise PDC Design for Entire Hole Section . https://doi.org/10.2118/149372-MS

Hammoutene, C., Bits, S., 2012b. FEA Modelled MSE/UCS Values Optimise PDC Design for Entire Hole Section . https://doi.org/10.2118/149372-MS

Han, C., Guan, Z., Li, J., Hu, H., Xu, Y., 2019. Equivalent Circulating Density Prediction Using a Hybrid ARIMA and BP Neural Network Model . https://doi.org/10.2118/197495-MS

Hassan, I., 2008. Application to differential transformation method for solving systems of differential equations. Appl. Math. Model. 12. https://doi.org/10.1016/j.apm.2007.09.025

Hemphill, T., Ravi, K., Bern, P., Rojas, J.C., 2008. A simplified method for prediction of ECD increase with drillpipe rotation. Proc. - SPE Annu. Tech. Conf. Exhib. 2, 1092–1098. https://doi.org/10.2118/115378-ms

Hopkin, E.A., 1967. Factors Affecting Cuttings Removal During Rotary Drilling. J. Pet. Technol. 19, 807–814. https://doi.org/10.2118/1697-PA

Huang, H., Babadagli, T., Li, H.A., Develi, K., Wei, G., 2019. Effect of injection parameters on proppant transport in rough vertical fractures: An experimental analysis on visual models. J. Pet. Sci. Eng. 180, 380–395. https://doi.org/https://doi.org/10.1016/j.petrol.2019.05.009

Iyoho, A.W., 1980. Drilled-cuttings Transport by Non-Newtonian Drilling Fluids Through Inclined, Eccentric Annuli. University of Tulsa.

Jacobs, C., Jendrassak, M., Gurka, R., Hackett, E., 2015. Experimental study of particle settling velocitiesle [WWW Document]. Sch. Coast. Environ. Student Exp. URL https://scmss.coastal.edu/sites/default/files/student_experience/Present_AGU_04_Final.pdf

Jalaal, M., Bararnia, H., Domairry, G., 2011. A series exact solution for one-dimensional non-linear particle equation of motion. Powder Technol. 207, 461–464. https://doi.org/https://doi.org/10.1016/j.powtec.2010.10.025

Jayaweera, K., Mason, B., 1965. The Behaviour of Freely Falling Cylinders and Cones in a Viscous Fluid. J. Fluid Mech. 22, 709–720. https://doi.org/10.1017/S002211206500109X

Johnsen, M., 2014. Particle Transport and Hole Cleaning in Wells During Drilling. Masters degree thesis Submitt. to Dep. Pet. Eng. Univ. Stavanger, Norway.

Kamyab, M., Dawson, R., Farmanbar, P., 2016. A New Method to Determine Friction Factor of

Cuttings Slip Velocity Calculation in Vertical Wells Using Neural Networks, in: SPE Asia Pacific Oil & Gas Conference and Exhibition. Society of Petroleum Engineers, pp. 1–7. https://doi.org/10.2118/182359-MS

Kamyab, M., Sampaio, J.H.B., Qanbari, F., Eustes, A.W., 2010. Using artificial neural networks to estimate the z-factor for natural hydrocarbon gases. J. Pet. Sci. Eng. 73, 248–257. https://doi.org/https://doi.org/10.1016/j.petrol.2010.07.006

Katende, A., Segar, B., Ismail, I., Sagala, F., Saadiah, H.H.A.R., Samsuri, A., 2020. The effect of drill–pipe rotation on improving hole cleaning using polypropylene beads in water-based mud at different hole angles. J. Pet. Explor. Prod. Technol. 10, 1253–1262. https://doi.org/10.1007/s13202-019-00815-1

Kelessidis, V., 2004. Terminal velocity of solid spheres falling in Newtonian and non-Newtonian liquids. Tech. Chron. Sci. 24, 43–54.

Kelessidis, V., 2003. Terminal velocity of solid spheres falling in Newtonian and non-Newtonian liquids. Tech. Chron. Sci. J. TCG 24, 43–54.

Kenny, P., Sunde, E., Hemphill, T., 1996. Hole Cleaning Modelling: What's "n" Got To Do With It? IADC/SPE Drill. Conf. https://doi.org/10.2118/35099-MS

Kerunwa, A., 2020. Contributory Influence of Drill Cuttings on Equivalent Circulation Density Model in Deviated Wellbores. Int. J. Oil, Gas Coal Eng. 8, 82. https://doi.org/10.11648/j.ogce.20200804.12

Khatmullina, L., Isachenko, I., 2016. Settling velocity of microplastic particles of regular shapes. Mar. Pollut. Bull. 114. https://doi.org/10.1016/j.marpolbul.2016.11.024

Kristiansen, T.G., 2004. Drilling Wellbore Stability in the Compacting and Subsiding Valhall Field. IADC/SPE Drill. Conf. https://doi.org/10.2118/87221-MS

Krumbein, W.C., Sloss, L.L., 1951. Stratigraphy and sedimentation. LWW.

Kulkarni, D., Maghrabi, S., Wagle, V., 2014. Synergistic Chemistry Tailors Invert Emulsion Fluids (IEF) with Consistent Rheology to Minimize Equivalent Circulating Density (ECD) Fluctuations . https://doi.org/10.2118/171695-MS

Ladenburg, R., 1907. Über die innere Reibung zäher Flüssigkeiten und ihre Abhängigkeit vom Druck. Ann. Phys. 327, 287–309. https://doi.org/10.1002/andp.19073270206

Larsen, T.I., Pilehvari, A.A., Azar, J.J., 1997. Development of a New Cuttings-Transport Model for High-Angle Wellbores Including Horizontal Wells. SPE Drill. Complet. 12, 129–136. https://doi.org/10.2118/25872-PA

Larsen, T.I.F., 1990. A Study of the Critical Fluid Velocity in Cuttings Transport for Inclined Wellbores. University of Tulsa.

Li, M., Jv, Y.F., Wang, Z.Q., Hao, B.Y., Hong, Y.K., 2010. Simulation on the effect of drillstring rotation on hole cleaning for extended reach well. West-china Explor. Eng 5, 51–54.

Li, M., Zhang, G., Xue, J., Li, Y., Tang, S., 2014. Prediction of the Wall Factor of Arbitrary Particle Settling through Various Fluid Media in a Cylindrical Tube Using Artificial Intelligence. Sci. World J. 2014, 1–10. https://doi.org/10.1155/2014/438782

Lin, A., Alali, M., Almasmoom, S., Samuel, R., 2018. Wellbore Instability Prediction Using Adaptive Analytics and Empirical Mode Decomposition. IADC/SPE Drill. Conf. Exhib. https://doi.org/10.2118/189598-MS

Liu, H., Bedrikovetsky, P., Yuan, Z., Liu, J., Liu, Y., 2021. An optimized model of calculating optimal packing ratio for graded proppant placement with consideration of proppant embedment and deformation. J. Pet. Sci. Eng. 196, 107703.

https://doi.org/10.1016/j.petrol.2020.107703

Livescu, S., Craig, S., 2018. A critical review of the coiled tubing friction-reducing technologies in extended-reach wells. Part 2: Vibratory tools and tractors. J. Pet. Sci. Eng. 166, 44–54. https://doi.org/10.1016/j.petrol.2018.03.026

Loureiro, B.V., Paula, R.S., Serafim, M., Martins, A.L., 2010. Experimental Evaluation of the Effect of Drillstring Rotation in the Suspension of a Cuttings Bed. SPE Lat. Am. Caribb. Pet. Eng. Conf. https://doi.org/10.2118/122071-MS

Lunnon, R.G., 1928. Fluid resistance to moving spheres. Proc. R. Soc. London. Ser. A, Contain. Pap. a Math. Phys. Character 118, 680–694. https://doi.org/10.1098/rspa.1928.0077

Luo, X., Wang, S., Wang, Z., Jing, Z., Lv, M., 2014. Experimental research on rheological properties and proppant transport performance of GRF–CO2 fracturing fluid. J. Pet. Sci. Eng. 120, 154–162. https://doi.org/https://doi.org/10.1016/j.petrol.2014.06.009

Luo, Y., 1988. Non-Newtonian annular flow and cuttings transport through drilling annuli at various angles. Heriot-Watt University, Edinburgh.

Luo, Y., Bern, P.A., Chambers, B.D., 1992. Flow-Rate Predictions for Cleaning Deviated Wells. IADC/SPE Drill. Conf. https://doi.org/10.2118/23884-MS

Mahmoud, H., Hamza, A., Nasser, M.S., Hussein, I.A., Ahmed, R., Karami, H., 2020. Hole cleaning and drilling fluid sweeps in horizontal and deviated wells: Comprehensive review. J. Pet. Sci. Eng. 186, 106748. https://doi.org/10.1016/j.petrol.2019.106748

Maidla, E., Haci, M., 2004. Understanding Torque: The Key to Slide-Drilling Directional Wells . https://doi.org/10.2118/87162-MS

Malekzadeh, N., Mohammadsalehi, M., 2011. Hole Cleaning Optimization in Horizontal Wells: A New Method To Compensate Negative Hole Inclination Effects. Bras. Offshore.

https://doi.org/10.2118/143676-MS

Malhotra, S., Sharma, M.M., 2014. Experimental Measurement of Settling Velocity of Spherical Particles in Unconfined and Confined Surfactant-based Shear Thinning Viscoelastic Fluids. J. Vis. Exp. https://doi.org/10.3791/50749

Martin, M., Georges, C., Bisson, P., Konirsch, O., 1987. Transport of Cuttings in Directional Wells, in: Proceedings of SPE/IADC Drilling Conference. Society of Petroleum Engineers, pp. 293–303. https://doi.org/10.2523/16083-MS

Martins, A.L., Santana, C., 1992. Evaluation of Cuttings Transport in Horizontal and Near Horizontal Wells -A Dimensionless Approach, in: Proceedings of SPE Latin America Petroleum Engineering Conference. Society of Petroleum Engineers, pp. 155–161. https://doi.org/10.2523/23643-MS

Martins, A.L., Santana, M.L., Campos, W., Gaspari, E.F., 1999. Evaluating the Transport of Solids Generated by Shale Instabilities in ERW Drilling. SPE Drill. Complet. 14, 254–259. https://doi.org/10.2118/59729-PA

Mason, C.J., Chen, D.C.-K., 2006. The Wellbore Quality Scorecard (WQS). IADC/SPE Drill. Conf. https://doi.org/10.2118/98893-MS

Mehta, A., Barker, G.C., 1994. The dynamics of sand. Reports Prog. Phys. 57, 383–416. https://doi.org/10.1088/0034-4885/57/4/002

Menegbo, E.K., Charles, E., Dosunmu, A., 2019. Evaluation of Cuttings Transport in Well Annulus Using Power Law Model. SPE Niger. Annu. Int. Conf. Exhib. https://doi.org/10.2118/198825-MS

Merdan, M., Gokdogan, A., Yildirim, A., Mohyud-Din, S., 2012. Numerical Simulation of Fractional Fornberg-Whitham Equation by Differential Transformation Method. Abstr.

Appl. Anal. 2012, Spec. https://doi.org/10.1155/2012/965367

MFiX - Multiphase Flow Science Group at NETL [WWW Document], n.d. URL https://mfix.netl.doe.gov/mfix/ (accessed 2.2.20).

Mirhaj, S.A., Shadizadeh, R., Fazaeli-zadeh, M., 2007. Cuttings Removal Simulation for Deviated and Horizontal Wellbores, in: Proceedings of SPE Middle East Oil and Gas Show and Conference. Society of Petroleum Engineers. https://doi.org/10.2523/105442-MS

Missirlis, K.., Assimacopoulos, D., Mitsoulis, E., Chhabra, R.., 2001. Wall effects for motion of spheres in power-law fluids. J. Nonnewton. Fluid Mech. 96, 459–471. https://doi.org/10.1016/S0377-0257(00)00189-0

Mitchell, T., 2006. The Discipline of Machine Learning, in: CMU-ML-06-108. Pittsburgh. PA.

Mkuyi, F.R., 2016. Evidences of Poor Hole-cleaning or of Wellbore Instability through Hook load Response. Norwegian University of Science and Technology.

Mohammadsalehi, M., Malekzadeh, N., 2011. Optimization of Hole Cleaning and Cutting Removal in Vertical, Deviated and Horizontal Wells. SPE Asia Pacific Oil Gas Conf. Exhib. https://doi.org/10.2118/143675-MS

Mohan, K., Adil, F., Samuel, R., 2014a. Comprehensive Hydromechanical Specific Energy Calculation for Drilling Efficiency. J. Energy Resour. Technol. 137. https://doi.org/10.1115/1.4028272

Mohan, K., Adil, F., Samuel, R., 2014b. Comprehensive Hydromechanical Specific Energy Calculation for Drilling Efficiency. J. Energy Resour. Technol. 137. https://doi.org/10.1115/1.4028272

Mohan, K., Adil, F., Samuel, R., 2009a. Tracking Drilling Efficiency Using Hydro-Mechanical Specific Energy . https://doi.org/10.2118/119421-MS

Mohan, K., Adil, F., Samuel, R., 2009b. Tracking Drilling Efficiency Using Hydro-Mechanical Specific Energy . https://doi.org/10.2118/119421-MS

Moreira, B., Arouca, F., Damasceno, J., 2017. Analysis of suspension sedimentation in fluids with rheological shear-thinning properties and thixotropic effects. Powder Technol. 308, 290–297. https://doi.org/10.1016/j.powtec.2016.12.034

Mott, R.A., 1951. The Laws of Motion of Particles in Fluids and their Application to the Resistance of Beds of Solids to the Passage of Fluid, in: Some Aspects of Fluid Flow. Papers Presented at a Conference Organised by the Institute of Physics in October 1950. Edward Arnold & Company. London. 1951. 292 Pp. Illustrated. Index. 50s. Net. The Journal of the Royal Aeronautical Society, pp. 745–746. https://doi.org/10.1017/S0368393100122424

Munroe, H.S., 1889. The English versus the continental system of jigging: is close sizing advantageous. Trans. Am. Inst. Min. 23 p.

Nazari, T., Hareland, G., Azar, J.J., 2010. Review of Cuttings Transport in Directional Well Drilling: Systematic Approach. SPE West. Reg. Meet. https://doi.org/10.2118/132372-MS

Nguyen, D., Rahman, S.S., 1998. A Three-Layer Hydraulic Program for Effective Cuttings Transport and Hole Cleaning in Highly Deviated and Horizontal Wells. SPE Drill. Complet. 13, 182–189. https://doi.org/10.2118/51186-PA

Nolan, G.F., 1970. Drag of free-falling spheres in water for Reynolds numbers near critical. Naval Postgraduate School, Monterey, California.

Nouri, R., Ganji, D.D., Hatami, M., 2014. Unsteady sedimentation analysis of spherical particles in Newtonian fluid media using analytical methods. Propuls. Power Res. 3, 96–105. https://doi.org/10.1016/j.jppr.2014.05.003

Nwagu, C., Awobadejo, T., Gaskin, K., 2014. Application of Mechanical Cleaning Device: Hole Cleaning Tubulars To Improve Hole Cleaning. https://doi.org/10.2118/172403-MS

Okrajni, S., Azar, J.J., 1986. The Effects of Mud Rheology on Annular Hole Cleaning in Directional Wells. SPE Drill. Eng. 1, 297–308. https://doi.org/10.2118/14178-PA

Oliveira, C., 2015. Solving ODEs and PDEs, in: Practical C++ Financial Programming. Apress, Berkeley, CA, pp. 221–236. https://doi.org/10.1007/978-1-4302-6716-4_11

Osborne, M.R.; W.R.O., 1977. Chapter 8: Artificial Intelligence, Simulation and Modelling, in: Simulation and Modelling.

Oseen, C.W., 1911. Über die Stoke'sche Formel und über eine verwandte Aufgabe in der Hydrodynamik: Mitteilung 2, Arkiv för matematik, astronomi och fysik. Almqvist & Wiksell.

Oseh, J.O., Mohd Norddin, M.N.A., Ismail, I., Gbadamosi, A.O., Agi, A., Ismail, A.R., 2020. Experimental investigation of cuttings transportation in deviated and horizontal wellbores using polypropylene–nanosilica composite drilling mud. J. Pet. Sci. Eng. 189, 106958. https://doi.org/10.1016/j.petrol.2020.106958

Ozbayoglu, E.M., Miska, S.Z., Takach, N., Reed, T., 2009. Sensitivity analysis of major drilling parameters on cuttings transport during drilling highly-inclined wells. Pet. Sci. Technol. 27, 122–133. https://doi.org/10.1080/10916460701700195

Ozbayoglu, Mehmet Evren, Ettehadi Osgouei, R., Ozbayoglu, A., Yuksel, E., 2010. Estimation of Very-Difficult-to-Identify Data for Hole Cleaning, Cuttings Transport and Pressure Drop Estimation in Directional and Horizontal Drilling, in: IADC/SPE Asia Pacific Drilling Technology Conference and Exhibition. Society of Petroleum Engineers, pp. 668–685. https://doi.org/10.2118/136304-MS

Ozbayoglu, M.E., Saasen, A., Sorgun, M., Svanes, K., 2008. Effect of Pipe Rotation on Hole Cleaning for Water-Based Drilling Fluids in Horizontal and Deviated Wells. IADC/SPE Asia Pacific Drill. Technol. Conf. Exhib. https://doi.org/10.2118/114965-MS

Ozbayoglu, M E, Sorgun, M., Saasen, A., Svanes, K., 2010. Hole Cleaning Performance of Light-Weight Drilling Fluids During Horizontal Underbalanced Drilling. J. Can. Pet. Technol. 49, 21–26. https://doi.org/10.2118/136689-PA

Padé, H., 1892. Sur la représentation approchée d'une fonction par des fractions rationnelles. Ann. Sci. l'école Norm. Supérieure 9, 3–93.

Pang, B., Wang, S., Wang, Q., Yang, K., Lu, H., Hassan, M., Jiang, X., 2018. Numerical prediction of cuttings transport behavior in well drilling using kinetic theory of granular flow. J. Pet. Sci. Eng. 161, 190–203. https://doi.org/10.1016/j.petrol.2017.11.028

Parmar, M., Haselbacher, A., Balachandar, S., 2011. Generalized Basset-Boussinesq-Oseen Equation for Unsteady Forces on a Sphere in a Compressible Flow. Phys. Rev. Lett. 106, 84501. https://doi.org/10.1103/PhysRevLett.106.084501

Pašić, B., Gaurina-Međimurec, N., Davorin, M., 2007. Wellbore instability: Causes and consequences. Rud. Zb. 19.

Pastusek, P.E., 2018. Stabilizer selection based on physics and lessons learned. Soc. Pet. Eng. - IADC/SPE Drill. Conf. Exhib. DC 2018 2018-March, 6–8. https://doi.org/10.2118/189649-ms

Peden, J., Luo, Y., 1987. Settling Velocity of Variously Shaped Particles in Drilling and Fracturing Fluids. SPE Drill. Eng. 2, 337–343. https://doi.org/10.2118/16243-PA

Peden, J.M., Ford, J.T., Oyeneyin, M.B., 1990. Comprehensive Experimental Investigation of Drilled Cuttings Transport in Inclined Wells Including the Effects of Rotation and

Eccentricity. Eur. Pet. Conf. https://doi.org/10.2118/20925-MS

Pereira, C.E.G., da Cruz, G.A., Pereira Filho, L., Justino, L.R., Paraiso, E.C.H., Rocha, J.M., Calçada, L.A., Scheid, C.M., 2019. Experimental analysis of pressure drop in the flow of Newtonian fluid in coiled tubing. J. Pet. Sci. Eng. 179, 565–573. https://doi.org/10.1016/j.petrol.2019.04.082

Pessier, R.C., Fear, M.J., 1992a. Quantifying Common Drilling Problems With Mechanical Specific Energy and a Bit-Specific Coefficient of Sliding Friction . https://doi.org/10.2118/24584-MS

Pessier, R.C., Fear, M.J., 1992b. Quantifying Common Drilling Problems With Mechanical Specific Energy and a Bit-Specific Coefficient of Sliding Friction . https://doi.org/10.2118/24584-MS

Pigott, R.J.S., 1941. Mud flow in drilling. Drill. Prod. Pract. 1941 91–103.

Pilehvari, A.A., Azar, J.J., Shirazi, S.A., 1996. State-Of-The-Art Cuttings Transport in Horizontal Wellbores. Int. Conf. Horiz. Well Technol. https://doi.org/10.2118/37079-MS

Piroozian, A., Ismail, I., Yaacob, Z., Babakhani, P., Ismail, A.S.I., 2012. Impact of drilling fluid viscosity, velocity and hole inclination on cuttings transport in horizontal and highly deviated wells. J. Pet. Explor. Prod. Technol. 2, 149–156. https://doi.org/10.1007/s13202-012-0031-0

Prashant, Derksen, J.J., 2011. Direct simulations of spherical particle motion in Bingham liquids. Comput. Chem. Eng. 35, 1200–1214. https://doi.org/10.1016/j.compchemeng.2010.09.002

Rashidi, B., Hareland, G., Fazaelizadeh, M., Svigir, M., 2010. Title: Comparative Study Using Rock Energy And Drilling Strength Models .

Rashidi, M.M., LARAQI, N., Sadri, S., 2010. A Novel Analytical Solution of Mixed Convection

about an Inclined Flat Plate Embedded in a Porous Medium Using the DTM-Padé. Int. J. Therm. Sci. 49, 2405–2412. https://doi.org/10.1016/j.ijthermalsci.2010.07.005

Rasi, M., 1994. Hole Cleaning in Large, High-Angle Wellbores. IADC/SPE Drill. Conf. https://doi.org/10.2118/27464-MS

Razavi, F., Komrakova, A., Lange, C., 2019. CFD-DEM Model of Particulate Flow.

Reynolds, P.A., Jones, T.E.R., 1989. An Experimental Study of the Settling Velocities of Single Particles in Non-Newtonian Fluids. Int. J. Miner. Process. - INT J Min. Process 25, 47–77. https://doi.org/10.1016/0301-7516(89)90056-2

Richardson, J.F., Harker, J.H., Backhurst, J.., 1986. Sedimentation, in: Coulson and Richardson's Chemical Engineering Volume 2 - Particle Technology and Separation Processes. Elsevier. https://doi.org/10.1016/b978-0-08-049064-9.50017-5

Rooki, R., Doulati Ardejani, F., Moradzadeh, A., Kelessidis, V.C., Nourozi, M., 2012. Prediction of terminal velocity of solid spheres falling through Newtonian and non-Newtonian pseudoplastic power law fluid using artificial neural network. Int. J. Miner. Process. 110–111, 53–61. https://doi.org/10.1016/j.minpro.2012.03.012

Rouse, H., 1938. Nomogram for the settling velocity of spheres. Washington.

Rushd, S., Hassan, I., Sultan, R.A., Kelessidis, V.C., Rahman, A., Hasan, H.S., Hasan, A., 2019. Terminal settling velocity of a single sphere in drilling fluid. Part. Sci. Technol. 37, 943–952. https://doi.org/10.1080/02726351.2018.1472162

Ryder, R., Qiang, J., Mccabe, P., Nuccio, V., Persits, F., 2003. Qingshankou-Putaohua/Shaertu and Jurassic Coal– Denglouku/Nongan Total Petroleum Systems in the Songliao Basin, China. US Geol. Surv. Bull. 2203-A.

Saasen, A., Løklingholm, G., 2002. The Effect of Drilling Fluid Rheological Properties on Hole

Cleaning. IADC/SPE Drill. Conf. https://doi.org/10.2118/74558-MS

Sadat-Helbar, S.M., Shirazi, H., Zare, D., 2009. Fall velocity of sediment particles in Water Reservoirs. IASME/WSEAS Int. Conf. Water Resour. Hydraul. Hydrol. 39–45.

Saeid, N., Busahmin, B., 2016. CFD analysis of drilling fluid flow in vertical wells.

Samni, E.S.A., 1949. Hydrodynamic Forces Acting on Particles in the Surface of a Stream Bed. University of California, Berkeley.

Sanchez, R.A., Azar, J.J., Bassal, A.A., Martins, A.L., 1997a. The Effect of Drillpipe Rotation on Hole Cleaning During Directional Well Drilling. SPE/IADC Drill. Conf. https://doi.org/10.1061/(ASCE)0733-9399(2005)

Sanchez, R.A., Azar, J.J., Bassal, A.A., Martins, A.L., 1997b. The Effect of Drillpipe Rotation on Hole Cleaning During Directional Well Drilling. SPE/IADC Drill. Conf. https://doi.org/10.2118/37626-MS

Seeberger, M.H., Matlock, R.W., Hanson, P.M., 1989. Oil Muds in Large-Diameter, Highly Deviated Wells: Solving the Cuttings Removal Problem. SPE/IADC Drill. Conf. https://doi.org/10.2118/18635-MS

Shadizadeh, S.R., Zoveidavianpoor, M., 2012. An Experimental Modeling of Cuttings Transport for an Iranian Directional and Horizontal Well Drilling. Pet. Sci. Technol. 30, 786–799. https://doi.org/10.1080/10916466.2010.490816

Sharma, M., Chhabra, R., 1991. An Experimental Study of Free Fall of Cones in Newtonian and Non-Newtonian Media: Drag Coefficient and Wall Effects. Chem. Eng. Process. Process Intensif. 30, 61–67. https://doi.org/10.1016/0255-2701(91)80012-E

Shu, Q., 2005. Experimental Research on the Flow Law of the Annular Liquid by the Action of Cyclone Centralizer. West-china Explor. Eng. 10, 55–57.

Shu, Q., Liu, C., 2006. Pressure Drop Study on Annular Helical Flow Field under Action of Cyclone Centralizer. Nat. Gas Ind. 26, .86-87.

Shu, Q., Liu, C., 2005. Research on the Helical Flow Attenuation Law in Annular Flow Field by the Action of Cyclone Centralizer. Nat. Gas Ind. 25, 57–60.

Sifferman, T.R., Becker, T.E., 1992. Hole Cleaning in Full-Scale Inclined Wellbores. SPE Drill. Eng. 7, 115–120. https://doi.org/10.2118/20422-PA

Sifferman, T.R., Myers, G.M., Haden, E.L., Wahl, H.A., 1974. Drill Cutting Transport in Full Scale Vertical Annuli. J. Pet. Technol. 26, 1295–1302. https://doi.org/10.2118/4514-PA

Singh, A.N.R.K.C., 1969. Study of the effects of orientation and shape on the settling velocity of non-isometric particles. Chem. Eng. Sci. 24, 1185.

Sivanandam, S., Sumathi, S., Deepa, S., 2006. Introduction to neural networks using MATLAB 6.0. Tata McGraw-Hill.

Skalle, P., 2011. Drilling Fluid Engineering, 1st ed. Ventus Publishing ApS.

Song, X., Xu, Z., Li, G., Pang, Z., Zhu, Z., 2017. A new model for predicting drag coefficient and settling velocity of spherical and non-spherical particle in Newtonian fluid. Powder Technol. 321, 242–250. https://doi.org/10.1016/j.powtec.2017.08.017

Song, X., Zhu, Z., Xu, Z., Li, G., Faustino, M.A., Chen, C., Jiang, T., Xie, X., 2019. Experimental study on the wall factor for spherical particles settling in parallel plates filled with power-law fluids. J. Pet. Sci. Eng. 179, 941–947. https://doi.org/https://doi.org/10.1016/j.petrol.2019.05.018

Soo, S.L., 1990. Multiphase fluid dynamics. Science Press ; Gower Technical, Beijing; Aldershot; Brookfield, USA.

Sorgun, M., 2010. Modeling of Newtonian Fluids and Cuttings Transport. Middle East Technical

University.

Stenevik, B.C., 1991. Design and Construction of a Large-scale Wellbore Simulator and Investigation of Hole Size Effects on Critical Cuttings Transport Velocity in Highly Inclined Wells. University of Tulsa, The Graduate School.

Stokes, G.G. (Ed.), 2009. On the Effect of the Internal Friction of Fluids on the Motion of Pendulums, in: Mathematical and Physical Papers, Cambridge Library Collection - Mathematics. Cambridge University Press, Cambridge, pp. 1–10. https://doi.org/DOI: 10.1017/CBO9780511702266.002

Stokes, G.G., 1850. On the Effect of the Internal Friction of Fluids on the Motion of Pendulums, in: Mathematical and Physical Papers. Cambridge University Press, Cambridge, pp. 1–10. https://doi.org/10.1017/CBO9780511702266.002

Strack, O.D.L., Cundall, P.A., 1978. The distinct element method as a tool for research in granular media. Department of Civil and Mineral Engineering, University of Minnesota, Minneapolis.

Tan, C.P., Yaakub, M.A., Chen, X., Willoughby, D.R., Choi, S.K., Wu, B., 2004. Wellbore Stability of Extended Reach Wells in an Oil Field in Sarawak Basin, South China Sea. SPE Asia Pacific Oil Gas Conf. Exhib. https://doi.org/10.2118/88609-MS

Teale, R., 1965a. The concept of specific energy in rock drilling. Int. J. Rock Mech. Min. Sci. Geomech. Abstr. 2, 57–73. https://doi.org/https://doi.org/10.1016/0148-9062(65)90022-7

Teale, R., 1965b. The concept of specific energy in rock drilling. Int. J. Rock Mech. Min. Sci. Geomech. Abstr. 2, 57–73. https://doi.org/https://doi.org/10.1016/0148-9062(65)90022-7

Time, R.W., Rabenjafimanantsoa, A.H., 2014. Flow Regimes of Particle Settling in Suspensions and Non-Newtonian Fluids with Relevance to Cuttings Transport during Drilling. Annu.

Trans. Nord. Rheol. Soc. 22, 115–124.

Tomren, P.., 1979. The Transport of Drilled Cuttings in an Inclined Annulus. University of Tulsa.

Tomren, P.H., Iyoho, A.W., Azar, J.J., 1986. Experimental Study of Cuttings Transport in Directional Wells. SPE Drill. Eng. 1, 43–56. https://doi.org/10.2118/12123-PA

Tong, S., Gu, M., Singh, R., Mohanty, K.K., 2019. Proppant transport in foam fracturing fluid during hydraulic fracturing. J. Pet. Sci. Eng. 182, 106279. https://doi.org/https://doi.org/10.1016/j.petrol.2019.106279

Torabi, M., Yaghoobi, H., 2011. Novel solution for acceleration motion of a vertically falling spherical particle by HPM–Padé approximant. Adv. Powder Technol. 22. https://doi.org/10.1016/j.apt.2011.02.013

Trofa, M., D'Avino, G., Hulsen, M., Greco, F., Maffettone, P.L., 2015. Numerical simulations of the dynamics of a slippery particle in Newtonian and viscoelastic fluids subjected to shear and Poiseuille flows. J. Nonnewton. Fluid Mech. 228. https://doi.org/10.1016/j.jnnfm.2015.12.001

Vajargah, A.K., Fard, F.N., Parsi, M., Hoxha, B.B., 2014. Investigating the Impact of the "Tool Joint Effect" on Equivalent Circulating Density in Deep-Water Wells . https://doi.org/10.2118/170294-MS

van Oort, E., Hale, A.H., Mody, F.K., Roy, S., 1996. Transport in Shales and the Design of Improved Water-Based Shale Drilling Fluids. SPE Drill. Complet. 11, 137–146. https://doi.org/10.2118/28309-PA

Wachs, A., Frigaard, I., 2016. Particle settling in yield stress fluids: Limiting time, distance and applications. J. Nonnewton. Fluid Mech. 238. https://doi.org/10.1016/j.jnnfm.2016.09.002

Wadell, H., 1935. Volume, Shape, and Roundness of Quartz Particles. J. Geol. 43, 250–280. https://doi.org/10.1086/624298

Wang, H., Xisheng, L., Hongqian, L., Ding, G., 1995. An Experimental Study of Transport of Drilling Cutting in a Horizontal Well. ACTA Pet. Sin. 16, 125–132.

Wang, J., He, X., 2020. Special issue on advanced simulation in engineering. Int. J. High Perform. Comput. Appl. 34, 157–158. https://doi.org/10.1177/1094342020905932

Wang, J., Huang, Y., Zhou, F., Liang, X., 2020. The influence of proppant breakage, embedding, and particle migration on fracture conductivity. J. Pet. Sci. Eng. 193, 107385. https://doi.org/10.1016/j.petrol.2020.107385

Wang, Y., Zhou, L., Wu, Y., Yang, Q., 2018. New simple correlation formula for the drag coefficient of calcareous sand particles of highly irregular shape. Powder Technol. 326. https://doi.org/10.1016/j.powtec.2017.12.004

Wang, Z., Zhai, Y., Hao, X., Guo, X., Sun, L., 2010. Numerical simulation on three layer dynamic cutting transport model and its application on Extended Reach Drilling. IADC/SPE Asia Pacific Drill. Technol. Conf. Exhib. https://doi.org/10.2118/134306-MS

Wei, G., Babadagli, T., Huang, H., Hou, L., Li, H., 2020a. A visual experimental study: Resin-coated ceramic proppants transport within rough vertical models. J. Pet. Sci. Eng. 191, 107142. https://doi.org/https://doi.org/10.1016/j.petrol.2020.107142

Wei, G., Babadagli, T., Huang, H., Hou, L., Li, H., 2020b. A visual experimental study: Resin-coated ceramic proppants transport within rough vertical models. J. Pet. Sci. Eng. 191, 107142. https://doi.org/10.1016/j.petrol.2020.107142

Wicks, M., 1971. TRANSPORT OF SOLIDS AT LOW CONCENTRATION IN HORIZONTAL PIPES, in: Presented at the ASCE-Pennsylvania University International

Symposium, “Advances in Solid-Liquid Flow in Pipes and Its Applications”, Philadelphia, Pennsylvania, March 4-6, 1968.

Williams, C.E., Bruce, G., 1951. Carrying Capacity of Drilling Muds. J. Pet. Technol. - J Pet. TECHNOL 3, 111–120. https://doi.org/10.2118/951111-G

Wilson, K.C., 1970. Slip Point of Beds in Solid-Liquid Pipeline Flow. J. Hydraul. Div. 96, 1–12.

Wilson, M.A., 2009. Talus cones on the north shore of Isfjorden, Svalbard, Norway. [WWW Document]. URL https://commons.wikimedia.org/wiki/File:TalusConesIsfjorden.jpg

Woods, B.H., Lubinski, A., 1955. Use of Stabilizers in Controlling Hole Deviation. Am. Pet. Inst.

Xiang, Y.L., Liu, G., Vertex, P., 2012. Impact of Cuttings Concentration on ECD during Drilling. AADE Fluids Tech. Conf. Exhib.

Xiaofeng, S., Tie, Y., LiWei, WuYanze, 2013. Study on cuttings transport efficiency affected by Stabilizer’s Blade shape in Vertical Wells. Open Pet. Eng. J. 6, 7–11. https://doi.org/10.2174/1874834101306010007

Xu, Z., Song, X., Li, G., Liu, Q., Pang, Z., Zhu, Z., 2017. Predicting fiber drag coefficient and settling velocity of sphere in fiber containing Newtonian fluids. J. Pet. Sci. Eng. 159. https://doi.org/10.1016/j.petrol.2017.09.046

Yaghoobi, H., Torabi, M., 2012. Novel solution for acceleration motion of a vertically falling non-spherical particle by VIM–Padé approximant. Powder Technol. 215–16. https://doi.org/10.1016/j.powtec.2011.09.049

Yan, T., Qu, J., Sun, X., Li, Z., Li, W., 2019. Investigation on horizontal and deviated wellbore cleanout by hole cleaning device using CFD approach. Energy Sci. Eng. 7, 1292–1305. https://doi.org/10.1002/ese3.346

Yu, M., Takach, N.E., Nakamura, D.R., Shariff, M.M., 2007. An Experimental Study of Hole Cleaning Under Simulated Downhole Conditions, in: SPE Annual Technical Conference and Exhibition. Society of Petroleum Engineers, pp. 1186–1199. https://doi.org/10.2118/109840-MS

Zaidi, A., Tsuji, T., Tanaka, T., 2015a. Hindered Settling Velocity & Structure Formation during Particle Settling by Direct Numerical Simulation. Procedia Eng. 102, 1656–1666. https://doi.org/10.1016/j.proeng.2015.01.302

Zaidi, A., Tsuji, T., Tanaka, T., 2015b. Hindered Settling Velocity & Structure Formation during Particle Settling by Direct Numerical Simulation. Procedia Eng. 102, 1656–1666. https://doi.org/10.1016/j.proeng.2015.01.302

Zakerian, A., Sarafraz, S., Tabzar, A., Hemmati, N., Shadizadeh, S.R., 2018. Numerical modeling and simulation of drilling cutting transport in horizontal wells. J. Pet. Explor. Prod. Technol. 8, 455–474. https://doi.org/10.1007/s13202-018-0435-6

Zamora, M., Hanson, P., 1991a. Rules of thumb to improve high-angle hole cleaning. Pet. Eng. Int. 63, 4–44.

Zamora, M., Hanson, P., 1991b. More rules of thumb to improve high-angle hole cleaning. Pet. Eng. Int. 63, 4–22.

Zeidler, U.H., 1972. An Experimental Analysis of the Transport of Drilled Particles. Soc. Pet. Eng. J. 12, 39–48. https://doi.org/10.2118/3064-PA

Zhang, F., Miska, S., Yu, M., Ozbayoglu, E., Takach, N., Osgouei, R.E., 2015. Is Well Clean Enough? A Fast Approach to Estimate Hole Cleaning for Directional Drilling, in: SPE/ICoTA Coiled Tubing & Well Intervention Conference & Exhibition. Society of Petroleum Engineers, pp. 603–618. https://doi.org/10.2118/173681-MS

Zhou, J.K., 1986. Differential transformation and its applications for electrical circuits. Huazhong Univ. Press 1279–1289.

Zhu, C., Fan, L.S., 1998. Chapter 18 - Multiphase flow: Gas/Solid, in: Handbook of Fluid Dynamics. CRC Press, pp. 20.1-20.104 BT-Handbook of Fluid Dynamics.

Zhu, J., Yang, Z., Li, X., Song, Z., Liu, Z., Xie, S., 2019. Settling behavior of the proppants in viscoelastic foams on the bubble scale. J. Pet. Sci. Eng. 181, 106216. https://doi.org/https://doi.org/10.1016/j.petrol.2019.106216